AD-A140 194 WORKSHOP ON DYNAMIC FRACTURE HELD AT PASADENA CALIFORNIA ON 17-18 FEBRUARY 1983(U) CALIFORNIA INST OF TECH PASADENA W G KNAUSS ET AL. OCT 83 1/3

UNCLASSIFIED ARO-19961.1-EG-CF DAAG29-83-M-0101 F/G 11/6 NL

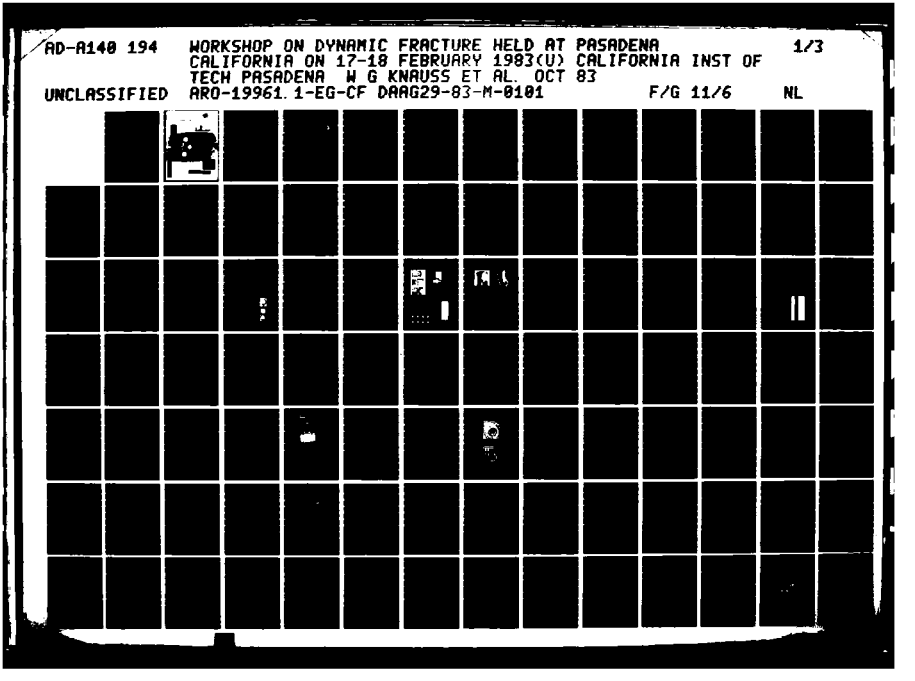

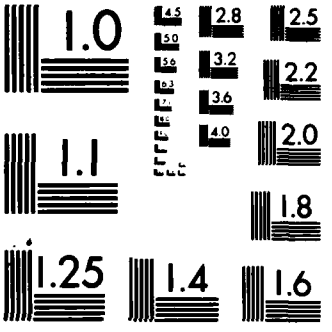

Workshop on

Dynamic Fracture

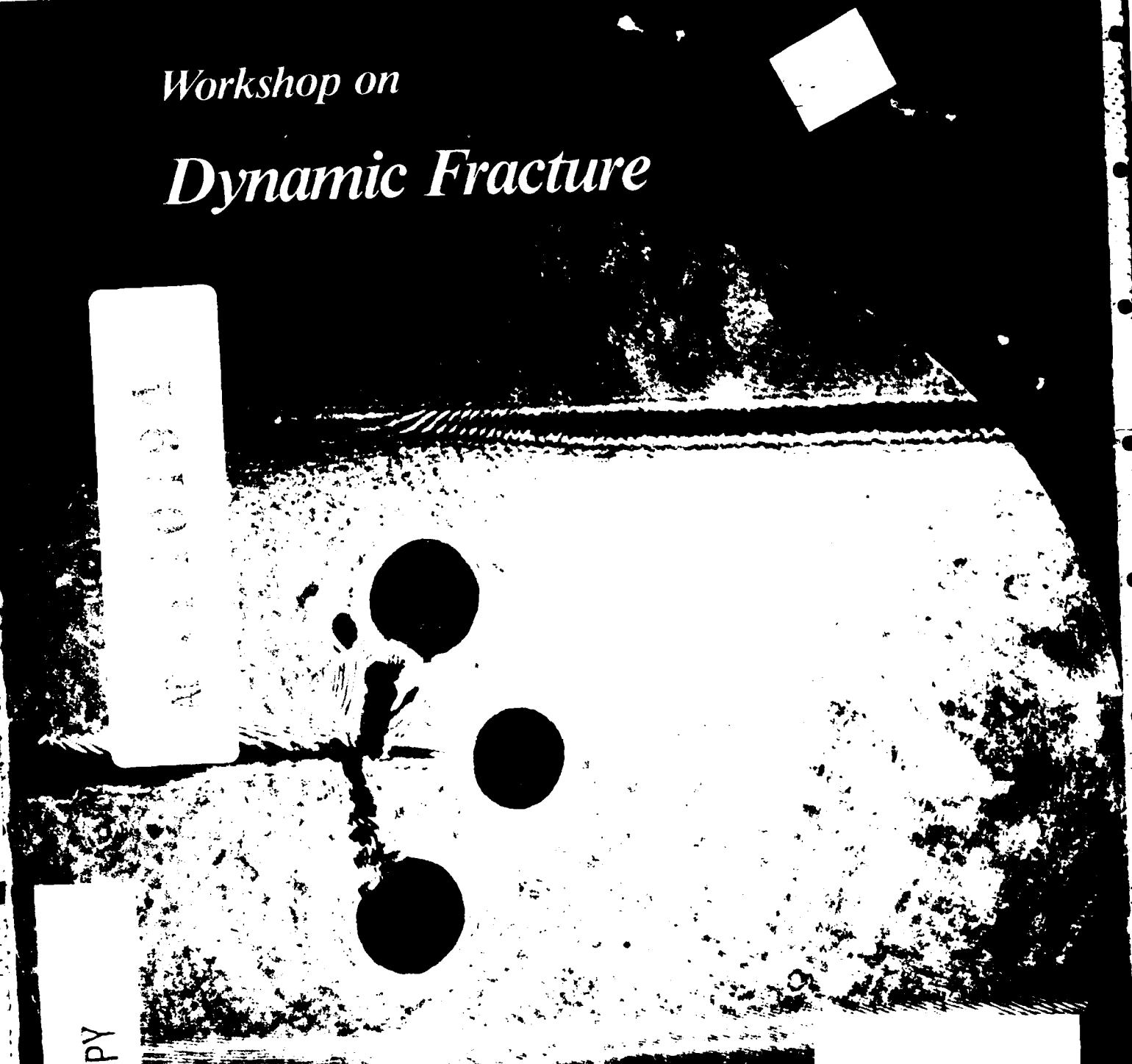

California Institute of Technology February 17-18, 1983

Sponsored by the National Science Foundation and the Army Research Office

Unclassified

SECURITY CLASSIFICATION OF THIS PAGE (When Data Entered)

REPORT DOCUMENTATION PAGE		READ INSTRUCTIONS BEFORE COMPLETING FORM
1. REPORT NUMBER: 19961.1-EG-CF	2. GOVT ACCESSION NO.: AD-A140 194	3. RECIPIENT'S CATALOG NUMBER:
4. TITLE (and Subtitle): Workshop on Dynamic Fracture		5. TYPE OF REPORT & PERIOD COVERED: 1 Dec 82-30 Nov 83 Final Report
		6. PERFORMING ORG. REPORT NUMBER: N/A
7. AUTHOR(s): W. G. Knauss		8. CONTRACT OR GRANT NUMBER(s): DAAG29-83-K-0101
9. PERFORMING ORGANIZATION NAME AND ADDRESS: California Institute of Technology, Pasadena, California		10. PROGRAM ELEMENT, PROJECT, TASK AREA & WORK UNIT NUMBERS:
11. CONTROLLING OFFICE NAME AND ADDRESS: U. S. Army Research Office, Post Office Box 12211, Research Triangle Park, NC 27709		12. REPORT DATE: Oct 83
		13. NUMBER OF PAGES: 236
14. MONITORING AGENCY NAME & ADDRESS (if different from Controlling Office)		15. SECURITY CLASS. (of this report): Unclassified
		15a. DECLASSIFICATION/DOWNGRADING SCHEDULE:

16. DISTRIBUTION STATEMENT (of this Report)

Approved for public release; distribution unlimited.

17. DISTRIBUTION STATEMENT (of the abstract entered in Block 20, if different from Report)

18. SUPPLEMENTARY NOTES

The view, opinions, and/or findings contained in this report are those of the author(s) and should not be construed as an official Department of the Army position, policy, or decision, unless so designated by other documentation

19. KEY WORDS (Continue on reverse side if necessary and identify by block number)

Fracture properties
Fracture (Mechanics)
Explosives
Impact
Workshops

20. ABSTRACT (Continue on reverse side if necessary and identify by block number)

This workshop was proposed to provide a forum for the discussion of problems to be overcome and research to be undertaken in the future in the area of dynamic fracture. Fundamental aspects of the problems were to dominate over the applied or engineering design facets. Practical problems were to be related to the mechanisms of explosives and impact damage.

DD FORM 1 JAN 73 1473 EDITION OF 1 NOV 65 IS OBSOLETE

UNCLASSIFIED

COMPONENT PART NOTICE

THIS PAPER IS A COMPONENT PART OF THE FOLLOWING COMPILATION REPORT:

(TITLE): Workshop on Dynamic Fracture Held at Pasadena, California on 17-18 February 1983.

(SOURCE): California Inst. of Tech., Pasadena, CA.

TO ORDER THE COMPLETE COMPILATION REPORT USE AD-A140 194.

THE COMPONENT PART IS PROVIDED HERE TO ALLOW USERS ACCESS TO INDIVIDUALLY AUTHORED SECTIONS OF PROCEEDINGS, ANNALS, SYMPOSIA, ETC. HOWEVER, THE COMPONENT SHOULD BE CONSIDERED WITHIN THE CONTEXT OF THE OVERALL COMPILATION REPORT AND NOT AS A STAND-ALONE TECHNICAL REPORT.

THE FOLLOWING COMPONENT PART NUMBERS COMPRISE THE COMPILATION REPORT:

AD#:	TITLE:
AD-P003 102	On Some Current Problems in Experimental Fracture Dynamics.
AD-P003 103	A Plate Impact Experiment for Studying Crack Initiation at Loading Rates K(I) Approximately 10(8) MPa m/s.
AD-P003 104	Applying Molecular Dynamics to Fracture.
AD-P003 105	Short Pulse Fracture Mechanics.
AD-P003 106	Dynamic Crack Growth in Polymers.
AD-P003 107	Dynamic Crack Growth Criteria in Structural Metals.
AD-P003 108	Processes Controlling the Dynamic Fracture of Brittle Solids.
AD-P003 109	Some Theoretical Results on the Dependence of Dynamic Stress Intensity Factor on Crack Tip Speed.
AD-P003 110	On Crack Paths.
AD-P003 111	Path-Independent Integrals in Dynamic Fracture Methanics.
AD-P003 112	Crack Branching, Crack Arrest and Rapid Tearing.
AD-P003 113	Dynamic Kinking and Bifurcation of Cracks in Plane Strain.
AD-P003 114	Dynamic Steady-State Crack Propagation in Linear Isotropic Viscoelastic Material.
AD-P003 115	Viscoelastic Effect on Dynamic Crack Propagation in Homalite 100.
AD-P003 116	Some Thoughts on the Subject of Dynamic Elastic-Plastic Analyses of Rapid Crack Propagation and Crack Arrest.

WORKSHOP ON DYNAMIC FRACTURE

February 17 and 18, 1983

California Institute of Technology

Pasadena, California

Feb. 1983

Sponsored by

the National Science Foundation and

the Army Research Office

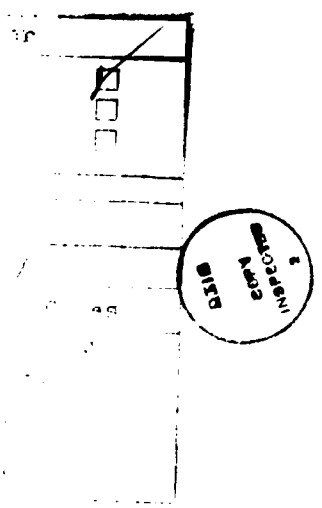

A-1

PROGRAM - TABLE OF CONTENTS

INTRODUCTORY COMMENTS

by

W.G. Knauss

By far most situations involving fracture result from quasi-static conditions so that material inertia has (essentially) no effect on the development of the fracture process. No doubt this preponderance of static fracture occurrences in engineering applications accounts substantially for the fact that dynamic fracture problems have, historically, attracted less attention. However, an additional and obvious reason for this apparent quasi-static bias in the study of fracture is that dynamic fracture problems are analytically more complicated and experimentally more demanding than their quasi-static counterparts.

These limitations notwithstanding there has been a steadily increasing interest devoted to dynamic fracture problems which is motivated by diverse engineering problems of serious concern; these problems relate to the need for both fracture prevention as well as fracture promotion.

In the latter category we find the problems of comminution: these are of interest in the pharmaceutical and in the chemical engineering industry where generating small particles in an energy efficient way is important. On the more macroscopic scale the technology of developing cracks and "porosity" in geological formations for improving recovery of oil, natural gas or thermal energy draws on the results of dynamic fracture research.

In the more preventive vein of designing against dynamic fracture the need exists to understand the propagation of cracks in pressurized gas pipe lines as well as their behavior in structures such as ships or large rocket motors. There, as in pressure vessels for nuclear reactors, both the conditions leading to crack initiation, growth and arrest need to be understood in order to minimize risks. In addition to these typical crack propagation problems those connected with projectile penetration of rock or metal targets are important. Moreover, there are many situations where postmortem evaluation of an accomplished failure is important in analyzing

the source and process of a failure in an engineering structure in order to prevent a failure recurrence through design improvements. In these latter cases the fractography of dynamically generated fracture surfaces is of prime importance.

It is clear that such a broad range of problems generates an equally broad spectrum of needs and questions. For convenience of discussion purposes, these may be divided into design-oriented needs on the one hand, and understanding of basic phenomena on the other, even though all serve to enhance our ability to cope more effectively with the problems of prevention or promotion of (dynamic) fracture.

For design purposes it may be necessary to draw on limited available information which serves to construct relatively simple theoretical concepts. Such stiuations arise often in connection with engineering analyses. Simultaneously one needs to develop additional knowledge on a somewhat short term basis (advancing engineering concepts), yet fully recognizing that a still more satisfactory resolution of important questions must await answers from long range research which are geared to clarify the fundamental phenomena. Within this spectrum of concern with detail and investigative sophistication this conference was structured to emphasize the more fundamental aspects of dynamic fracture rather than those of immediate engineering concern, although the awareness of the latters' importance was clearly the driving force behind the presentations and discussions.

There are many issues of need and concern that can be expressed and differentiated in various ways in order to introduce some kind of classifying framework for discussion purposes. A basic question underlying most dynamic fracture investigations is whether the difference between dynamic and quasi-static fracture problems is primarily the effect of material inertia and/or of material rate sensitivity. If one were to suppose that material inertia alone accounted for the major difference between static and dynamic fracture, then this inertia effect could be "factored out" analytically: This is to say that stress analyses could account for inertia effects, but otherwise criteria of fracture could remain unchanged. Thus the dynamic fracture problem could be reduced essentially to "quasi-static fracture behavior" which is much more easily characterized in

laboratory tests than its dynamic counterpart.

The belief that such a simple reduction may be possible - if only for a select class of materials - seems to be the basis for deliberate attempts to devise (small) test geometries that lead to quasi-static stress fields under rapid loading. Similarly, the attempt of explaining crack arrest as a "reverse crack initiation problem" governed by the same stress field parameter has its root in this belief; yet such a simple viewpoint is not supported by experiment. Instead, it appears that history effects are significant. However, it is not yet clear to what extent - and in which material types - absolute time rates of deformations and/or merely the sequential nature of material deformations are important.

A resolution of this question has a fundamental impact on the developments of dynamic fracture for it is intimately connected with the choice of a laboratory test geometry and the application of a load history to it. More importantly, the resolution of this question affects our assumption that the results obtained on small specimens in the laboratory accurately reflect aspects of dynamic fracture behavior and are, therefore, transferable to large structures in which moving crack tips may experience load histories that are significantly different from those generated in specialized geometries in the laboratory. That crack tip history effects are indeed important is clear from tests on small specimens where the relation between crack speed and associated fracture toughness is found to depend on specimen geometry (presentations by A. Kobayashi and by J. Kalthoff). Moreover, tests on large specimens (of Homalite 100) demonstrate that such a relation does not even always exist (presentation by Kalthoff, Ravi-Chandar/Knauss, and Rosakis/Duffy/Freund). In addition to these questions relating to test geometry and loading type there is another concern: The complicated wave actions associated with small specimens can, conceivably, blurr or mask the physical behavior of crack growth so much that the physical phenomena that govern crack growth (in a large structure) are not resolved or recognized clearly enough.

Another example that should caution us to extrapolate our current test results without question to large geometries is the observation that loading far from the crack (crack in a

stretched sheet) produces crack growth behavior that is significantly different from that when loading is applied to the crack faces. This latter situation arises when pressure follows the moving crack tip as for example in the fracture of pipes, or other gas pressurized vessels. Whether these observed differences can be accounted for simply by following multiple interactions of the crack tip with waves needs to be clarified. At any rate, there appears to be enough uncertainty in our explanation of observed phenomena that one must question whether our view of dynamic fracture, heavily colored by quasi-static concepts, as it is, is sufficient to clarify the basic understanding of dynamic fracture phenomena.

Of overriding concern in fracture problems is the effect which material behavior plays in the fracture process. Clearly both the behavior on the microscopic scale (crack tip) and in bulk (far field) is significant. Problems considered analytically (or numerically) still compromise the degree of analytical difficulty with the choice of material description; however, there is a definite trend towards incorporating more realistic constitutive behavior in such analyses. Most likely, carefully executed numerical procedures will provide the most powerful tool to deal with real, highly non-linear material behavior, provided the characterization of such materials can be accomplished with sufficient precision. Linearly elastic and brittle material behavior is analyzed most easily, with plastic or even viscoelastic/viscoplastic behavior offering considerably more difficulty in both analysis and experiment. Progress with understanding these latter materials seems to be primarily a matter of time (no pun intended).

Because dynamic fracture is a discipline that is, relatively speaking, in its infancy, the interaction between experimental and analytical work is very important. The obvious reason is that wave analyses provide the backbone for time resolution in interpreting experiments and that idealized assumptions need to be tested against real material behavior. Concurrently, experimental observations provide vital input into analyses because they are the basis for analytically modelling the fracture process. For these reasons it was hoped that a review of both experimental and analytical work would benefit this interchange.

Perhaps here another remark is in order with respect to present interaction between experimental and analytical work in dynamic fracture. While this interaction is, on the whole, mutually reinforcing one perceives a possible shortcoming that needs to be addressed, perhaps first by the experimentally inclined investigator. Because detailed analytical studies examining physical phenomena at the crack tip are extremely complex, one tends to describe the fracture process or the stress/strain field in terms of parameters like the stress intensity factor or fracture energy. In order to add new information into the analysis/experiment cycle it would seem necessary for the experimentalist to provide refined or more detailed information which transcends such a "global" description to which the analyst has to limit himself. For example, it would be very satisfying if a fairly detailed description of the crack tip behavior were available which could then be averaged or integrated somehow to develop an analysis framework that is still consistent with the current analytical description of the fracture process in terms of stress intensity (or similar) data.

In this way one would - for the present - avoid the enormous analytical complexities, yet still be assured that the less detailed analytical description conforms to experiment at the more detailed level. Analysis techniques required for the detailed description would, no doubt, follow later and more closely scrutinize the self-consistency of the experimental results. By contrast, an experimental investigation that limits itself to a characterization of the fracture process in terms of the same gross parameters accessible to the analyst will, generally, not contribute new information beyond the modelling assumption incorporated in the analysis. It seems, therefore, highly desirable to make efforts at generating rather detailed experimental information, even if each detail does not yet have its analytical counterpart.

Because of the considerable breadth of dynamic fracture problems it is sometimes useful to distinguish categories of related problems. True, problems are of interest here only if crack motion is involved under steady or transient conditions. It is reasonable, however, to distinguish narrow categories such as initiation, crack speed behavior, fracture path, branching phenomena and arrest, for example. In addition, all phenomena of crack growth depend on the micro- and on the bulk-behavior of the material, which we may divide roughly into brittle and linearly

elastic (small deformation), linearly viscoelastic, rate independent and rate dependent plastic behavior. When one considers that each one of these material behaviors can have an effect on the different categories of crack behavior, one is confronted with a large number of subproblems which can be summarized in terms of an interaction matrix as in Figure 1. This matrix may clarify our current level of understanding of dynamic fracture processes: Thus it is of interest to examine the attention that these individual problem areas have received in the past. As an indication of how attentively I perceive these to have been treated, I let the size of the circles suggest the relative level of past effort in these particular areas. No doubt the reader will wish to modify the relative sizes somewhat, but, on the whole, the areas that have received no attention stand out clearly.

In fairness to many investigators it should be said that the need to understand most of these "untouched" areas is well-recognized and that contributions and propositions exist; but in virtually all such cases these contributions are (important) by-products of investigations originating to a large extent in concepts of linear fracture mechanics. In the event where apparently no direct effort has been made to elucidate the effect of material behavior on a particular aspect of crack growth, no entry is made in the table. (For example, there appears to be no investigation recorded to date in the open literature that addresses the effect of viscoelastic material behavior on crack arrest.)

For the purpose of organizing this meeting, the interaction matrix provided a reasonable guide. Clearly, other choices would have been equally acceptable, but inasmuch as the workshop discussions were left rather unstructured, this rough guide was not deemed very restrictive.

PHENOM-ENON / MATERIAL	INITIATION	SPEED	PATH	BRANCHING	ARREST	GENERATION
BRITTLE		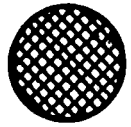				
RATE DEP: BRITTLE						
RATE INDEP: PLASTICITY						
RATE DEP: PLASTICITY						

SYNOPSIS OF SESSION I: CRACK INITIATION

G.T. Hahn
Vanderbilt University

Summary of Discussion

Prior to the session W.G. Knauss made introductory comments which anticipated many of the workshop discussions. The first paper reviews recent work by J.F. Kalthoff and associates on dynamic initiation, propagation and arrest. In the discussion period that followed, questions from the floor sought to clarify the origins of the oscillations detected during the dynamic loading of single and paired edge cracks. It is apparent that for many workers, including this reporter, intuition remains an unreliable source of insights to dynamic effects. The issue that prompted the most lively discussion is the inequality J.F. Kalthoff allows for between K_I^d-field, the advancing crack stress field parameter determined from caustics, and K_{ID}-material, the advancing crack toughness as evaluated from local temperature rise measurements. The discussion failed to resolve whether these two quantities must be identical under LEFM conditions (as it seems to this reporter), whether the temperature rise measurements are accurate enough for a meaningful interpretation, and whether any real differences are accounted for by departures from LEFM such as the plastic flow in the "wake" region as suggested by L.B. Freund. It was brought to this reporter's attention later that earlier work along these lines (Döll, Int. J. Fracture, Vol. 12, p. 595, 1976) favors agreement between the 2 quantities.

In order to minimize wave reflection effects on crack propagation J.F. Kalthoff proposed the use of a special test geometry. The merits of this "butterfly" crack arrest specimen were questioned in view of earlier work by the author's group (Kalthoff, Beinert, Winkler and Klemm, ASTM STP 711, p. 109, 1980) which shows that dynamic effects at arrest in the compact specimen are small. The 1980 study provides justification for current practice in this country, which evaluates K_{Ia} with the easier-to-machine compact specimen using a static LEFM analysis. J.F. Kalthoff responded that his group has since concluded that the dynamic effects at arrest in the

compact specimen are larger than reported in the 1980 reference. This motivated the development of the "butterfly" specimen which minimizes wave reflections and makes it possible to derive K_{Ia} from the crack length at arrest with a static LEFM analysis and without foreknowledge of the shape of the K_{ID}-crack velocity curve. Kalthoff agreed that K_{Ia} can be evaluated with similar ease from the compact specimen by applying existing dynamic analyses (Kanninen, Popelar and Cohlen, ASTM STP 627, p. 19, 1977), but it seems to this reporter that the dynamic interpretation depends on the shape of the K_{ID}-crack velocity curve.

The paper by R.J. Clifton and G. Ravichandran describes a new dynamic loading procedure with the potential of increasing the upper bound of stationary crack loading rates by 2 orders of magnitude. The discussion of the paper was stimulated by R.J. Clifton's request for suggestions of alternative ways of detecting the position of the crack tip and the instant the crack extends in his dynamically loaded test piece. The diffraction of ultra sound and the detection of electromagnetic surface waves were among ideas offered by participants. Several concerns about the technique were aired. According to R.J. Clifton the crack faces are not expected to impede the passage of the initial compression loading wave because the fatigue crack is closed. R.J. Clifton agreed that the evaluation of K_{IC} hinges on the dominance of the singular field and its extent relative to the estimated $\sim$ 80 μm plastic zone, and discussed how these features can be controlled.

The paper by W.G. Hoover and B. Moran descirbes efforts to use an atomistic model to characterize the field of a large, rapidly advancing crack. Doubts were expressed in the discussion period about the merits of treating continuum-scale features with such a highly refined model. As noted in the author's paper, the existing atomistic model is altogether too small and inflexible to simulate even the most rudimentary crack tip plastic deformation. It seems to this reporter that, in the absence of plasticity, an atomistic model of a non-brittle material is no better than a much coarser, elastic, finite element representation. There were questions about the exact elastic wave velocities that result from the piecewise-linear force law used by the authors. One discusser

wondered whether a liquid-like, "disorganized" state at the crack tip has implications for crack speed.

The paper by D.A. Shockey, J.F. Kalthoff, H. Homma and D.C. Erlich - the last in this session - examined the criterion for crack extension under a short duration stress pulse. The discussion of this work centered on experimental methods and the need for more detailed modelling. It was suggested that the 25 μm-root radius imbedded flaws be pulsed twice, the first time to sharpen the cracks, and that lasers could be used to generate internal cracks in transparent materials. Inspired by the authors' thesis, that crack extension can involve a K_I^{dyn}-sensitive, minimum time criterion, a number of participants argued in favor of more detailed analyses of the processes in the "non-continuum" physical damage zone at the crack tip. The need for "matching" the non-continuum with the continuum, incorporating the details of the fracture surface and linking crack extension to the events in the "process zone" were advocated.

ON SOME CURRENT PROBLEMS IN EXPERIMENTAL FRACTURE DYNAMICS

J.F. Kalthoff
Fraunhofer-Institut für Werkstoffmechanik
Freiburg, West Germany

1. INTRODUCTION

The term fracture dynamics includes both crack tip motion effects and dynamic loading of cracks. Based on the research work at the Fraunhofer-Institut für Werkstoffmechanik (IWM) several topics are discussed regarding the subjects (see Fig. 1): crack propagation, arrest of fact running cracks, time dependent loading in general, and loading of cracks by sharp stress pulses of short duration. Following the guidelines of the workshop, previous results are briefly summarized to state the current situation, but special consideration is given to still open questions and problems not yet resolved.

2. EXPERIMENTAL TECHNIQUE

Most experimental data reported in this paper have been generated by means of the shadow optical method of caustics. The caustics technique is an optical tool for measuring stress intensifications. The method has been applied very successfully in the field of fracture mechanics for determining stress intensity factors. Crack tip caustics are of a simple form and can easily be evaluated. The technique, therefore, is very well suited for investigating complex fracture problems, as for example in fracture dynamics.

The physical principle of the shadow optical method of caustics is illustrated in Fig. 2. A precracked specimen under load is illuminated by a parallel light beam. A cross-section through the specimen at the crack tip is shown in Fig. 2b for a transparent specimen, and in Fig. 2c for a non-transparent steel specimen. Due to the stress concentration the physical conditions at the crack tip are changed. For transparent specimens both the thickness of the specimen and the

refractive index of the material are reduced. Thus, the area surrounding the crack tip acts as a divergent lens and the light rays are deflected outwards. As a consequence, on a screen (image plane) at a distance z_o behind the specimen a shadow area is observed which is surrounded by a region of light concentration, the caustic (see Fig. 3a). Figure 2c shows the situation for a non-transparent steel specimen with a mirrored front surface. Due to the surface deformations, light rays near the crack tip are reflected towards the center line. An extension of the reflected light rays onto a virtual image plane at the distance z_o behind the specimen results in a light configuration which is similar to the one obtained in transmission. Consequently a similar caustic is obtained. In Fig. 3b experimentally observed caustics are shown which were photographed in transmission and in reflection with different materials.

The method of caustics was introduced by Manogg [1,2] in 1964. Later on, Theocaris [3] further developed the technique. The author and his co-workers extended and applied Manogg's method for investigating dynamic fracture phenomena [4-7]. For further details of the technique see [8,9].

3. DYNAMIC CRACKS

In this chapter dynamic effects associated with crack tip motion are discussed.

3.1 Crack Propagation

The stress intensification and the path stability of dynamically propagating cracks are considered in the following two sections.

3.1.1 Stress Intensity - Crack Velocity - Relationship Data on the dynamic stress intensity factor as a function of crack velocity (K-v-curve) have been obtained by the author and his colleagues from many crack arrest experiments with various types of specimens made from the model material Araldite B (see Fig. 4, and [4,5,10]). All data lie within a broad band. Large scatter is observed for each type of specimen, but a tendency for lower or higher values is observed when different types of specimens are considered. The large variations in stress intensity for the same crack velocity could be due to modifications in the experimental

conditions, which were unavoidable in the course of the investigations (e.g., due to different batches of material). Therefore, experiments were carried out under practically identical conditions with DCB- and SEN-specimens (see Fig. 5). Two clearly separated K-v-curves were obtained, the one for the DCB-specimen showing significantly higher (up to 20 %) values than the one for the SEN-specimen. Additional experiments with a DCB/SEN-combination specimen (see insert in Fig. 6) confirmed these differences: Data measured in the DCB-section of the specimen fell on the previously measured curve for the DCB-specimen, and accordingly for the SEN-section. It must be speculated, therefore, that K-v-curves are not unique, but dependent on specimen geometry. Kobayashi, et al. [11] and Dally, et al. [12] measured similar data for the material Homalite-100 by means of photo-elastic techniques (Figs. 7 and 8). Kobayashi concludes that the scatter in the data is an indication of the non-uniqueness of K-v-curves. Dally [12], however, argues that the different results are due to insufficiencies of the current data evaluation procedures and speculates that the K-v-relationship, in particular the stem of the curve, is unique.

In the following paragraph it is assumed for the moment that K-v-curves are <u>not unique</u>. In order to discuss consequences of this assumption it is worthwhile to introduce and to distinguish between the following two quantities: the dynamic stress intensity factor K_I^{dyn}, i.e., a pure stress field quantity and the dynamic fracture toughness K_{ID}, i.e., a material property. In an energy consideration, K_I^{dyn} represents a measure of the energy which is available at the crack tip, whereas K_{ID} represents a measure of the energy which is actually consumed at the crack tip for propagation. Experimental techniques as shadow optics or photoelasticity measure the stress intensity factor, K_I^{dyn}. The above discussion on the uniqueness or non-uniqueness, therefore, first of all, applies for K_I^{dyn}-v-curves. Thus, it is very well possible that the dynamic fracture toughness $K_{ID}(v)$ is nevertheless represented by a unique curve. As a consequence, it would be necessary, however, to assume that the two quantities K_I^{dyn} and K_{ID} can take different values. $K_{ID}(v)$ could be the lower bound of all possible $K_I^{dyn}(v)$-curves, $K_{ID}(v) \leqslant K_I^{dyn}(v)$ (see schematic representation in Fig. 9). This would imply that more energy can be available at the tip of the

propagating crack than is actually absorbed by the propagating crack.

The speculation of an imbalance between the dynamic stress intensity factor K_I^{dyn} and the dynamic fracture toughness K_{ID} raises several questions: Is a single parameter (K) description adequate for dynamic fracture problems? Can there be different results if procedures for determining the dynamic stress intensity factor are based on different approaches: a localized consideration of information obtained from a confined area around the crack tip (experimental techniques) or a global consideration of total energy changes in the whole specimen (numerical techniques)? Are there retardation effects if information at finite observation distances ahead of the crack tip is utilized for determining the dynamic stress intensity factor? (See contribution of L.B. Freund, this volume.)

More theoretical and experimental investigations are necessary to clarify these points. Experiments have been performed by the author and his colleagues [13] to simultaneously measure both quantities, the dynamic stress intensity factor, K_I^{dyn}, and the dynamic fracture toughness, K_{ID}, by two different techniques (see Fig. 10). The shadow optical technique was applied for determining K_I^{dyn}, and temperature measurements were performed to determine the heat production at the tip of the propagating crack, which is a measure of the energy consumption [14] and hence of the dynamic fracture toughness K_{ID}. Preliminary results obtained from experiments with high strength steel specimens are shown in Fig. 11. All data lie within a large scatter band, but there is a tendency for $K_I^{dyn} > K_{ID}$ at high crack velocities. More measurements with improved accuracy are needed and are currently performed to get more definite results.

After this discussion based on the assumption that K-v-curves are not unique it shall be assumed now that K-v-curves are unique. This would imply that the experimental techniques are insufficient to resolve the uniqueness. In principle, the accuracy of evaluation procedures which utilize information at finite distances away from the crack tip can be improved by incorporating higher order terms of the stress field around the crack tip. Work is carried out at IWM in cooperation with colleagues from the University of Maryland to study the effects of higher

order terms on the K-determination by caustics. The resulting changes in shape and size of caustics are shown in Fig. 12. Information on the absolute magnitude of the higher order coefficients is necessary to give quantitative estimates on the conditions under which a one-parameter K-evaluation yields data of sufficient accuracy. The influences of higher order terms in general are considered to be less severe in shadow optics than in photoelasticity.

More fundamental research is needed to resolve the uncertainties regarding the uniqueness or non-uniqueness of K-v-curves.

3.1.2 Crack Path: The crack propagation direction in brittle materials is controlled by the mixed mode stress intensity factors K_I and K_{II} [15,16]; the directional stability is determined by the sign of the second order coefficient a_2 [17]. The formation of a definite crack branching angle (see Fig. 13) is an example of crack propagation in such a direction that pure mode I loading results: As was found by the author [18], the crack tip stress fields of the branches interact with each other, leading to a mixed mode loading. The mode-II stress intensity factor varies in magnitude and changes sign when different branching angles are considered. Accordingly, branches with large/small angles attract/repel each other, and crack propagation in the preexisting direction is possible only for a critical branching angle.

The crack propagation path in bend specimens, in particular under impact loading, shows another interesting feature (see Fig. 14). When the crack approaches the rear end of the specimen it slows down and the following crack path shows a characteristic S-shaped deviation from the original direction. High speed photoelastic investigations (see Fig. 15, [19]) reveal a change from forward loops to backward loops, which occurs prior to the actual change in the crack propagation direction. (See Fig. 15, photographs for times > 420 μs). Backward loops are an indication of a positive value of the second order coefficient a_2. Thus instability of crack propagation direction is expected according to Cotterell's theory [17]. Caustic investigations some time later, when the crack has reached almost zero crack velocity, show a mixed mode loading (see Fig. 16, [7]) which then initiates the change in the crack propagation direction. This problem is investigated

further by studying the effect of stress wave interaction with the propagating crack.

3.1.3 Crack Arrest: Stress wave effects were also found to have a significant influence on the crack arrest process. Shadow optical investigations have shown (see Fig. 17, [4,5]): At the beginning of the crack propagation event the dynamic stress intensity factor K_I^{dyn} is smaller than the stress intensity factor of an equivalent stationary crack, $K_I^{dyn} < K_I^{stat}$. This is due to elastic waves which are generated by the propagating crack. Kinetic energy is radiated into the specimen. At the end of the crack propagation event, in particular at arrest $K_I^{dyn} > K_I^{stat}$, since waves after reflection at the finite boundaries of the specimen interact with the crack (see Fig. 18) and contribute to the stress intensity factor. Only after arrest, the dynamic stress intensity factor K_I^{dyn} approaches the equivalent static stress intensity factor at arrest, K_{Ia}^{stat}, via an oscillation with damped amplitude. The wave effects during the run-arrest event initiate a vibration of the total specimen. The observed experimental findings confirm the Battelle concept of recovered kinetic energy [20,21].

Thus, a statically determined crack arrest toughness K_{Ia}^{stat} can not represent a true material property. Only a dynamically determined crack arrest toughness, K_{Ia}^{dyn}, or K_{Im} [5,21] can reflect the true arrest behavior of the material. However, since dynamic effects in large scale structures in general are smaller than in the relatively small laboratory test specimens, static crack arrest analyses will yield conservative safety predictions [22]. On the basis of this understanding the static crack arrest concept can be applied by the practical engineer. Crack arrest safety analyses would be more widely used in practice if a standardized procedure for measuring the crack arrest toughness K_{Ia} would have been released by ASTM already.

In order to minimize errors in the static crack arrest concept resulting from neglected dynamic effects an RDE-(reduced dynamic effects)-specimen has been developed at IWM (see Figs. 19 and 20). Edges and boundary of the specimen were shaped to reduce wave reflection and to defocus reflected waves. Damping material and additional weights are attached to the "wings" of the specimen to absorb kinetic energy and to increase the period of the

eigenoscillation of the specimen in order to reduce the recovery of kinetic energy. Statically determined crack arrest toughness values K_{Ia}^{stat} are shown in Fig. 21 for the RDE-specimen in comparison to data obtained with other crack arrest specimens. The dependence on crack jump distance is about three to four times smaller for RDE-specimens than for the most commonly used C-specimen.

4. DYNAMIC LOADING OF CRACKS

The fracture behavior of cracks under time dependent loads in general is discussed in the following chapter. The loading times are assumed to be considerably larger than the time it takes waves to travel the distance given by the crack length. Effects resulting for shorter load durations are discussed in a separate chapter.

4.1 Time Dependent Loading

4.1.1 Stationary Cracks: A procedure [23] has been proposed to ASTM for measuring the impact fracture toughness K_{Id} of steels with precracked Charpy specimens. The procedure assumes that dynamic stress intensity factors can be determined from loads registered at the tup of the striking hammer via a static analysis, if the times of interest are larger than three times the period η of the eigenoscillation of the specimen (see Fig. 22). A comparison of such stress intensity factors, denoted K_I^{stat}, with the actual dynamic stress intensity factors, K_I^{dyn}, determined by shadow optics, is shown in Fig. 23, [6]. The results were obtained with specimens of enlarged size made from Araldite B or a high strength steel, tested under drop weight loading at 0.5 m/s. Marked differences were measured between K_I^{stat} and K_I^{dyn}, even for times $t > 3\ \eta$. Furthermore, such large times to fracture could be obtained only by utilizing low impact velocities. The specimen behavior was investigated further by also measuring the specimen reaction at the anvils [24]. Figure 24 compares the load measured at the striking hammer (a), the stress intensity factor measured at the crack tip (b), the load measured at the anvils (c), and the position of the specimen ends with regard to the anvils (d). The late registration of load at the anvil results from a loss of contact between the specimen ends and the anvils. This loss of contact can later occur for

a second time and loss of contact can also take place between the hammer and the specimen (see Fig. 25). These effects demonstrate the strong influence of inertial effects during impact loading. It is concluded, therefore, that the determination of reliable impact fracture toughness values K_{Id} at reasonably high loading rates does require a fully dynamic evaluation procedure.

Therefore, the author and his colleagues developed the dynamic concept of impact response curves (see Fig. 26, and [25]): For fixed test conditions (i.e., specimen geometry, hammer mass, impact velocity, etc.) the dynamic stress intensity factor versus time relationship is determined by means of the shadow optical method of caustics with a high strength steel specimen. The K_I^{dyn}-t-curve (impact response curve) applies for all steels, provided the conditions for small scale yielding are fulfilled. In the real test-experiment with the steel to be investigated, then only the time to fracture is measured (e.g., by an uncalibrated strain gage near the crack tip). This time together with the preestablished impact response curve determines the impact fracture toughness value K_{Id}. This procedure has been applied successfully with two structural steels (see Fig. 27) impacted at 5 m/s. Although fracture occurred at about 0.5 η only, the concept of impact response curves gave reliable data.

Work is continued to extend this technique to increased loading rates. Data at loading rates sufficiently higher than those obtained in drop weight experiments allow to discriminate between the following behavior: the existence of a minimum fracture toughness, a continuous decrease or a final increase of toughness with increasing loading rate (see Fig. 28). Experiments were performed with a gas gun by firing a projectile against a precracked SEN-specimen (see Fig. 29). After reflection of compressive stress waves at the free ends of the specimen, the crack is loaded in tension (Fig. 30). Shadow optical analyses indicate dynamic fracture toughness values K_{Id} which are equal to or larger than the static fracture toughness K_{Ic} (see Fig. 31). A toughness increase with increasing loading rate, i.e., with decreasing time to fracture, was also observed by Ravi-Chandar and Knauss [26] with Homalite 100 specimens loaded by electromagnetic techniques (see Fig. 32). Such a behavior can be explained by assuming the existence of an

incubation time (see Fig. 33): According to this assumption the crack tip would have to experience a supercritical stress intensity factor for a constant (very likely material related) minimum time before onset of rapid crack propagation can occur. More data at varying loading rates are necessary to verify this assumption.

4.1.2 Interaction of Multiple Cracks: Due to mutual interaction, the stress intensity factors K_I of two parallel cracks under static loading condition are smaller than the stress intensity factor for an equivalent single crack. In addition a superimposed mode II loading results (see Fig. 34). Experiments were carried out to study the interaction of two parallel cracks under stress pulse loading (see Fig. 35). Shadow optical photographs and the resulting quantitative data are shown in Figs. 36 and 37 [27]. At very early times the crack which is hit by the tensile pulse first shows a similar behavior as the single crack, and the second crack is only less loaded. Some time later, however, the situation changes and the second crack exhibits the larger stress intensity factor. This process varies periodically. At larger times the average stress intensity factor of the parallel cracks is smaller than the one of the single crack, just as in the static case. This behavior is of significance for the fracture behavior of multiple crack configurations under dynamic loading conditions.

4.1.3 Propagating Cracks: Problems are more complex for propagating cracks under time dependent loading. Kanninen, et al. [28,29] analyzed the crack initiation and crack propagation behavior in precracked bend specimens under quasi-static and under impact loading conditions (see Fig. 38). Dynamic fracture toughness values $K_{ID}(v)$ inferred from these tests were roughly a factor of two different [29]. This finding relates to the question of the uniqueness or non-uniqueness of K-v_curves and would be of great significance for the relevance of safety considerations based on impact test data. The problem is addressed and further clarified in the contribution of M.F. Kanninen, in this volume.

4.2 Short Pulse Loading

The author and his colleagues at SRI-International studied the fracture behavior of cracks loaded by stress pulses of durations which are comparable or even smaller than the time it takes waves to travel the distance given by the crack length [30-32]. If the pulse duration is decreased below a certain limit, a stress intensity factor according to a simple $\sigma_o \sqrt{\pi a_o}$-relationship does not apply anymore. Instead the behavior is controlled by a rather complex stress intensity history [30]. The stress intensity increases with time to a maximum value which is reached at the end of the pulse; the stress intensity factor then drops off again. The maximum value is $\sigma_o \sqrt{\pi a_{eff}}$, with $a_{eff} \approx c \cdot T_o$, and $a_{eff} < a_o$. T_o is the pulse duration; c is a wave speed. Assuming that the crack has to experience a supercritical stress intensity factor for at least a certain minimum time in order to become unstable a short pulse fracture criterion was developed. According to this criterion and the stress intensity history discussed above, higher critical stresses are predicted to bring a crack to instability than in the equivalent static case. Furthermore, the instability stresses should not depend on crack length. The general instability behavior of cracks with different lengths subjected to different loading conditions, i.e., pulse amplitude and pulse duration, is shown in a three-dimensional (σ_o–a_o–T_o)-diagram, see Fig. 39, [30]. The short pulse fracture behavior is represented in the rear right section of the diagram. The front left regime (long pulse durations, short crack length) shows the usual static behavior. Short pulse fracture experiments were performed by Shockey, et al. [31,32]. Cracks of different lengths in various materials were subjected to stress pulses of different durations (see Figs. 40 and 41, and contribution of D.A. Shockey, et al. in this volume). The good agreement with the theoretical predictions demonstrates the applicability of the developed short pulse fracture criterion.

5. CONCLUSIONS

Several different problems in the field of fracture dynamics have been discussed. In many cases the physical principles which control the dynamic event are well understood. So it is evident that dynamic processes as crack arrest, impact loading of cracks, short pulse loading of

cracks, can accurately be described only by dynamic analyses. Static procedures can lead to erroneous results and are applicable only with restrictions. Some fundamental problems in fracture dynamics, e.g., the energy transfer at the tip of propagating cracks, the crack path stability, the applicability of a single parameter (K) description, the influence of far field effects, etc., seem to need further clarification from both the theoretical and the experimental point of view.

REFERENCES

1. Manogg, P., "Anwendung der Schattenoptik zur Untersuchung des Zerreißvorgangs von Platten," Dissertation, Universität Freiburg, West Germany, (1964).

2. Manogg, P., "Schattenoptische Messung der spezifischen Bruchenergie während des Bruchvorgangs bei Plexiglas," Proceedings, International Conference on the Physics of Non-Crystalline Solids, Delft, The Netherlands (1964) 481-490.

3. Theocaris, P.S., "Local Yielding Around a Crack Tip in Plexiglas," J. Appl. Mech., 37 (1970) 409-415.

4. Kalthoff, J.F., Beinert, J., and Winkler, S., "Measurements of Dynamic Stress Intensity Factors for Fast Running and Arresting Crack in Double-Cantilever-Beam-Specimens," ASTM STP 627 - Fast Fracture and Crack Arrest, American Society for Testing and Materials, Philadelphia, U.S.A. (1977) 161-176.

5. Kalthoff, J.F., Beinert, J., Winkler, S., and Klemm, W., "Experimental Analysis of Dynamic Effects in Different Crack Arrest Test Specimens," ASTM STP 711 - Crack Arrest Methodology and Applications, American Society for Testing and Materials, Philadelphia, U.S.A. (1980) 109-127.

6. Kalthoff, J.F., Böhme, W., Winkler, S., and Klemm, W., "Measurements of Dynamic Stress Intensity Factors in Impacted Bend Specimens," CSNI Specialist Meeting on Instrumented Precracked Charpy Testing, EPRI, Palo Alto, Calif., U.S.A. (1980).

7. Kalthoff, J.F., Böhme, W., and Winkler, S., "Analysis of Impact Fracture Phenomena by Means of the Shadow Optical Method of Caustics," VIIth Intl. Conf. Experimental Stress Analysis, Society for Experimental Stress Analysis, Haifa, Israel, Aug. 23-27, 1982.

8. Beinert, J., and Kalthoff, J.F., "Experimental Determination of Dynamic Stress Intensity Factors by Shadow Patterns," in Mechanics of Fracture, 7, G.C. Sih (ed.), Martinus Nijhoff Publishers, The Hague, Boston, London (1981) 281-330.

9. Kalthoff, J.F., "Stress Intensity Factor Determination by Caustics," Intl. Conf. Experimental Mechanics, Society for Experimental Stress Analysis and Japan Society of Mechanical Engineers, Honolulu, Maui, Hawaii, U.S.A., May 23-28, 1982.

10. Kalthoff, J.F., Beinert, J., and Winkler, S., "Influence of Dynamic Effects on crack Arrest," Draft of Final Report prepared for Electric Power Research Institute, Palo Alto, Calif. under Contract No. RP 1022-1, IWM-Report W 4/80, Freiburg, 1980.

11. Kobayashi, A.S., and Mall, S., "Dynamic Fracture Toughness of Homalite-100," Experimental Mechanics, 18 (1978) 11-18.

12. Kobayashi, T., Dally, J.W., and Fourney, W.L. , "Influence of Specimen Geometry on Crack Propagation and Arrest Behavior," VIth Intl. Conf. Experimental Stress Analysis, Society for Experimental Stress Analysis, München, West Germany, Sept. 18-22, 1978.

13. Shockcy, D.A., Kalthoff, J.F., Klemm, W., and Winkler, S., "Simultaneous Measurements of Stress Intensity and Toughness for Fast Running Cracks in Steel," to appear in Experimental Mechanics (1983).

14. Wells, A.A., "The Mechanics of Notch Brittle Fracture," Welding Res., 7 (1953) 34r-56r.

15. Erdogan, F., and Sih, G.C., "On the Crack Extension in Plates under Plane Loading and Transverse Shear," J. Basic Engineering, Trans. ASME, 85 D (1963) 519-525.

16. Kerkhof, F., "Wave Fractographic Investigations of Brittle Fracture Dynamics," Proceedings, International Conference on Dynamic Crack Propagation, G.C. Sih (ed.), Lehigh University, Bethlehem, Pa., U.S.A., July 10-12, 1972.

17. Cotterell, B., "Notes on the Paths and Stability of Cracks," International Journal of Fracture, 2 (1966) 526-533.

18. Kalthoff, J.F., "On the Propagation Direction of Bifurcated Cracks," Proceedings, International Conference on Dynamic Crack Propagation, G.C. Sih (ed.), Lehigh University, Bethlehem, Pa., U.S.A., July 10-12, 1982.

19. Böhme, W., and Kalthoff, J.F., "Untersuchungen des Bruchverhaltens schlagbelasteter Dreipunktbiegeproben unter Einsatz verschiedener Meßverfahren der Spannungsanalyse," 15. Sitzung, Arbeitskreis Bruchvorgänge im Deutschen Verband für Materialprüfung, Darmstadt, Febr. 22-23, 1983 and 7th Symposium, Gemeinschaft Experimentelle Spannungsanalyse, Schliersee, May 2-3, 1983.

20. Hahn, G.T., Hoagland, R.G., Kanninen, M.F., and Rosenfield, A.R., "A Preliminary Study of Fast Fracture and Arrest in the DCB Test Specimen," Proceedings, International Conference on Dynamic Crack Propagation, G.C. Sih (ed.), Lehigh University, Bethlehem, Pa., U.S.A. July 10-12, 1972.

21. Hahn, G.T., Gehlen, P.C., Hoagland, R.G., Kanninen, M.F., Rosenfield, A.R. et al., "Critical Experiments, Measurements and Analyses to Establish a Crack Arrest Methodology for Nuclear Pressure Vessel Steels," BMI-1937, 1959, 1995, Battelle Columbus Laboratories, Columbus, Ohio, Aug. 1975, Oct. 1976, May 1978.

22. Kalthoff, J.F., Beinert, J., and Winkler, S., "Einfluß dynamischer Effekte auf die Bestimmung von Rißarrestzähigkeiten und auf die Anwendung von Rißarrestsicherheitsanalysen," 8. Sitzung, Arbeitskreis Bruchvorgänge im Deutchen Verband für Materialprüfung, Köln, West Germany, Oct. 6-7, 1976.

23. ASTM E 24.03.03, "Proposed Standard Method of Tests for Instrumented Impact Testing of Precracked Charpy Specimens of Metallic Materials," Draft 2C, American Society for Testing and Materials, Philadelphia, U.S.A. (1980).

24. Böhme, W., and Kalthoff, J.F., "The Behavior of Notched Bend Specimens in Impact Testing," International Journal of Fracture, 20 (1982) R139-143.

25. Kalthoff, J.F., Winkler, S., Böhme, W., and Klemm, W., "Determination of the Dynamic Fracture Toughness K_{Id} in Impact Tests by Means of Response Curves," 5th Intl. Conf. Fracture, Cannes, March 29 - April 3 1981, Advances in Fracture Research, D. Francois et al. (eds.), Pergamon Press, Oxford, New York (1980).

26. Ravi-Chandar, K., and Knauss, W.G., private communication.

27. Kalthoff, J.F., and Winkler, S., "Fracture Behavior under Impact," Progress Reports prepared for United States Army, European Research Office, London, under Contract No. DAJA 37-81-C-0013, Freiburg, 1983.

28. Kanninen, M.F., Gehlen, P.C., Barnes, C.R., Hoagland, R.G., and Hahn, G.T., "Dynamic Crack Propagation under Impact Loading," Nonlinear and Dynamic Fracture Mechanics, ASME Winter Annual Meeting, New York, Dec. 2-7, 1979, N. Perrone and S.N. Atluri (eds.), ASME Publication AMD 35 (1979).

29. Ahmad, J., Jung, J., Barnes, C.R., and Kanninen, M.F., "Elastic-Plastic Finite Element Analysis of Dynamic Fracture," Engineering Fracture Mechanics, 17 (1983) 235-246.

30. Kalthoff, J.F., and Shockey, D.A., "Instability of Cracks under Impulse Loads," J Appl. Phys., 48 (1977) 986-993.

31. Shockey, D.A., Kalthoff, J.F., and Ehrlich, D.C., "Evaluation of Dynamic Crack Instability Criteria," to appear in Int. Journ. of Fracture.

32. Homma, H., Shockey, D.A., and Muragama, Y., "Response of Cracks in Structural Materials to Short Pulse Loads," submitted to J. Mech. Phys. Solids.

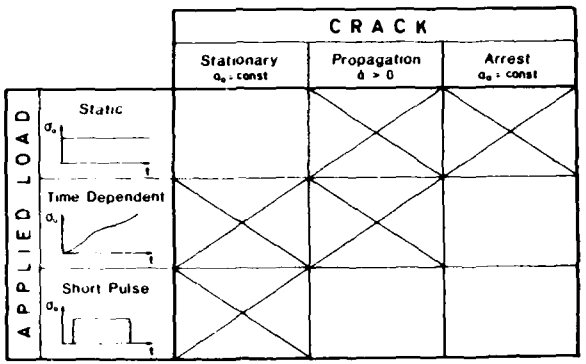

Figure 1. Dynamic fracture problems.

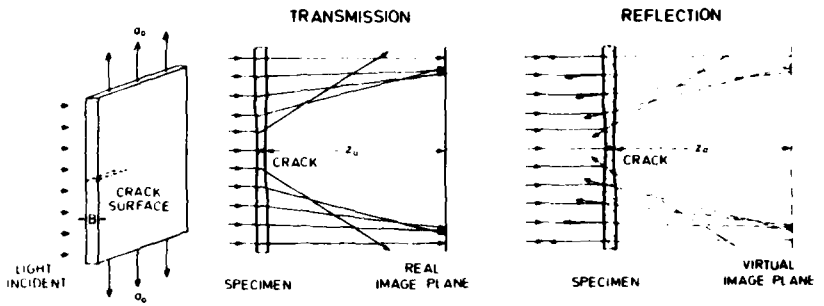

Figure 2. Shadow optical method of caustics, physical principles.

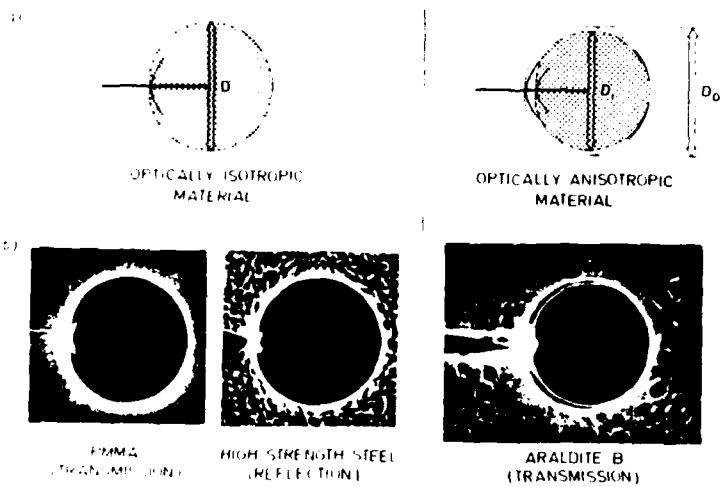

Figure 3. Caustics.

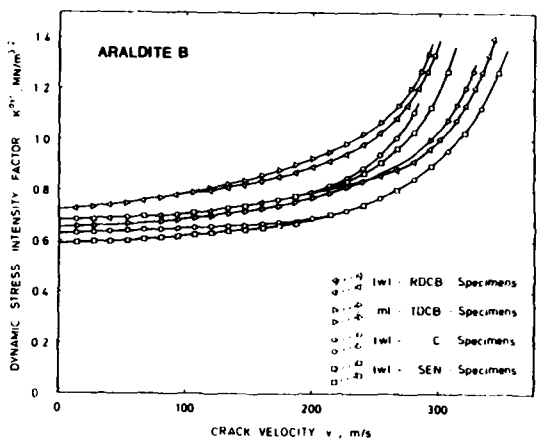

Figure 4. K-v-data for different test geometries.

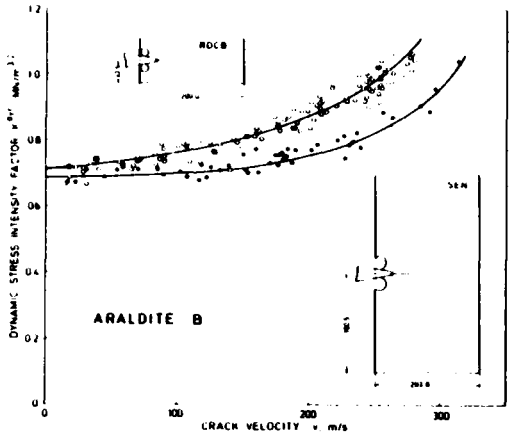

Figure 5. k-v-data for DCB- and SEN-specimens.

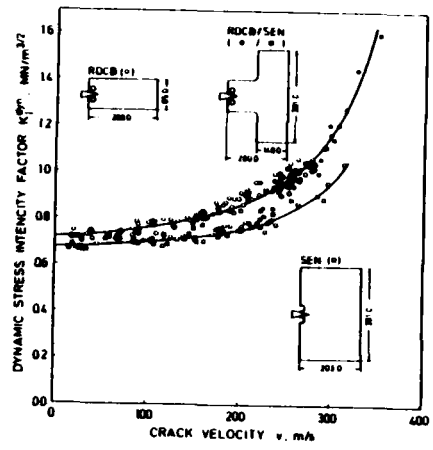

Figure 6. k-v-data for DCB/SEN-combination specimens.

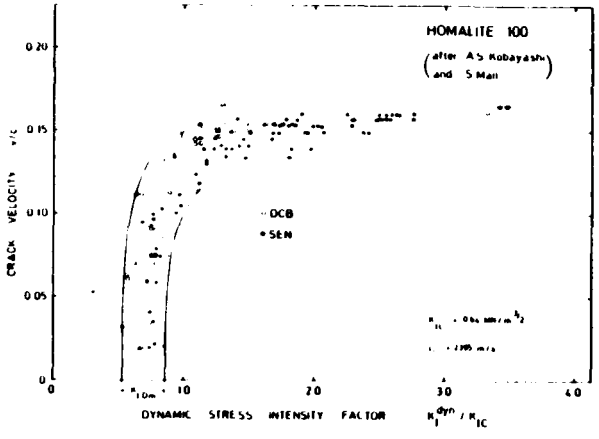

Figure 7. k-v-data.

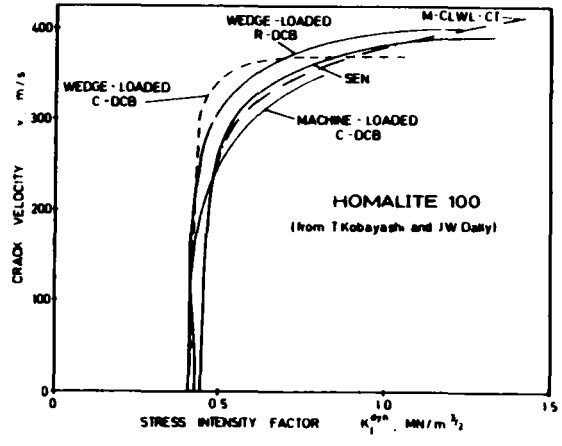

Figure 8. k-v-data.

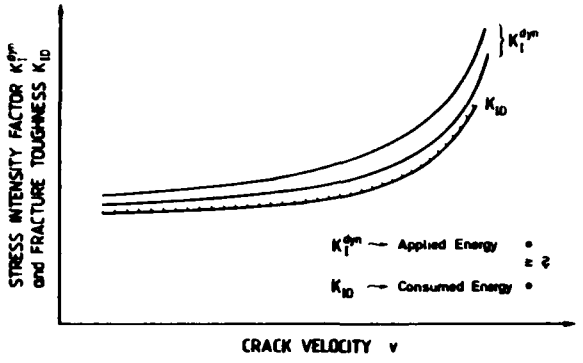

Figure 9. Dynamic stress intensity factor and fracture toughness.

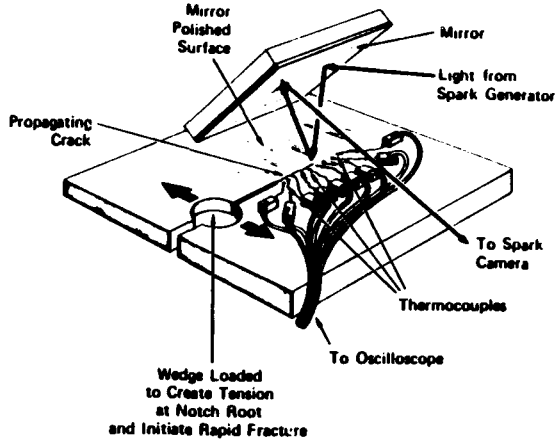

Figure 10. Simultaneous measurement of K_I^{dyn} and K_{ID}.

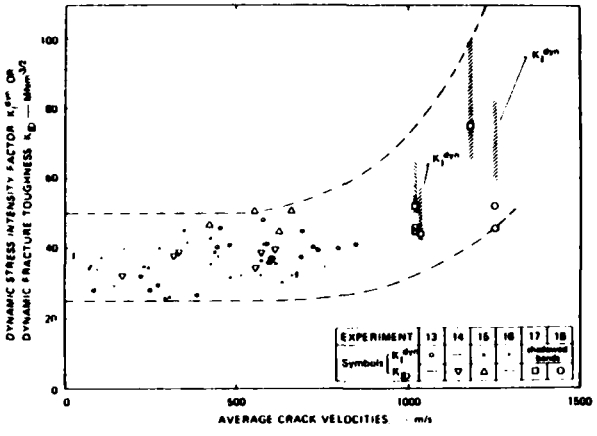

Figure 11. Measured K_I^{dyn} - and K_{ID}-values.

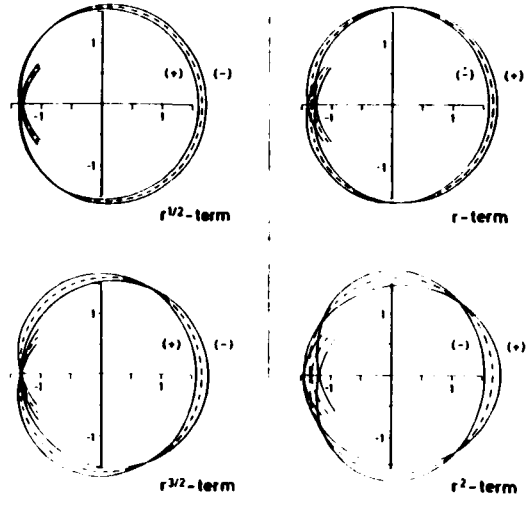

Figure 12. Influence of higher order terms on caustics.

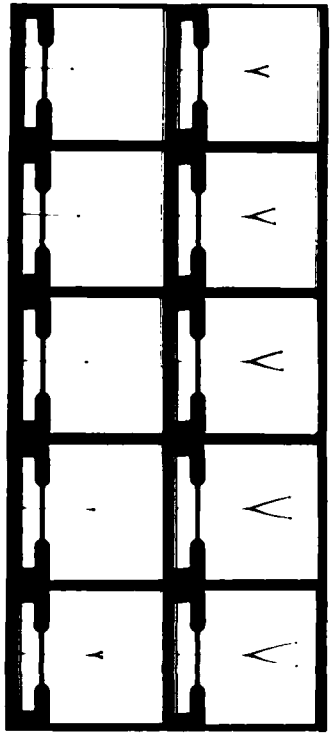

Figure 13. Crack branching.

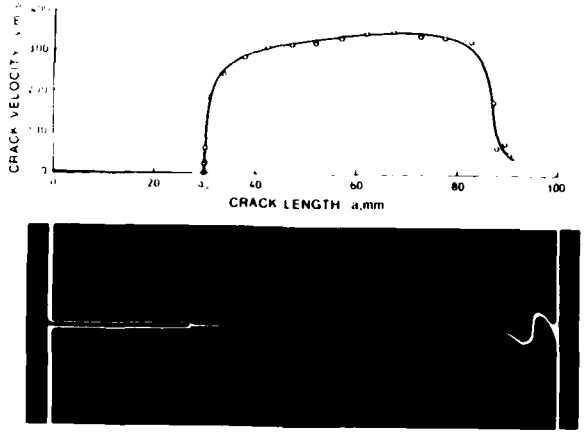

Figure 14. Fracture behavior of impacted bend specimens.

Figure 15. Photoelastic Investigation of crack propagation in Impacted bend specimen.

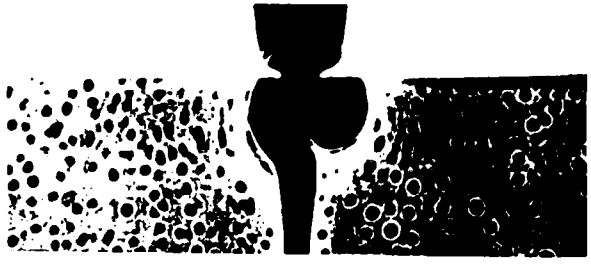

Figure 16. Mixed mode caustic in impacted bend specimen.

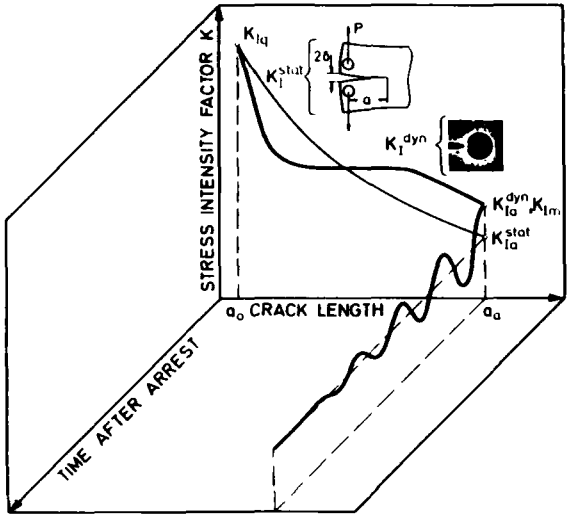

Figure 17. Crack arrest behavior.

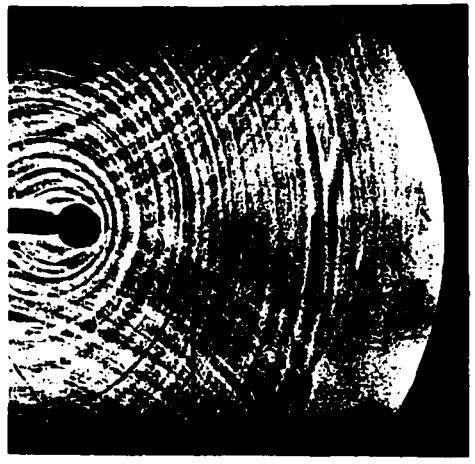

Figure 18. Shadow optical photograph of a propagating crack in steel.

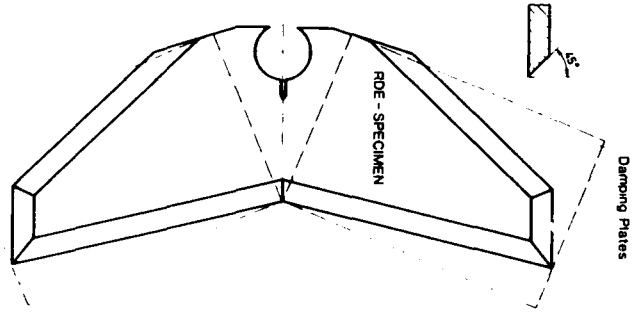

Figure 19. RDE-crack arrest specimen.

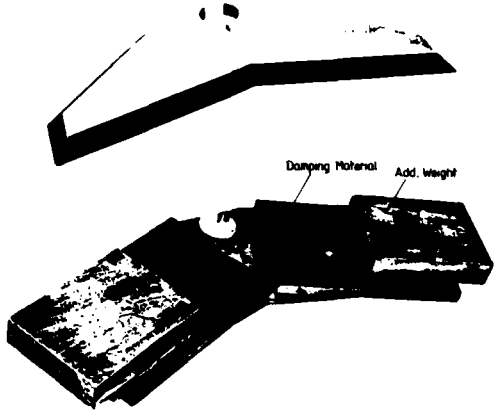

Figure 20. Photograph of RDE-crack arrest specimen.

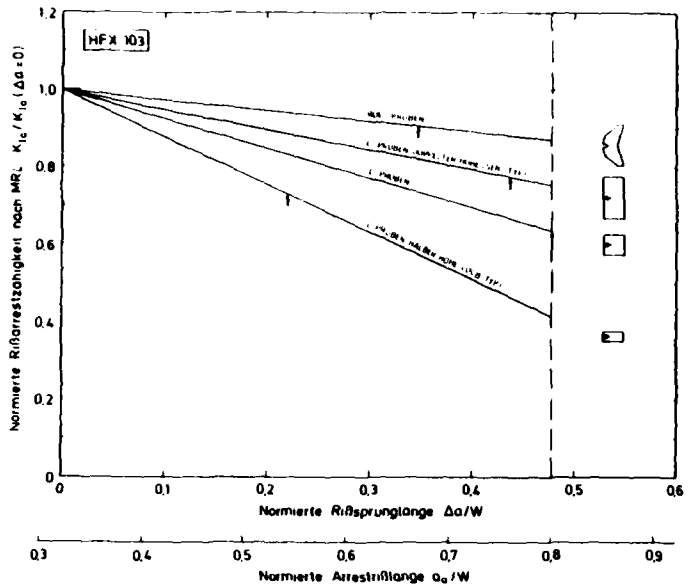

Figure 21. Dynamic effects for different crack arrest specimens.

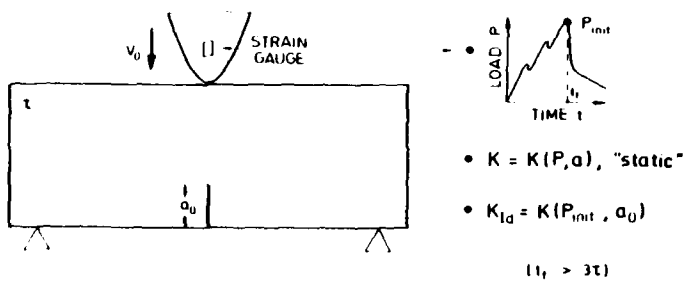

Figure 22. Determination of the impact fracture toughness.

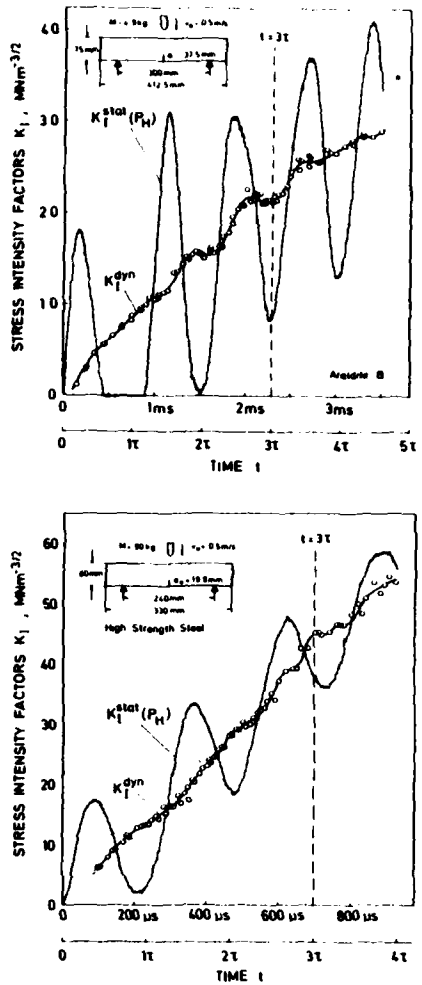

Figure 23. Stress intensity factors for impacted cracks.

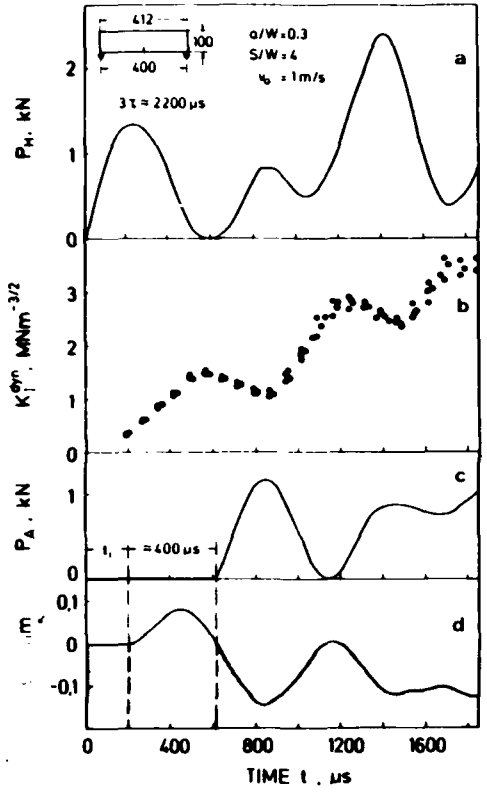

Figure 24. Specimen behavior under impact loading.

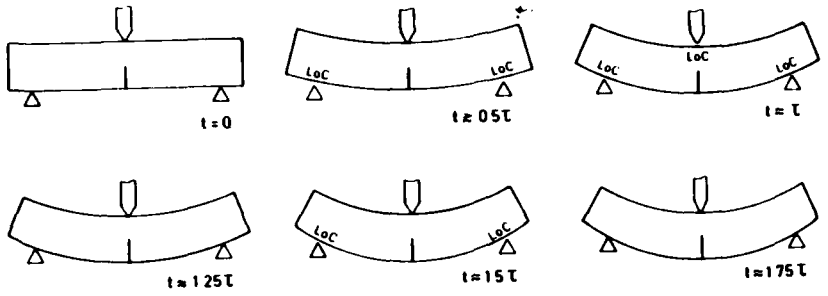

Figure 25. Loss of contact effects.

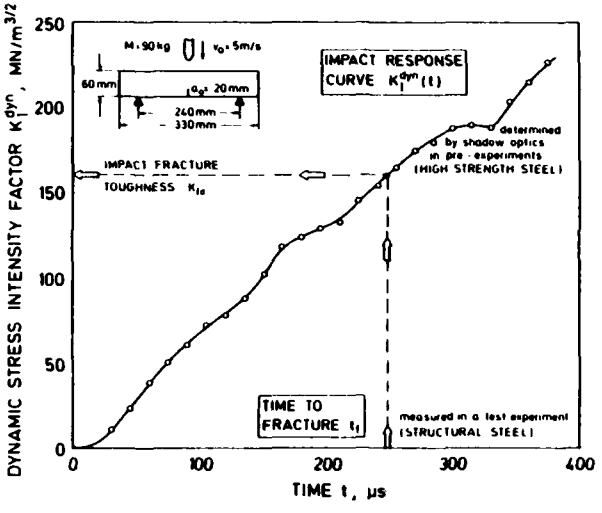

Figure 26. K_{Id}-determination by impact response curves.

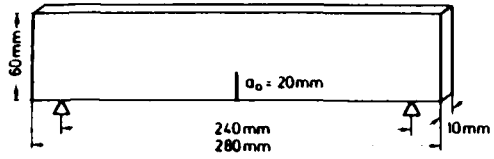

HAMMER MASS 90kg

IMPACT VELOCITY 5m/s

Figure 27. Impact fracture toughness data.

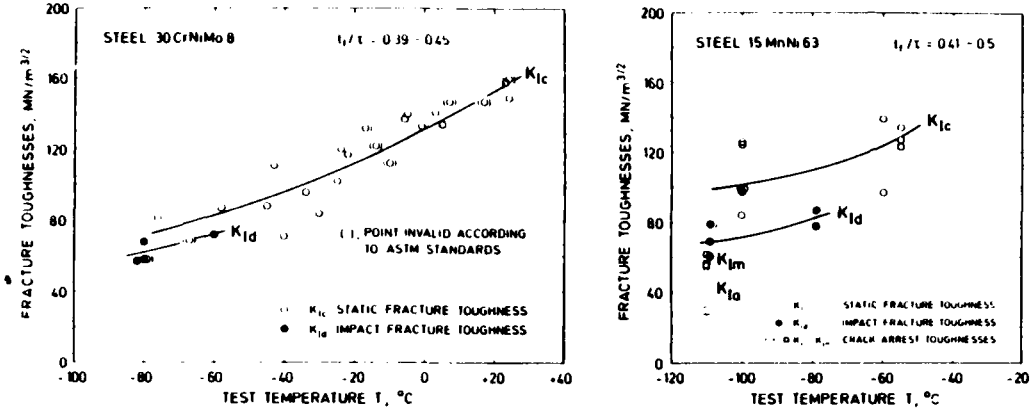

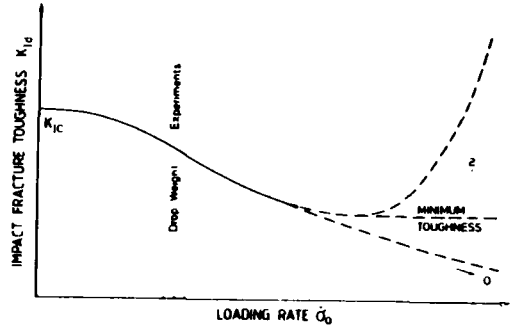

Figure 28. Influence of loading rate.

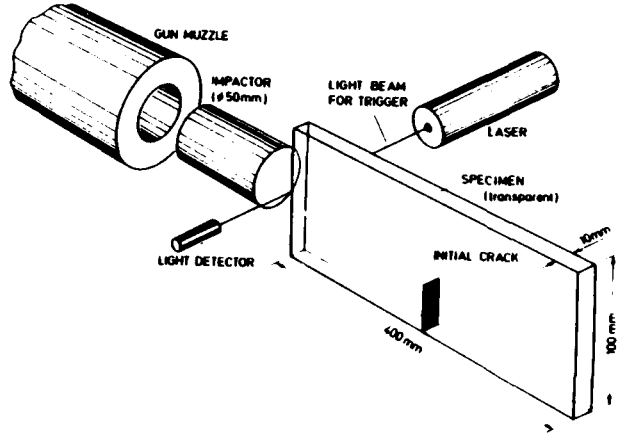

Figure 29. Projectile loading arrangement.

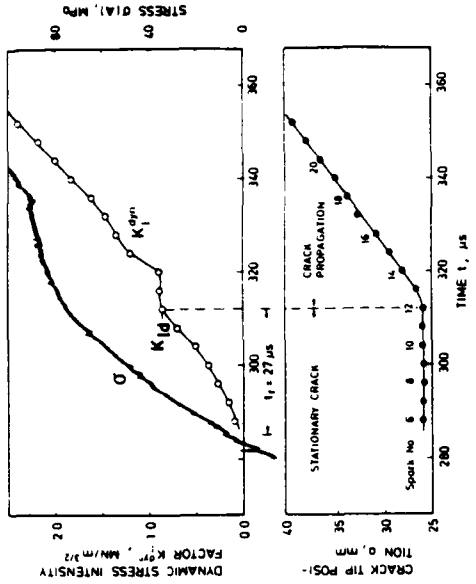

Figure 31. Fracture behavior under impact loading.

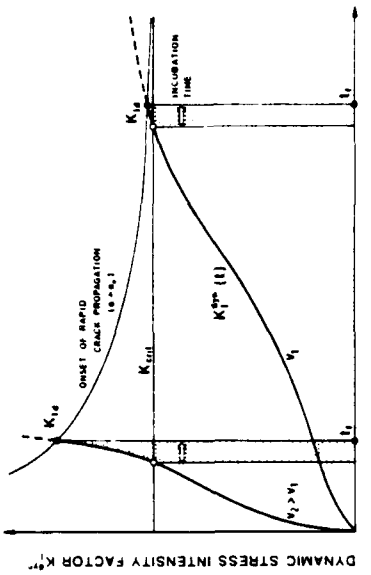

Figure 33. Incubation time.

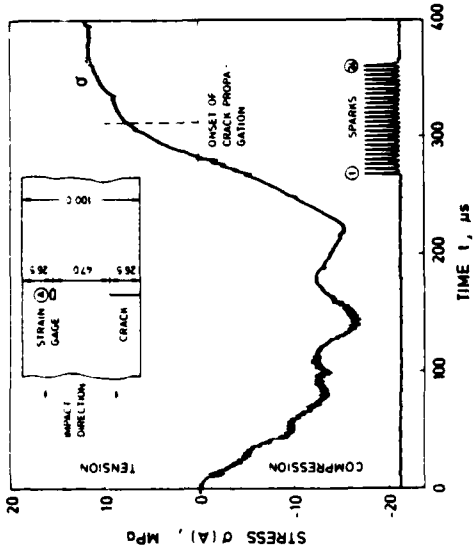

Figure 30. Load history.

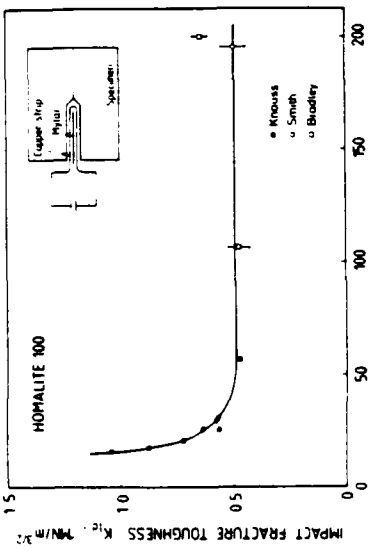

Figure 32. Loading rate influence.

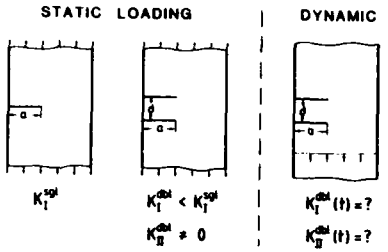

Figure 34. Interaction of cracks.

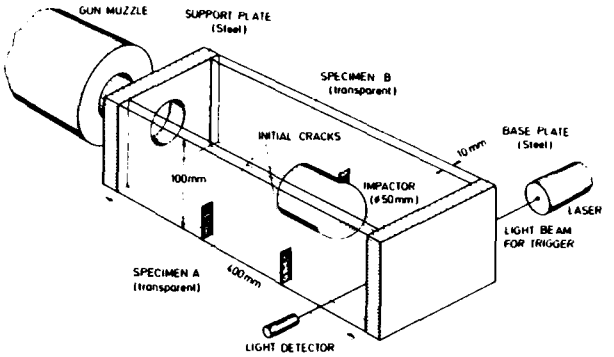

Figure 35. Loading arrangement.

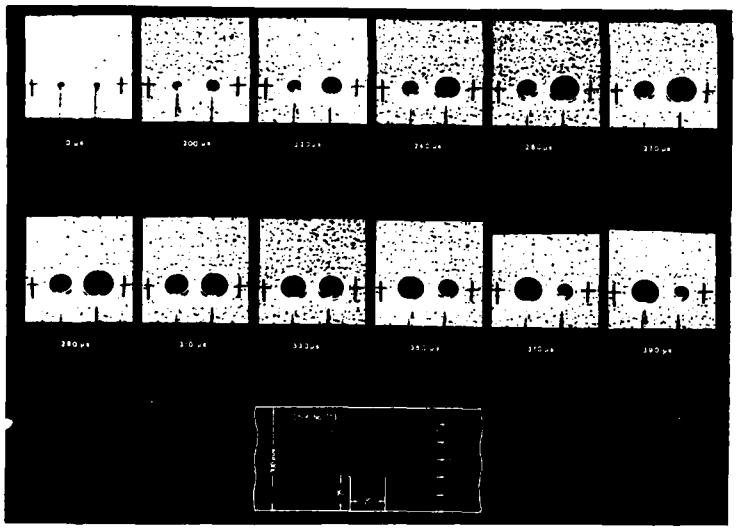

Figure 36. Dynamic interaction of cracks.

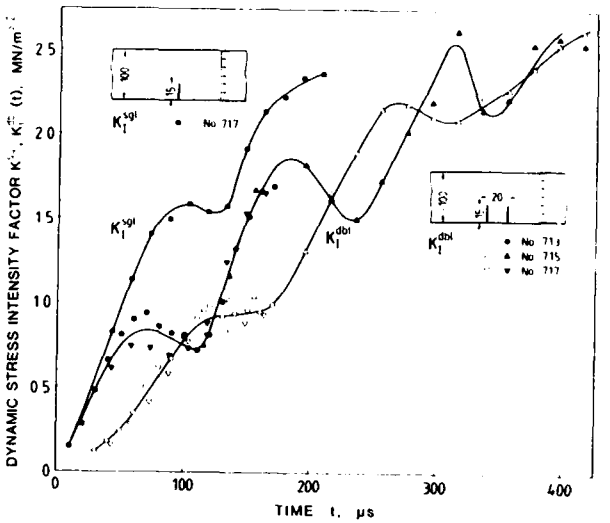

Figure 37. Stress intensity factors for interacting of cracks.

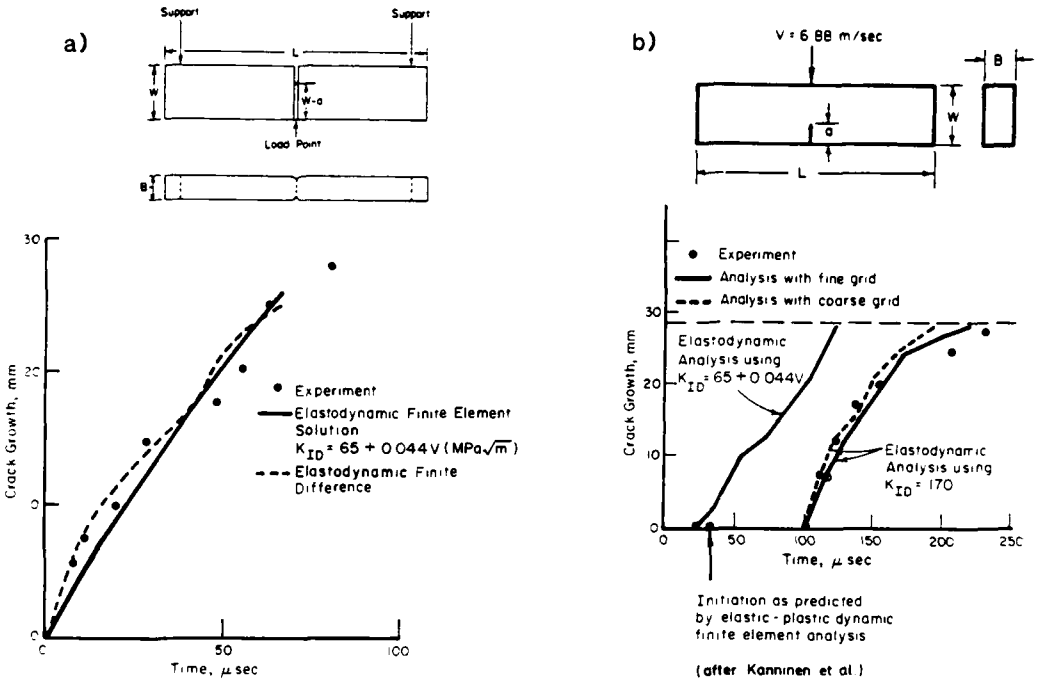

Figure 38. Crack growth in 4340 steel under a)quasi-static and b) impact loading (after Kanninen et al. [28,29]).

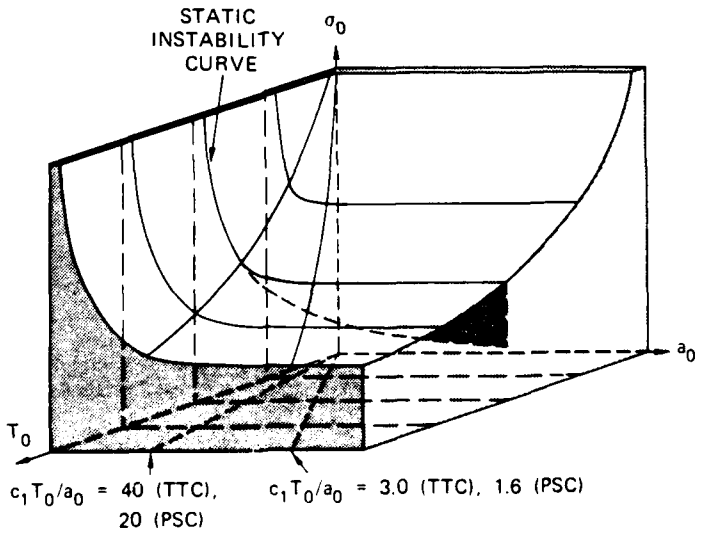

Figure 39. Dynamic instability surface.

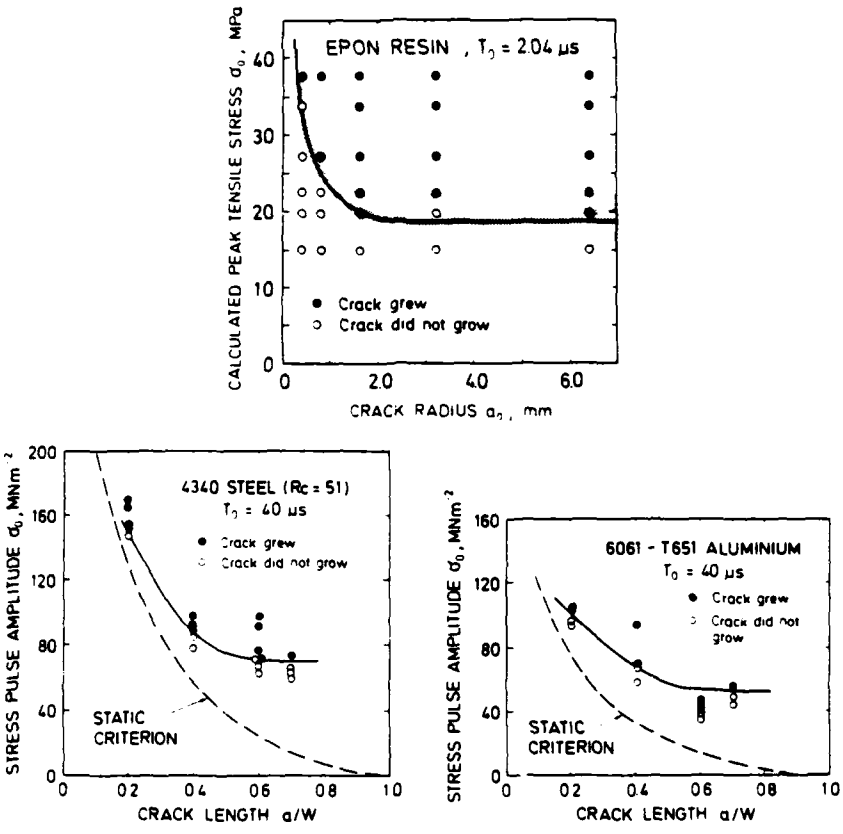

Figure 40. Dynamic instability data.

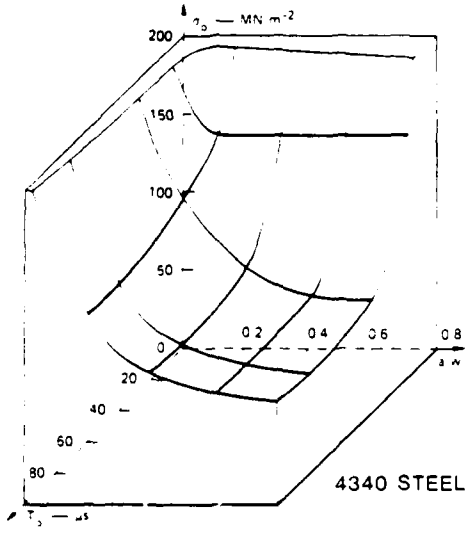

Figure 41. Measured dynamic instability surface.

A PLATE IMPACT EXPERIMENT FOR STUDYING CRACK INITIATION AT LOADING RATES $K_I \approx 10^8$ MPa $m^{\frac{1}{2}} s^{-1}$*

R.J. Clifton and G. Ravichandran
Division of Engineering
Brown University

ABSTRACT

A symmetric plate impact technique is being developed for establishing the critical conditions for dynamic fracture initiation at extremely high loading rates - in excess of $K_I = 10^8$ MPa $m^{\frac{1}{2}} s^{-1}$. The specimen consists of a circular disc with a mid-plane, prefatigued, edge crack that has propagated halfway across the diameter. A compressive pulse propagates through the specimen, reflects from the rear surface, and subjects the crack plane to a step tensile pulse. The motion of the rear surface of the specimen is monitored with a laser interferometer system in order to determine the loading time required for crack extension to begin. Using this time in the elastodynamics solution of the stress wave diffraction problem, one can obtain the critical value of the stress intensity factor for dynamic fracture initiation. Preliminary experiments are being conducted on SAE 4340 VAR steel.

1. INTRODUCTION

Impact loading of structures causes pre-existing cracks to be loaded by stress waves. Under these conditions the crack tip loading rates, expressed in terms of K_I - the rate of the change of the crack tip stress intensity factor - are generally much larger than obtained in quasi-static laboratory experiments. Charpy tests [1], which are commonly used to evaluate a material's resistance to dynamic fracture, are attractive because of the ease of conducting the tests; however the results are difficult to interpret within the framework of fracture mechanics. Furthermore, the loading times, which are approximately 10-50 μs, are too long to allow investigation of

* This research is supported by the Army Research Office through Contract No. DAAG29-81-K-0121 with Brown University.

fracture processes that occur on the scale of a few microseconds or less. Difficulties of interpretation within the framework of fracture mechanics have been greatly reduced by the introduction of the Kolsky bar technique [2]. The loading times, which are approximately 20-25 μs, are again too long to allow microsecond-scale fracture processes to be investigated. Such loading times result because of the mass of an end piece that must be accelerated in order to generate the tensile wave. Geometric dispersion precludes the possibility of obtaining risetimes less than approximately 10 μs, even for step loading at the end of the bar. Loading rates, K_I of the order of 10^6 MPa $m^{\frac{1}{2}} s^{-1}$, are obtained in these experiments. Extension of this technique to substantially higher loading rates does not appear to be possible because of the risetime limitation and because of the yield stress limitation for the uniaxial stress state in the bar.

The objective of the present work is to investigate dynamic fracture initiation at loading rates, say $K_I \approx 10^8$ MPa $m^{\frac{1}{2}} s^{-1}$, that allow for the study of dynamic fracture processes which occur when loading times are in the sub-microsecond range. Such loading rates are to be expected for the impact loading of structures made of high strength materials when the impacted region is near a pre-existing flaw and a free surface. Under these conditions, loading of the crack by large amplitude, reflected tensile waves with sharp wave-fronts can cause crack extension to occur in less than a microsecond. Investigation of dynamic fracture at these high loading rates should also contribute to better understanding of dynamic fracture at lower loading rates by clarifying the trends in the response at the upper limits of the rates attainable with current techniques.

The underlying concept in the design of the experiment is to make the measurements as amenable as possible to interpretation within the framework of fracture mechanics. To this end the experiment is designed to cause loading of a semi-infinite plane crack by a plane, step, tensile wave at normal incidence. Elastodynamics solutions for this problem have been obtained by Achenback and Nuismer [3] and by Freund [4]. A principal result of the analysis [4] is that the crack tip stress intensity factor K_I increases with time according to

$$K_I(t) = \frac{2\sigma_o}{(1-\nu)} \left[\frac{C_L(1-2\nu)}{\pi} \right]^{\frac{1}{2}} t^{\frac{1}{2}} \tag{1}$$

where σ_o is the tensile stress in the incident wave, C_L is the longitudinal elastic wave speed, ν is Poisson's ration, and t is time measured from the time of arrival of the step wave at the crack plane. The experiment is designed to allow measurement of σ_o and of the time $t = \tau$ at which crack extension begins so that the value $K_I(\tau)$ or K_{IC} at fracture initiation can be computed from (1). Because of the square root dependence of K_I on time in (1), the experiment has the attractive feature that the fractional error in $K_I(\tau)$ due to an error in the measurement of τ is less than the fractional error in the measured value of τ. Details of the experimental technique and preliminary results from experiments on a 4340 VAR steel are outlined in the remainder of this note.

2. EXPERIMENTAL TECHNIQUE

The new experimental configuration for dynamic fracture is shown in Fig. 1. A disc containing a mid-plane, pre-fatigued, edge crack that has propagated halfway across the diameter is impacted by a thin flyer plate of the same material. This generates a square compressive pulse with duration

$$t_L = \frac{2h}{C_L} \tag{2}$$

and amplitude

$$\sigma_o = \frac{1}{2} \rho C_L |V_o| \tag{3}$$

where h and v_o are, respectively, the thickness and the initial velocity of the flyer plate, ρ is the mass density. The compressive pulse propagates through the specimen, reflects from the rear surface, and subjects the crack plane to approximately a square tensile pulse. The amplitude of this pulse is determined by means of (3) with measured values of the projectile velocity. The motion of the rear surface of the specimen is monitored with a laser interferometer system. This

measured velocity-time profile is to be compared with one computed for the case of no crack extension. The time at which the computed and measured profiles deviate is to be interpreted as indicative of the time at which crack extension begins.

The specimen is a 62.5 mm diameter circular disc, 8 mm thick, cut from a cylindrical bar of the same diameter. A fatigue crack is propagated into the specimen by notching the bar to a diameter of 53 mm and subjecting the bar to cyclical pure bending. Growth of the fatigue crack is monitored by monitoring the change in compliance, using a clip gauge to record the crack opening at the notch. The pre-fatiguing is conducted in accordance with guidelines proposed for fracture toughness testing [5]. Once the fatigue crack is extended approximately halfway across the specimen, the specimen is cut from the bar such that the fatigue crack is in its mid-plane. The specimen is then ground and lapped flat to within 1-2 Newton rings over its diameter. Four contact pins, electrically isolated from the specimen, are placed near the periphery of the impact face before lapping so that they are lapped to lie in the plane of the impact face. The times at which these voltage-biased pins are shorted out during impact are recorded in order to determine the angle of tilt between the faces of the flyer and the specimen at impact.

The specimen is placed in a holder attached to an adjustable frame that is used to align the specimen parallel to the flyer plate. The flyer plate, a 59 mm diameter disc with a thickness of 3 mm, is lapped flat and mounted at the front of a projectile. An optical technique [6] is used to align the impact faces to be parallel to an accuracy of 2×10^{-5} radians. The projectile is propelled down the gun barrel by nitrogen gas. A keyway in the barrel prevents the rotation of the projectile. Impact occurs in vacuum. The velocity of impact is determined from the times at which the flyer contacts five accurately spaced pins mounted at the muzzle of the barrel. Tilt angles obtained from the times of contact of the four contact pins are generally better than 1×10^{-3} radians. After impact the specimen, flyer plate and projectile are decelerated in a catcher tank by a series of corrugated lead plates.

Motion of the rear surface of the specimen at a point near the axis of the disc is monitored with a laser interferometer system consisting of a displacement interferometer [7] and a velocity

interferometer [8]. The light source is a 1.5 w Argon ion laser with a wavelength λ = 514 nm. The intensity of the combined beams is detected with photodiodes and monitored by two 500 MHz oscilloscopes. One peak-to-peak variation in intensity of the light from the displacement interferometer corresponds to a displacement of $\lambda/2$. Similarly, a peak-to-peak variation in intensity for the velocity interferometer corresponds to a change in velocity of $\lambda/2\tau_D$ where τ_D is the time required for the light to go around a delay leg. The velocity interferometer is used to obtain a complete record of the history of the motion of the rear surface from the arrival of the incident wave until the arrival of unloading waves from the periphery of the specimen; arrival of the latter waves marks the end of the experiment. The displacement interferometer is used to obtain a detailed record of the motion during the time when an indication of crack extension is expected.

The time-distance diagram for the experiment is shown in Fig.2. The compressive step pulse passes through the specimen and causes a jump in the rear surface particle velocity at time t_1. The free surface velocity remains constant at the velocity V_o until the unloading wave reflected from the rear surface of the flyer arrives at time t_{ul}. This brings the rear surface velocity to zero. The wave reflected from the rear surface arrives at the crack plane as a tensile wave at time t_c. This tensile wave is diffracted as shown in Fig. 3. The cylindrical diffracted longitudinal wave arrives at the rear surface at a point directly opposite to the crack tip at the time t_d in Fig. 2. Tensile loading of the crack plane continues until the time t_e at which the end of the tensile pulse arrives. The cylindrical diffracted longitudinal wave emanating from the crack tip at time t_e arrives at the rear surface at time t_f. Thus, the time interval (t_d,t_f) is the interval during which the velocity-time profile is to be examined for indications that crack advance has begun. If the observation point is behind the crack tip (e.g., point (A) in Fig. 3), then the plane wave reflected from the crack would be detected before the cylindrical wave. On the other hand, if the observation point is ahead of the crack tip (e.g., point (B) in Fig. 3), then the reflected plane wave would not be observed. Accurate location of the observation point relative to the crack front is essential

if the comparison of computed and measured wave profiles is to reveal the time at which crack advance begins.

3. PRELIMINARY EXPERIMENTS

Preliminary experiments are being conducted on specimens of SAE 4340 VAR steel. The material was austenitized at 870°C for 2 hours, oil quenched, and tempered at 100°C for 2 hours. This heat treatment produces a relatively homogeneous martensitic microstructure that results in a high yield strength and comparatively low fracture toughness. Three experiments have been conducted at impact velocities V_o of approximately 0.08 mm μs^{-1}. For an acoustic impedance ρc_L = 45,400 MPa mm^{-1} μs, (ρ = 7600 kg m^{-3}, c_L = 5983ms^{-1}) the corresponding stress amplitude, from (3), is 1816 MPa. This value is approximately 58 percent of the expected yield stress in uniaxial strain (i.e., the "Hugoniot elastic limit") for the specimen material. If the stress at fracture initiation is taken to be comparable to the value, say $K_I(\tau)$ or K_{IC} = 40 MPa $m^{\frac{1}{2}}$, for cleavage fracture of this material at lower loading rates, then the loading duration τ obtained from (1) (with ν = 0.3) is 75 ns. The corresponding loading rate given by

$$\dot{K}_I(\tau) = \frac{K_I(\tau)}{2\tau} \tag{4}$$

is 2.67 x 10^8 MPa $m^{\frac{1}{2}} s^{-1}$.

Two of the experiments were conducted with the observation point at positions comparable to (B) in Fig. 3. In the other experiment the observation point corresponds to point (a) in Fig. 3. The incident wave has the expected features. Even with the observation point at (A) the front of the wave is a step with nearly 70 percent of the final amplitude reached in less than 20 ns. The rise to the final level takes approximately 450 ns. This risetime is believed to be the time required for the crack surfaces to close completely so that the compression wave can be transmitted fully. As expected, the plane wave reflected from the crack surface is evident when the observation point is at (A), but not when the observation point is at (B). Later regions of the wave

profile have not been compared with predictions because the predicted wave profiles have not yet been evaluated. Also, improved resolution of the motion during the time interval (t_d, t_f) appears to require the use of an additional 500 MHZ oscilloscope so that this interval can be covered with overlapping displacement interferometer records.

Examination of the specimens after impact reveals that, in the central region of the specimen, the crack has advanced approximately 1.75 mm uniformly along the crack front. The appearance of the fracture surface differs markedly from that of the fatigue crack surface and the fracture surface resulting from quasi-static separation of the specimens after the experiment. Thus, the measurement of the extent of crack advance appears to be quite reliable. Presumably this advance occurred during the loading interval (t_c, t_e) since later reflected waves that could load the crack plane in tension are expected to be much smaller in amplitude and to lack the uniformity required to give uniform crack advance. Although the time of fracture initiation has not been established, a lower bound on the average velocity at which the cracks advanced can be estimated by dividing the crack advance by the total loading duration $(t_f - t_d)$, which is approximately 1 μs. Thus, a lower bound on the average crack velocity appears to be approximately 1.75 mm μs^{-1}, which is 54 percent of the elastic shear wave speed.

4. CONCLUDING REMARKS

Detailed computations are under way to predict the motion of the rear surface of the specimen for the case of diffraction of a plane longitudinal wave by a stationary crack. This predicted motion is required in order to determine the time of fracture initiation from the measured velocity-time profiles. Whether or not the comparison of predicted and measured rear surface motions will be sufficiently sensitive to fracture initiation to allow the initiation time to be determined with sufficient accuracy remains to be seen. Other means for determining crack initiation are being investigated. Improved accuracy in the location of the fatigue crack front is to be attempted by use of an acoustical microscope and by better understanding of the relationship between the crack length and the compliance.

REFERENCES

1. Barsom, J.M., and Rolfe, S.T., "Impact Testing of Materials," ASTM STP 466 (1970) 281.

2. Costin, L.S., Duffy, J., and Freund, L.B., "Fast Fracture and Crack Arrest," ASTM STP 627 (1977) 301.

3. Achenbach, J.D., and Nusimer, R., Int. Journ. of Fracture Mech., 7 (1971) 77.

4. Freund, L.B., J. Mech. Phys. Solids, 21 (1973) 47.

5. Plane Strain Crack Toughness Testing of High Strength Metallic Materials, ASTM STP 410 (1966).

6. Kumar, P., and Clifton, R.J., J. Appl. Phys. 48 (1977) 1366.

7. Barker, L.M., and Hollenbach, R.E., Rev. Sci. Instru. 36 (1965) 1617.

8. Barker, L.M., Proc. IUTAM Symp. on Behavior of Dense Media Under High Dynamic Pressure, Paris (1967) 483.

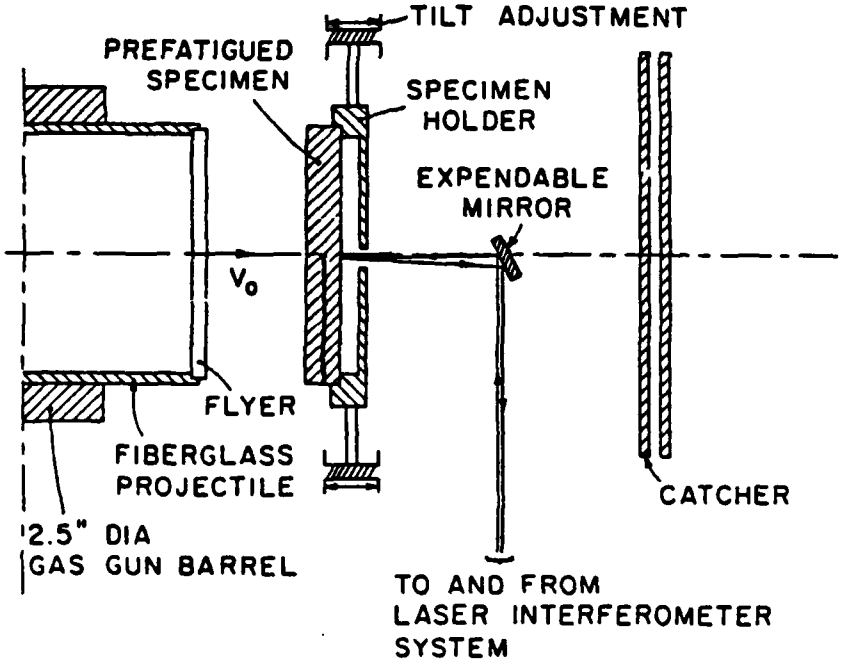

Figure 1. Schematic of experimental configuration.

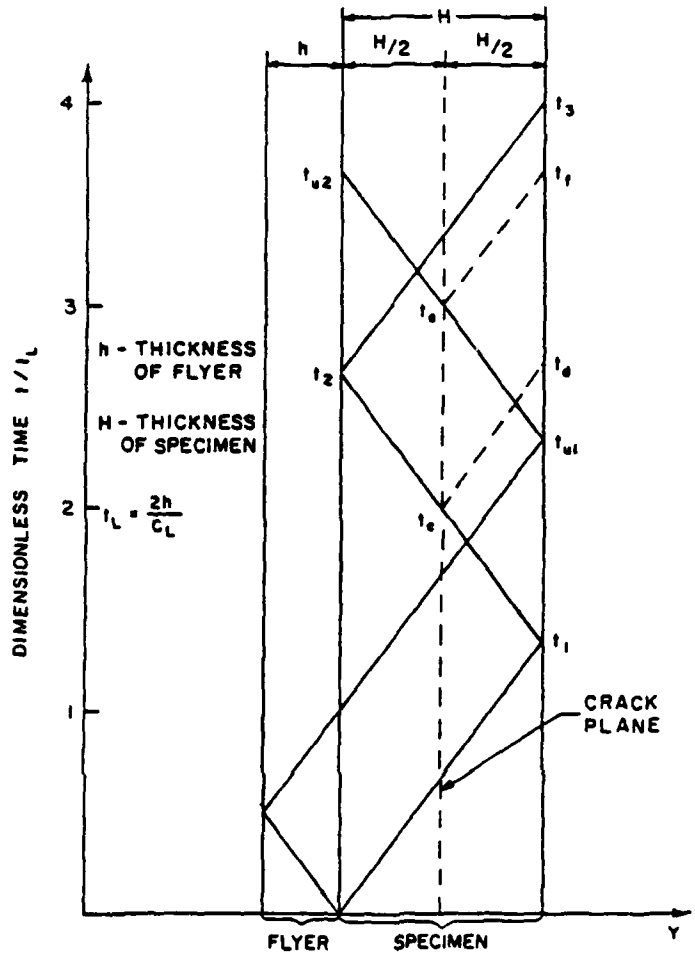

Figure 2. Time-distance diagram.

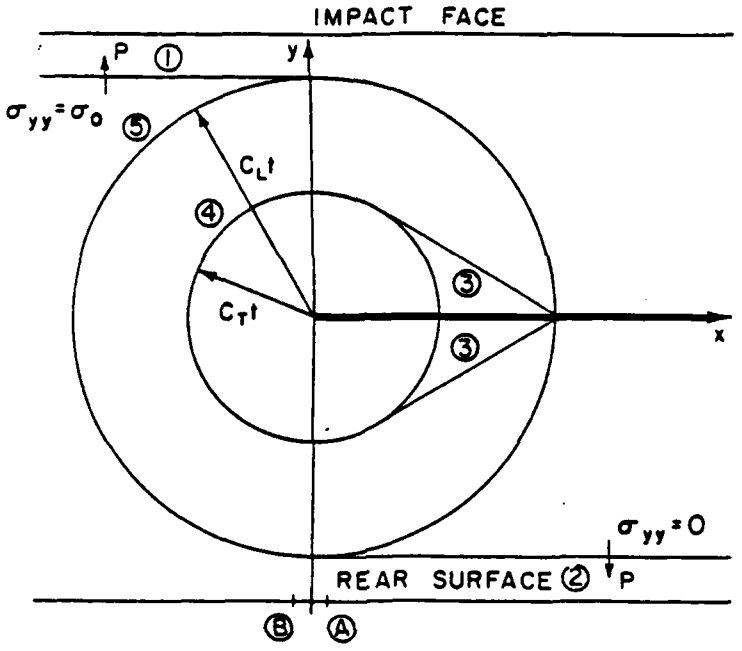

Figure 3. Pattern of wavefronts for diffraction of a plane wave by a semi-infinite crack.

APPLYING MOLECULAR DYNAMICS TO FRACTURE [1]

W.G. Hoover
Dept. of Applied Science
University of California at Davis-Livermore
B. Moran
Lawrence Livermore National Laboratory

1. MOTIVATION

The stress and strain fields of continuum fracture mechanics include unrealistic divergences at crack tips. These divergences can be avoided by using a detailed atomistic description. Such a description automatically characterizes the crack-propagation process. The main disadvantage of the more-detailed atomistic approach is the increased computer time requirement. As computational capability has improved, increasingly sophisticated atomistic simulations have been carried out. The early models, in which only a few degrees of freedom were treated explicitly, gave way to more realistic treatments [2]. With current computing capabilities there is no difficulty in treating three-dimensional crystal lattices with complicated interparticle forces.

In real metals the presence of lattice defects, including the crack tip itself, and the dependence of the forces on these defects preclude quantitative agreement with experiment, so that the computer simulations can be expected to provide understanding of experimental trends rather than replication of experimental results.

The experiments described by Kalthoff [3], using shadow patterns to measure the strength of strain fields near moving crack tips, contained interesting time dependent fluctuations. We have made an attempt to understand the structure of the rapidly moving cracks and to simulate the shadow patterns numerically. The particle trajectories are generated using molecular dynamics, and then shadow patterns are developed and compared with experimental results. This work will be described at length in a forthcoming thesis [4]. Here we only outline the methods used, results obtained, and the problems remaining.

2. TECHNIQUE

"Molecular Dynamics" means the solution of the microscopic atomistic equations of motion. Newtonian "equilibrium" molecular dynamics has been carried out ever since Fermi, Pasta, and Ulam used the Los Alamos Maniac computer to study the approach to equilibrium during World War II. The "nonequilibrium" molecular dynamics technique, in which constraints stabilize temperature, pressure, and other macroscopic variables rather than energy, has developed only during the last few years [5].

To carry out a dynamical calculation it is necessary to specify initial conditions, interparticle forces, equations of motion, and boundary conditions. All of the calculations described here use the "Piecewise-linear" forces illustrated in Figure 1. These forces are certainly not realistic. They do, however, capture the important features of real interactions, a repulsion, which prevents atoms from coalescing, and an attraction which stabilizes the liquid and solid phases of matter.

The fundamental simplification inherent in the atomistic approach is this: The entire constitutive behavior - sound speeds, yield strength, fracture velocity, and the rest - all follow from the interparticle forces. The macroscopic constitutive quantities need not be specified independently. The fly in the ointment is that these constitutive properties must all be measured, just as for real materials.

In our calculations we have used both displacement boundaries and boundaries upon which specified stresses are applied. A typical fracture specimen is illustrated in Figure 2. The 7680 nodes, many fewer than the 50,000 or so that can be treated with modern computers [6], all interact with the force-law of Figure 1. The crystal has been loaded by initially displacing the two loadpoints and relaxing the structure by solving the equations of motion with frictional damping, constraining the first few bonds to avoid fracture. After relaxation, the constraints are removed, and the crack proceeds to grow. High speed graphics is essential for displaying the fracture data in useful forms.

Shadow patterns can be produced by first using the plane stress equations to calculate hypothetical displacements perpendicular to the plane of the fracturing (two-dimensional) crystals. Then, by sampling over a large number of incident light beams and computing the image of these on a screen, the shadow pattern formed by reflection or transmission can be generated. For speed and clarity, the calculations we have carried out treat two-dimensional crystals. There is no difficulty in carrying out similar calculations in three dimensions.

3. RESULTS

It has long been known that stress waves invalidate static analyses of crack stability. A simple illustration of this wave effect appears in Figure 3. An elastic strip, with the horizontal boundaries displaced to produce a tensile stress, has an arrested stress intensity some fifteen percent below the static initiation value. This difference, similar to that found experimentally, was established by comparing the arrest strain to the initiation strain in a gradually tapered strip specimen. In the computer simulations there is a strong tendency for cracks to propagate unevenly, veering off the strip centerline. We overcome this tendency in either of two ways, by adding a small amount of viscous damping to the equations of motion or by using a slight compressive stress in the direction of propagation, as in the experiments described by Rosakis [7].

While propagating, the crack in Figure 3 moves at about one half of the transverse sound velocity. The small amount of damping changes the crack speed by less than one percent.

A second illustration of the importance of stress waves is shown in Figure 4. Two different specimens were loaded as in Figure 2, and the progress of brittle cracks was followed in time. The scaled data correspond closely despite the factor-of-two difference in sample size, indicating that the results obtained are close to the large-system macroscopic limit. The horizontal line indicates the position at which the crack would stop according to static analysis. The actual propagation slows, before reaching that position, but then accelerates beyond it when the tensile wave reflection from the free boundary reaches the crack tip.

Figure 5 shows a typical static shadow pattern. The diameter of the spot does correspond to the known stress intensity factor, but the numerical uncertainties are of order five to ten percent in the static case. Attempts to carry out the same analysis for dynamically moving cracks lead to much larger errors, of order a factor-of-two. The dynamic pattern shown in the Figure indicates a sound wave emanating from the crack tip.

4. DIFFICULTIES

Correlating macroscopic fracture results with microscopic calculations is difficult. On the macroscale a shadow spot must be analyzed to infer the stress state near the crack tip. The analysis is straightforward only for an elastic material. In the plastic case the link between the spot size and stress depends upon the unknown geometry-dependent [3] details of the constitutive relation for plastic flow.

On the microscopic level there are three kinds of difficulties. First, as Knauss has shown [8], very large strips are required if the region large enough to produce a spot is to be free of boundary influences. Second, thermal motion tends to increase the fluctuations in stress and strain, making a straightforward simulation impossible. Finally, there is not yet a model for plastic flow, valid on a microscopic level, which would preclude detailed description of individual dislocations [9].

It is true that by embedding an atomistic crack tip in a surrounding finite-element continuum the properties of a dynamic large-scale crystal could be simulated. This is a relatively large-scale task in two dimensions. Such a calculation is desirable, because it represents the only way to obtain fundamentally correct results. Calculations in which crack velocity is specified are useful for interpolation but have little predictive value.

REFERENCES

1. This work was supported by the Electric Power Research Institute, Contract RP-1326-2, at the University of California's Department of Applied Science, and performed under the auspices of the Department of Energy at the Lawrence Livermore National Laboratory, under contract W-7405-Eng-48.

2. Gehlen, P.C., and Kanninen, M.F., "An Atomic Model for Cleavage Crack Propagation in Alpha Iron," in Inelastic Behavior of Solids, M.F. Kanninen, W.F. Alder, A.R. Rosenfield, and R.I. Jaffee (eds.), McGraw-Hill (1972).
Weiner, J.R., and Pear, M., "Crack and Dislocation Propagation in an Idealized Crystal Model," J. Appl. Phys., Vol. 46, 2398 (1975).
Ashurst, W.T., and Hoover, W.G., "Microscopic Fracture Studies in the Two-Dimensional Triangular Lattice," Phys. Rev. B, Vol. 14, 1465 (1976).

3. Kalthoff, J.F., "On Some Current Problems in Experimental Fracture Dynamics," Proceedings, Workshop on Dynamic Fracture, California Institute of Technology (1983).

4. Moran, B., "Crack Initiation and Propagation in the Two-Dimensional Triangular Lattice," Ph.D. Dissertation, University of California at Davis (1983).

5. Hoover, W.G., "Nonequilibrium Molecular Dynamics," Annual Review of Physical Chemistry, 34 (1983).

6. Kinney, J.H., and Guinan, M.W., "Computer Simulation of Surface Effects on Defect Production in Tungsten," Phil. Mag. A, Vol. 46, 789 (1982).

7. Rosakis, A.J., "Dynamic Crack Growth Criteria in Structural Metals," Proceedings, Workshop on Dynamic Fracture California Institute of Technology (1983).

8. Knauss, W.G., "Stress in an Infinite Strip Containing a Semi-Infinite Crack," J. Appl. Mech., Trans. ASME, Vol. 33, 356 (1966).

9. Ladd, A.J.C., and Hoover, W.G., "Energy and Entropy of Interacting Dislocations," Phys. Rev. B, Vol. 26, 5469 (1982).

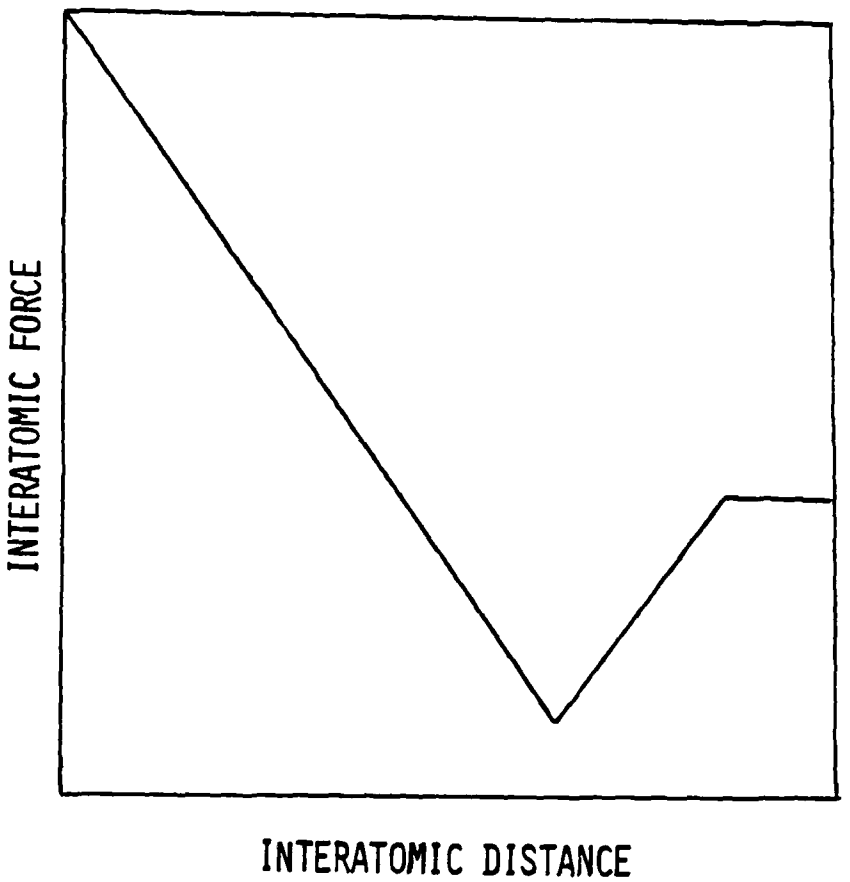

Figure 1. The piecewise-linear force law used in molecular dynamics simulations of fracture.

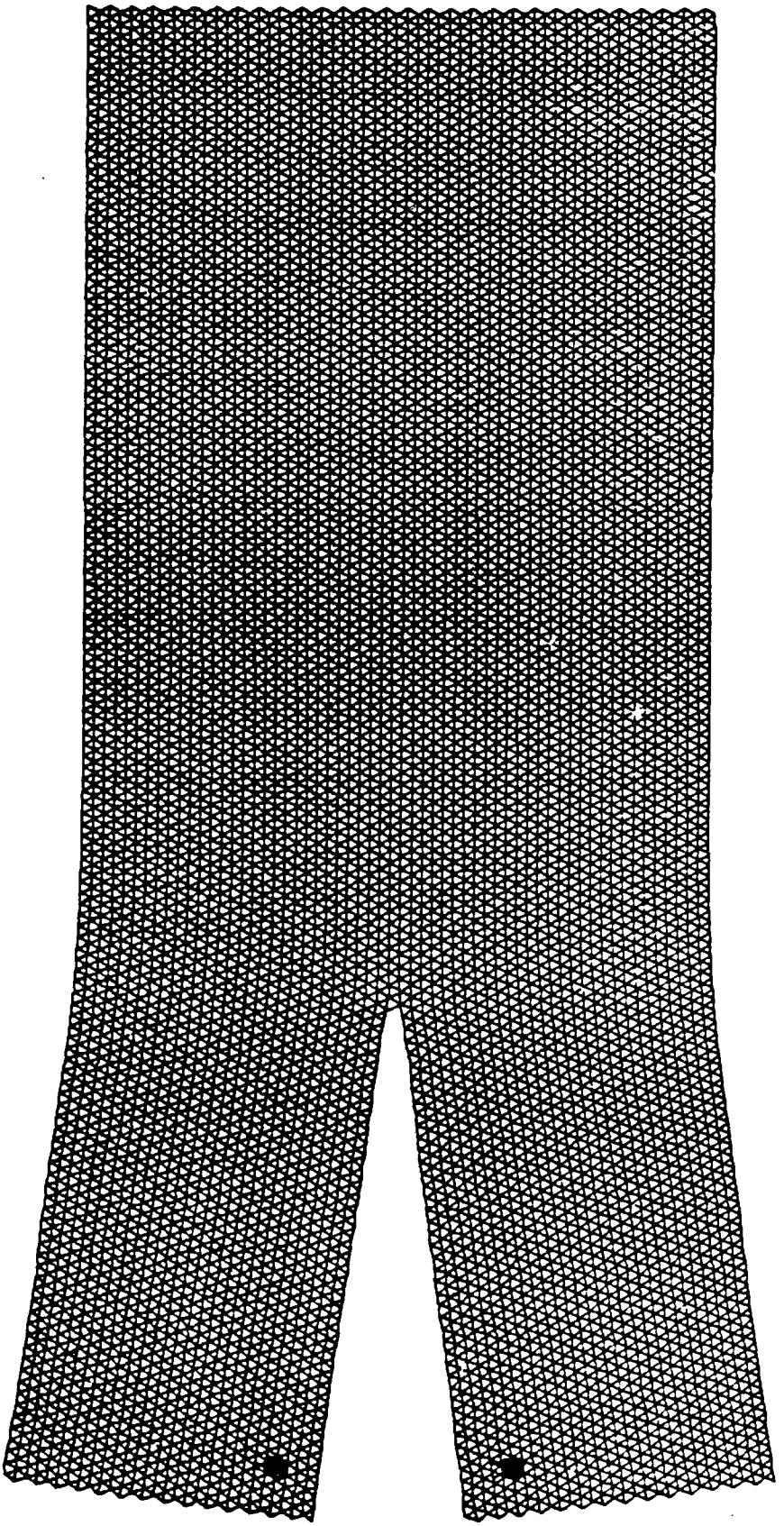

Figure 2. A 7680-node specimen loaded, with displacement boundaries, at two points.

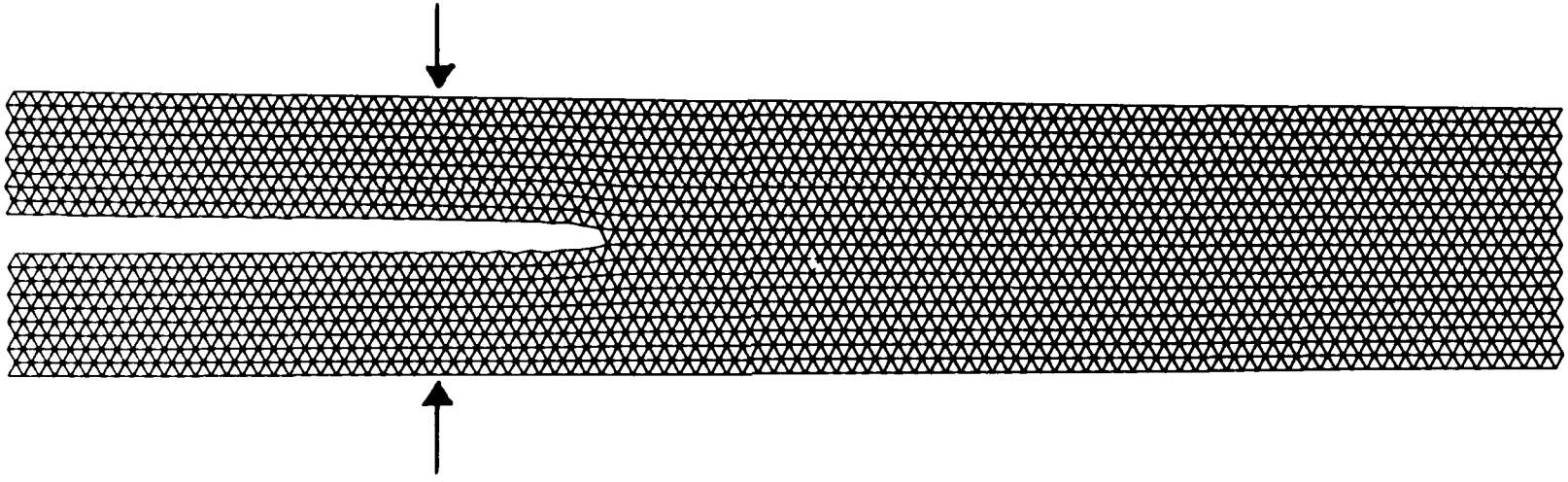

Figure 3. "Tapered" specimen with arrested crack. The tapered slope of the upper boundary is almost too small to see, 1.6%. The arrows indicate the location of the crack tip corresponding to the critical stress intensity.

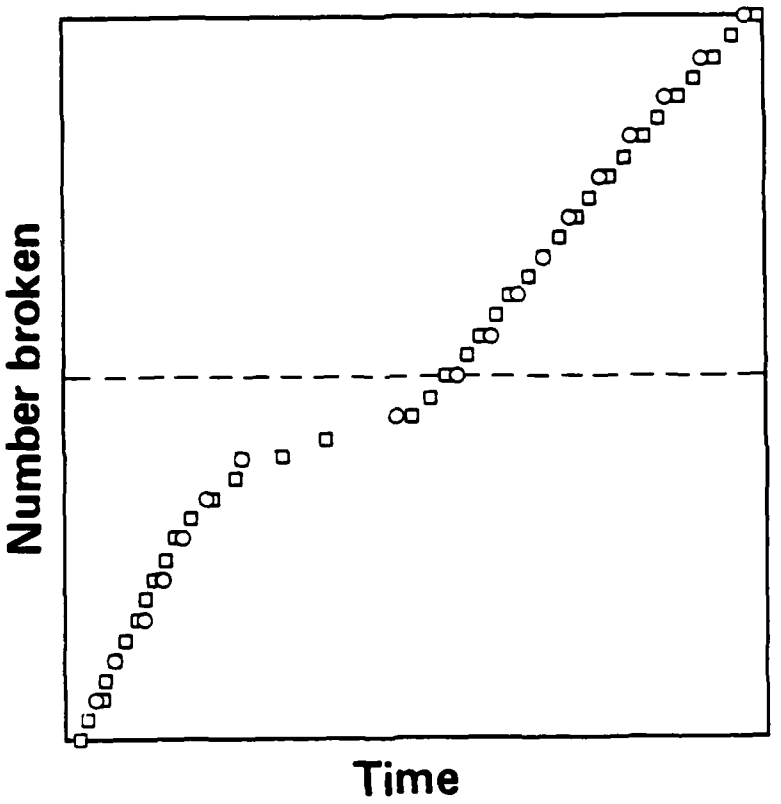

Figure 4. Crack length versus time for two specimens differing in scale by a factor of two. The specimens contained 1920 and 7680 nodes, respectively. The shape is that of Figure 2. The slowdown of the crack, followed by acceleration, corresponds well with the calculated reflection of stress waves from the top and bottom of the specimens.

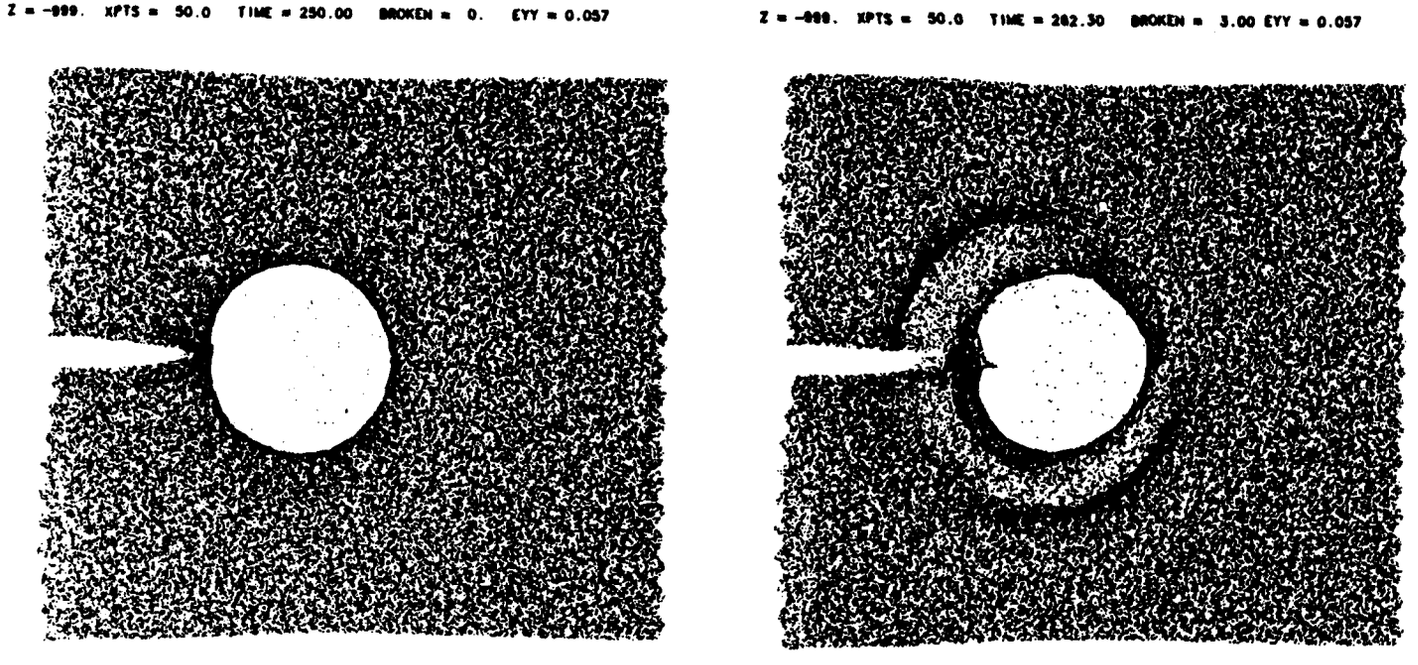

Figure 5. Shadow patterns generated for static (left) and dynamic (right) cracks. The pattern size on the left corresponds to the known static stress intensity factor. The dim circle seen at the right is a sound wave emanating from the crack tip. A recognizable dynamic shadow can be seen here.

SHORT PULSE FRACTURE MECHANICS

D.A. Shockey*, J.F. Kalthoff**, H. Homma***, and D.C. Erlich*

ABSTRACT

A research effort was begun eight years ago at SRI International to analyze the response of a crack struck by a short-lived tensile pulse and to modify static fracture mechanics concepts to allow predictions of dynamic crack instability. The results of this work, which have been presented in a series of papers over the past six years, comprise a unified extension of classical fracture mechanics and are summarized here.

We first review considerations of the stress intensity history experienced by a dynamically loaded crack tip and deduce the instability criterion. Then we describe the experiments that were performed to test the "minimum time" criterion, present the results, and compare them with predictions of the criterion.

The agreement between predictions and experimental results suggests that certain key aspects of crack instability under short pulse loads are understood and that this understanding can be applied to solve dynamic fracture problems. The current research effort at SRI is aimed at developing equipment and procedures for valid dynamic fracture testing, measuring K_{Id} for selected materials, and establishing minimum times for crack instability.

1. INTRODUCTION

The situation to be analyzed is shown schematically in Figure 1. A crack of length 2a in a material is impinged upon by a stress pulse whose amplitude σ_0 endures a period of time T_o. Such a situation could arise, for example, when a flawed structure is struck by a projectile, is

* SRI International, Menlo Park, CA 94025.

** Fraunhofer-Institut für Werkstoffmechanik, 78 Freiburg, West Germany.

*** Toyohashi University of Technology, Tempaki-cho, Toyohashi 440 Japan.

irradiated by a pulsed laser, or is in contact with a detonating explosive.

Predicting crack instability in a short load pulse situation is more involved than when the load is applied quasi-statically. Only stress level and crack length are important for the quasi-static case, but in the short pulse case pulse duration also influences instability behavior and must be accounted for in the instability criterion.

In Section 2 we review briefly the instability criterion of classical static fracture mechanics, discuss the time variation of crack tip stress intensity for a rapidly applied load, and deduce an instability criterion for a short load pulse. In Section 3 we describe and present the results of experiments in epoxy, steel, and aluminum designed to discriminate among the various proposed criteria for dynamic crack instability. Section 4 summarizes our current state of understanding of short pulse fracture mechanics and discusses the continuing research effort at SRI.

2. BACKGROUND

According to classical static fracture mechanics (Paris and Sih, 1964, for example) the stress σ necessary to cause crack instability varies inversely as the square root of the crack length a.[1] The usual instability criterion compares the crack tip stress intensity K with the fracture toughness K_c; that is, instability occurs when

$$K = f(\sigma, a^{\frac{1}{2}}) \geq K_c .$$

The fracture toughness K_c is a general measure of the resistance of a material to unstable crack growth. Under plane strain conditions K_c ($= K_{Ic}$) is geometry independent but may vary with strain rate and temperature.

When the load is applied very rapidly, the material may exhibit a different fracture resistance, and if the load duration is short and comparable to the time required for a stress wave to run the length of the crack, the crack tip stress intensity K_I^{dyn} may vary with time. Let us assume for

1. For simplicity of discussion we consider here only Mode I (opening, tensile mode) loading of a sharp crack in a perfectly elastic material.

simplicity that a constant dynamic fracture toughness value K_{Id} exists that characterizes the material for the strain rate considered (we will relax this assumption later), and let us next consider the time-dependence of the stress intensity and its effect on the instability condition.

When a stress wave strikes a crack, a complicated pattern of diffracted waves is generated and produces initial oscillations in the crack tip stress field. The time-dependent crack tip stress intensities produced by impinging step function loads have been computed by Sih (1968), Ravera and Sih (1969), Embley and Sih (1971), Sih, et al. (1972), Achenbach (1970, 1972) and others. These results, depicted in Figure 2, show that the dynamic stress intensity K^{dyn} rises sharply with time ($K^{dyn} \sim t^{\frac{1}{2}}$), overshoots the equivalent static stress intensity ($K^{stat} \sim a$) by a considerable amount, and then reaches a constant static value after several damped oscillations. At early times K^{dyn} is independent of crack length, depending only on time and on the amplitude of the stress pulse. This is because the effective crack length that contributes to the crack tip stress intensity increases linearly with time as the stress wave propagates along its length and loads it. If a single-valued parameter characterizing this complicated stress field existed, it could be compared to the material property to obtain an instability criterion.

Sih (1968, 1973) and Achenbach (1972) speculated that the maximum value of K^{dyn} determined crack instability. These authors thus suggested that dynamically loaded cracks may become unstable at lower stress levels than cracks under equivalent static loads, because K^{dyn} briefly exceeds K^{stat}.

However, the results of an experiment reported by Shockey and Curran (1973) could not be explained by the K^{dyn}_{max} criterion. In this experiment a plate specimen of polycarbonate containing a distribution of internal penny-shaped cracks was impacted by a flying plate to produce a tensile pulse of known amplitude and duration. Cracks above a certain size propagated, whereas smaller cracks remained stable. The dynamic fracture toughness was determined from the critical crack size, the amplitude of the tensile pulse, and the static fracture mechanics formula. However, when these results were used to calculate the crack instability behavior observed in a

similar experiment with a lower amplitude pulse, a discrepancy was evident, demonstrating the inadequacy of both the static fracture mechanics criterion and the K_{max}^{dyn} criterion to describe crack instability under short pulse loads.

Kalthoff and Shockey (1977) explained these results by analyzing the early time stress intensity histories experienced by cracks of different lengths under stress pulses of different durations and proposed that for instability to occur K^{dyn} must exceed K_{Id} for a certain minimum time. These authors postulated that static fracture mechanics can predict instability behavior when the ratio of pulse duration T_o to crack length a exceeds a certain value that depends on crack geometry. For penny-shaped cracks, the static criterion holds when $c_1 T_o/a > 20$, where c_1 is the longitudinal wave speed. Short cracks that can be traversed several times by a wave during the life of the stress pulse experience essentially constant stress intensity histories very similar to those produced by static loads, and hence their instability response is governed by the classical static fracture mechanics formulae.

Larger cracks experience more of the transient aspects of the stress intensity history, so the dynamic instability curve in stress-crack length space lies above the static curve, $\sigma \sim \sqrt{a}$. For cracks longer than a certain length, a constant critical stress is predicted, since all cracks longer than a certain length (postulated to be $c_1 T_o/a < 1.6$ for a penny-shaped crack) experience identical stress intensity histories. Thus for short pulse loads, crack instability may be a function of applied load, crack length, and pulse duration, and not simply applied load and crack length as in the static case.

These instability deductions are depicted graphically in Figure 3 as a surface in stress amplitude/stress duration/crack length space. Unstable crack growth is expected for conditions of σ, T_o,and a that lie above the surface, whereas stable behavior is predicted for points below this surface. For short crack lengths and long stress durations, the instability surface is defined by the static criterion. However, for long crack lengths and short stress durations, time, and not crack length, is important. In this regime, the instability stress is a function only of the stress duration,

so that all cracks longer than a certain length exhibit similar behavior. To check these hypotheses, stress wave loads were applied to cracks in an epoxy, in two steels, and in an aluminum alloy, and their instability response was observed.

3. EXPERIMENTS AND RESULTS

A data base for dynamic crack instability was generated by casting arrays of appropriately sized internal penny-shaped cracks in epoxy and subjecting the cracks to rectangular, 2.04-μs-duration stress pulses (Shockey, Kalthoff and Erlich 1983). Six plate impact specimens of Epon Resin 815 epoxy[2] were cast from a single batch of epoxy in an effort to minimize specimen-to-specimen variation in mechanical properties. The specimens were 6.35 mm thick by 63.5 mm in diameter and each contained six judiciously spaced, 50-μm-thick, circular Mylar[3] disks having radii of 6.35, 3.18, 1.59, 0.79, and 0.40 (two disks) mm. A light gas gun was used to accelerate a flyer plate against the specimen plates to achieve rectangular stress pulses of 2.04-μs duration. Impact velocities ranging from 110 to 275 m/s, corresponding to peak tensile stresses[4] ranging from 14.9 to 37.3 MPa, were chosen in an attempt to make different crack sizes grow in each specimen.

Figure 4 shows the results in stress-crack radius space at constant stress duration, T_o = 2.04 μs. The solid points, indicating crack instability, and the open circles, denoting no crack growth, define the regimes of crack instability and stability, respectively. The boundary between the two regimes represents the threshold conditions for crack instability and defines the curve required to evaluate proposed instability criteria. Some scatter exists in the data, so that comparisons of proposed criteria must be made with a band rather than a sharp curve.[5] Nevertheless, the band provides a reliable indication of the shape and average location of the instability curve and thus allows discriminative evaluations of the proposed criteria.

2. Epon Resin 815, Trademark, Shell Corporation, Houston, Texas.
3. Trademark, E.I. DuPont de Nemours Co., Wilmington, Delaware 19898.
4. A one-dimensional elastic wave propagation code, SWAP, computed the durations and amplitudes of the peak tensile stresses experienced by the individual specimens.
5. Scatter is attributable in part to the relatively large inherent variability in mechanical properties, as has been found in static fracture toughness data, $K_{Ic} = 1.1 \pm 0.46$ MPa $m^{\frac{1}{2}}$.

Figure 5 compares the experimentally observed instability curve for epoxy with curves predicted by several proposed criteria. All criteria predict well the observed behavior at short crack lengths ($a < 0.3$ mm, $c_1T_o/a > 20$). In this region, the stress wave has time to run the length of the crack several times before the pulse vanishes, so that the crack tip stress field approaches equilibrium and static conditions apply. For longer crack lengths, where crack tip stress conditions are further from equilibrium, the constant critical stress observed for cracks larger than about 2 mm disagrees with the continuous decrease in critical stress with increasing crack length predicted by static LEFM. The maximum dynamic stress intensity criterion predicts constant behavior for cracks greater than 2.5 mm,[6] but the magnitude is significantly less than observed. Moreover, the magnitude of the critical stress predicted for shorter cracks is also less than observed. The data are best described by the minimum time criterion, which accurately predicts the shape and location of the instability curve.

Further verification of the minimum time instability criterion was sought in structural materials (Homma, Shockey and Murayama 1983). Cracks in single-edge-notched strip specimens 1016 x 88.9 x 9.5 mm^3 of 4340 steel, 1018 steel, and 6061-T651 aluminum were subjected to 40-μs-long haversine-shaped tensile pulses of various amplitudes. Pulse loads were applied by pneumatically accelerating a cylindrical projectile along the specimen and against a massive block attached to one end of the specimen. This caused a tensile wave, whose profile was measured by a strain gage, to run back to the crack location. The amplitudes of successive pulses were increased in small steps until incremental crack growth could be detected by replicating the crack tip on the side of the specimen.

The results are shown in Figure 6. For all three materials the stress for crack instability decreased strongly with crack length at short crack lengths, but tended to reach a constant value for crack lengths greater than about 60% of the specimen width. These trends in the variation of critical stress with crack length observed in structural materials are similar to those observed in

6. For $c_1T_o/a > 2.2$, the stress for instability stays constant although the crack length increases, because the stress pulse vanishes before the loading wave can run the length of the crack.

epoxy.

The instability curve resulting from the static criterion (dashed line) is shown in Figure 6 for comparison and predicts a more rapid decrease with crack length in the amplitudes of the critical pulses. Furthermore, the maximum value of the dynamic stress intensity [as calculated by a dynamic finite element method (Homma, Shockey, and Murayama, 1983)] varied with crack length for the two steels, showing again that $K_{I_{max}}^{dyn}$ is not a useful dynamic crack instability criterion.

However, the structural alloy results are in accord with the minimum time instability criterion. The instability curves at constant stress duration fall rapidly with crack length at short crack lengths, and then appear to approach a constant stress value at longer crack lengths (compare Figures 3 and 5). Thus, the observed shape of the instability curve agrees with the predicted shape.

The effect of pulse duration on crack instability stress was investigated for 4340 steel by performing experiments using a shorter and a longer projectile. The results for 18-μs and 80-μs long pulses are shown in Figure 7. The instability curve for the 80-μs pulse decreased with increasing crack length in a manner similar to the curve for the 40-μs pulse. The constant critical stress was reached at longer crack lengths and the amplitude of the stress was less than under 40-μs pulses. The critical stress for the 18-μs pulse was significantly higher than for the 40-μs pulse and independent of crack length in the range investigated, $0.2 < a/w < 0.8$.

When these curves are plotted in 3-dimensional critical stress-crack length-pulse duration space along with the 40-μs curve for 4340 steel shown in Figure 6(a), an instability surface results, Figure 8. The similarity in shape of this experimentally determined surface and that predicted by the minimum time criterion (Figure 3) further confirms the validity of this criterion.

4. DISCUSSION AND CONCLUSIONS

The experimental results obtained in epoxy, aluminum, and two steels agree with predictions of the minimum time crack instability criterion, suggesting that certain aspects of the instability response of cracks under short pulse loads are understood. We conclude that the crack instability criterion of classical static fracture mechanics can be modified to apply to high-rate, short-duration load situations. When the load is applied as a tensile pulse whose duration is comparable to or less than the time required for a wave to run the length of the crack, unstable crack growth can occur only if the crack tip stress intensity exceeds the dynamic fracture toughness for a certain minimum time.

This understanding allows simple equipment and procedures to be developed for valid determination of K_{Id}. Optimum geometries for specimens and impactors can be specified that produce stress pulses of suitable amplitude and duration for rectangular stress intensity histories and hence well-defined, readily interpretable crack tip stress conditions. Thus measured changes in instability parameters (σ,a,T_o) can be attributed to material resistance changes, and hence variations of K_{Id} with loading rate, pulse duration, and the like can be investigated and established. This means that the assumption of constant K_{Id} made in the introduction of this paper can now be relaxed and tested.

This understanding also allows fracture response in the transient stress intensity history region to be evaluated. The minimum time for crack instability, thought to arise from the time required for the plastic and process zones at the crack tip to mature, can be investigated to establish its dependence, if any, on loading parameters. Intuition suggests that minimum time may be a decreasing function of $K_I^{dyn} - K_{Id}$.

The current research effort in short pulse fracture mechanics at SRI International addresses the above two topics.

ACKNOWLEDGEMENT

This research was sponsored by the Air Force Office of Scientific Research (AFSC) under Contract No. F459620-77-C-0059. Technical Monitor was Dr. A.H. Rosenstein.

REFERENCES

1. Achenbach, J.D., "Brittle and Ductile Extension of a Finite Crack by a Horizontally Polarized Shear Wave," Int. J. Eng. Sci., 8 (1970) 947-966.

2. Achenbach, J.D., "Dynamic Effects in Brittle Fracture," in Mechanics Today, S. Nemat-Nasser (ed.), Vol. 1, Pergamon (1972).

3. Embley, G.T., and Sih, G.C., Proc. 12th Midwestern Mechanics Conference, 6 (1971) 473. See G.C. Sih (1973). Handbook of Stress-Intensity Factors, Institute of Fracture and Solid Mechanics, Lehigh University, Bethlehem, PA. p. 8.5.2-1.

4. Homma, H., Shockey, D.A., and Murayama, Y., "Response of Cracks in Structural Materials to Short Pulse Loads," J. Mech. Phys. Solids, in press (1983).

5. Kalthoff, J.F. and Shockey, D.A., "Instability of Cracks under Impulse Loads," J. Appl. Phys., 48 (3) (1977) 984-993.

6. Paris, P.C., and Sih, G.C., "Stress Analysis of Cracks," in Fracture Toughness Testing and Its Applications, ASTM Special Technical Publication No. 381 (1964).

7. Ravera, R.J., and Sih, G.C., "Transient Analysis of Stress Waves Around Cracks under Antiplane Strain," J. Acous. Soc. Amer., 47 (1969) 875-880.

8. Shockey, D.A., and Curran, D.R., A Method for Measuring K_{Ic} at Very High Strain Rates, ASTM Special Technical Publication No. 536 (1973).

9. Shockey, D.A., Kalthoff, J.F., and Erlich D.C., "Evaluation of Dynamic Crack Instability Criteria," Int. J. Frac. Mech., in press (1983).

10. Sih, G.C., "Some Elastodynamic Problems of Cracks," Int. J. Frac. Mech., 4 (1968) 51-68.

11. Sih, G.C., Handbook of Stress-Intensity Factors, Institute of Fracture and Solid Mechanics, Lehigh University, Bethlehem, PA (1973).

12. Sih, G.C., Embley, G.T., and Ravera, R.J., "Impact Response of a Plane Crack in Extension," Int. J. Solids Structures, 8 (1972) 977-993.

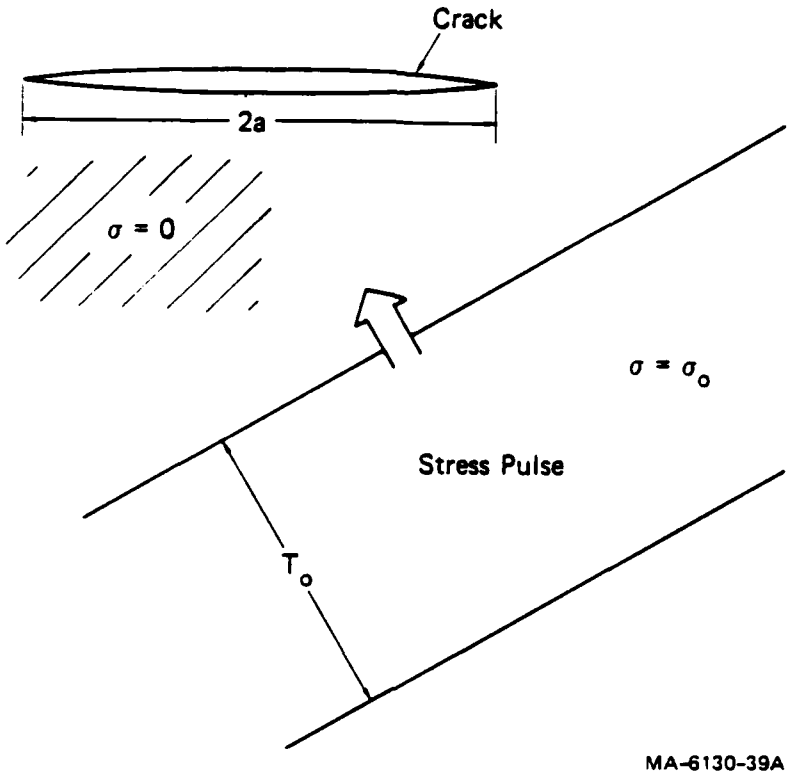

Figure 1. Stress pulse about to impinge on a crack.

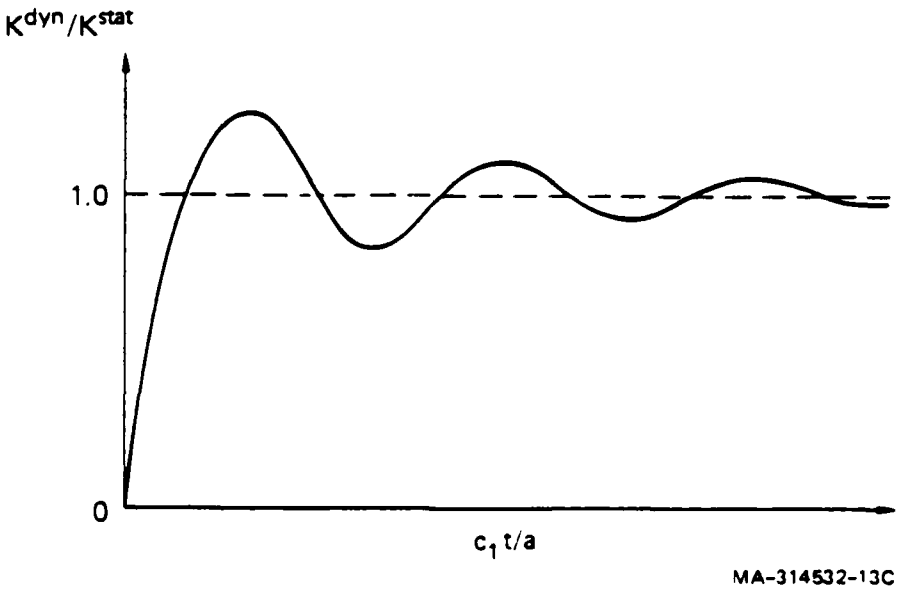

Figure 2. Variation of K^{dyn}/K^{stat} with time for a crack loaded by a step wave (schematic).

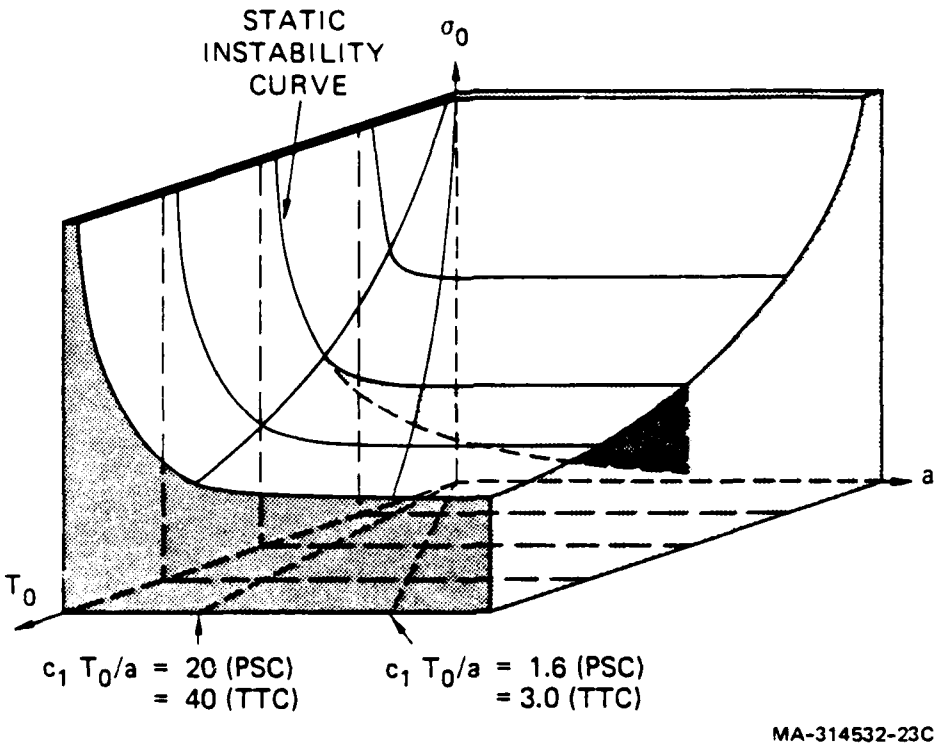

Figure 3. Crack instability surface for penny-shaped cracks (PSC) and through thickness cracks (TTC) according to dynamic minimum time-stress intensity criterion.

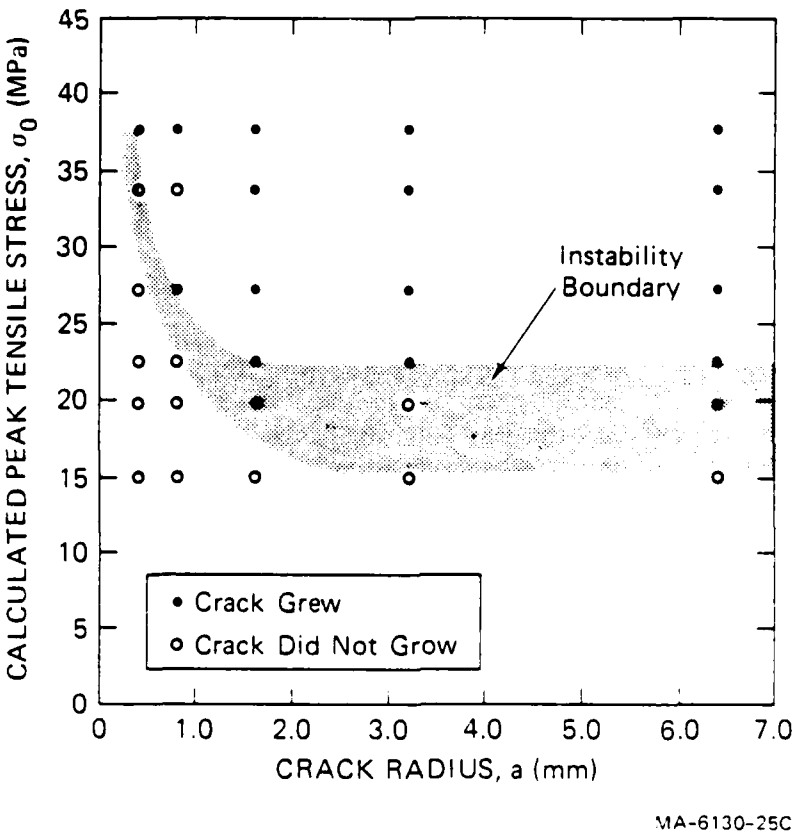

Figure 4. Instability response of penny-shaped cracks in epoxy under 2.04-μs duration stress pulses.

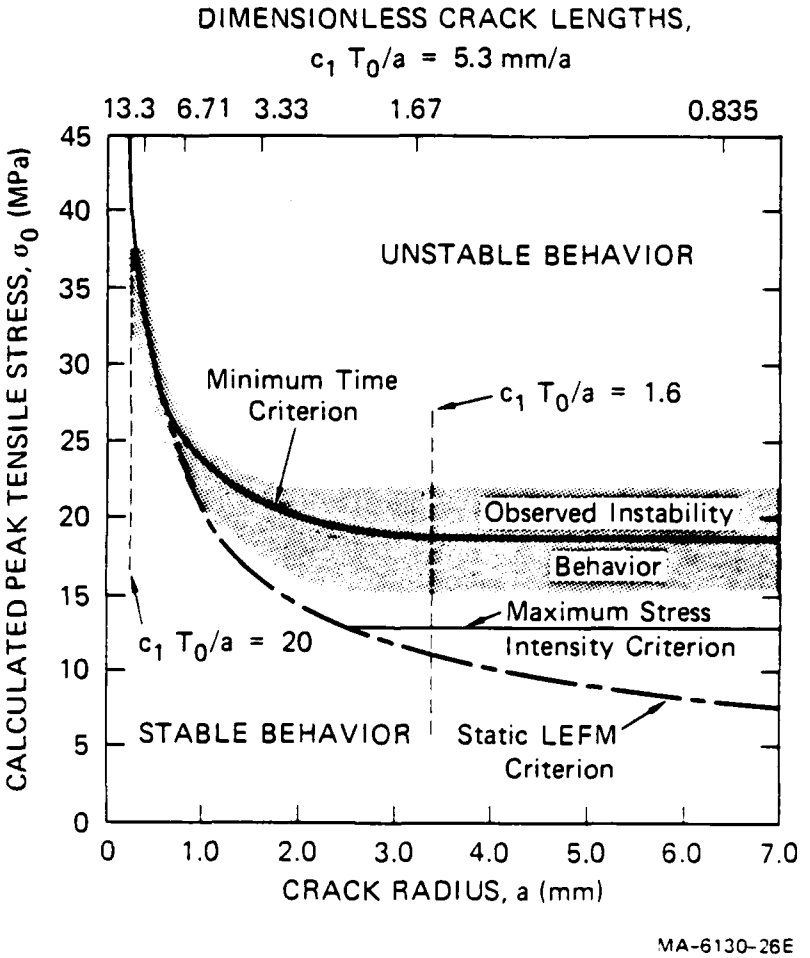

Figure 5. Comparison of experimentally determined dynamic crack instability behavior with curves predicted by proposed instability criteria.

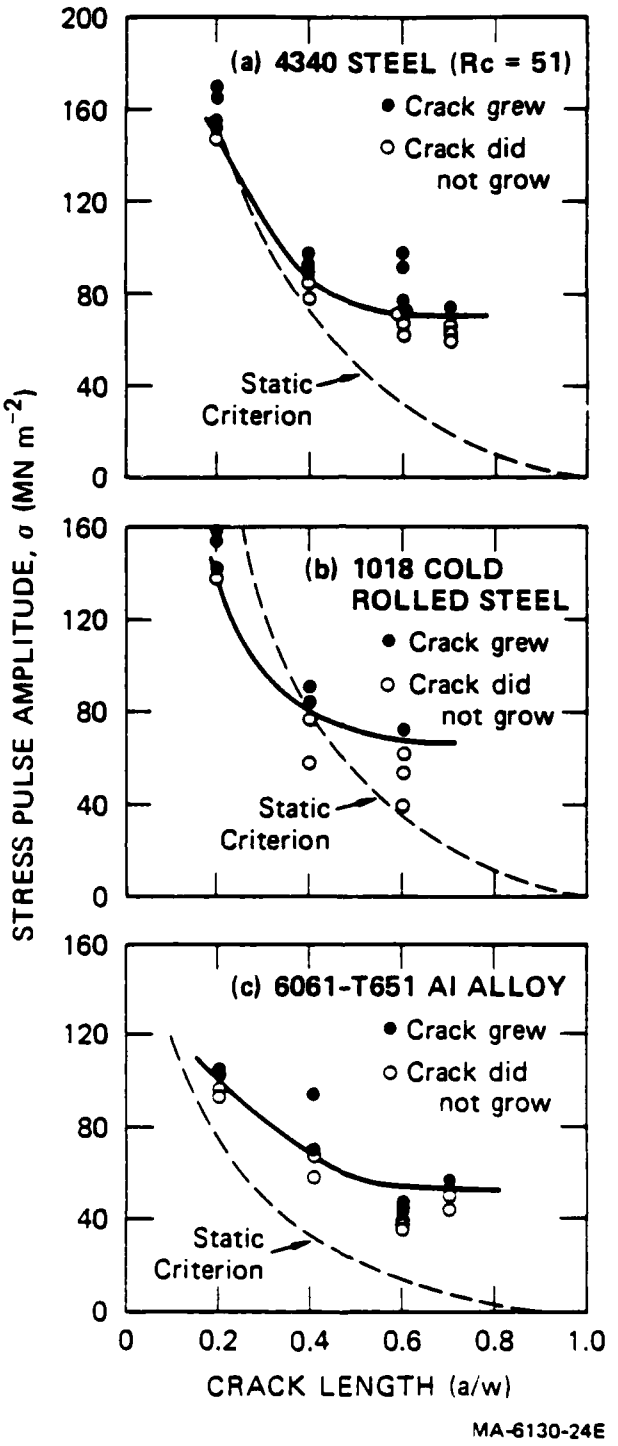

Figure 6. Observed instability behavior of cracks in three structural materials loaded by a 40-μs stress pulse.

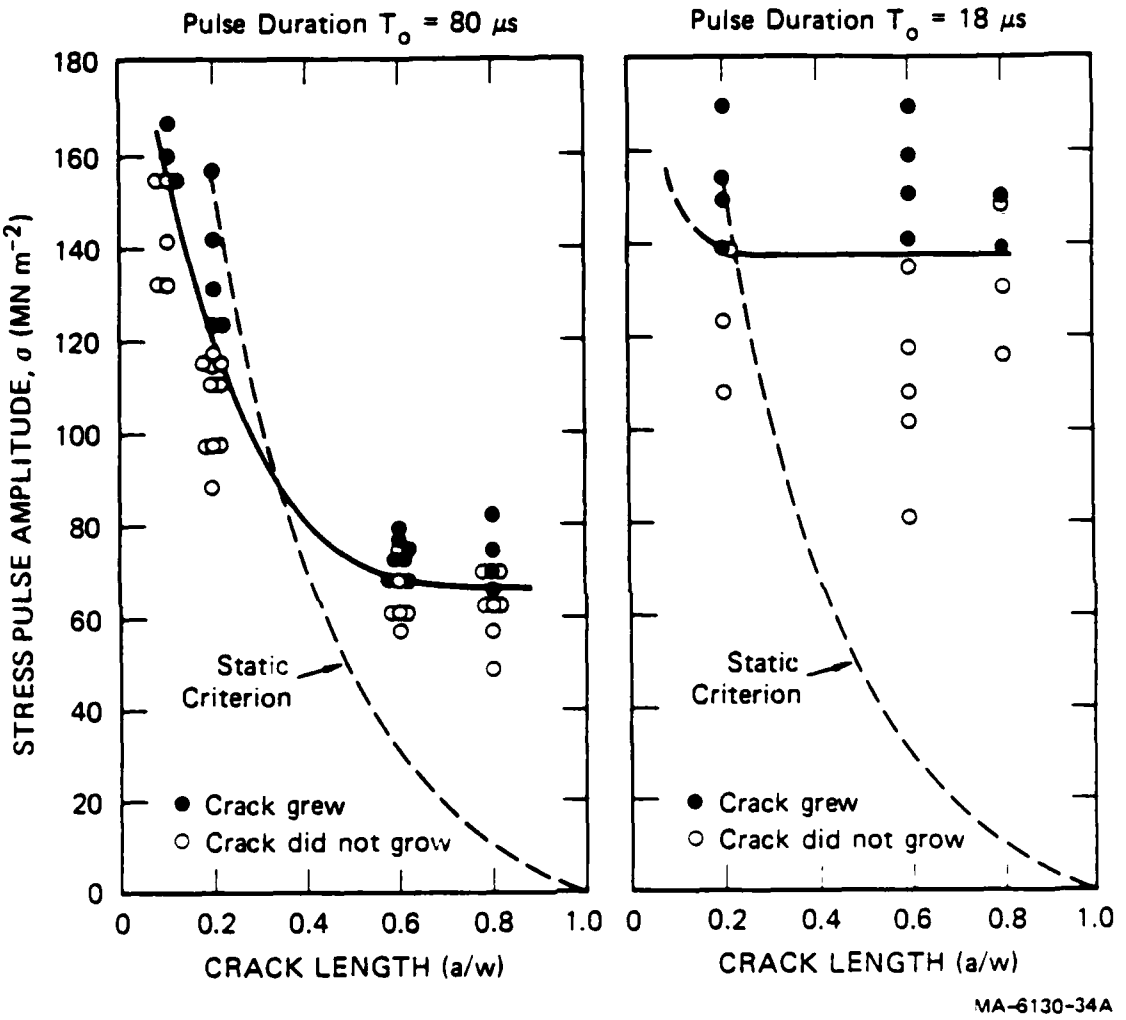

Figure 7. Effect of pulse duration on instability stress for cracks in 4340 steel.

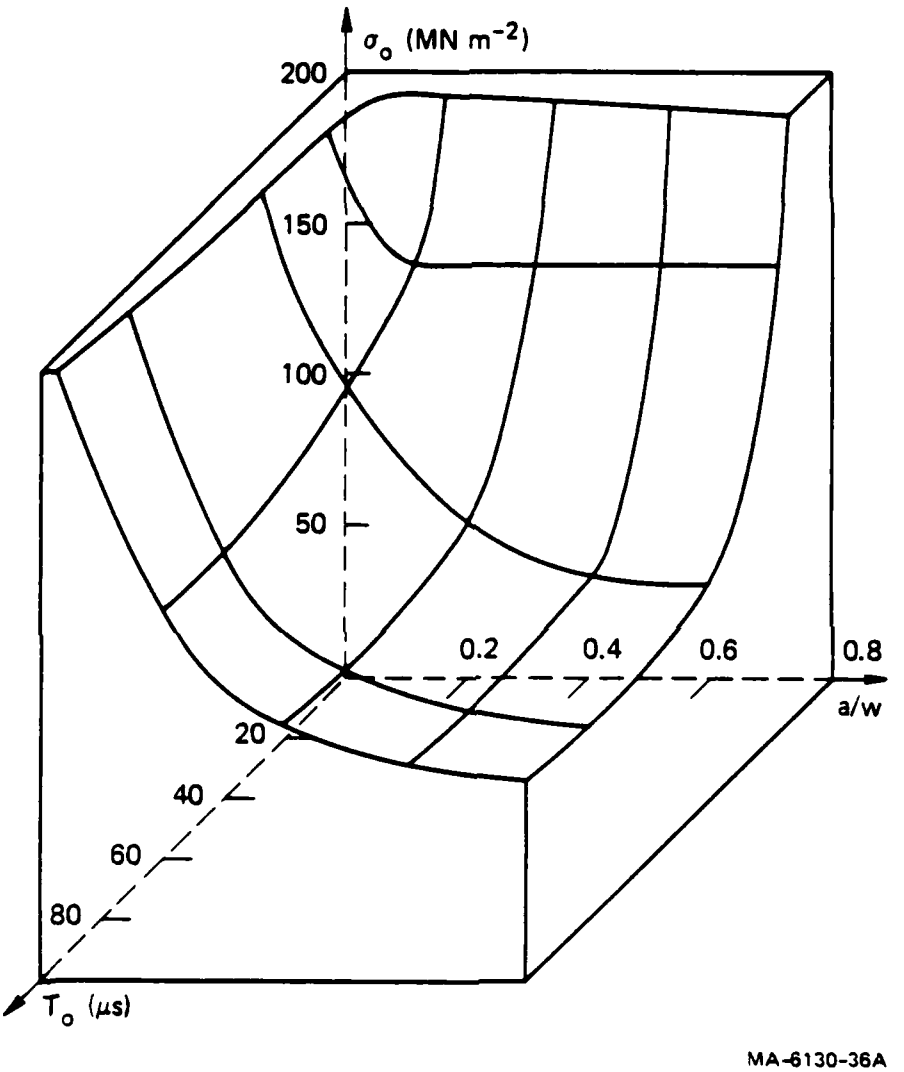

Figure 8. Instability surface for cracks in 4340 steel struck by short-lived stress pulses.

SYNOPSIS OF SESSION II: DYNAMIC CRACK GROWTH CRITERIA

F. Erdogan
Lehigh University

In this session the main emphasis of the prepared statements as well as of the discussions was on the crack growth criteria in the presence of "Dynamic Effects". The basic thrust of the experimental work presented was on the determination of the intensity of the stress field around the propagating crack tip, interpretation of the results in terms of some kind of a "stress intensity factor" K, on making additional measurements with regard to the crack velocity $\dot{a}$ or length a, and on trying to arrive at a material characterization for the dynamic crack growth by relating measured K and $\dot{a}$. The technique used to measure the stress intensity factor was photoelasticity in W. Fourney's work and the method of caustics in A.J. Rosakis' and K. Ravi-Chandar's works.

Directly or indirectly, the most important question addressed was whether or not there exists a material unique relationship that connects K_D and $\dot{a}$ which represents the instantaneous dynamic crack propagation behavior of the material. (This relation would then be a "material property".) A unique K_D vs. $\dot{a}$ relationship characterizing the dynamic crack growth behavior of the material is, of course, a very attractive notion. With the material thus characterized, dynamic crack growth problems can then be solved by using the finite element method, possibly including the problem of crack branching. The latter might correspond to some limiting value of K_D - the termination of the K_D vs. $\dot{a}$ relation. At best the evidence indicated (and the consensus appeared to be) that the measured K vs. $\dot{a}$ depends on the specimen geometry and hence the existence of a unique K_D vs. $\dot{a}$ as a material property does not appear to be likely. Furthermore, K. Ravi-Chandar's results showed that (at least for Homalite 100) measured K values may vary considerably while the crack velocity $\dot{a}$ remains constant.

In the work presented by A. Rosakis there were discussions regarding the details of the experimental techniques and related dynamic analysis, the effect of the machine stiffness on the

measured results, which might be the real cause of the oscillations in measured K values observed in some experiments; the effect of the initial arm length in the DCB specimens on the measured results (as they appear to act as a wave guide in transferring energy to the crack tip); the effect of the reflected waves on the crack velocity (the stress waves reflecting from "fixed" surfaces tend to decrease and those reflecting from the "free" surfaces tend to increase the intensity of the stress field around the crack tip); and the concept of critical (plastic) strain at a characteristic distance from the crack tip as a possible criterion for dynamic crack propagation were discussed at some length. Part of L.B. Freund's analytical results showed that the basic features of the experimental observations (regarding K vs. t) made by K. Ravi-Chandar and W.G. Knauss may be theoretically predicted, when the rise time of the loading pulse is smaller than the time to initiate fracture. The converse problem was not discussed.

There was discussion concerning the crack branching phenomenon. It was pointed out that, because of the mixed mode effects on the crack path, in the case of two equal branches with small included angles, the cracks repel each other and for large angles they attract each other - implying a likelihood of an optimal angle. It was also observed that, for branched cracks with unequal lengths, at "low" velocities the K value for the short branch tends to decrease and that for the long branch tends to increase with increasing time, whereas at "high" velocities K values for both cracks tend to increase with increasing time. This observation may provide a partial explanation for the arrest of the shorter crack branches (and hence, for the unsuccessful attempt at the crack branching) at lower crack velocities. K. Ravi-Chandar's real time photography appears to provide a plausible explanation for the initiation of branching, i.e., growth of existing voids, formation of many microcracks, and growth of the most favorably oriented microcracks into macrocrack branches. The same work also provides a possible explanation of the mechanism of heckle or "riverline" formation on fracture surfaces in amorphous solids under high stress intensities. The caustics taken with the specimens inclined with respect to the lightbeam indicate the formation of secondary fracture surfaces (presumably triggered by the existing localized imperfections) which grow into heckles.

The search for the elusive "universal K_D vs. $\dot{a}$ relationship" no doubt will go on. However, some general remarks on the subject may perhaps be useful. First, it must be realized that any local criterion must be a necessary condition. In solids which are not ideally brittle (i.e., the materials in which the zone of the energy dissipation around the propagating crack front possesses a sizeable nonzero volume), the global energy balance must also be satisfied for crack growth to occur. The geometries and loading conditions in (real) structural materials undergoing dynamic fracture the size and shape of the zone of the energy dissipation around the crack front as well as the dimensions of the wake region of residual stresses. Consequently the fracture energy which must be supplied should depend on the geometry of the medium (including the current crack size), the nature of the external loads and the environmental conditions (primarily temperature) as well as on the crack velocity. It is, therefore, unrealistic to expect that the dynamic fracture resistance of such a material may be characterized by a single K_D (or some other fracture parameter) vs. $\dot{a}$ curve.

It appears that the real problem of a complete and rational characterization of the fracture dynamics process is, for the moment, very complicated. In practical applications one will still have to use the best available concepts. This may mean that for some materials a proper K_D vs. $\dot{a}$ curve (parametrized perhaps with regard to the initial stress and temperature levels) may continue to be useful at least until more definite limitations are established. In other materials one may instead use an appropriate "necessary condition" by selecting a characteristic material constant which is a measure of the intensity of the plastic deformations near the crack front, such as, for example, the crack opening stretch or (maximum) plastic strain.

DYNAMIC CRACK GROWTH IN POLYMERS

W.L. Fourney, R. Chona, and R.J. Sanford
Dept. of Mechanical Engineering
University of Maryland

1. INTRODUCTION

Over the past several years, considerable effort has been directed towards developing two-dimensional, finite-element computer codes to predict crack propagation behavior in large structures [1-3]. One of the input parameters to these computer codes is the relationship between the crack extension force (or the stress intensity factor) and the velocity of crack propagation in the material. Experimental investigations of the dynamic behavior of crack propagation and arrest in several different polymers, epoxies, and structural steels have been conducted at, among other places, the University of Washington at Seattle, Brown University, the California Institute of Technology, IFKM-Freiburg (West Germany), and the University of Maryland's Photomechanics Laboratory [4-12]. This paper summarizes briefly the highlights of the work performed at the University of Maryland over the period 1972-1982 using dynamic photoelasticity, high speed multi-flash photography, and finite element modeling to study crack propagation.

2. FINITE ELEMENT MODELING OF DYNAMIC FRACTURE

SAMCR, developed at the University of Maryland under the sponsorship of the Nuclear Regulatory Commission and Oak Ridge National Laboratory, is a dynamic, finite-element-type code for the Stress Analysis of Moving CRacks, in which a straight, moving crack is modeled by the controlled release of nodal forces perpendicular to the crack face. The nodal displacement field is updated at each time step, and a J-integral type computation carried out along a contour that moves with the crack tip. The mode I stress intensity factor is then calculated from the numerical value of the J-integral, and the crack tip velocity, $\dot{a}$, determined from an $\dot{a}$-K relationship which has to be specified. Fig. 1 shows the geometry of a Crack-Line-Wedge-Loaded

Modified-Compact-Tension (CLWL-MCT) fracture specimen, and the corresponding finite element mesh used to study this test case. Data on the $\dot{a}$-K relationship for the specimen material (Homalite 100, a brittle polymer) had been obtained previously using dynamic photoelasticity, and complete crack extension behavior records were available for comparison with the computer code predictions. The particular relationship between K and crack speed that was used is shown in Fig. 2. The resulting predictions for crack extension as a function of time are shown in Fig. 3, which also shows the results for the same problem from a finite difference code developed by Battelle Columbus Laboratories (BCL). It can be seen that both computer codes tend to overpredict the total crack extension, and this is felt to be due to energy losses and damping phenomena which are not incorporated into the linear elastic computer code [13]. Another observation that was made in this preliminary study was the dependence of the predicted crack extension behavior on the specified $\dot{a}$-K relation, an observation that has been confirmed in later work on thermal-shock steel cylinders both at the University of Maryland and at BCL [14].

3. PHOTOELASTIC DETERMINATION OF THE $\dot{a}$-K RELATIONSHIP

A Cranz-Schardin-type, multiple spark camera [15] was used to record the isochromatic fringe patterns at the tip of propagating cracks in fracture test specimens fabricated from transparent, birefringent materials such as Homalite 100 and Araldite B. The optical arrangement of a typical Cranz-Schardin camera is illustrated in Fig. 4. The spark gaps are initially charged to 15 kVdc and then, upon a trigger signal, are discharged in a time-controlled sequence. The light from each spark gap is collected with a field lens system and focused on a set of geometrically similar camera lenses. With this arrangement each image is recorded at a different location on a sheet of stationary film. The framing rate can be varied from about 30,000 fps to 800,000 fps. Since the run-arrest event in a typical fracture experiment is relatively long, the camera is normally operated at a low framing rate so that the 16 frame sequence provides an observation period of about 400-500 μs.

A typical sequence of 16 isochromatic fringe patterns which represent high-velocity crack propagation and crack division in a Single-Edge-Notched (SEN) specimen is shown in Fig. 5. The crack tip velocity is determined by taking the slope of the crack position - time curve and the instantaneous stress intensity factor extracted from the isochromatic fringe data using techniques that will be described in the next section of this paper.

Using these techniques, the dynamic behavior of propagating cracks has been characterized over the entire range from crack arrest to high-velocity crack propagation and crack division, in terms of the relationship between instantaneous crack tip velocity and stress intensity factor. Studies at the University of Maryland [2, 8-12] have been conducted with six different types of fracture test specimens, which include the Single-Edge-Notched (SEN), Compact-Tension (CT), Modified-Compact-Tension (MCT), Rectangular-Double-Cantilever-Beam (RDCB), Contoured-Double-Cantilever-Beam (CDCB), and a Ring segment. The results obtained for the $\dot{a}$-K relationship from this very extensive research program are summarized in Fig. 6. Considering that these results were (1) obtained with four different shipments of Homalite 100, (2) over a five year period, (3) involved four different investigators, and (4) with experimental errors ranging from $\pm$ 10 percent on individual values of K, the agreement between the $\dot{a}$-K relations for the different specimen geometries is felt to be quite satisfactory.

While the $\dot{a}$-K relation characterizes many aspects of dynamic crack behavior, three special topics do require further consideration. These include branching of high-velocity running cracks, super-high-velocity cracks observed during explosive loading, and crack acceleration and deceleration. The first two items will be discussed in a preliminary fashion in subsequent sections.

4. THE INFLUENCE OF NON-SINGULAR STRESSES IN FRACTURE TEST SPECIMENS

It is generally recognized that the near-field equations suggested by Irwin [16] adequately describe the state of stress in the neighborhood of a stationary crack tip, excluding a very small region around the crack tip itself. With suitable modifications for the effects of inertia, this

two-parameter representation (in terms of K and a superimposed constant stress in the crack extension direction, σ_{ox}) can be extended to crack tip stress patterns that are moving with gradual changes in speed [17]. Situations arise, however, for which a one-parameter or even a two-parameter characterization of the stress field is not adequate. This can occur due to a spreading out of the fracture process zone or a reduction in size of the singularity-dominated-zone at the crack tip. For example, when using isochromatic fringes for the evaluation of K, it is rarely possible to use measurements very close to the crack tip for a number of practical reasons. Some of these are illustrated in Fig. 7, and include an unknown degree of plane-strain constraint, light scattering from the dimple (caustic) at the crack tip, crack front curvature, fringe clarity, etc. In such cases it is desirable to define and measure additional stress field parameters. Considerable work has been done in recent years to investigate the influence of non-singular (or higher-order) terms on the stress field around but not immediately adjacent to the crack tip. The effect of these non-singular terms on the interpretation of fringe patterns obtained from photoelasticity, optical interferometry, and the method of caustics has also been examined [2]. It has been shown [2,18], that in order to completely describe the stress state associated with two-dimensional cracks under static opening-mode loading, a generalized form of the Westergaard [19] equations is necessary. This generalization follows from an Airy stress function of the form:

$$F = Re\overline{\overline{Z}} + y\,Im\,\overline{Z} + y\,Im\,\overline{Y} \tag{1}$$

where

$$Z(z) = \frac{K}{\sqrt{2\pi W}}\,(z/W)^{-\frac{1}{2}} \sum_{j=0}^{j=J} A'_j (z/W)^j \tag{2}$$

and

$$Y(z) = \frac{K}{\sqrt{2\pi W}}\,(z/W)^{-\frac{1}{2}} \sum_{m=0}^{m=M} B'_m (z/W)^{m+\frac{1}{2}} \tag{3}$$

where the A'_j and B'_m are dimensionless real constants ($A'_0 \equiv 1$) and W is a characteristic in-plane dimension of the specimen, such as the specimen width.

One immediate consequence of using a complete stress field representation such as eqn. (1) is that one is now able to predict the presence of fringes crossing the crack line such as those seen in Fig. 8, where the crack is approaching a normal boundary. By combining this stress field representation with the non-linear least-squares method of Sanford [20], and using a small desk-top microcomputer, it becomes possible to greatly enhance the accuracy of K-determination from photoelastic fringe data. This in turn allows the extension of photoelastic methods to problems such as fracture specimen characterization [21], and permits the calculation of quantities such as the singularity-dominated zone size in specimens of finite dimensions [22,23].

Briefly, the isochromatic fringe pattern analysis procedure can be summarized as follows. A data acquisition region is selected for a given experimental pattern, and data points taken over the entire region in a distributed fashion. This data set is then input to the least squares algorithm to obtain a best-fit solution for the unknown A'_j and B'_m coefficients. The number of coefficients necessary for an adequate representation of the stress field over the data acquisition region can be estimated by examining, as a function of the number of parameters, the average fringe order error, the values of K and σ_{ox}, and the reconstructed (computer-generated) fringe pattern corresponding to a given set of coefficients. Stability of the error term and leading coefficients, as well as a good visual match between experimental and reconstructed patterns indicates convergence to a satisfactory solution. A typical example consisting of the experimental fringe pattern, the data set selected therefrom, and the reconstructed pattern, is shown in Fig. 9. The data points in this case have been taken over a region of radius 0.25 W, centered at the crack tip, which is located at an a/W of 0.40 in a Three-Point-Bend (TPB) specimen. The reconstructed pattern is based upon an eight-parameter stress field representation, and can be seen to match the salient features of the experimental pattern over the sampled region around the crack tip. Fig. 10 shows the decrease in error and increased stability of K and σ_{ox} that occurs with an increasing order model for the same case as Fig. 9. Fig. 11 shows a comparison between photoelastic results and boundary collocation computations of the function f(a/W) for the TPB specimen. Both sets of results are in good agreement but the photoelastic technique has the

advantage of being easier and less costly to perform.

The methodology described above can be extended to the analysis of dynamic isochromatic fringe patterns, by making the crack-speed-dependent coordinate transformation shown in Fig. 12. Irwin [17,24] has shown that, for a crack tip stress pattern translating in the positive x-direction at a fixed speed, the dilatation, Δ, and rotation, ω, can be expressed as

$$\Delta = \frac{\partial u}{\partial x} + \frac{\partial v}{\partial y} = A(1 - \lambda_1^2)\ Re\ \Gamma_1(z_1)$$
$$\text{and} \quad \omega = \frac{\partial v}{\partial x} - \frac{\partial u}{\partial y} = B(1 - \lambda_2^2)\ Im\ \Gamma_2(z_2)\ . \tag{4}$$

It then follows that

$$\begin{aligned} \sigma_x &= \mu[A(1 + 2\lambda_2^2 - \lambda_2^2)\ Re\ \Gamma_1 - 2B\lambda_2 Re\ \Gamma_2] \\ \sigma_y &= \mu[-A(1 + \lambda_2^2)\ Re\ \Gamma_1 + 2B\lambda_2 Re\ \Gamma_2] \\ \tau_{xy} &= \mu[-2A\lambda_1 Im\ \Gamma_1 + B(1 + \lambda_2^2)\ Im\ \Gamma_2] \end{aligned} \tag{5}$$

where the constants A and B have to be evaluated, after selecting general stress functions, Γ_1 and Γ_2, so as to satisfy the boundary conditions for the crack problem. Suitable choices for the general stress functions are

$$Z_1 = \sum_{j=o}^{j=J} C_j z_1^{j-\frac{1}{2}} \qquad with \qquad Z_2 = \sum_{j=o}^{j=J} C_j z_2^{j-\frac{1}{2}} \tag{6}$$

and

$$Y_1 = \sum_{m=o}^{m=M} D_m z_1^m \qquad with \qquad Y_2 = \sum_{m=o}^{m=M} D_m z_2^m \tag{7}$$

which provide a complete representation of the dynamic stress field in a manner analogous to that described previously for the static situation.

Fig. 13a shows the $\dot{a}$-K curve for Homalite 100 determined from a Ring segment in 1978 using a two-parameter (K and σ_{ox}) dynamic stress field representation. Fig. 13b shows the results obtained in 1981 after re-analysis of the same fringe patterns with the multi-parameter least-squares technique of [20] and equations (5)-(7). The scatter in the data was substantially reduced and the $\dot{a}$-K relationship formulated with greater confidence, which is particularly important if this is to be input to the finite element code for further calculations.

5. EFFECTS OF NON-SINGULAR TERMS ON CRACK BRANCHING AND HIGH-VELOCITY CRACK PROPAGATION

Past work has been helpful in bringing to light major features of crack propagation behavior. There is evidence that in special situations, such as high-velocity crack propagation and crack branching, the cracking behavior is influenced by stress field parameters other than K. At the present time, efforts to see consistent influences of, for example, σ_{ox} in our present $\dot{a}$-K data have not been pursued to the point where definitive conclusions are possible. However, certain qualitative observations can be made.

Fig. 14 shows a schematic representation of the $\dot{a}$-K curves obtained for Homalite 100 with various mechanically-loaded fracture test specimens, as well as with explosively-driven cracks. Notice that as the value of σ_{ox} goes from large positive (DCB specimens) to large negative values (explosively-driven cracks), the plateau in the $\dot{a}$-K curve disappears. Fig. 15 shows fringe patterns associated with attempted and successful branching of high velocity propagating cracks in SEN specimens, with the cracks propagating at about 16,000 in/s (400 m/s).

In testing with explosive loading, much higher crack velocities have been recorded before successful branching has been observed. Fig. 16 shows the decomposition of the stresses within a P-wave propagating outwards from an explosive source. Note that the state of stress is basically biaxial compression, with the magnitude of the radial stress, σ_r, being about 2.5 times the tangential stress, σ_θ. This translates into a high negative value of σ_{ox}.

Fig. 17 shows three frames from an explosive test. In the first frame, taken 85 μs after detonation, 10 major radial cracks can be seen propagating from the borehole, with unsuccessful attempts to branch. These cracks are propagating at speeds in excess of 25,000 inches/sec (625 meters/sec), much higher than any recorded velocities for mechanically loaded fracture specimens. It is felt that a combination of the interaction from stress fields at neighboring crack tips and the compressive stress field due to the explosive loading prevents these cracks from branching successfully. The later two frames show the radial crack behavior as the reflected waves generated by the P-wave striking the free boundary pass over the crack tips. (The outward

P-wave reflects so as to provide a tensile field.) Notice that the cracks turn in a circumferential direction and "explode" into a multiple-branched condition as the reflected P-wave passes. Once the wave has passed by, the cracks resume their original radial orientation and continue to propagate.

The analysis models which have been developed, when combined with microcomputer based numerical algorithms, provide the tools necessary for a systematic study of such phenomena, and this area of investigation is currently being pursued.

6. FRACTURE INITIATION IN A JOINTED MEDIA

This section describes results obtained in the testing of polymeric models to investigate the mechanisms associated with fragmentation blasting. The mechanisms observed in laboratory tests were also seen in rock fragmentation field testing, and are discussed here in the hope of stimulating discussion and analysis from a fracture mechanics viewpoint, which would be very helpful.

In a quarry blasting situation, it is normal to find the geologic medium separated by bedding planes and joint sets. These joints are varied in properties and can range from open, mud-filled joints to calcite-filled joints whose strength approaches that of the surrounding rock. A series of tests with layered plastic models was conducted in an effort to determine what effect these joints would have on the resulting fragmentation.

The models were fabricated from sheets of 6 mm thick Homalite 100, which were machined into 50 mm wide strips. The strips were then bonded together with a cyanoacrylate ester cement. The bond was extremely thin (0.025 mm or less) and tests showed the tensile strength of the bond to be of the order of 7 MPa, while the shear strength was greater than that of the model material. The finished model was 300 mm x 450 mm and normally contained two boreholes. Pressure containment devices were used to retain the detonation pressures for as long a time as possible.

Fig. 18 shows results typical of some twenty tests that were conducted using the Cranz-Schardin camera. Fig. 18a, taken 34 μs after detonation of the right-hand borehole, shows

the presence of fractures above and below the borehole in the vicinity of the bond lines. The next frame, Fig. 18b. taken 28 μs later (62 μs after detonation) shows the intense fracture system developed along the bond lines adjacent to the borehole. These cracks form angles of about 70° to the bondline and were observed to always travel away from the borehole layer. They appear to be most intense and longest in the region where radial lines from the borehole make an angle of $\pm$ 30° with the bond line. Figs. 18c and 18d show details of crack growth later in the event. Note the lack of fractures within the borehole layer itself. This layer was observed to fracture much later in the dynamic event, when stress waves reflected from the model boundaries passed through the layer.

It is thought that this phenomenon, which we have termed joint-initiated-fracturing, is caused by the shear component in the outgoing P-Wave and the closely following S-wave. The probable initiation sites are felt to be large numbers of small imperfections along the bond lines, which result in initiation of cracks when loaded in shear. Further details of the investigations of explosively loaded models can be found in [25-27].

7. CLOSURE

Analyses of running cracks in large structures can be performed using large numerical computing programs which take account of the inertia of the material. Alternatively, the problem of interest can be modeled and studied experimentally using, for example, dynamic photoelasticity. Because of the complexities and approximations involved in large structure modeling, comparisons of computational and experimental results are both valuable and necessary. The recently acquired ability to determine K-values accurately from photoelastic data represents an important step in this direction. The simultaneously gained information about non-singular stress field influences enhances the capability for studying fracture phenomena not controlled by K alone.

ACKNOWLEDGEMENTS

The research work described in this paper has been made possible by support provided by the U.S. Nuclear Regulatory Commission and Oak Ridge National Laboratory. Support for the work

on explosively loaded models came from the National Science Foundation. Computational Work has been made possible by the support provided by the University of Maryland Computer Science Center. The investigations described here would not have been possible without the guidance of Professor George Irwin and the efforts of the Photomechanics Laboratory personnel.

REFERENCES

1. Hahn, G.T., et al., "Critical Experiments, Measurements and Analyses to Establish a Crack Arrest Methodology for Nuclear Pressure Vessel Steels," 2nd Annual Report to NRC, BMI-1937, Battelle Report (1975).

2. Irwin, G.R., et al., "Photoelastic Studies of Damping, Crack Propagation, and Crack Arrest in Polymers and 4340 Steel," NUREG/CR-1455, University of Maryland (1980).

3. Nishioka, T., and Atluri, S.N., "Finite Element Simulation of Fast Fracture in Steel DCB Specimen," Engineering Fracture Mechanics, 16 (1982) 157-175.

4. Bradley, W.B., and Kobayashi, A.S., "An Investigation of Propagating Cracks by Dynamic Photoelasticity," Experimental Mechanics, 10 (1970) 106-113.

5. Kobayashi, A.S., Emery, A.F., and Mall, S., "Dynamic Finite Element and Dynamic Photoelastic Analysis of Crack Arrest in Homalite 100 Plates," Fast Fracture and Crack Arrest, ASTM STP 627 (1977) 95-108.

6. Kalthoff, J.F., et al., "Experimental Analysis of Dynamic Effects in Different Crack Arrest Test Specimens," Crack Arrest Methodology and Applications, ASTM STP 711 (1980) 109-127.

7. Beinert, J., and Kalthoff, J.F., "Experimental Determination of Dynamic Stress Intensity Factors by the Method of Shadow Patterns," Mechanics of Fracture VII, Noordhoff International (1980).

8. Irwin, G.R., et al., "A Photoelastic Study of the Dynamic Fracture Behavior of Homalite 100," U.S. NRC Report NUREG-75-107, University of Maryland (1975).

9. Irwin, G.R., et al., "A Photoelastic Characterization of Dynamic Fracture," U.S. NRC Report NUREG-0072, University of Maryland (1976).

10. Irwin, G.R., et al., "Photoelastic Studies of Crack Propagation and Arrest," U.S. NRC Report NUREG/CR-0342, University of Maryland (1977).

11. Irwin, G.R., et al., "Photoelastic Studies of Crack Propagation and Arrest in Polymers and 4340 Steel," U.S. NRC Report NUREG/CR-0542, University of Maryland (1978).

12. Kobayashi, T., and Dally, J.W., "The Relation Between Crack Velocity and the Stress Intensity Factor in Birefringent Polymers," Fast Fracture and Crack Arrest, ASTM STP 627 (1977) 257-273.

13. Shukla, A., Fourney, W.L., and Irwin, G.R., "Study of Energy Loss and Its Mechanisms in Homalite 100 During Crack Propagation and Arrest," NUREG/CR-2150 (ORNL/Sub-7778/1), ORNL/HSST Report No. 61, University of Maryland (1981).

14. Whitman, G.D., and Bryan, R.H., "Heavy-Section Steel Technology Program Quarterly Progress Report for January-March 1981," NUREG/CR-2141/V1 (ORNL/TM-7822), Oak Ridge National Laboratory (1981).

15. Riley, W.F., and Dally, J.W., "Recording Dynamic Fringe Patterns with a Cranz-Schardin Camera," Experimental Mechanics, 9 (1969) 27N-33N.

16. Irwin, G.R., "Discussion of: The Dynamic Stress Distribution Surrounding a Running Crack - A Photoelastic Analysis," Proceeding SESA, 16 (1958) 93-96.

17. Irwin, G.R., "Constant Speed Semi-Infinite Tensile Crack Opened by a Line Force, P, at a Distance, b, from the Leading Edge of the Crack Tip," Lehigh University Lecture Notes (1968).

18. Sanford, R.J., "A Critical Re-examination of the Westergaard Method for Solving Opening-Mode Crack Problems," Mechanics Research Communications, 6 (1979) 289-294.

19. Westergaard, H.M., "Bearing Pressures and Cracks," Trans. ASME, 61 (1939) A49-A53.

20. Sanford, R.J., "Application of the Least Squares Method to Photoelastic Analysis," Experimental Mechanics, 20 (1980) 192-197.

21. Sanford, R.J., and Chona, R., "Characterizing Fracture Test Specimens Using Photoelastic Methods," Proceedings of the 1982 SESA/JSME Joint Conference on Experimental Mechanics, (1982) 263-265.

22. Sanford, R.J., Chona, R., Fourney, W.L., and Irwin, G.R., "The Influence of Non-Singular Stresses in Fracture Test Specimens," NUREG/CR-2179 (ORNL/Sub-7778/2), University of Maryland (1981).

23. Chona, R., Irwin, G.R., and Sanford, R.J., "The Effect of Specimen Size and Shape on the Singularity-Dominated Zone," Proceedings of the ASTM 14th National Symposium on Fracture Mechanics, Los Angeles, CA, ASTM STP in press (1983).

24. Irwin, G.R., "Series Representation of the Stress Field Around Constant Speed Cracks," University of Maryland Lecture Notes (1980).

25. Barker, D.B., Fourney, W.L., and Dally, J.W., "Photoelastic Investigation of Fragmentation Mechanism Part I - Borehole Crack Network," Report to the National Science Foundation,

University of Maryland (March 1978).

26. Barker, D.B., and Fourney, W.L., "Photoelastic Investigation of Fragmentation Mechanisms Part II - Flaw Initiated Network," Report to the National Science Foundation, University of Maryland (August 1978).

27. Fourney, W.L., Barker, D.B., and Holloway, D.C., "Mechanism of Fragmentation in a Jointed Formation," Report to the National Science Foundation, University of Maryland (July 1979).

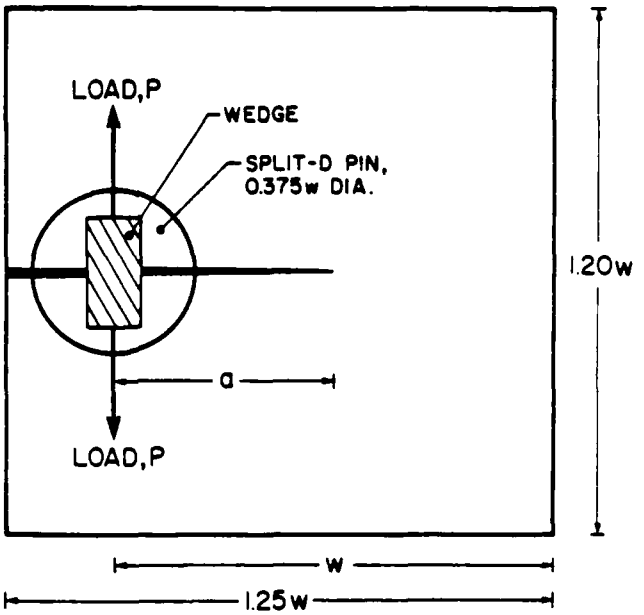

Figure 1a. Geometry of the crack-line-wedge-loaded modified-compact-tension fracture test specimen.

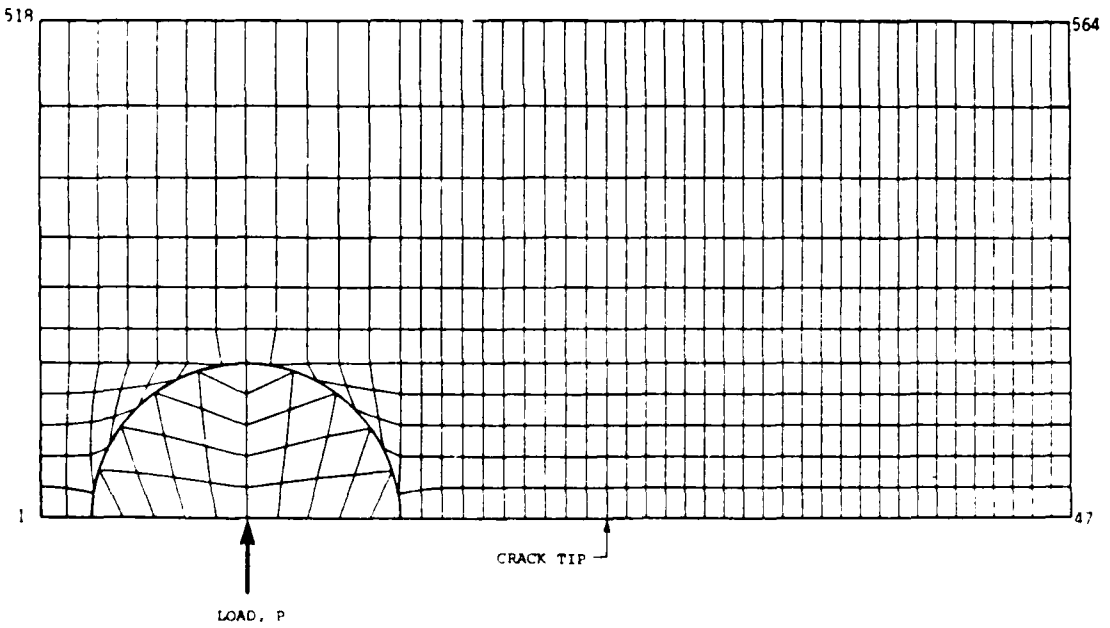

Figure 1b. Symmetric (upper) half of the MCT specimen showing the finite element mesh used for analysis by the SAMCR code.

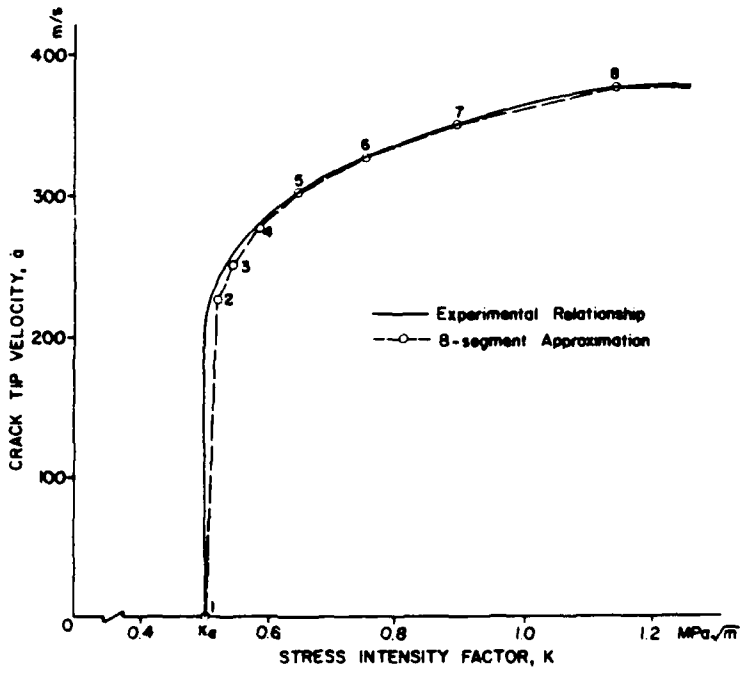

Figure 2. The experimentally determined ȧ-K relationship input to SAMCR.

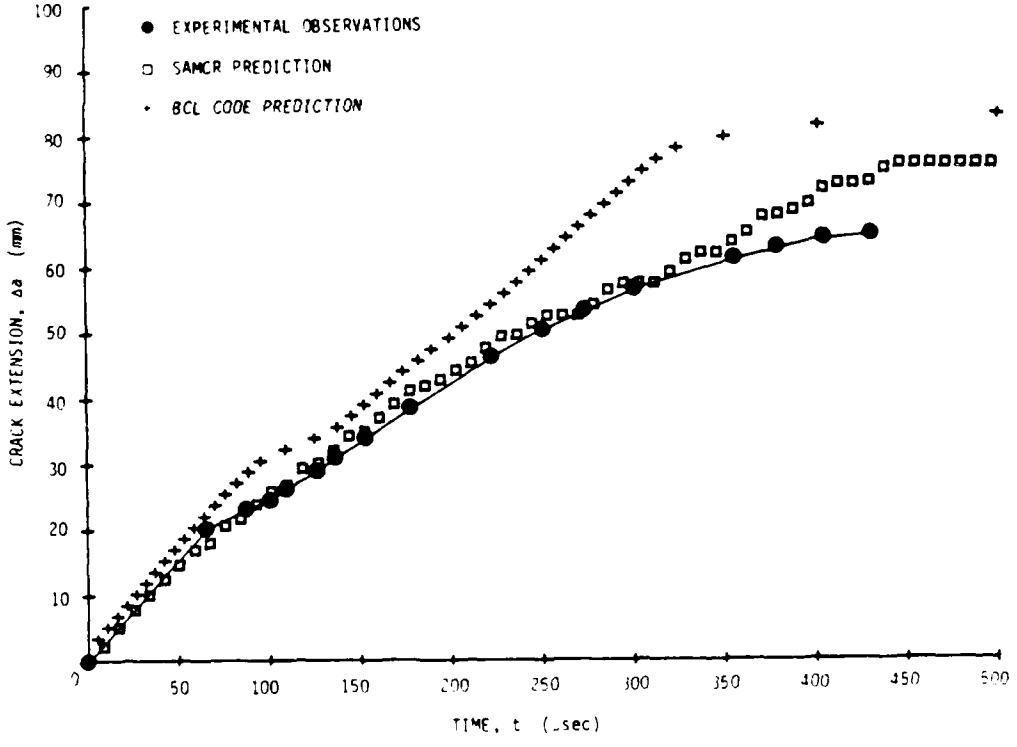

Figure 3. Experimental observations and computer code predictions for crack extension as a function of time in an MCT specimen.

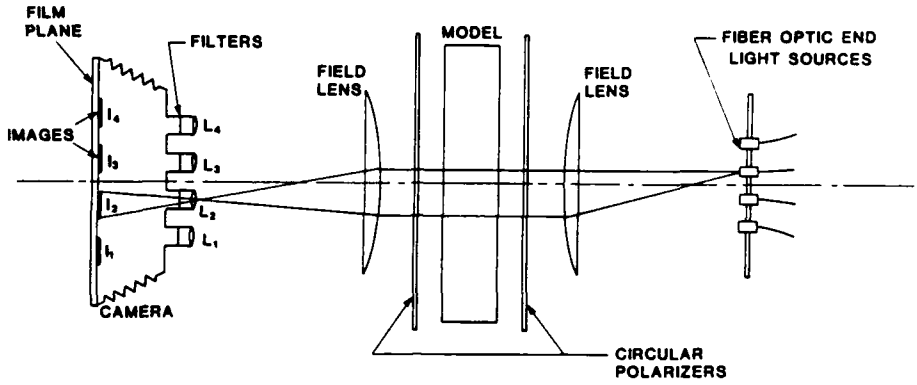

Figure 4. The optical arrangement of a typical Cranz-Schardin, multiple-spark, high-speed photography camera.

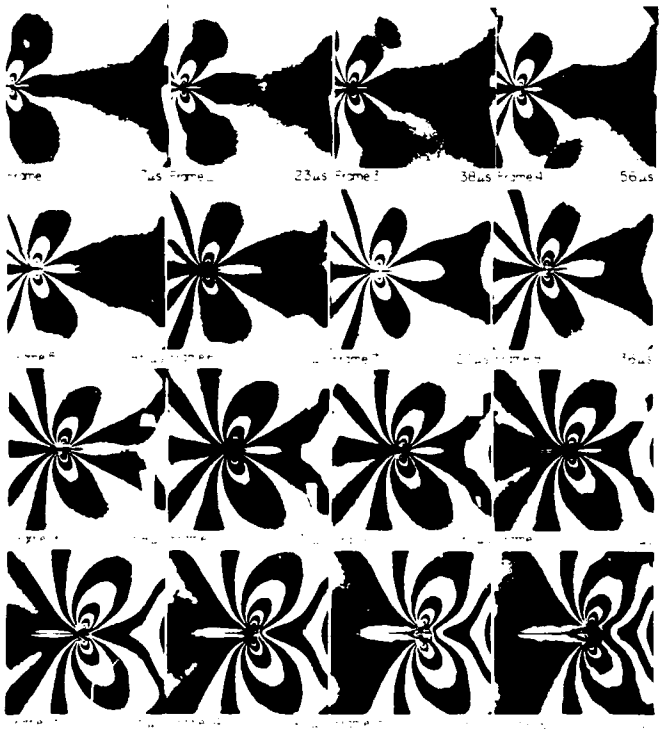

Figure 5. A typical sequence of 16 isochromatic fringe patterns recorded with the Cranz-Schardin camera, showing high-velocity crack propagation and crack branching in an SEN specimen.

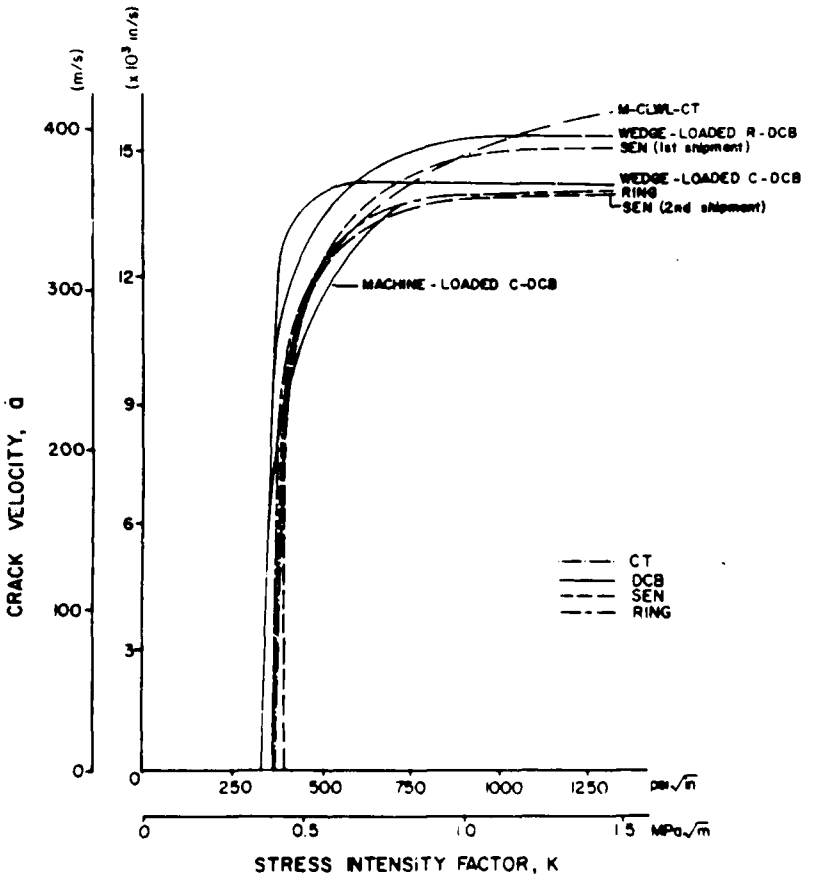

Figure 6. The relationship between crack speed and crack tip stress intensity factor as determined from several different test specimen geometries for Homalite 100.

AD-A140 194 WORKSHOP ON DYNAMIC FRACTURE HELD AT PASADENA CALIFORNIA ON 17-18 FEBRUARY 1983(U) CALIFORNIA INST OF TECH PASADENA W G KNAUSS ET AL. OCT 83 2/3

UNCLASSIFIED ARO-19961.1-EG-CF DAAG29-83-M-0101 F/G 11/6 NL

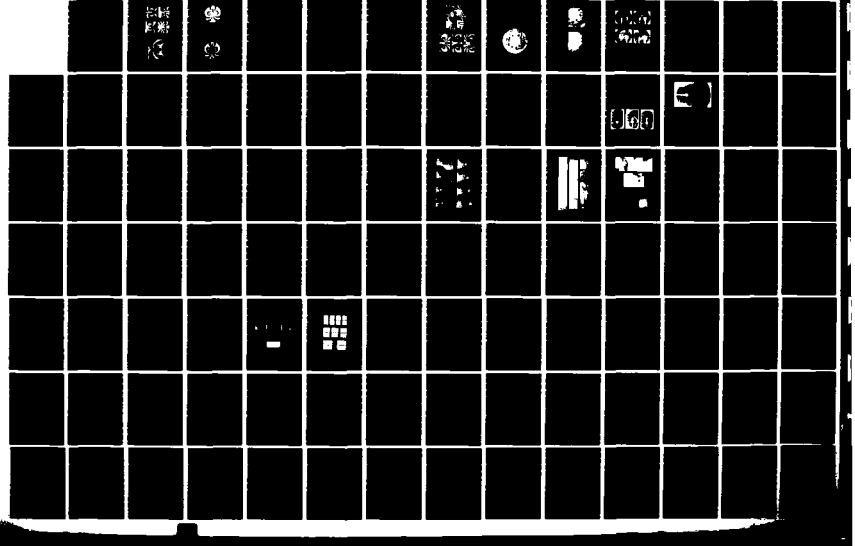

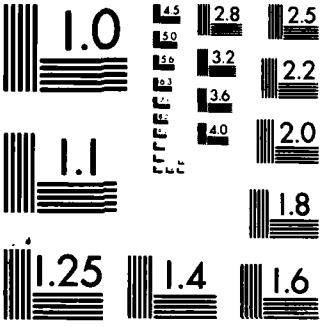

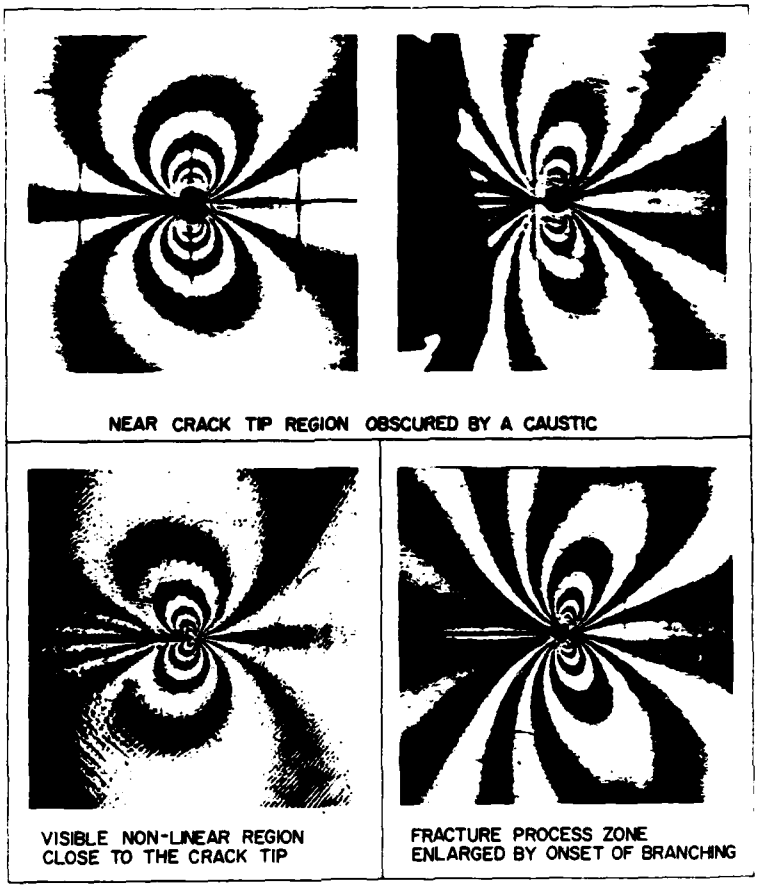

Figure 7. Some examples of isochromatic fringe patterns which cannot be analyzed by taking data close to the crack tip.

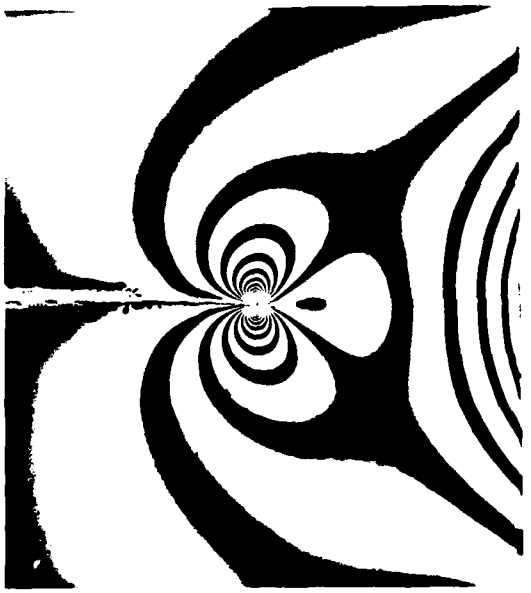

Figure 8. Isochromatic fringe pattern surrounding a deep crack (a/W = 0.8) in an MCT specimen illustrating the effects of a near boundary on the fringe distribution.

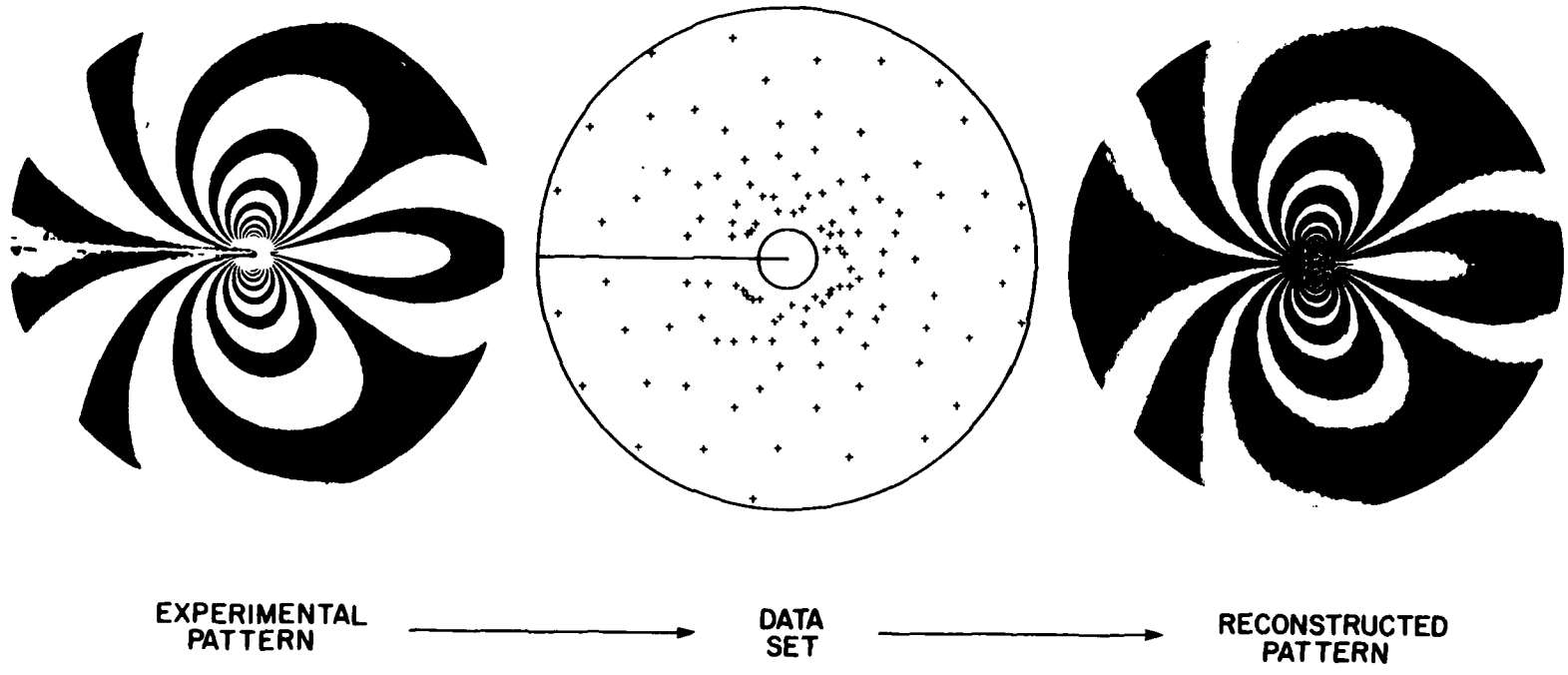

Figure 9. A typical crack-tip isochromatic fringe pattern in a three-point-bend specimen, the data set used for analysis, and the reconstructed pattern corresponding to an eight-parameter solution.

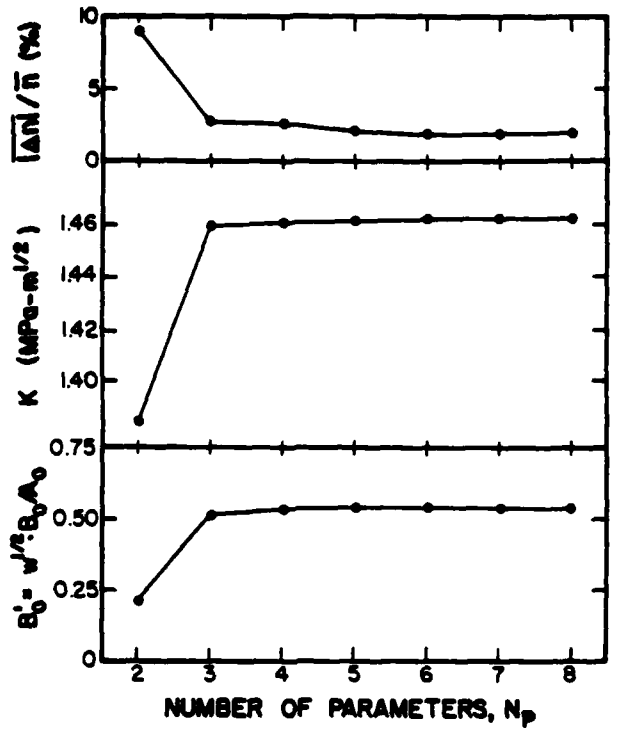

Figure 10. The changes in fringe order error, K, and B'_0 observed as the order of the analysis model increases.

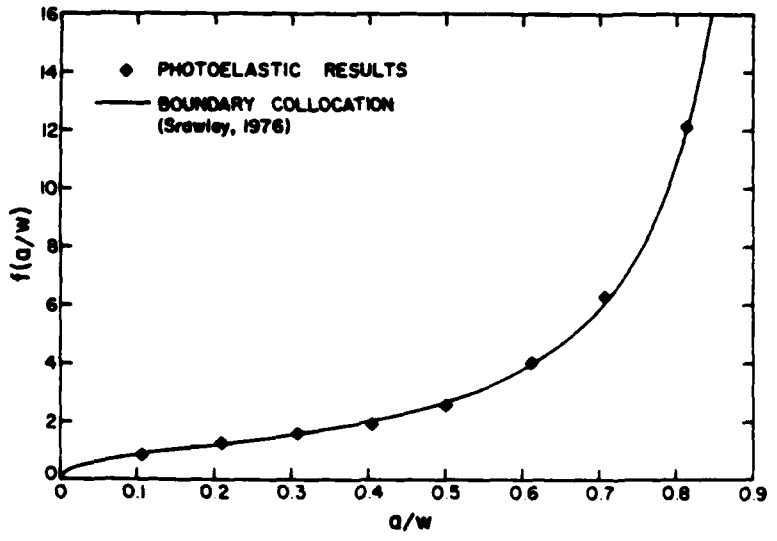

Figure 11. The geometric shape function, f(a/W), for a three-point-bend specimen, as determined by boundary collocation and photoelastic methods.

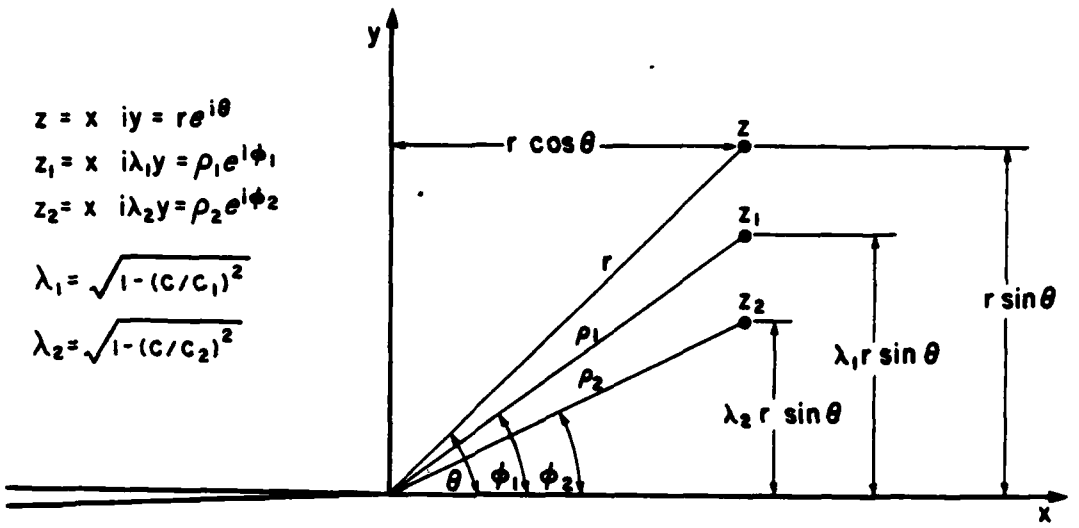

Figure 12. The coordinate system employed for the dynamic analysis of constant-speed running cracks.

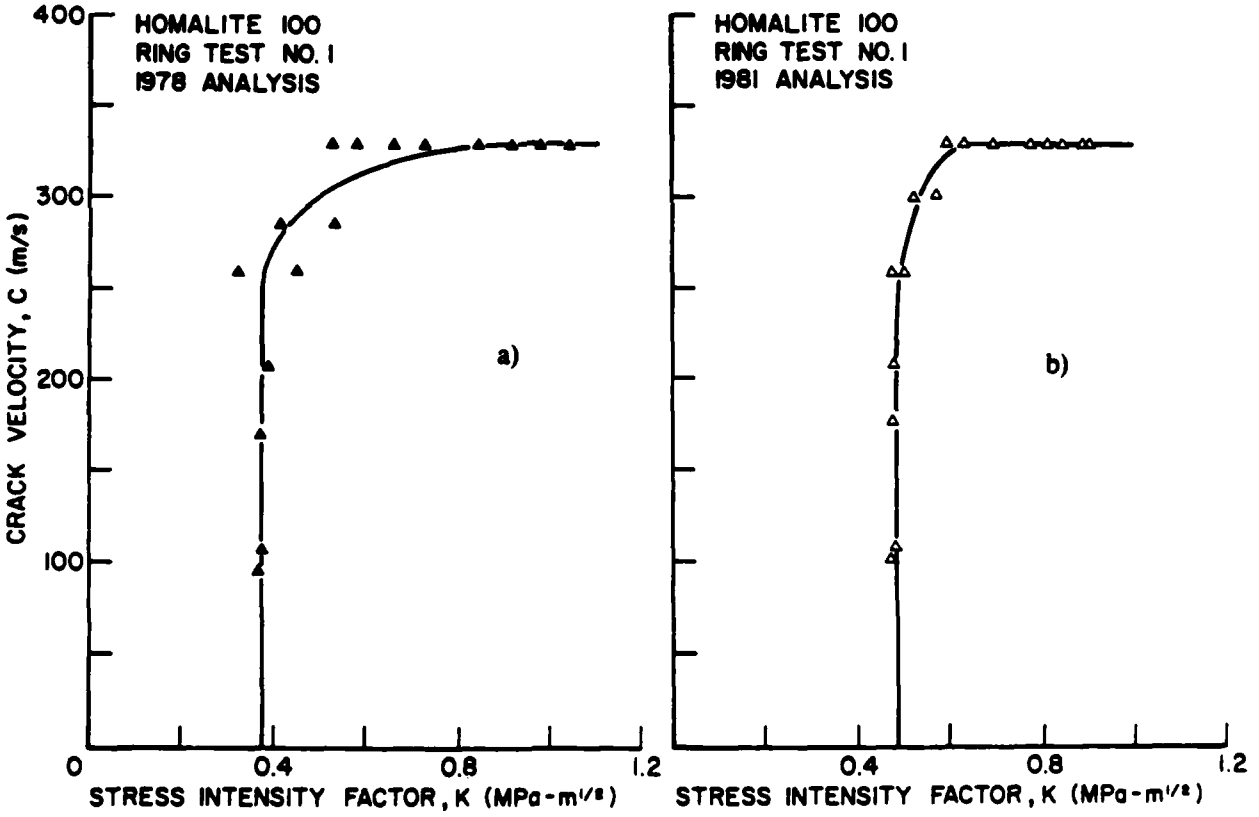

Figure 13. The ȧ-K relationship for Homalite 100 as determined from a ring specimen using a two-parameter and a higher-order analysis model.

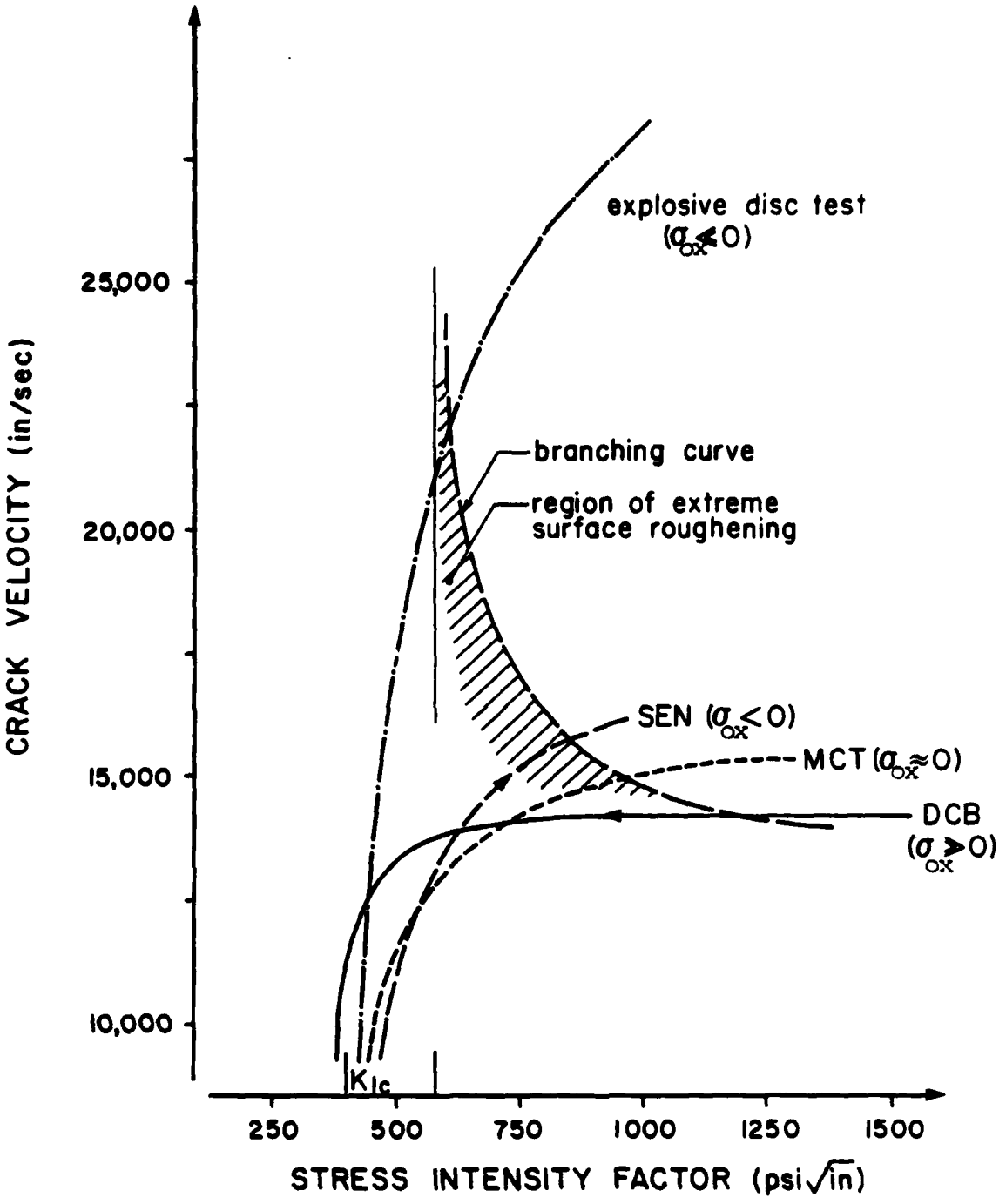

Figure 14. Schematic representation of the á-K curve showing the effects of σ_{ox} on crack branching and the plateau region.

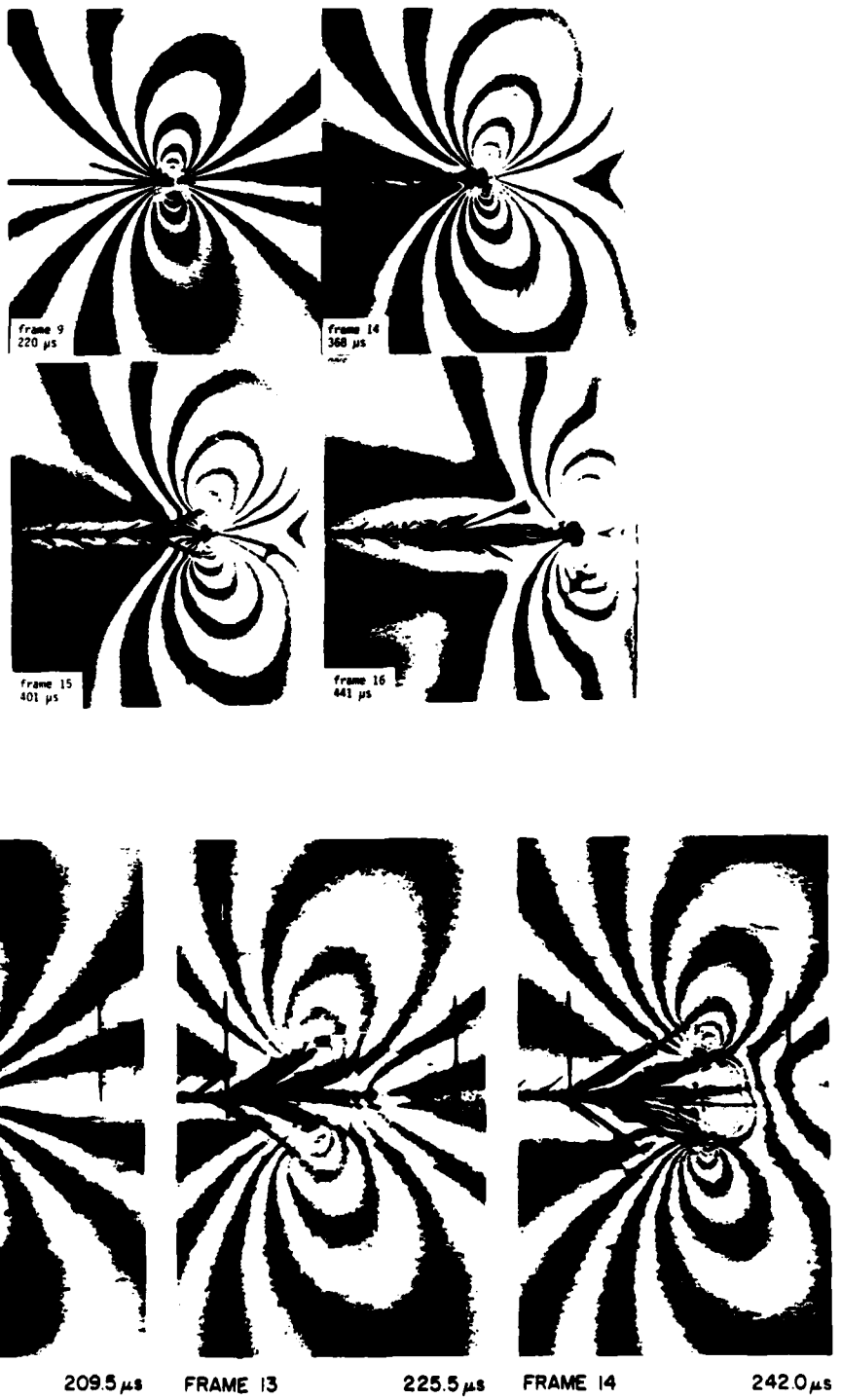

Figure 15. Isochromatic fringe patterns from two tests in an SEN specimen, showing high-velocity propagating cracks attempting to branch and successful branching.

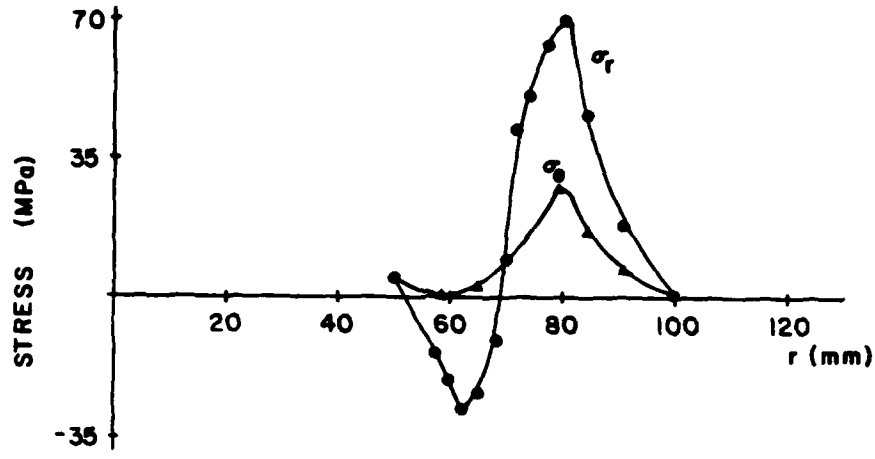

Figure 16. The decomposition of stresses in a P-wave propagating in Homalite 100, 40 μs after detonation of the explosive.

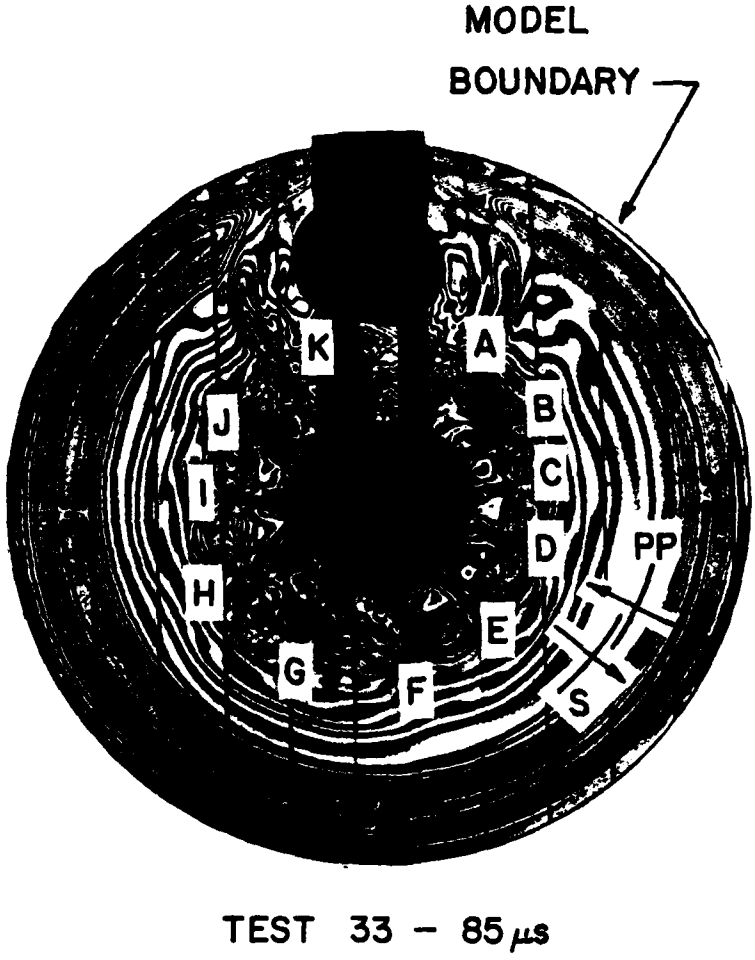

Figure 17. Three frames from a circular fragmentation model showing the behavior of radial cracks before and after interaction with reflected stress waves.

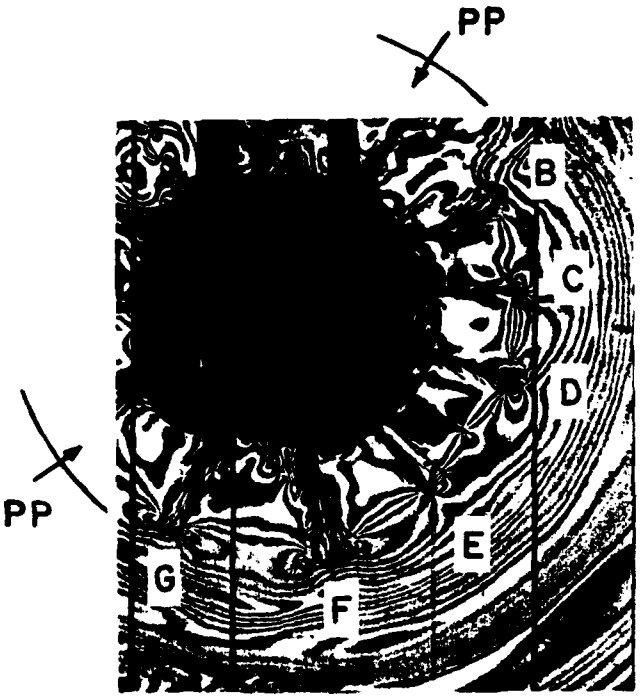

TEST 33 – 104 μs

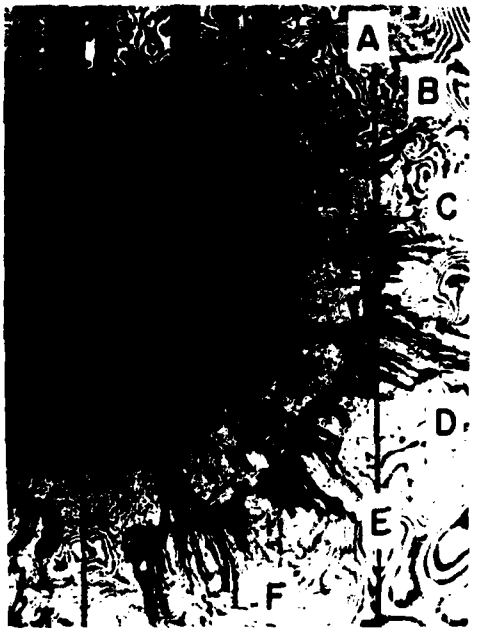

TEST 33 – 153 μs

Figure 17. Continued.

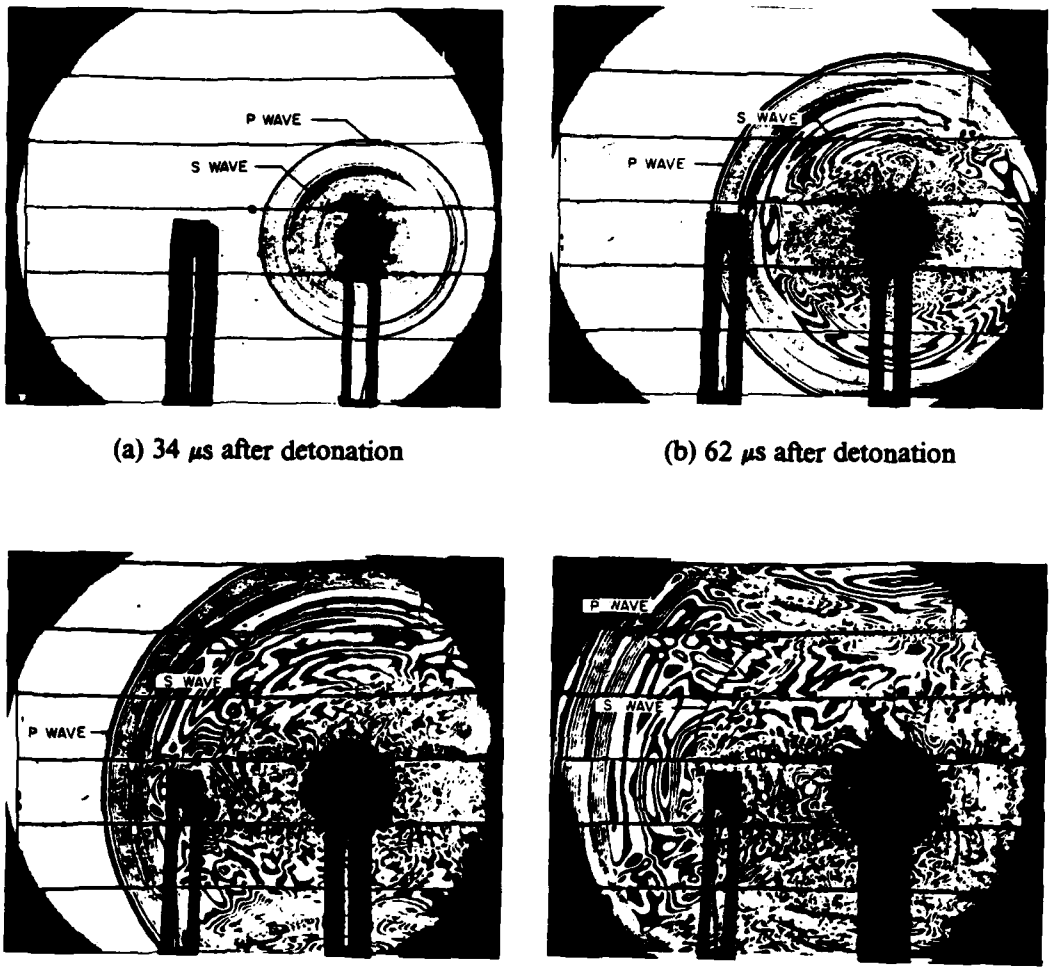

Figure 18. Four frames from a layered model test showing joint-initiated-fracturing.

DYNAMIC CRACK GROWTH CRITERIA IN STRUCTURAL METALS

A.J. Rosakis
California Institute of Technology

J. Duffy and L.B. Freund
Brown University

1. INTRODUCTION

Analytical difficulties associated with the dynamic crack propagation problem have limited the available dynamic solutions to idealized situations. The major limitations introduced by these analytical solutions make both numerical methods and direct experimental observations necessary for the complete understanding of the dynamic fracture process. A principal purpose of experimental studies is to observe directly the instantaneous stress intensity factor as a function of crack speed, and to determine whether or not the observed variation constitutes a material characteristic.

The present paper provides a description of dynamic crack propagation experiments on double cantilever beam specimens of a high strength steel. Measurements of the crack tip deformation field and of crack speed during propagation have been made using the optical method of caustics in reflection. A principal advantage of a measurement made directly at the crack tip is that the interpretation of data does not rely on a complete transient stress analysis of the entire specimen. The inherent time dependence of crack propagation experiments requires that many sequential measurements of field quantities be made in an extremely short time and in a way that does not interfere with the process to be observed. Furthermore, the area over which the field quantities are to be measured advances along with the crack tip, and often in a nonuniform way. The method of caustics is attractive for meeting these experimental requirements.

2. THE FORMATION OF CAUSTICS BY REFLECTION

For opaque specimens the caustic image is formed by the reflection of light from the specimen surface. The specimen must be planar and polished, and mounted with parallel rays of light striking normal to its surface. When the specimen is loaded, the presence of a crack results in stress concentration, causing a dimple to form in the specimen surface. If a beam of parallel light rays is incident upon the deformed specimen surface, then, upon reflection, the light rays no longer will be parallel. Furthermore, if certain geometric conditions are met by the reflecting surface, then the virtual extension of the reflected rays will form an envelope describing a three dimensional surface in space. This surface, called the caustic surface is the locus of points of maximum luminosity. Its intersection with a vertical plane gives the caustic curve, which can be recorded photographically. For this purpose a camera is positioned in front of the specimen and focused onto a plane, called the "screen", at a distance z_o behind the plane of the undeformed specimen surface. The reflected light field provides an image of the caustic curve at the focal plane of the camera. The complete analysis required to obtain an expression for the dynamic stress intensity factor, K_I^d in terms of the caustic width, D, is presented in [1] and includes the dynamic effects associated with the velocity, v, of the moving crack tip. It is found that the instantaneous value of K_I^d is related to D by:

$$K_I^d(t) = C(\alpha_l)\,\frac{2(2\pi)^{\frac{1}{2}}\,E\,[\,4\alpha_l\alpha_s - (1+\alpha_s^2)^2\,]}{z_o \nu d(1+\alpha_s^2)(\alpha_s^2-\alpha_l^2)}\,D^{\frac{5}{2}} \qquad (1)$$

where: $\alpha_{l,s} = (1 - \nu^2 / c_{l,s}^2)^{\frac{1}{2}}$, d is the specimen thickness, ν Poisson's ratio and E Young's modulus. $C(\alpha_l)$ has been numerically determined and can be accurately expressed as $C(\alpha_l) = (6.8 + 14.4\alpha_l + 2.6\alpha_l^2) \times 10^2$. Expression (1) was used throughout the present work in the interpretation of the results of the dynamic propagation experiments performed with the DCB 4340 steel specimens.

3. THE DYNAMIC CRACK PROPAGATION EXPERIMENTS

The specimens used in this investigation were of the single-edge crack configuration commonly known as the double cantilever beam or DCB. The specimens were machined from steel plates of commercial AISI 4340 steel. Their final dimensions were 229 mm by 76 mm, with a thickness of 12.7 mm. The precrack, which is introduced by means of a spark cutter, runs along the center line of each specimen to a depth of 63.5 mm and ends at a 1.40 mm drill hole. Figure 1 shows the experimental arrangement, including the two wedges used to force open the crack. These wedges bear on two hardened steel pins of 16 mm diameter, one in each arm of the specimen. During a test, the wedges are brought down by a slow-moving hydraulic ram, while the other end of the specimen is clamped on a firm base.

Specimen preparation began with machining, which included drilling the 1.40 mm hole that later formed the tip of the crack. The heat treatment consisted of austenitizing at 843^oC (1550^oF) for one hour, followed by an oil quench and a temper to 316^oC (600^oF) for one hour. After this heat treatment, the crack was spark-cut to the drilled hole; then one face of the specimen was ground, lapped and polished to produce a surface with high reflectivity and a high degree of flatness. In separate tests, it was determined that the flow stress of this material in tension is approximately 1300 MPa and that it has a hardness of 45 on the Rockwell C scale.

The caustic patterns formed during the course of the experiments were recorded by means of a high speed camera of the Cranz-Schardin type. The present camera employs twelve flash tubes arranged in a 3 x 4 array, as shown schematically in Fig. 1, to provide the light sources for a sequence of twelve pictures. Each flash has an effective duration of approximately one microsecond. To obtain a predetermined time interval between flashes, each flash tube is triggered separately, within the range 0.8 to 740 microseconds. The light from the flash tubes strikes a parabolic mirror which then directs it onto the polished surface of the specimen. Upon reflection from this surface, the light rays converge and are focused on the 12 objective lenses of the camera. The camera is focused to a plane behind the specimen, indicated by the word "screen" on the diagram.

During a test, when the load supplied by the wedge reaches a critical value, a sharp crack starts to propagate from the notch tip. The camera is then triggered by the crack itself as it starts to move and breaks a conducting strip cemented to the reverse side of the specimen. As the crack advances the reflective surface of the specimen deforms and a series of twelve caustic patterns is recorded sequentially on 8" x 10" photographic film. In the resulting photograph, each image of the specimen measures 25 by 35 mm and shows a shadow spot and a caustic curve surrounding the moving crack tip. An enlargement of three of these images is shown in Figure 2.

In Figure 2, the event of initiation is recorded. The first photograph shows the caustic corresponding to the static loading of the blunted notch. In the second photograph the crack has initiated, emitting unloading waves, which will be reflected from the specimen boundaries and will subsequently interfere with the motion of the propagating crack. Some of these waves are visible in the picture as dark circles surrounding the shadow pattern. Such waves are also clearly visible in the dynamic shadowgraph simulations reported in this volume by Hoover, et al. [2].

After completing a test, two measurements are made from each image to provide values of the stress intensity factor and the corresponding crack speed. The speed is calculated from the instantaneous position of the crack tip by locating the position of the maximum transverse diameter of each caustic relative to a scale drawn on the specimen surface. The second measurement made is that of the transverse diameter D of the shadow spot, as recorded for instance in Fig. 3. This measurement leads to an instantaneous value of the dynamic stress intensity factor in accordance with the dynamic analytical models presented in [1], and in particular on the basis of Equation (1).

4. DISCUSSION AND RESULTS

For dynamic crack propagation, under conditions of small scale yielding, fracture criteria based on the stress intensity factor are expressed in an equivalent way to the static case. This is done by the introduction of a time dependent amplitude factor $K_I^d(t)$ and an experimentally

determined critical value K_c^d that is assumed to be a material property.

For a propagating crack the fracture criterion is assumed to take the form

$$K_I^d = K_{Ic}^d(v) \tag{2}$$

where v is the crack-tip speed. The actual dependence of K_{Ic}^d on v must be determined by experiment.

In order to analyze the experimental results, the instantaneous crack length, a(t), and the dynamic fracture toughness value, $K_{Ic}^d(t)$, are plotted as functions of time for each experiment. Typical results, obtained for specimen number 9, are displayed as the points shown in Fig. 4. For all specimens tested, the curves of $K_{Ic}^d(t)$ as a function of time are very similar in nature but are not identical. The main differences are due to the stress waves which are reflected from the specimen boundaries and interact with the crack tip motion. This interaction produces sudden variations in the crack tip velocity and in the stress intensity factor. The phenomenon will be discussed in detail in a later section, but it is worth observing here that the curves of a(t) and $K_{Ic}^d(t)$ show oscillations, and that the peaks and jumps in these curves occur at different instants for different tests, depending on the velocity history of the crack tip. It is noted that corresponding results reported for polymers [3,4] do not show the large oscillations in the value of K_{Ic}^d and of the crack velocity seen here for metals. As discussed later, this difference seems to be due to the relatively low ratio of specimen stiffness to loading mechanism stiffness in experiments with polymer specimens.

An alternative way of presenting the data is shown in Fig. 5. Here the dynamic fracture toughness and the crack tip velocity are plotted as functions of crack length. Again we observe oscillations in the values of K_{Ic}^d and v to either side of the mean levels indicated by the dotted lines in both curves. The oscillations in K_{Ic}^d and v occur in phase with each other, suggesting the existence of a relationship between K_{Ic}^d and v. The crack tip motion does not appear to exhibit inertia effects, and it would seem reasonable to expect that K_{Ic}^d does not depend on the time

derivatives crack speed. These observations lead to the conclusion that for a fixed specimen geometry, the dynamic fracture toughness is a function of crack tip velocity only. Fig. 6 shows a plot of K_{Ic}^{d} as a function of v, obtained from the results of experiments number 8, 9 and 10. The initial crack tip velocity history differed in each of these three tests, although the geometry and material properties of the specimens were the same. Fig. 6 shows that, for values of crack tip velocity less than about $700 ms^{-1}$, the dynamic fracture toughness is nearly independent of crack velocity. The quasi-static value predicted here is approximately 50 MN $m^{-3/2}$. But for velocities greater than about 800 ms^{-1} the dynamic fracture toughness increases quite sharply with velocity. Nevertheless these data do not furnish evidence that crack velocity is limited to an asymptotic value.

Fig. 6 is one of the first K_{Ic}^{d} vs. v relationship reported for a metal as a result of a direct observation. Caustics by reflection have been used in the past [3] for the study of the arrest process in high-strength steels, but no such relation between K_{Ic}^{d} and v was reported.

For crack propagation in rate insensitive metals under conditions of contained yielding, as in the case considered here, some theoretical speculations can be made about the nature of the K_{Ic}^{d} vs. v behavior. From a purely intuitive point of view, it can be argued that, in the fracture of rate-independent elastic-plastic materials, the plastic zone surrounding the crack tip will give rise to greater inertial forces as the velocity of crack propagation increases and that this effect will be larger than in elastic materials. Approaching the problem from both an analytical and a numerical point of view, Freund and Douglas [5] and Douglas [6] obtained K_{Ic}^{d} as a function of v for the dynamic propagation of a Mode III crack in elastic-plastic and elastic-viscoplastic materials. Their results for rate insensitive materials predict the general behavior exhibited in Fig. 6. Under conditions of small scale yielding, the elastic-plastic field in the crack tip region is controlled by the intensity of the surrounding elastic field; namely, the remote stress intensity factor. As pointed out in [6], in order to determine the level of the remotely applied stress intensity factor required to sustain growth at a predetermined speed v, a ductile fracture criterion must be

introduced. A possible fracture criterion might be one requiring that a critical level of plastic strain occurs at a characteristic distance ahead of the crack tip in order for the crack to grow. Suppose now that a crack propagating in a metal undergoes a velocity increase. As a result of such an increase, the plastic zone size will shrink in the direction of propagation, and the plastic strain at the critical distance will be reduced. In order to sustain crack growth, the strain level has to be restored to its critical level and that is achieved with an increase of the far field stress intensity factor.

The results of Freund and Douglas, presented here in Fig. 7, show the far field dynamic stress intensity factor K (normalized with respect to the initiation toughness) plotted versus the normalized crack tip speed. Different curves correspond to different values of the critical plastic strain γ_c^p. Higher γ_c^p values represent higher ductility levels. The analytical predictions are qualitatively consistent with the experimental results displayed in Fig. 6 and seem to demonstrate that a K vs. v. relationship is a good description for a high strength, low ductility metal which fails in a *locally ductile* manner and whose fracture behavior is well described by a ductile fracture criterion.

Figure 6 is also consistent with the experimental results of Kobayashi and Dally [7] who investigated the dynamic propagation of cracks in compact specimens of a 4340 steel. In their work, birefringent coatings were used to obtain dynamic isochromatic patterns for the direct measurement of the stress intensity factor during the dynamic event. Their results exhibit the same qualitative features as discussed above. More specifically, oscillations in the values of K_I^d corresp ng to abrupt changes of the crack tip velocity are observed. It is apparent from their resu d here in Fig. 8 that sudden changes in the velocity of the crack tip are caused by the i he reflected waves on the crack tip motion. Unfortunately, the specimen geometry emp oyed by Kobayashi and Dally does not allow for easy identification of the waves interacting with the crack tip. The analysis for such an identification, presented in the next section, holds for the case of a DCB specimen only. However, the K_{Ic}^d vs. v curve reported in [7] is

very similar to the one obtained here by caustics.

5. THE INFLUENCE OF REFLECTED WAVES ON DYNAMIC CRACK ADVANCE

In this section some of the reflected waves interacting with the propagating crack in a standard DCB specimen are identified. Simple calculations based on the geometry of the specimen show that the ratio of the specimen compliance to that of the loading system can account for the magnitude of the stress wave-crack interactions, as predicted by Freund [8,9,10].

In analyzing the DCB specimen, Freund [8] considered a simple model in which the arms of the specimen are constrained to deform as shear beams. In examining the influence of the dominant reflected waves, he concluded that the main contribution to the crack tip motion comes from the shear waves reflected from the loading pins, conveying information about the changing boundary conditions. In the formulation of this model two types of boundary conditions were considered. Initially, a perfectly rigid loading system (fixed-grip boundary conditions) was analyzed. The material was assumed to obey a fracture criterion of the form $\Gamma = \Gamma_o$= constant, where Γ is the specific fracture energy. The results, displayed in Fig. 9a, show that the crack propagates with a constant speed up to arrest, which coincides with the arrival of the reflected shear wave [8,9]. In an attempt to make the model more realistic, the assumption of a perfectly rigid loading apparatus was relaxed. Repeating the analysis for the new condition, the crack was found to propagate with a constant speed until the arrival of the shear wave. At that instant, the crack speed was shown to increase suddenly before decaying eventually to zero. The crack tip acceleration provides an additional amount of crack growth due to the flexibility of the loading apparatus (see Fig. 9b). The ratio of additional crack growth, Δl, to initial notch length, l_o, was found to be a function of the ratio of the flexibility of the specimen to that of the loading device.

Another assumption in the analysis that plays an important role in determining the motion of the crack tip was the fracture toughness dependence of crack tip velocity. If Γ is a monotonically increasing function of v, and if the loading device is stiff, the crack tip speed will vary in discontinuous steps, decreasing gradually between fracture initiation and crack arrest (see Fig.

9c). Further consideration of the effect of the flexibility of the loading device produces the result presented in Fig. 9d: a series of "steady states" is achieved connected by jumps Δl in crack length attributed to the flexibility of the loading device. The steady-state velocities decrease gradually to zero between initiation and arrest.

The last of the cases discussed above is the most realistic, since both the effects of loading flexibility and material inertia are incorporated. Comparison of Figs. 9d and 4 shows that good qualitative agreement exists between the results based on the one-dimensional model and the experimental values of crack length as a function of time. A simple calculation, based on the estimated time for a shear wave to travel from the initiating crack to the pins and subsequently overtake the propagating crack, serves to identify t_A as the time of the arrival of the shear wave. This is illustrated in Figure 5 where a jump in velocity is obtained at point A' corresponding to a jump in the stress intensity factor at point A. In some of the experiments performed, more than one jump in velocity and stress intensity factor was observed. In all specimens tested, the most intense of the jumps was always identified as the one corresponding to the arrival of the shear wave. The other crack tip velocity and stress intensity peaks were not positively identified.

The additional crack length Δl between the two steady states at the instant of arrival of the shear wave is due to loading device flexibility. A simple calculation was performed in which the compliance both of the specimen and of the loading mechanism was determined for the present specimen geometry and the present loading apparatus. Following the analysis in [8], the jump was estimated to be of the order of 10 mm, a value found to hold consistently for all experiments. The results obtained from specimen #9 are shown in Fig. 4.

To demonstrate the difference between experiments performed in steels and experiments performed in polymers, the calculation was repeated for a hypothetical polymer specimen. Both the specimen and loading device configurations were taken as identical to those in the experiments performed with the 4340 steel. For the polymer specimen, the ratio of the specimen flexibility to that of the loading device flexibility is very much lower than for a steel specimen. The calculation indicated that the effect of the reflected shear waves on the crack tip motion is

indeed negligible, and that the loading device can be considered to be perfectly rigid. The prediction is consistent with experiments conducted in polymers and explains the lack of oscillations in the K_{Ic}^{d} and v values for these materials. The discussion clearly demonstrates the advantages gained by keeping the ratio of specimen to loading device stiffness as low as possible.

At the onset of dynamic propagation, the crack accelerates very rapidly from zero velocity to the initial propagation velocity and the crack tip motion differs significantly from steady state. High accelerations at initiation cause the generation of Rayleigh surface waves at the crack tip. These waves propagate along the two faces of the crack surface, i.e., down the cantilever arms, until they reach the corners of the specimen where they are partially reflected. The reflection occurs without a change in phase and with a reflection coefficient of about 0.25 [10]. These reflected waves can overtake the running crack and it has been suggested by various authors that they play an important role in the arrest process [10,11]. The effect of such a reflected wave on the crack tip motion was considered initially by Freund [10]. He concluded that for crack tip velocities greater than 0.3 V_R, where V_R is the velocity of the Rayleigh wave, the drop in the value of the stress intensity factor associated with the arrival of the reflected Rayleigh wave was of the order of 10% of the value of K_I^d at the instant of the arrival. In the present experiments, it was found that crack deceleration or arrest was coupled with the estimated arrival time, t_B, of the reflected Rayleigh wave. This was true for all specimens and is consistent with Freund's analysis. Furthermore, the velocity of propagation just before the arrival of the wave was of the order of 0.3 V_R, and the associated fracture toughness decrease at $t = t_B$, was of the order of 0.1 $K_I^d(t_B)$, as shown in Figs. 5 and 6. The experimental evidence agrees well with the predictions of the analysis and indicates that the Rayleigh waves may play an important role in the crack arrest process.

6. DEVIATIONS FROM THE UNIQUE K vs. v BEHAVIOR

In the spirit of the Workshop, it was felt appropriate to conclude the discussion of the K versus v behavior by considering the results of several investigators that seem to disagree with the

existence of a unique K vs. v relationship.

Figure 10 shows the results of Kalthoff, et al. [4] for Araldite -B and for a HFX 760 high, strength steel. The figure displays the variation of normalized stress intensity factor (upper curves) and crack tip speed (lower curves), versus crack length.

Figure 10a to the left shows the experimental results for Araldite-B. As expected in the testing of polymers, the ratio of loading device stiffness to the specimen stiffness is very high (stiff loading). Such conditions are similar to the ones described by Figure 9c, and no substantial oscillations in stress intensity factor and crack tip velocity are predicted. Indeed no such oscillations are observed experimentally. For such a case a smoothly varying K vs. v curve can be obtained.

Figure 11b displays the results obtained from high strength steel. It corresponds to a much lower loading device to specimen stiffness ratio (compliant loading). Such conditions are very similar to the ones described in Figure 9d, where oscillations in both stress intensity factor and crack tip speed are predicted. The experimental results show the expected oscillations in stress intensity factor but do not show any oscillation in crack tip speed. The observed behavior suggests that a unique K vs. v curve does not exist for the steel tested. Plotting the K versus v behavior from Figure 11b shows a series of discreet straight lines perpendicular to the v axis. The straight lines indicate that the stress intensity factor K may vary without any change in crack tip speed v.

A similar result indicating non unique K vs. v behavior was recently reported by Ravi-Chandar and Knauss [12] who conducted experiments in Homalite-100. Their results, displayed in Fig.11, also show a series of lines normal to the velocity axis. In their experiments the stress intensity factor was also observed to change with time without any change in crack tip velocity.

At this point it is worth stressing that results of this nature, showing a non-unique K vs. v behavior, have only been reported for brittle solids (e.g., brittle polymers or the high strength HFX-760 steel). On the other hand, solids that fail in a locally ductile manner (e.g., the 4340 steel considered in the present work) seem to be well described by a unique K vs. v behavior. A

possible explanation of the observed differences could be sought in the differences in the micromechanics of separation between brittle materials and more ductile solids. In more ductile material the separation process is deformation controlled (separation by void growth) and a ductile crack growth criterion seems to be a good description. This explains the qualitative agreement of the experimental results presented here, and the analysis of Freund and Douglas [5] who employed such a ductile fracture criterion. On the other hand, for a brittle solid the separation process seems to be stress controlled and the fracture criterion must be based on the attainment of a critical stress. For such cases the non-uniqueness in the K vs. v behavior can be qualitatively explained by considering an atmosphere of microcracks propagating with the crack tip as discussed in detail in [12]. From the analytical viewpoint, strong evidence, based on existing elastodynamic solutions, and providing a possible explanation of the observed non-unique behavior for brittle solids, are reported in this volume by Freund [13].

As indicated from the above, additional analytical and experimental work is required for the resolution of the controversy over the existence of a unique K vs. v relation. Further, the accuracy and limitations of the experimental methods used in performing local near tip measurements must be systematically investigated and improved.

REFERENCES

1. Rosakis, A.J., "Experimental Determination of the Fracture Initiation and Dynamic Crack Propagation Resistance of Structural Steels by the Optical Method of Caustics," Ph.D. Thesis, Brown University (1982).

2. Hoover, W.G., and Moran, B., "Applying Molecular Dynamics to Fracture," Proceedings, Workshop on Dynamic Fracture, California Institute of Technology (1983).

3. Beinert, J., and Kalthoff, J.F., "Experimental Determination of Dynamic Stress Intensity Factors by the Method of Shadow Patterns," in Mechanics of Fracture, Vol. 3, G.C. Sih (ed.), Noordhoff International Publishing, Leyden, Netherlands (1979).

4. Kalthoff, J.F., Beinert, J., and Winkler, S., "Analysis of Fast Running and Arresting Cracks by the Shadow Optical Method of Caustics," Proceedings of the I.U.T.A.M. Symposium on Optical Methods in Mechanics of Solids, Poitiers, France (1979) 497-507.

5. Freund, L.B., and Douglas, A.S., "The Influence of Inertia on Elastic-Plastic Antiplane Shear Crack Growth," Brown University Report MRL E-126, February 1982; Journal of the Mechanics and Physics of Solids, 30 (1982) 59-74.

6. Douglas, A.S., "Dynamic Fracture Toughness of Ductile Metals in Antiplane Strain," Ph.D. Thesis, Brown University, (1982).

7. Kobayashi, T., and Dally, J.W., "Dynamic Photoelastic Determination of the a-K Relation for 4340 Alloy Steel," Crack Arrest Methodology and Applications, ASTM STP 711, G.T. Hahn and M.F. Kanninen (eds.), American Society for Testing and Materials (1980) 189-210.

8. Freund, L.B., "A One-Dimensional Dynamic Crack Propagation Model," in Mathematical Problems in Fracture Mechanics, R. Burridge (ed.), American Mathematical Society (1979) 21-37.

9. Freund, L.B., "A Simple Model of the Double Cantilever Beam Crack Propagation Specimen," Journal of the Mechanics and Physics of Solids, 25 (1977) 69-79.

10. Freund, L.B., "Influence of the Reflected Rayleigh Wave on a Propagating Edge Crack," International Journal of Fracture, 17 (1981) R83-R86.

11. Schmuley, F., Peretz, D., and Perl, M., "Effect of Rayleigh Waves in Dynamic Fracture Mechanics," International Journal of Fracture, 14 (1978) R69-R72.

12. Ravi-Chandar, K., and Knauss, W.G., "Processes Controlling the Dynamic Fracture of Brittle Solids," Proceedings, Workshop on Dynamic Fracture, California Institute of Technology (1983). This volume.

13. Freund, L.B., "Some Theoretical Results on the Dependence of Dynamic Stress Intensity Factor on Crack Tip Speed," Proceedings, Workshop on Dynamic Fracture, California Institute of Technology (1983).

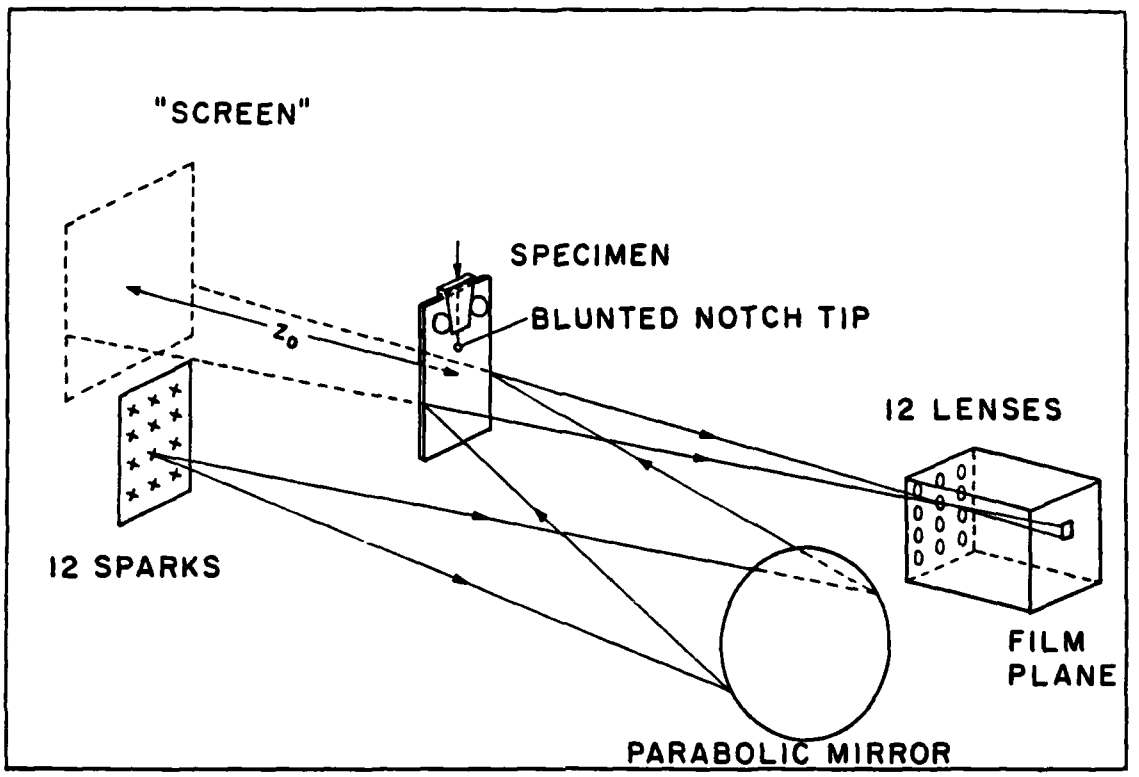

Figure 1. Schematic diagram of the optical set-up.

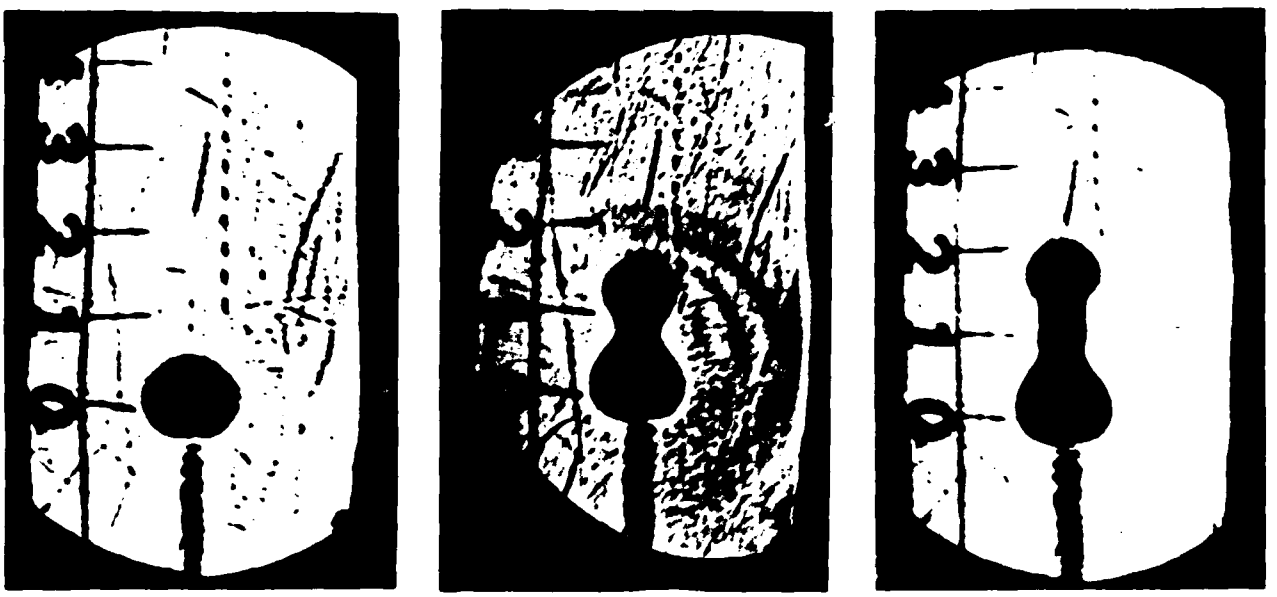

Figure 2. Caustic patterns formed just prior to and after crack initiation.

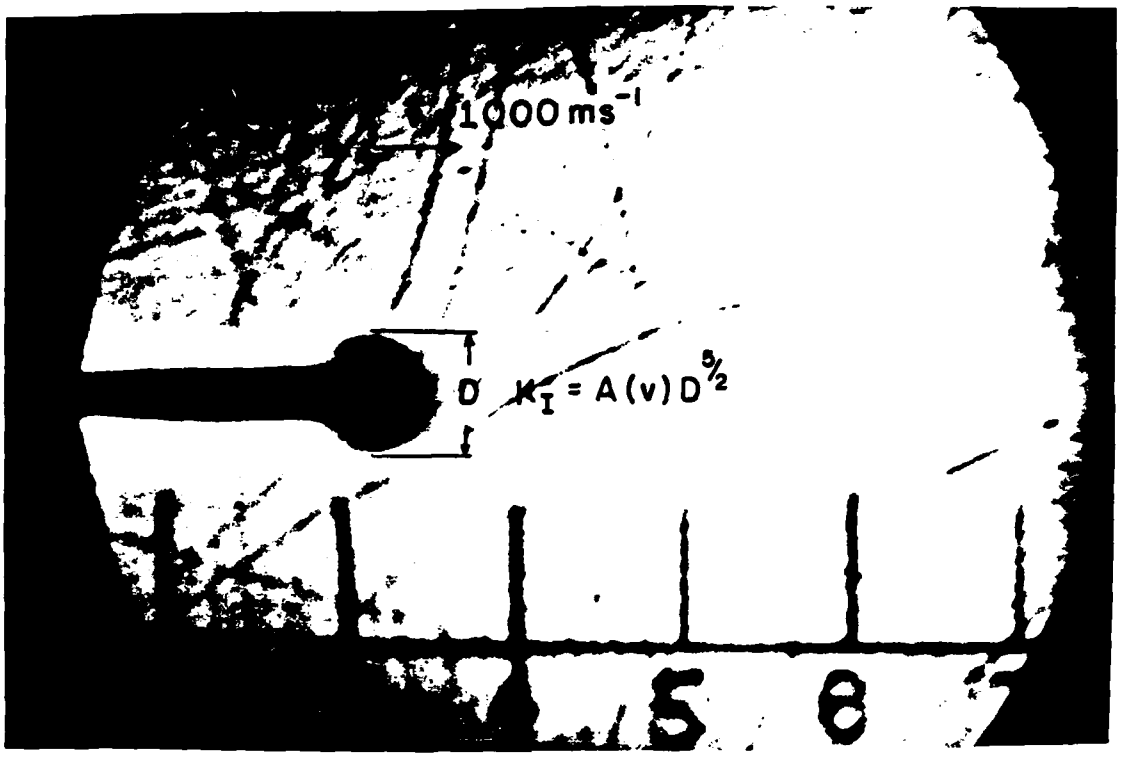

Figure 3. A typical caustic pattern, showing the measurement of D as required to calculate the dynamic stress intensity factor.

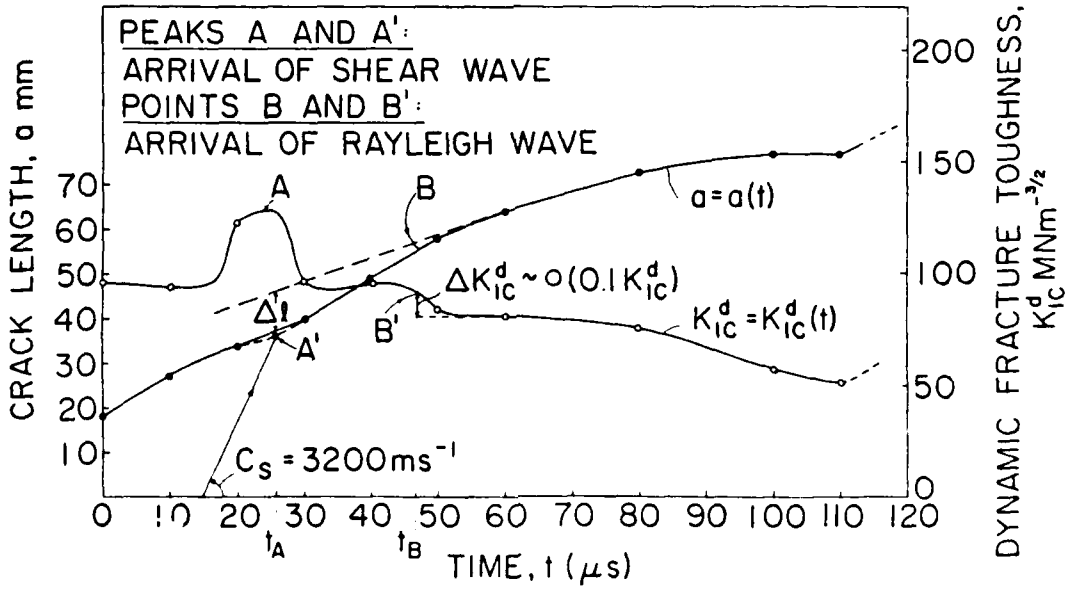

Figure 4. Crack length and dynamic fracture toughness as functions of time (specimen #9).

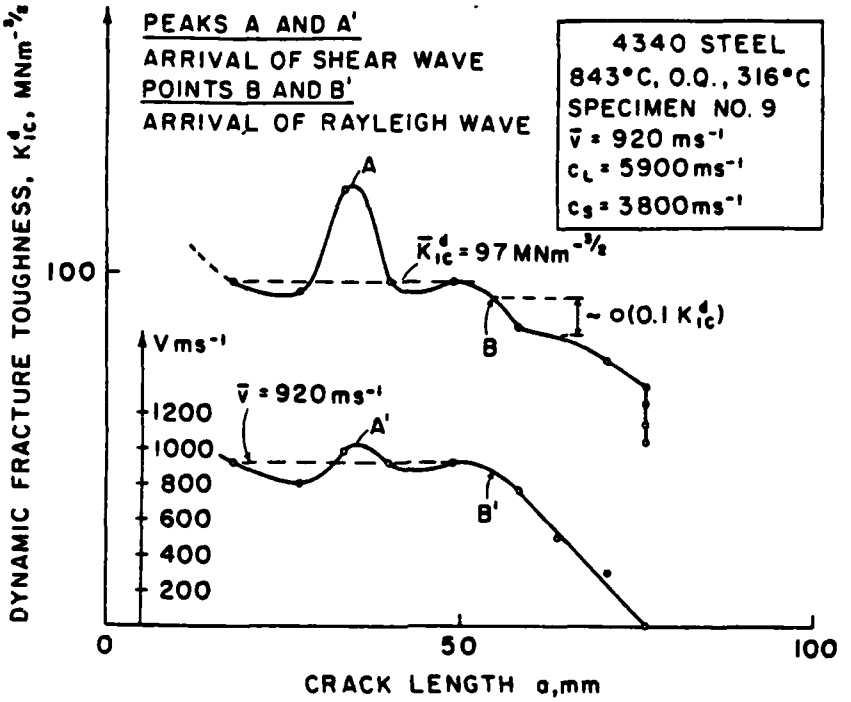

Figure 5. Crack tip speed and dynamic fracture toughness as functions of crack length (specimen #9). The dashed lines indicated by K^d_{Ic} and by v represent mean values of the respective quantities. The letters A and B identify, respectively, the crack lengths at which the reflected shear wave and Rayleigh wave will meet the crack tip.

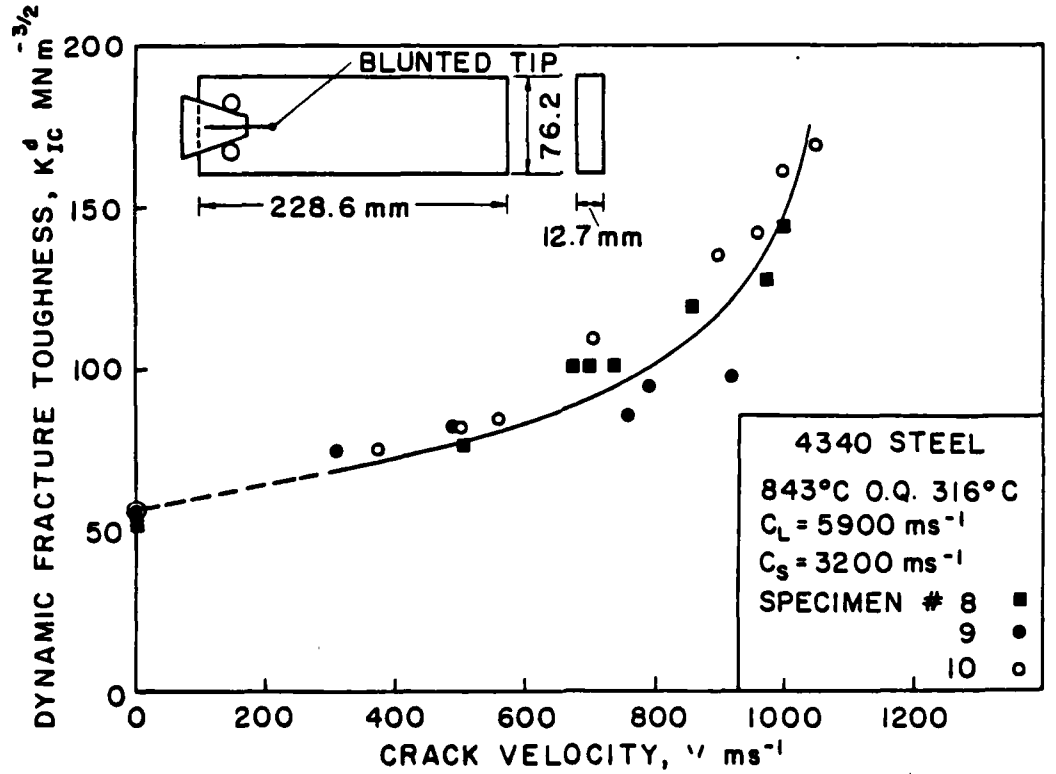

Figure 6. Dynamic fracture toughness as a function of crack tip speed (specimens #8,9,10).

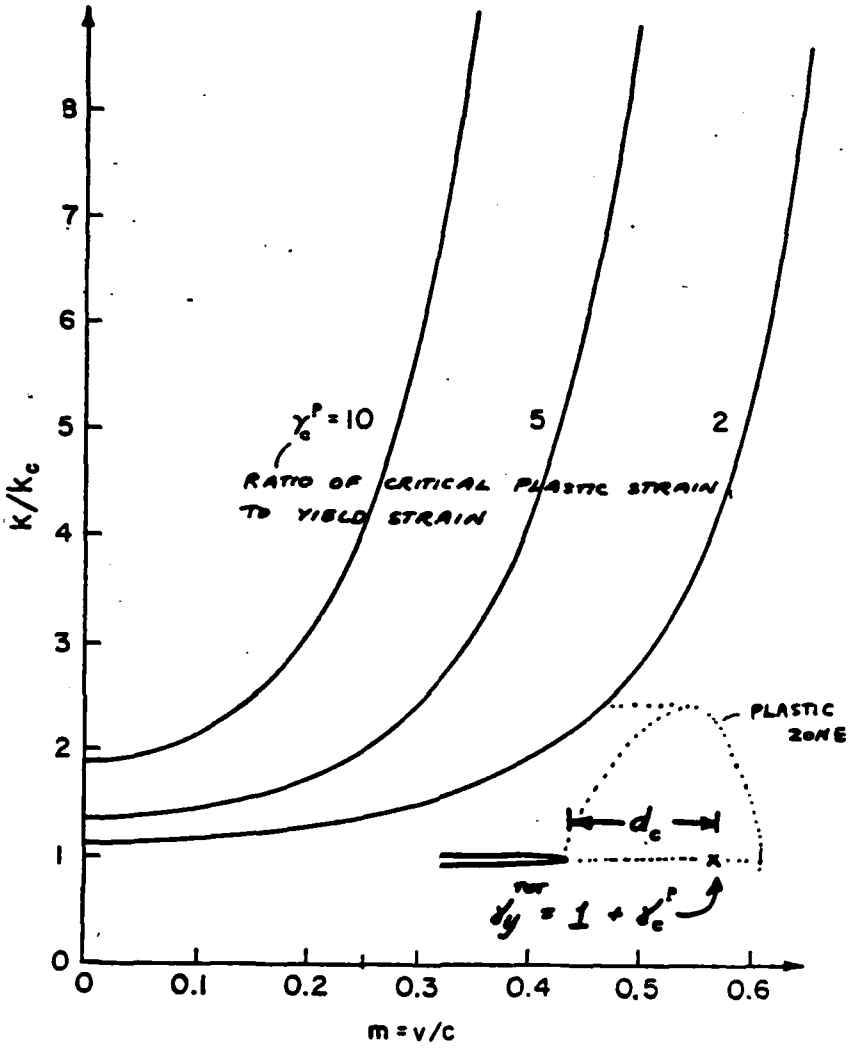

Figure 7. The load level K required to sustain crack growth at speed v according to the "critical strain at a characteristic distance" fracture criterion (from Freund and Douglas [5]).

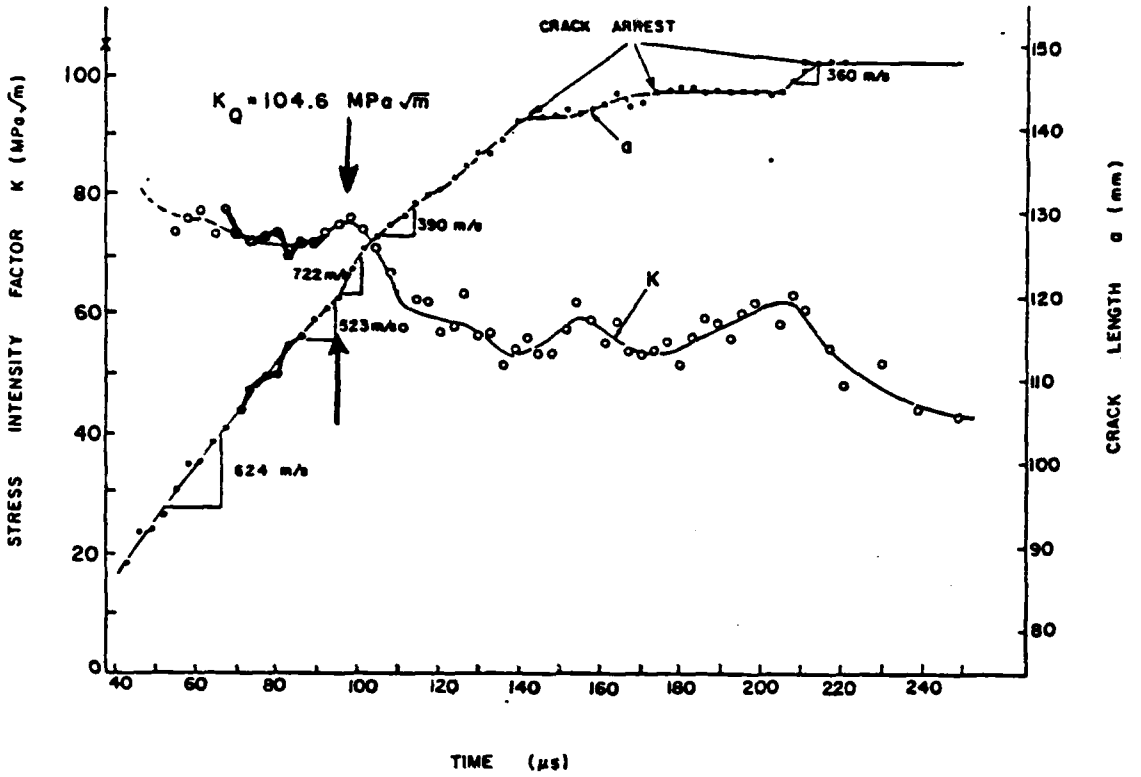

Figure 8. Stress intensity factor K and crack length as a function of time for specimen 362 (from Kobayashi and Dally [7]).

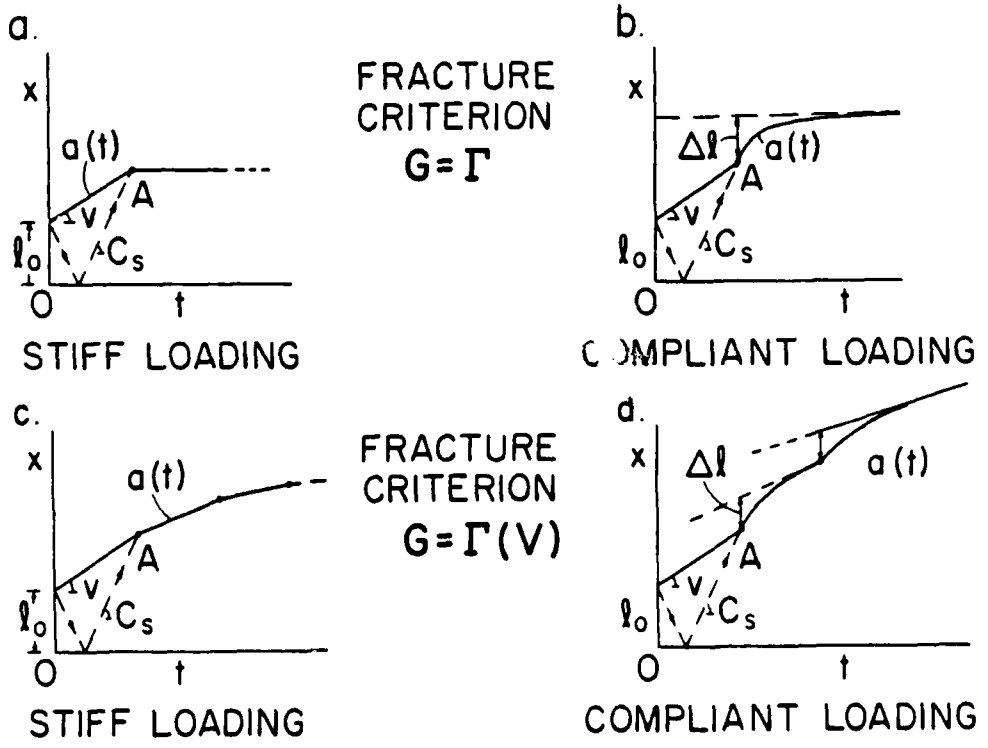

Figure 9. Crack tip motion in DCB specimens.

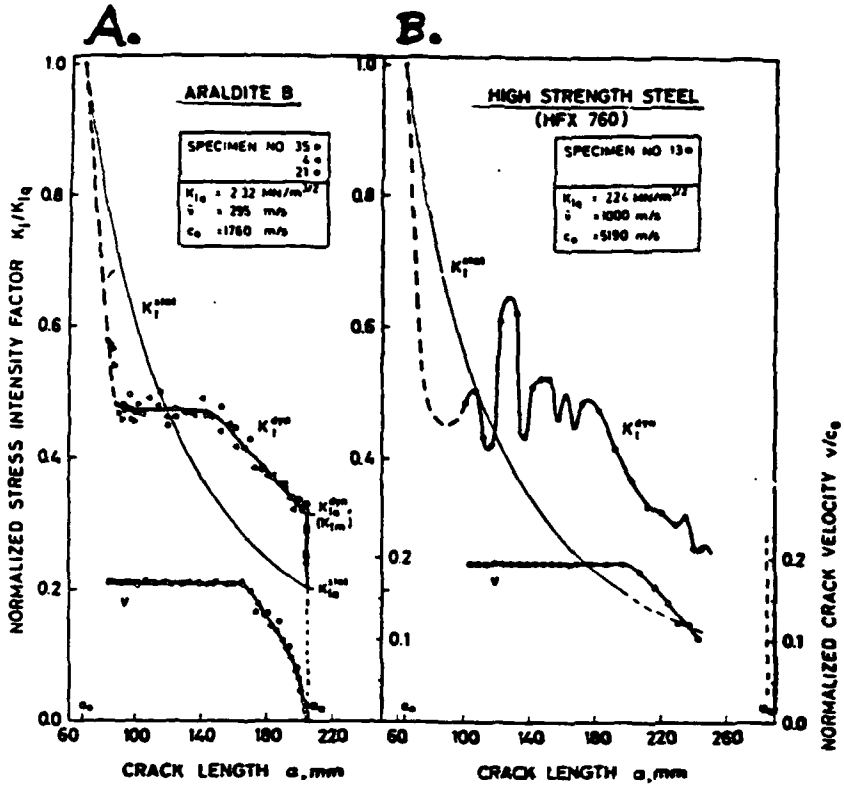

Figure 10. Stress intensity factors for propagating cracks in Araldite B and the high strength steel HFX-760 (from Kalthoff,et al. [3]).

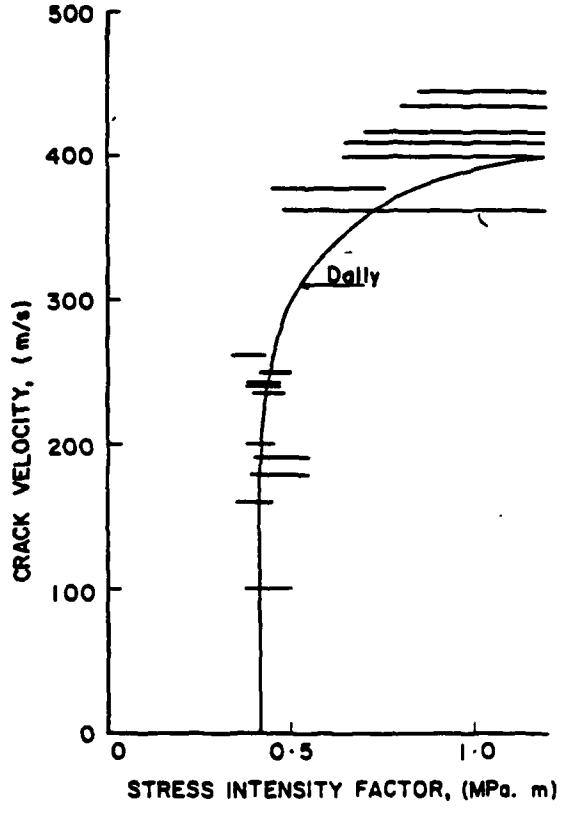

Figure 11. Relationship between the instantaneous stress intensity factor and crack velocity (from Ravi-Chandar and Knauss [12]).

PROCESSES CONTROLLING THE DYNAMIC FRACTURE OF BRITTLE SOLIDS

K. Ravi-Chandar and W.G. Knauss
California Institute of Technology

1. INTRODUCTION

A brief summary of some experimental results on dynamic fracture of brittle solids is presented. A complete presentation of the various aspects of dynamic fracture can be found in [1-5].

2. EXPERIMENTAL PROCEDURE

The experimental configuration used in these experiments simulate pressurized semi-infinite cracks in an unbounded medium (for the duration of the experiment: 150 μsec). The pressure loading on the crack faces is achieved by an electromagnetic loading device. The principle of the method is as follows: A copper strip is doubled up and inserted into a slit machined into a large plate. A high current on the order of several thousand amperes is passed through the copper strip. The current in one leg of the strip interacts with the magnetic field generated by the other leg, and the result is a pressure force on the faces of the machined slit. The current is derived from a capacitor-inductor circuit and the time dependence of the current pulse and hence that of the pressure resembles a trapezoidal history with a 25 μsec rise time and 160 μsec total duration. This device is capable of delivering crack face pressures of up to $\sim$ 60 MPa.

The stresses at the crack tip are determined in terms of the stress intensity factor by the method of caustics. The dynamic fracture process is recorded using a stationary film, rotating mirror type high speed camera, capable of obtaining 128 frames at rates of up to 200.000 frames per second. The exposure time of each frame is 20 nsec. Selected frames from a typical series of high speed cinematographs of the dynamic crack propagation process are shown in Fig.1. From such records, the stress intensity factor history and the crack extension history can be

determined. The reliability of the complete experimental scheme has been investigated in detail and is documented fully in [1].

3. CRACK PROPAGATION RESULTS OR DYNAMIC CRACK GROWTH CRITERIA

Let us first consider the crack propagation problem. It has been suggested that there is a unique relationship between the instantaneous stress intensity factor, K, and the crack velocity, v, which can be considered to be a material property. The analytical basis for such a claim arises from the balance of energy rates at the crack tip. Figure 2 shows such a K-V relationship for Homalite-100, obtained by Dally and co-workers [6]. There have been some doubts raised about such characterization, mainly pertaining to the effects of specimen geometry and the higher order terms in the asymptotic crack tip stress field.

The results of our investigation do not exhibit a one to one relationship between K and V. Two typical stress intensity factor histories and their corresponding crack extension histories are shown in Figure 3. It is seen that while the stress intensity factor changes significantly the velocity remains constant. If these results are plotted on a $K-V$ plane, the horizontal lines shown in Figure 2 are obtained. Furthermore, we find that the velocity of propagation depends on the stress intensity factor at initiation. Changes in the velocity (discontinuous) were found to be caused only by stress waves interacting with the propagating cracks. In order to explain these aspects of crack propagation, it is necessary to study the processes that occur on a microscopic scale and determine the controlling parameters or processes. This is the objective of the next section, and the results of that microstructural investigation will then be used in the last section to describe macroscopic crack propagation behavior.

4. MICROSTRUCTURAL ASPECTS OF DYNAMIC FRACTURE

A detailed examination of the fracture surface shows that the roughness of the surface increases continuously along the crack path (as illustrated in Figure 4). It should be noted that all along this path the crack velocity was constant and only the stress intensity factor increased monotonically. Therefore, the fracture surface roughness should be related directly to the stress

intensity factor. The roughness of the fracture surface results from "independent" fracture origins at the front of the main crack. Such fracture sources generate many of the parabolic and hyperbolic markings. That these fracture sources do indeed occur ahead of the main crack was verified by direct real time photography. Figure 5 shows projected views of the crack front viewed at an angle of 45° with respect to the specimen. The three photographs are representative of conditions of low, medium and high stress intensity factors. The dark regions at the intersection of the crack front with the specimen surfaces are shadow areas; the scallops at the front of the main crack are also caustics generated by the local point fractures ahead of the main crack. It is clear that at a low stress intensity factor the crack front assumes the curved shape typical of quasi-static cracks. At higher stress intensities the average crack is straight; it is, however, no longer appropriate to speak of a single crack front but rather of a front of a crack ensemble.

The high speed photomicrography used in capturing crack front evolution described above was also used to study the evolution of crack branching. In this case, the camera was focused onto a very small region where crack branching was expected. One observes then a through-the-thickness view of all the microcracks. Figure 6 shows tracings from high speed micrographs of a branching event. One observes that

a. a number of attempted branches exist

b. the microbranches evolve continuously from planes parallel to the main crack planes and

c. only a few of them grow larger while the rest are arrested.

From post-mortem examination, we also know that the microbranches do not span the plate thickness, some occurring on the faces of the plate while others are entirely in the middle of the plate. The branching phenomenon is then truly a three-dimensional problem. Figure 7 shows a frame from another branching event, at a higher magnification. The continuous change in the direction of growth of branches is evident.

5. DISCUSSION

With the microstructural aspects of the dynamic fracture process described in the previous section, we now attempt to describe crack propagation behavior. We believe that the rate of growth, coalescence and interaction of microcracks in the fracture process zone essentially control the dynamic fracture process.

Let us first consider the constancy of the velocity of crack propagation. As the stress intensity factor increases prior to crack initiation, the high stresses ahead of the crack tip induce microfractures, and the value of the stress intensity factor at initiation then establishes the size and general geometry of the fracture process zone. Thereafter, the crack propagates due to the interaction of and communication between these microcracks in the fracture process zone. As the stress intensity factor increases further, two consequences are possible: First the rate of microcrack coalescence could increase, thus leading to faster crack propagation (with a constant process zone). Secondly, the process zone could increase in size, leaving the crack velocity constant. In our experiments, it seems that when the stress intensity factor varies slowly, the latter mechanism operates.

The microcrack growth model of dynamic crack propagation also describes the crack branching phenomenon. The proposed mechanism is illustrated in Figure 8. As the stress intensity factor increases, the voids ahead of the crack experience high stresses and start to grow ahead of the main crack. The size of the zone of damage in which microcracks nucleate depends on the stress intensity factor. Significant interaction of stress fields of these microcracks occurs and this is suggested as the reason for microcracks deviating from main plane of propagation into microbranches. While no analytical solutions to the problem of dynamically interacting cracks exist, some idea of the naure of crack interaction may be gleaned from the quasi-static interaction solution by Pucik [7]. This solution shows that for two parallel cracks with a separation distance much smaller than their length, the cracks tend to deviate from each other markedly. Once a number of microbranches have been established, one would expect them to communicate through stress waves. If all of them were of equal size geometrical instability would permit only a

few of the microbranches to propagate. In reality, the microbranches vary in size and thus the larger ones are more likely to develop into full fledged branches. This points to some statistical effects in branching which is indeed evident to a small extent in our measurements: Under the same loading conditions, there is a variability in the branch location as well as in the branch angle close to the branch point.

ACKNOWLEDGEMENT

This work was performed under a program entitled "Fundamental Experiments in Dynamic Fracture," sponsored by the National Science Foundation. We also acknowledge gratefully the Office of Naval Research support under contract no. N00014-78-C-0634 during part of this investigation in conjunction with a parallel effort on dynamic fracture in viscoelastic solids.

REFERENCES

[1] Ravi-Chandar, K. and Knauss, W.G., "Dynamic Crack Tip Stresses under Stress Wave Loading - A Comparison of Theory and Experiment," International Journal of Fracture, 20 (1982) 209-222.

[2] Ravi-Chandar, K. and Knauss, W.G., "An Experimental Investigation into Dynamic Fracture - I. Crack Initiation and Crack Arrest," GALCIT SM Report No. 82-8, California Institute of Technology, September 1982.

[3] Ravi-Chandar, K. and Knauss, W.G., "An Experimental Investigation into Dynamic Fracture - II. Microstructural Aspects," GALCIT SM Report No. 82-9, California Institute of Technology, October 1982.

[4] Ravi-Chandar, K. and Knauss, W.G., "An Experimental Investigation into Dynamic Fracture - III. On Steady State Crack Propagation and Branching," GALCIT SM Report No. 82-3, California Institute of Technology, March 1983.

[5] Ravi-Chandar, K. and Knauss, W.G. "An Experimental Investigation into Dynamic Fracture - IV. On Stress Wave Interaction," GALCIT SM Report No. 82-4, California Institute of Technology, May 1983.

[6] Dally, J.W., "Dynamic Photoelastic Studies of Fracture," Experimental Mechanics, 19 (1979) 349-381.

[7] T.A. Pucik, Ph.D. Thesis, California Institute of Technology, Pasadena, 1972.

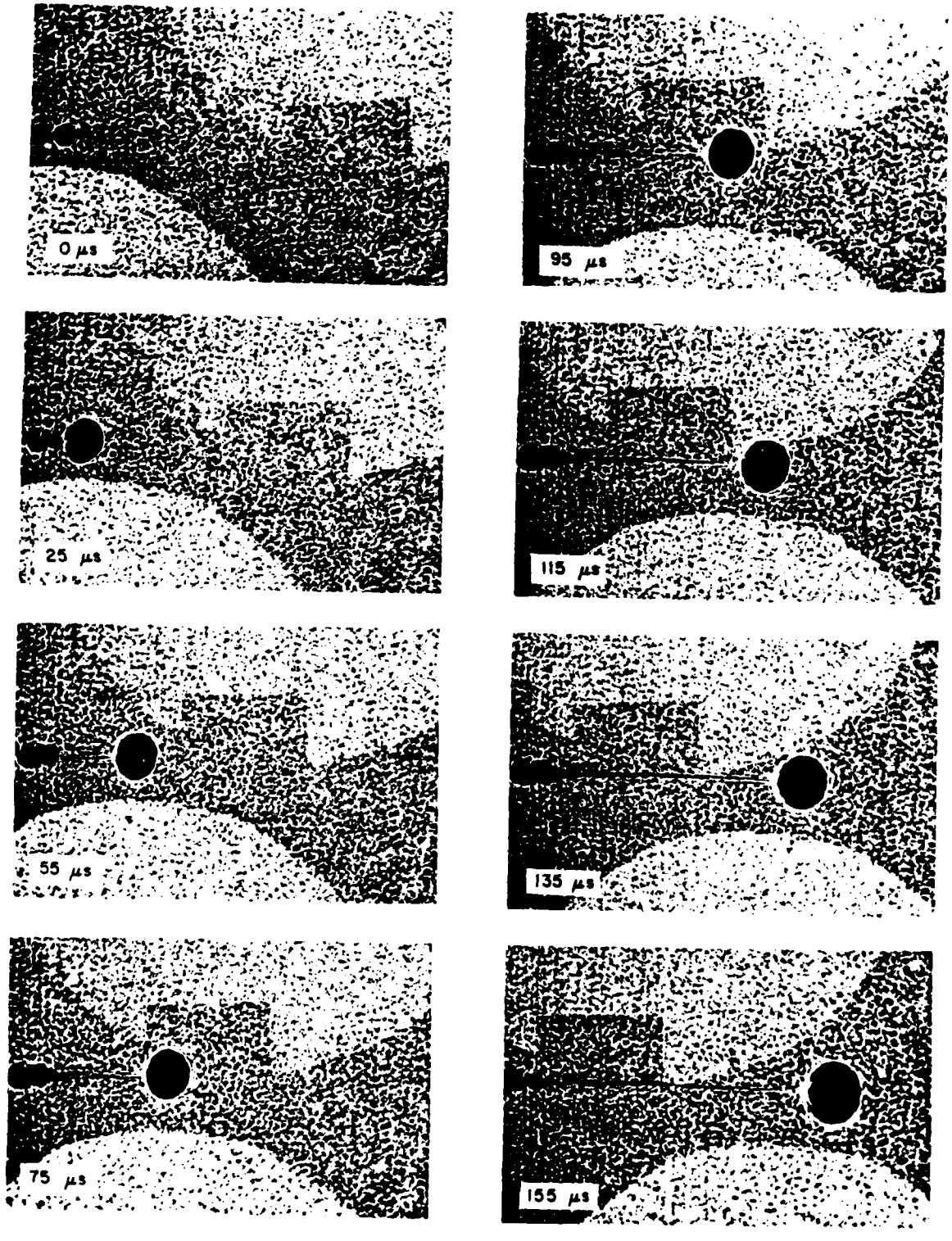

Figure 1. High speed cinematographs of a running crack.

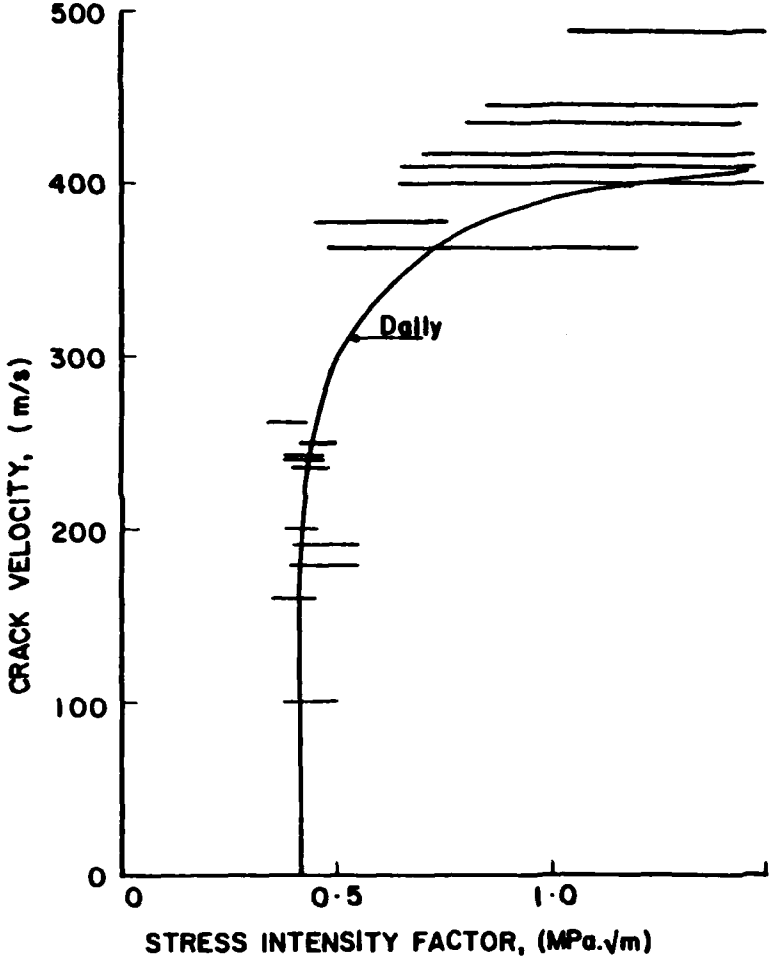

Figure 2. Stress intensity factor velocity relationship.

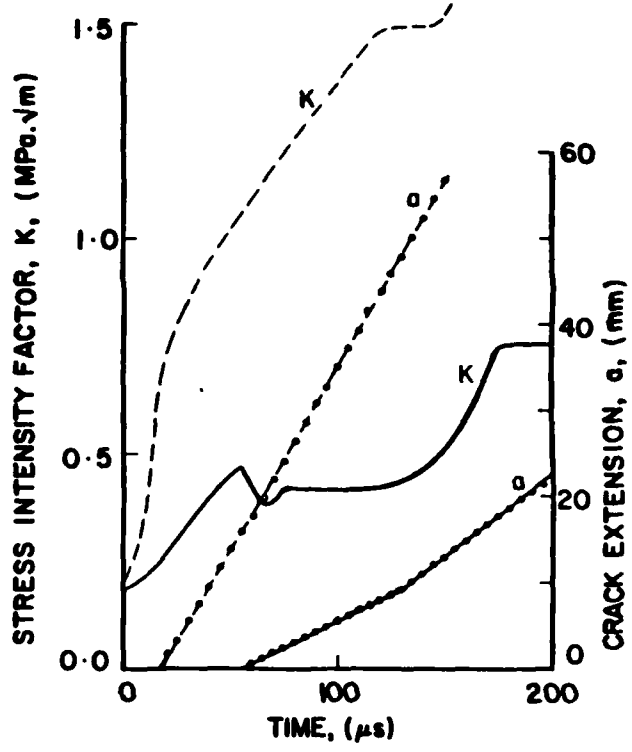

Figure 3. Stress intensity factor and crack extension histories.

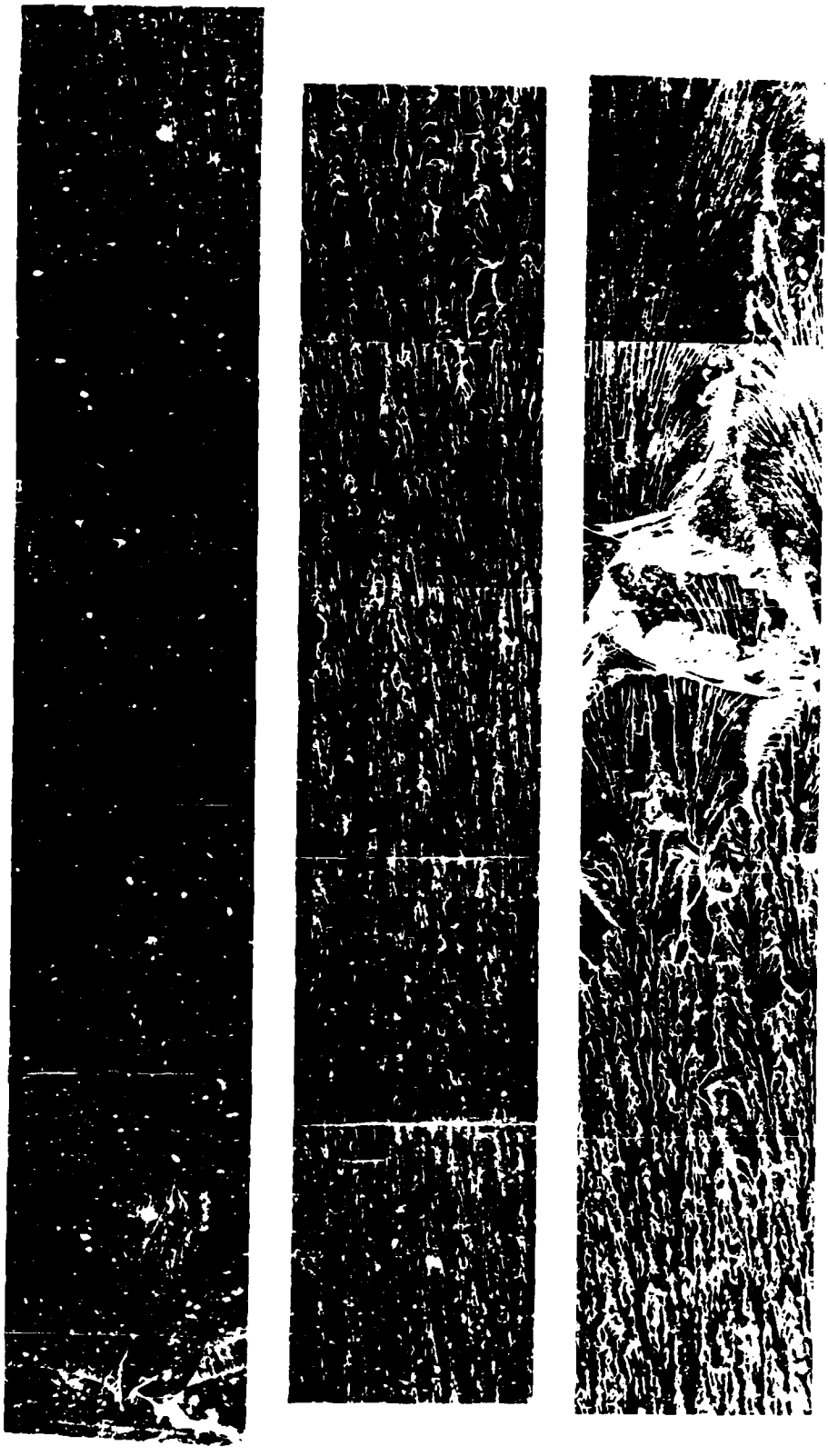

Figure 4. Fracture surface appearance.

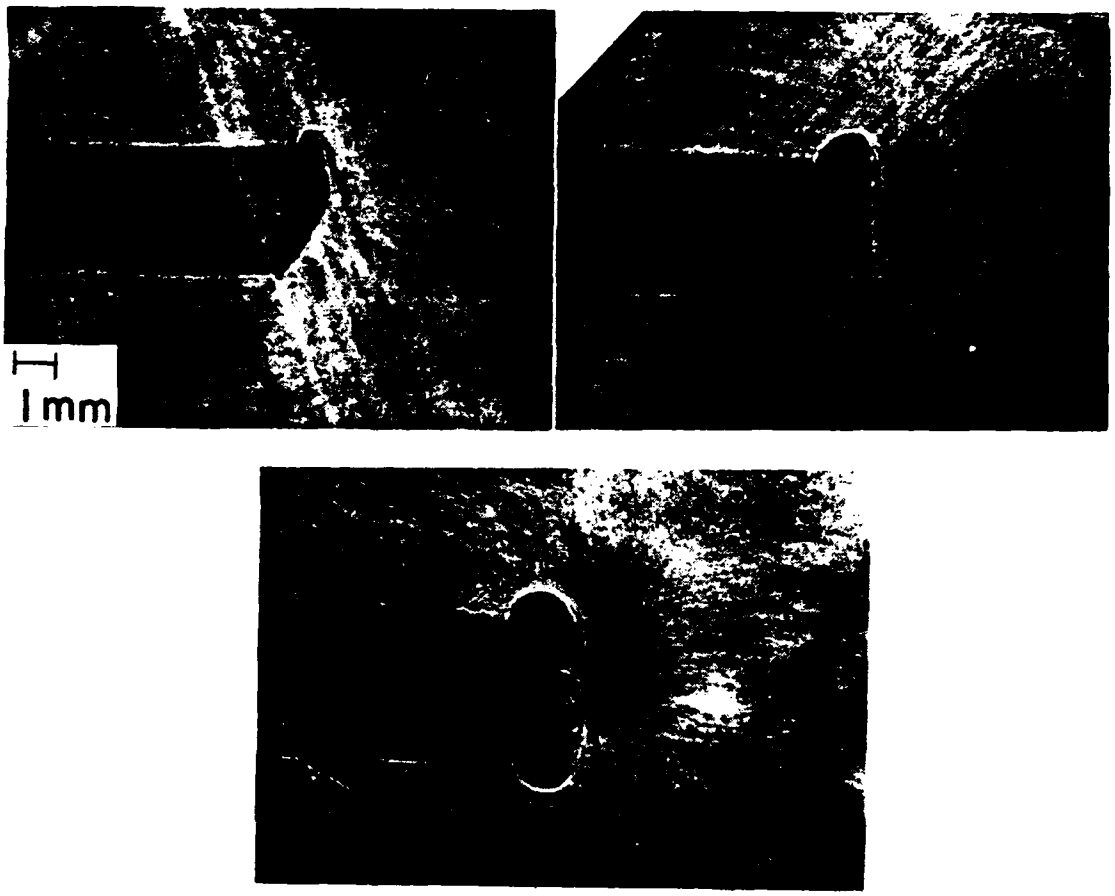

Figure 5. High speed photographs of crack front.

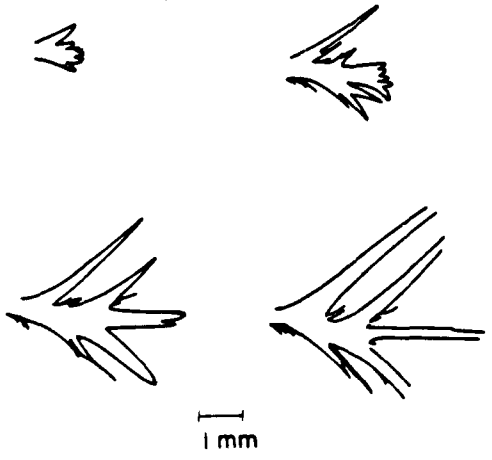

Figure 6. High speed micrograph of crack branching.

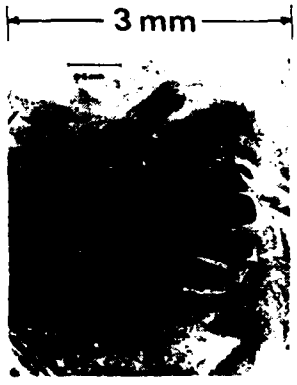

Figure 7. High speed micrograph of crack branching.

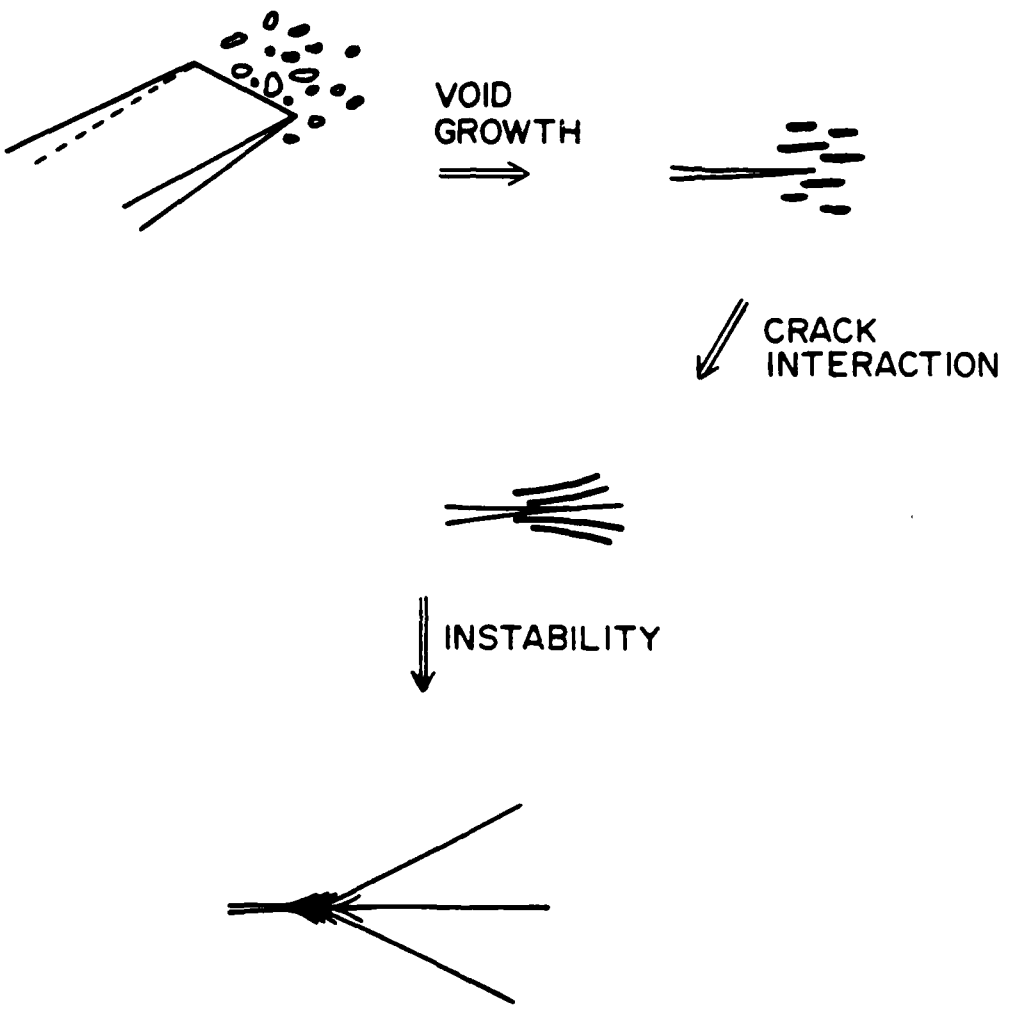

Figure 8. Crack branching mechanism.

SOME THEORETICAL RESULTS ON THE DEPENDENCE OF DYNAMIC STRESS INTENSITY FACTOR ON CRACK TIP SPEED

L.B. Freund
Division of Engineering
Brown University

1. INTRODUCTION

Two specific topics are discussed under this common heading. The first is concerned with elastic-plastic crack growth and, in particular, with developing theoretical models to explain the dependence of dynamic fracture toughness on crack tip speed observed for 4340 steel [1] and other high strength, low ductility materials which fail in a locally ductile manner. The second topic is concerned with limitations on the use of crack tip singular fields to describe actual stresses in elastic brittle materials during dynamic fracture. The analyses described in this connection are motivated by the experimental results on Homalite 100 reported by Ravi-Chandar [2].

2. DYNAMIC ELASTIC PLASTIC CRACK GROWTH IN ANTIPLANE SHEAR

The problem discussed is the steady-state growth of a crack in the antiplane shear mode under small scale yielding conditions. Inertial resistance of the material is taken into account explicitly but, for steady state growth, the deformation is time independent as viewed by an observer fixed at the moving crack tip. Results are considered for two material models, elastic-ideally plastic and elastic-viscoplastic. According to the small scale yielding hypothesis, the (possibly nonlinear) crack tip stress and deformation fields are controlled by the surrounding elastic field. The commonly used measure of this surrounding field, for any given crack tip speed v, is the linear elastic stress intensity factor K. For present purposes, the value of the stress intensity factor is assumed to be known in terms of the body geometry and applied loads from a suitable elastic crack problem.

The field equations governing this process include the equation of momentum balance, the strain-displacement relations, and the condition that the stress distribution far from the crack tip must be the same as the near tip stress distribution in a corresponding elastic problem. For elastic-ideally plastic material response, the stress state is assumed to lie on the Mises yield locus, and stress and strain are related through the incremental Prandtl-Reuss flow rule. The material is linear elastic outside of plastically deformed regions. The full set of field equations is presented in [3].

With a view toward deriving a theoretical relationship between the crack tip speed and the imposed stress intensity factor required to sustain this speed according to a critical plastic strain crack growth criterion, attention was focused on (a) the strain distribution on the crack line in terms of the plastic zone size and (b) the relationship between the remote applied stress intensity factor and the plastic zone size. It was found that the strain distribution on the crack line could be determined exactly, and results are presented in [3] and [4]. The main observation on the strain distribution is that the level of plastic strain is significantly reduced from its corresponding slow crack growth levels due to material inertia. This implies that, if a fixed level of plastic strain is to be maintained at a given distance ahead of the crack tip for growth to occur, then the level of applied stress intensity factor would necessarily increase with increasing crack tip speed. To quantify this idea, the remote applied stress intensity factor was related to the plastic zone strain distribution through a full-field numerical solution; see [3] for details. The main result is reproduced in Fig. 1, which gives the value of stress intensity factor K required to drive crack growth steadily at speed v according to a critical plastic strain at a characteristic distance growth criterion [5]. The material parameters appearing in Fig. 1 are the elastic shear wave speed c, the yield strain γ_o, the critical plastic strain γ_1, and the level of applied stress intensity K_1 required to satisfy the same fracture criterion for a stationary crack under quasi-static conditions in the same material. Results are shown for three levels of critical plastic strain. Each curve in Fig. 1 represents a theoretical fracture toughness versus crack speed relationship for a material which fails in a locally ductile manner. The general features of this relationship are consistent with the

limited data on dynamic growth in relatively rate insensitive steels as presented by Dahlberg, Nilsson and Brickstad [6], Kobayashi and Dally [7], and Rosakis, Duffy and Freund [1].

A similar analysis has been carried out for an elastic-viscoplastic material model. The material is essentially the power-law overstress material introduced by Malvern [8], with the additional feature that unloading (i.e., reduction in magnitude of the effective stress) can only occur elastically. The material model is described in detail in [9]. No features of the deformation field have been determined exactly in this case, and all results have been obtained by means of the numerical finite element method. One particularly interesting observation which follows from this material model concerns the level of strain within the active plastic zone, compared to the strain level for the equivalent rate-insensitive material at the same level of applied stress intensity factor and same crack tip speed. It is found that for points away from the crack tip the effect of rate sensitivity is to reduce the strain, while for points near to the tip the effect is to increase the strain. The distance of this "cross over point" from the tip compared to the characteristic distance in the ductile growth criterion is important in assessing the influence of rate sensitivity on theoretical toughness or applied stress intensity levels.

3. STRESS HISTORIES ASSOCIATED WITH TRANSIENT CRACK GROWTH

Suppose that a crack in a planar elastic brittle solid suddenly begins to grow under the action of applied loads. The resistance of such materials to crack growth is commonly expressed in terms of the actual values of the stress intensity factor during growth. Data on deformations in the crack tip region are frequently obtained by measurements involving optical techniques. Measurements are typically made over a plane region with transverse dimensions varying from a few millimeters to a centimeter or more, and toughness values are inferred by assuming that some theoretical near tip field is fully established over the region of observation. The actual time required for such a field to become established is an important element in the interpretation of rapid crack propagation experiments, and some preliminary calculations have been performed in order to estimate this time. Two representative results are described below.

Consider a half-plane crack in an unbounded elastic solid under plane strain conditions. The crack faces are subjected to equal but opposite point loads of magnitude P which are applied at a distance L behind the crack tip and which tend to separate the crack faces. No other loads act on the solid, and the material is initially at rest. At time t = 0 the crack begins to extend with constant crack tip speed, v, and attention is focussed on the component of stress s_{22} normal to the plane of the crack at some material point on the prospective fracture plane. An exact solution of this problem is given in [10].

A typical result is shown in Fig. 2 for crack tip speed equal to 30% of the longitudinal wave speed of the material c_1 and for an observation point at a distance of 0.75 L from the initial position of the crack tip. The normalized stress $s_{22}L/P$ has the initial static value until the first wave arrival at normalized time $tc_1/L = 0.75$. The stress decreases slightly upon arrival of the longitudinal wave, and it decreases further upon arrival of the shear wave at time 1.3. The stress does not increase above its initial value until after a point travelling from the initial position of the crack tip with the Rayleigh speed passes the observation point. Thereafter, the stress increases rapidly. The dashed curve in Fig. 2 is the stress which would be predicted by the stress intensity factor controlled singular solution alone.

The general features of the stress history in Fig. 2 can be explained in terms of well-known results in wave propagation. The initial transient in the process is the sudden application of large compressive loads (i.e., the sudden release of large tensile stresses ahead of the tip). The dilatational response is compressive, and this accounts for the initial reduction of stress in Fig. 2. Only after the shear wave passes does the stress history begin to approach the corresponding K-controlled stress history. The result in Fig.2 is typical in that the complete stress history was less than the singular stress history for all combinations of crack speed and observation distance which were considered.

As the basis for a second sample calculation, again consider a half-plane crack in an unbounded elastic solid under plane strain conditions. The material is initially at rest and stress

free. The crack faces are then subjected to a spatially uniform suddenly applied pressure at time t=0. At some later time, say $t=t_o$, the crack begins to grow with crack tip speed v. As the crack grows, the pressure does not spread; that is, it continues to act only over the initial crack faces. An exact solution of this problem is given in [11].

Attention is focused on a moving point which is always a fixed distance, say β, ahead of the moving crack tip. Of particular interest is the time required for the stress level at this point obtained from a complete stress distribution to approach the stress level obtained from the stress intensity factor controlled singular distributions. A graph of the ratio of these two stress levels versus time is shown in Fig. 3. The nondimensional delay time is $t_o c_1/\beta = 50$ and the crack speed is $v = 0.20\ c_1$. The time required for the ratio to approach unity is surprisingly large. For example, if $c_1 = 2000 m/s$ and $\beta = 2 mm$ then the ratio becomes 0.9 about 30 microseconds after initiation, and it becomes 0.95 about 70 microseconds after initiation. For high rate fracture phenomena, this is a significant observation time and the result suggests that the times over which shadow spot or photoelastic near tip data can be interpreted on the basis of a singular crack tip solution are subject to some constraints. Further work is required in order to quantify these limitations.

ACKNOWLEDGEMENT

The research summarized here was supported by the National Science Foundation (Solid Mechanics Program) and by the NSF Materials Research Laboratory at Brown University. The calculations leading to Fig. 3 were performed by C.C. Ma, Research Assistant at Brown University.

The computations were performed on the VAX11/780 Engineering Computer Facility at Brown University. This facility was made possible by grants from the National Science Foundation, the General Electric Foundation, and the Digital Equipment Corporation.

REFERENCES

1. Rosakis, A.J., Duffy, J., and Freund, L.B., "Determination of the Fracture Initiation and Crack Propagation Resistance of Structural Steels by the Optical Method of Caustics," Brown University Report, September 1982.

2. Ravi-Chandar, K., "An Experimental Investigation into the Mechanics of Dynamic Fracture," Ph.D. Thesis, California Institute of Technology (1982).

3. Freund, L.B. Douglas, A.S., Journal of the Mechanics and Physics of Solids, 30 (1982) 59-74.

4. Dunayevsky, V., and Achenbach, J.D., International Journal of Solids and Structures, 18 (1982) 1-12.

5. McClintock, F.A., and Irwin, G.R., in Fracture Toughness Testing and Applications, ASTM STP 381 (1965) 84-113.

6. Dahlberg, L., Nilsson, F., and Brickstad, B., in Crack Arrest Methodology and Applications, G. Hahn and M. Kanninen (eds.), ASTM STP 711 (1980) 89-108.

7. Kobayashi, T., and Dally, J.W., ibid., 189-210.

8. Malvern, L.E., Journal of Applied Mechanics, 18 (1951) 203-208.

9. Freund, L.B., and Douglas, A.S., "Dynamic Growth of an Antiplane Shear Crack in a Rate Sensitive Elastic-Plastic Material," in Elastic-Plastic Fracture Mechanics, J. Gudas and C.F. Shih (eds.), ASTM STP, to appear.

10. Freund, L.B., Journal of the Mechanics and Physics of Solids, 20 (1982) 129-140.

11. Freund, L.B., Journal of the Mechanics and Physics of Solids, 21, (1973) 47-61.

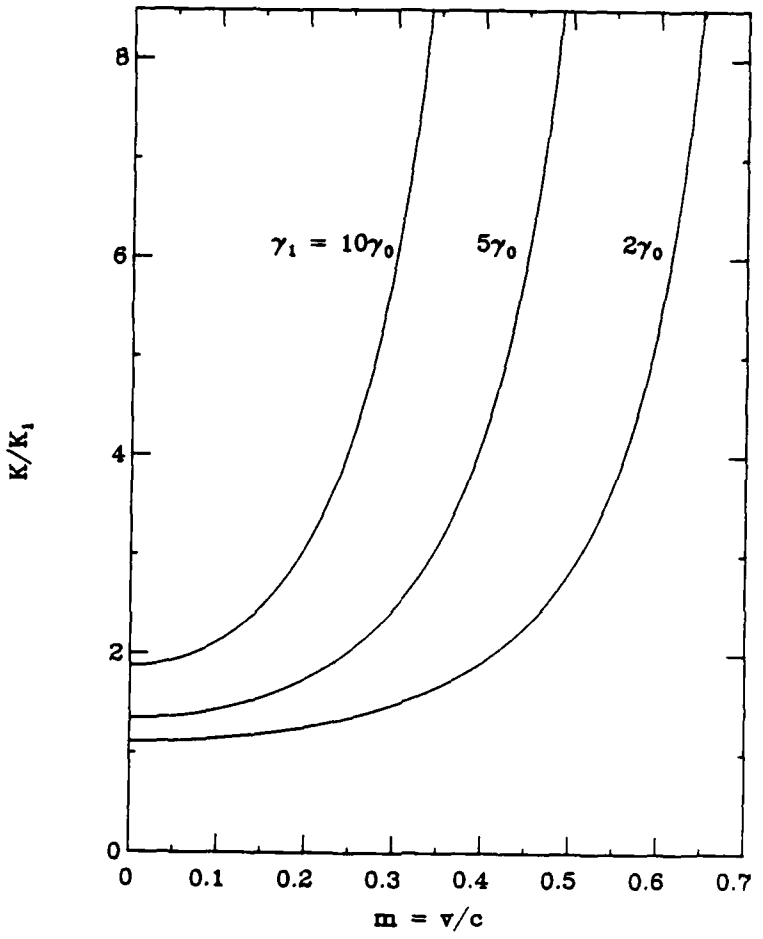

Figure 1. The applied stress intensity level required to sustain steady crack growth according to a critical plastic strain at a characteristic distance criterion.

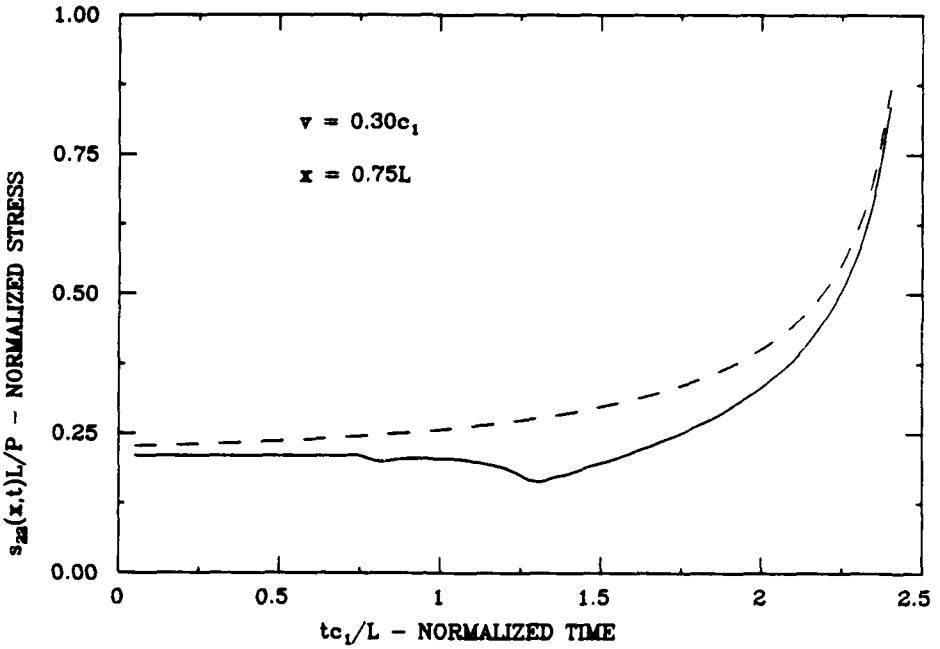

Figure 2. An example of the tensile traction at a material point on the prospective fracture plane versus time for dynamic crack growth with time-independent loading.

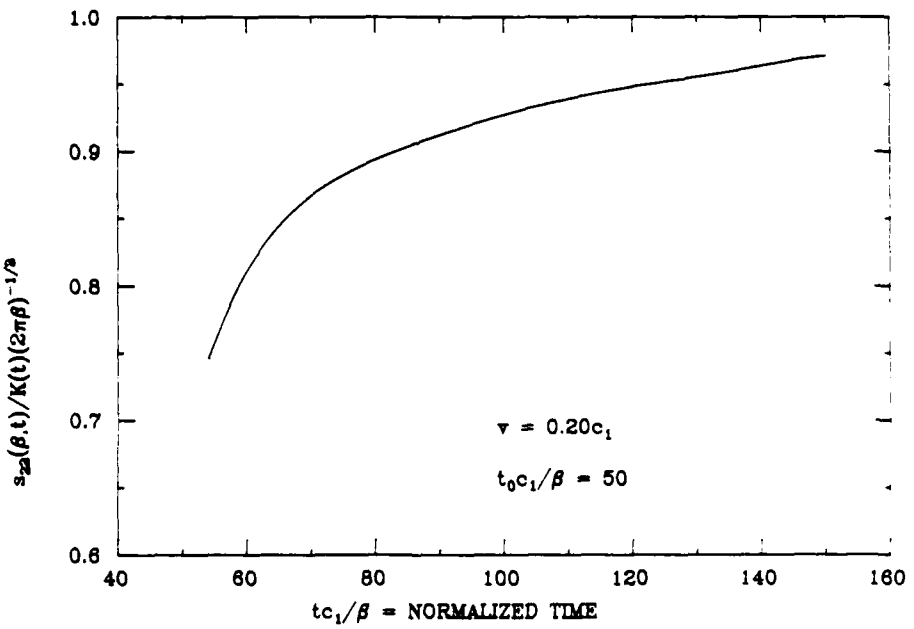

Figure 3. An example of the ratio of traction on the prospective fracture plane at a fixed distance ahead of the moving crack tip to the traction due to the singular solution alone versus time for dynamic crack growth with transient loading.

SYNOPSIS OF SESSION III: CRACK PROPAGATION AND BRANCHING

Carl Popelar and the Organizers
Ohio State University,
California Institute of Technology

In many instances a knowledge of the way in which crack paths develop are useful, primarily when one wishes to deduce from a "post mortem" investigation what the state of stress was in a structure as the crack grew. Similarly it is important, for example in comminution problems, to understand the reason for successful or unsuccessful crack branching events. In this context K.B. Broberg discussed crack path problems, primarily from the quasi-static point of view. Crack path stability is discussed as a more global phenomenon rather than the local occurrence envisioned by Cotterel and Rice; consequential differences are pointed out between the two criteria. Examples based on a periodic array of cracks suggest that collinear cracks may not tend to coalesce readily, a thought of importance in the process of microcrack coalescence at the tip of a macrocrack.

The effect of stress state with compressive component(s) was considered when friction affects the growth process much as is prevalent in rock or seismic problems. Friction can have a marked effect on the direction in which cracks can grow.

In a contribution to understanding the branching process K.B. Broberg recounted analytical-numerical work by Pärletun. The essence of that work showed that the pre-branch velocity of the crack has a possibly strong effect on the arrest of (off-axis) branches or their success to lead to full branches: Low speed cracks (20% of C_d) tended to arrest at the expense of the growth of the main crack, while for a crack speed of 65% of C_d multiple crack paths were sustained. These computations, though based on the K_B-vs $\dot{c}$ relation for PMMA, which relation may not exist as discussed in Session II, tended to be in general agreement with some experimental observations on crack branching (see e.g. synopsis for Session II).

An alternative approach to the analytical modeling of crack branching was taken by P. Burgers who considered a two dimensional self-similar model for the process. His approach was based on the approximation of small scale yielding and assumes that the region in which bifurcation attempts are made is small with respect to any characteristic length of the problem. His analytical predictions, coupled to the crack branching criterion $K_{II}^{BRANCH} = 0$, give bifurcation angles of about 10^o with the original crack axis. Comparison with results presented in Session II shows reasonable agreement with experiment and also justifies the use of the branching criterion. It is also worth noting here that on the cover page of this volume the caustics for the branched cracks exhibit no apparent Mode II deformation.

In parallel to the application of path independent integral(s) in quasi-static fracture problems the formulation of integrals and their path independence for dynamic problems were discussed in connection with numerical (FEM) solutions by S. Atluri. For linearly elastic bodies the dynamic stress intensity factors K_{ID} and K_{IID} were computed as an example. Work on the non-linear counterpart is in progress. However, reservations were expressed by members of the audience regarding physical interpretation of some of the resulting expressions. Additional comments by G. Herrmann alluded to the potential usefulness of contour integrals encompassing cracks entirely instead of the crack tip alone.

The application of dynamic fracture concepts to the failure of ceramic heat engine components was discussed by A. Kobayashi. It was observed that in contrast to the growth behavior in polymers and metals a crack acceleration phase exists in ceramics. Reaction bonded silicon nitride, the ceramic used in the tests, exhibits an atypical K-$\dot{c}$ that was double valued: In fact a decrease in the stress intensity factor resulted in lower crack growth rates but did not even lead to arrest at an intensity level below that required for crack initiation. A. Kobayashi also discussed the effect of plastic deformation in the interpretation of experiments.

The effect of a narrow, plastically deformed region ahead of the crack tip is to distort the isochromatics obtained in photoelastic experiments. If (distorted) isochromatics are generated

analytically using a Dugdale line plastic zone model they seem to compare favorably with the experimental isochromatics in the far field.

ON CRACK PATHS

K.B. Broberg
Lund Institute of Technology

1. INTRODUCTION

In general the direction of crack propagation depends upon the propagation velocity, the ambient stress state (including its time variation), and the processes in the process region.

In several cases the propagation velocity plays an insignificant role. These cases include certain fractures of thin plates at which the crack direction is outlined as a band of necking already before start of unstable crack growth. They also include certain fractures at plane strain, when the crack direction seems to be determined essentially by symmetry relations.

In some cases the influence of the propagation velocity on crack directions is obvious but still of minor interest. These cases include stability questions of the type: "Is the straight path stable or not?" Then the answer "Yes" or "No" is of primary interest, not the precise path at deviation from the straight line, which, moreover, generally depends upon the initial disturbance. In such cases a static analysis ought to be sufficiently informative.

Even though branching in rare cases might appear at slow crack growth it is generally closely connected with rapid crack propagation. Thus the dynamic character of the phenomenon must be taken under consideration.

2. NECKING TYPE FRACTURE OF THIN PLATES

Experiments with thin plates often show a necking type fracture. Necking regions then appear at the crack tips before unstable crack growth takes place. Sometimes these regions extend only a short distance ahead of the tips; sometimes they traverse the plate ligaments. Subsequent crack propagation proceeds along the mid-line of the necking region.

Altogether 79 experiments on aluminum plates (SIS 4007-14 and SIS 4007-18) have been performed in order to study the direction of crack growth. Different plate thicknesses (1,2 and 3 mm) were used as well as different plate widths and crack lengths. The cracks were always placed symmetrically and normal to the load direction (center-cracked specimens). The direction of rolling was parallel to the load direction in some tests, normal to in other tests.

In no case the crack traversed the whole specimen in the original crack direction, but in a few cases it continued along this direction on the one side and at an angle on the other side, see Fig. 1. In most cases, however, the cracks extended on both sides at an angle to the original direction, forming an antisymmetrical path, see Fig. 2. In some of these cases the crack at first grew in the original direction and thereupon changed direction, usually rather abrupt, even though in one case (Fig. 3, showing a test interrupted before completed fracture) the change was very gradual. Figure 4 shows schematically the result of some of the tests performed.

The angle formed to the original direction turned out to be independent of original crack length and plate width but dependent on the plate thickness and the orientation of the rolling direction, see Fig. 5. This fact suggests that the angle should equal the one found by well-known plasticity analysis (see, for instance, Hill [1] for necking in thin plates without cracks). Fig. 6 recapitulates the essentials of such an analysis: Since the velocity direction is normal to the yield surface, the angle of necking depends upon yield criterion and transverse stress (which in the experiments consisted only in the stress introduced by the constraints at the clamped ends and by the presence of the crack). The Tresca yield criterion always implies necking along the original crack direction, i.e., β (see Fig. 5) equals zero. The von Mises yield criterion implies $\beta \approx 35.3^o$ for isotropic material and zero transverse stress. For zero transverse stress and anisotropy introduced by rolling the von Mises Hypothesis implies $\beta < 35.3^o$ if the rolling direction is parallel to the load direction and $\beta > 35.3^o$ if it is normal to the load direction.

3. PLANE STRAIN CRACK PATHS

The discussion in this section refers to plane strain conditions but is also applicable to cases of plates in which the fracture mechanism is essentially the one encountered at plane strain even though the gross field might be much closer to plane stress. The term "crack" is used here, even in some cases when the term "slip" would be more appropriate. The model studied consists of a straight crack of length 2a forming an angle θ to the direction of σ_1 the smaller one of the two in-plane principal stresses σ_1 and σ_2, see Fig. 7. The stress intensity factors K_I and K_{II} are calculated. In a simple case the crack surfaces do not touch each other and then

$$(\pi a)^{-\frac{1}{2}} K_I = \frac{1}{2}(\sigma_2 + \sigma_1) + \frac{1}{2}(\sigma_2 - \sigma_1)\cos 2\theta \tag{1}$$

$$(\pi a)^{-\frac{1}{2}} K_{II} = \frac{1}{2}(\sigma_2 - \sigma_1)\sin 2\theta \, . \tag{2}$$

In another simple case the crack surfaces are pressed together by such a high compressive normal stress $|\sigma_n|$ that the tangential stress τ_{nt} is lower than the friction stress. Then no slip occurs and

$$K_I = K_{II} = 0 \, . \tag{3}$$

In intermediate cases the crack surfaces are pressed together ($\sigma_n < 0$) but τ_{nt} reaches the friction stress. Then

$$K_I = 0 \tag{4}$$

$$(\pi a)^{-\frac{1}{2}} K_{II} = \frac{1}{2}(\sigma_2 - \sigma_1)\sin 2\theta - \tau_{nt} \, . \tag{5}$$

With a Coulomb type friction,

$$\tau_{nt} = -\mu\sigma_n \tag{6}$$

where μ is the coefficient of friction, one obtains

$$(\pi a)^{-\frac{1}{2}} K_{II} = \mu \cdot \frac{1}{2}(\sigma_2 + \sigma_1) + \frac{1}{2}(\sigma_2 - \sigma_1)(\sin 2\theta + \mu\cos 2\theta) \, . \tag{7}$$

Six distinctly different cases can appear, depending on the relation between σ_1, σ_2 and μ. These relations are ($\alpha = (1+\mu^2)^{\frac{1}{2}} - \mu$) (see Figs. 8-13):

$\sigma_1 > 0$	$\sigma_1 \leqslant \sigma_2$	Fig. 8
$\sigma_1 < 0$	$\lvert\sigma_1\rvert \leqslant \sigma_2$	Fig. 9
$\sigma_1 < 0$	$\alpha^2\lvert\sigma_1\rvert \leqslant \sigma_2 < \lvert\sigma_1\rvert$	Fig. 10
$\sigma_1 < 0$	$0 < \sigma_2 < \alpha^2\lvert\sigma_1\rvert$	Fig. 11
$\sigma_1 < 0$	$-\alpha^2\lvert\sigma_1\rvert < \sigma_2 \leqslant 0$	Fig. 12
$\sigma_1 < 0$	$\lvert\sigma_1\rvert \leqslant \sigma_2 \leqslant -\alpha^2\lvert\sigma_1\rvert$.	Fig. 13

In Figs. 8-13 K_I and K_{II} are shown for different directions. Regions marked A are characterized by non-vanishing K_I andK_{II}. Regions marked C are characterized by vanishing K_I andK_{II}. Regions marked B are characterized by vanishing K_I but non-vanishing K_{II}. The maximum of K_{II} may lie outside region B (B1), thus in region A, between region B (B2) and region A or inside region B (B3). When maximum of K_{II} lies in region A, then it occurs for $\theta = 45^o$, otherwise for $\theta < 45^o$. Between B2 and A it occurs for $\theta = \frac{1}{2}\cos^{-1}[(\sigma_1+\sigma_2)/(\sigma_1-\sigma_2)]$ and in B3 it occurs for $\theta = \frac{1}{2}\cos^{-1}[\mu(1+\mu^2)^{-\frac{1}{2}}]$.

Numerous experiments corresponding to the case shown in Fig. 8 indicate that a pure mode I growth results in this case. One can see that, for instance, a criterion of type

$$K_I^2 + \kappa^2 K_{II}^2 = C^2 \quad , \qquad \kappa^2 < 2 \tag{8}$$

would lead to this result; i.e. the crack direction would be $\theta = 0$ and $K_I = C = K_{IC}, K_{II} = 0$. In crack path predictions the criterion $K_{II} = 0$ can therefore be used [2,3,4,5].

Since pure mode II growth is the only possibility in the case shown in Fig. 12 there must be a transition from mode I to mode II somewhere between these cases. In principle this transition might occur either gradually in a mixed mode I-II region, or abruptly.

In the case shown in Fig. 8 a crack with original direction $\theta = \theta_d = 0$ will continue to grow straightforwards and so will a crack in the case shown in Fig. 12 if its original direction is $\theta = \theta_d = \frac{1}{2}\cos^{-1}[\mu(1+\mu^2)^{-\frac{1}{2}}]$. In each intermediate case a θ_d-value always exists such that a pre-existing crack in this direction will continue to grow straightforwards. The θ_d-value in question is the one predicted by the appropriate crack growth criterion, which, however, is rarely known in the intermediate cases.

If the direction of the original crack does not coincide with θ_d the crack will curve during gorwth and tend towards direction θ_d. This has been demonstrated by means of directional stability analysis for the case shown in Fig. 8.

The case in Fig. 12 is typical for sliding motion such as at earthquakes. One observes that the slip direction forms an angle with the direction of largest shear stress. This angle $45^o - \theta_d$, is shown in Table I as a function of μ.

Table I. Crack growth direction as a function of the coefficient μ.

μ	θ_d	$45^o - \theta_d$
0	45°	0
0.2	39.3°	5.7°
0.4	34.1°	10.9°
0.6	29.5°	15.5°
0.8	25.7°	19.3°
1.0	22.5°	22.5°

It should be noticed that the direction θ_d found by using the criterion $K_{II} = K_{II\max}$ coincides with the direction found by using the fact that

$$\tau_{nt}(\theta) + \mu\sigma_n(\theta) \tag{9}$$

must be non-negative; i.e., the shear stress must reach the friction stress. This condition is met first for $\theta = \theta_d$ such that expression (9) is maximum.

4. COMMENTS ON MODE I AND MODE II CRACK GROWTH

A question by Fazil Erdogan regarded the nature of mode II crack growth. It is sometimes assumed that crack growth in materials like metals takes place at mode I and not at mode II. However, as can be judged from Figs. 8-13, high compressive in-plane principal stresses ought to promote a mode II growth so that under certain circumstances (difficult to satisfy experimentally) mode II growth should be obtained for virtually all materials. On the other hand one can argue that tensile forces always occur close to the tip of a mode II crack. The micro-structural properties (at a certain overall compressive stress composition) may be such that a micro-separation occurs at an angle to the crack direction due to such tensile forces. This might be referred to as an opening mode separation, but such a separation cannot be propagated more than a short distance from the tip of the main crack because compressive forces close the separation at its end. Continued crack growth must therefore occur in the direction of the main crack. On a micro-scale it could consist of repeated micro-separations at an angle to the crack direction due to tensile forces of short reach near the crack tip (echelon cracks). In other cases the micro-separation mechanism could consist of pure shear, i.e. unambiguously a shear mode separation. Both micro-structural properties and overall stress composition influence the choice of micro-separation mechanism.

It should be noticed that mode I crack propagation is analogous: The micro-separation mechanism may be (and usually is) of opening mode character (opening of voids or micro-cracks due to tensile forces), but zig-zag crack paths sometimes appear on a micro-scale, indicating a shear mode micro-separation. (This is, for instance, a frequently used model of fatigue crack growth.)

5. STABILITY OF STRAIGHT CRACK PATHS

It is a known experimental fact that two originally collinear cracks seem to avoid each other rather than to coalesce tip to tip. Fig. 14 shows a typical example. In a recent study, Melin [5] shows that this behavior becomes predicted by an elastostatic analysis of the crack path. She

regards a periodic array of cracks, -2a + 2nd < x < 2a + 2nd, y(-x + 2nd) = -y(x), |y'(x)| << 1. The stress intensity factor K_{II} turns out to be

$$K_{II}(a) = \sigma_y^{\infty}(d/2)^{\frac{1}{2}}[\tan(\pi a/2d)]^{\frac{1}{2}} \left[y'(a) + 2\tau_{xy}/\sigma_y^{\infty} - \pi y(a)/[d\sin(\pi a/d)] \right.$$

$$\left. + (1/d)(1-\sigma_x^{\infty}/\sigma_y^{\infty}) \int_{-a}^{a} y'(\xi)\cos(\pi\xi/2d)W(\xi)d\xi \right] \tag{10}$$

where σ_x^{∞} , σ_y^{∞} , andτ_{xy}^{∞} are the remote stresses and

$$W(\xi)=[\sin^2(\pi a/2d)-\sin^2(\pi\xi/2d)]^{-\frac{1}{2}} .$$

By using the criterion $K_{II}(a) = 0$ an integral equation is obtained. The assumption $\tau_{xy}^{\infty}/\sigma_y^{\infty} = 0$ and y(x) = 0 for $x < a_o < d$, $y(x) \neq 0$ for $a_o < x < a_o + \delta < d$, $\delta/a_o << 1$ (i.e. a disturbance at $x \approx a_o$) leads to the result that y(a) increases beyond any predetermined value when a comes sufficiently close to d, i.e. the cracks avoid each other.

The analysis can also be used for the case of a single crack, by letting a/d → 0 in eq. (10). The case $\tau_{xy}^{\infty}/\sigma_y^{\infty} = 0$, $\sigma_x^{\infty}/\sigma_y^{\infty} = 1$ is illustrative. It gives, simply, the equation

$$y'(a) = y(a)/a . \tag{11}$$

For an originally straight crack, y(x) = 0 for $x \leq a_o - \delta$, $\delta/a_o << 1$ with a disturbance, $y(x) = y_o > 0$ for $x = a_o$ one arrives at

$$y'(a) = y_o/a_o \qquad \text{for} \qquad x > a_o . \tag{12}$$

i.e.,

$$\frac{y(a)}{a} = \frac{y_o}{a_o} \qquad \text{for} \qquad x < a_o . \tag{13}$$

Even though y(a) actually increases with a, eq. (13) should not be taken to imply instability of the straight path. The same y(a) may imply a large deviation from straightness - if a is small enough - or a very small deviation from straightness - if a is large enough. Thus, obviously,

y(a)/a and not y(a) should be taken as a measure of straightness, and instability of the straight path should be regarded to prevail if y(a)/a exceeds any predetermined value if a/a_o is sufficiently large and y_o/a_o infinitesimal. Eq. (13) thus does not show instability, because y(a)/a is infinitesimal if y_o/a_o is infinitesimal, but it is easy to show that the case $\sigma_x^\infty > \sigma_y^\infty$ implies instability.

Actually, if one should use the criterion that the straight path is unstable if y(a) continues to increase with a after an initial disturbance $y_o > 0$, then one would arrive at the misleading result that the straight path is unstable not only for $\sigma_x^\infty/\sigma_y^\infty > 1$ but also for $1-\pi/4 < \sigma_x^\infty/\sigma_y^\infty \leqslant 1$ [5].

6. CRACK BRANCHING

Crack branching takes place at high crack propagation velocities and therefore the dynamic character should be taken into account. However, a quasi-dynamic approach can be used in order to demonstrate the essentials. This was done by Pärletun [4] who used the condition $K_{II} = 0$ in a static FEM-analysis to determine the paths, assuming that bifurcation actually occurred and that it was symmetrical. By assuming branching to occur again when the K_I-value at the first branching was recovered, also secondary branching could be included. The crack pattern turned out to come very close to experimentally obtained patterns.

Perhaps one does not understand precisely why branching is initiated, but micro-structural inhomogeneities probably play an important part. Still the question remains why a bifurcation, once initiated, develops into branches travelling with almost the same velocity. A difference in initial branch length ought to cause a smaller stress intensity factor for the shorter branch and this in turn will cause this branch to grow slower than the longer one. This might lead to decreasing stress intensity factor for the shorter branch and thereby a deceleration and finally arrest.

Pärletun looked upon the growth of two branches of originally different lengths. The stress

intensity factors were determined by means of a static FEM-analysis for different length ratios. The relations obtained were used in a quasi-dynamic analysis suggested by Bergkvist [6]. The result showed a surprisingly great sensitivity to the propagation velocity. Thus, assuming that the energy flow to the two crack tips just after branching equalled the energy flow to the single crack tip just before branching, almost sudden arrest of the shorter branch occurred when the pre-branching crack tip velocity was low (20 per cent of the equivoluminal wave velocity) but almost parallel growth resulted when the pre-branching crack tip velocity was high (65 per cent of the equivoluminal wave velocity). Data pertinent to PMMA were used.

Some of the results by Pärletun are shown in Figs. 15-16.

REFERENCES

1. Hill, R., The Mathematical Theory of Plasticity, Clarendon Press, Oxford (1950).

2 Erdogan, F., and Sih, G.C., "On the Crack Extension in Plates Under Plane Loading and Transverse Shear," Trans. ASME, D, 85 (1963) 4.

3. Kalthoff, J.F., "On the Propagation Direction of Bifurcated Cracks," in Dynamic Crack Propagation, G.C. Sih ed., Noordhoff, Leyden (1972) 449-458.

4. Pärletun, L.G., "Determination of the Growth of Branched Cracks by Numerical Methods," Engineering Fracture Mechanics, 1 (1979) 343-358.

5. Melin, S., "Why do Cracks Avoid Each Other?" to appear in Int. J. Fracture.

6. Bergkvist, H., "The Motion of a Brittle Crack," J. Mech. Phys. Solids, 21 (1973) 229-239.

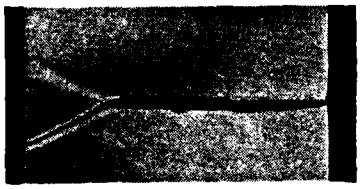

Figure 1. Asymmetrical crack growth.

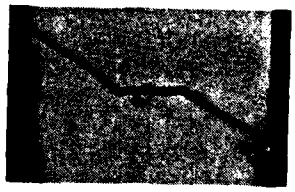

Figure 2. Antisymmetrical crack growth.

Figure 3. Incipient crack growth in the original crack direction followed by asymmetrical growth.

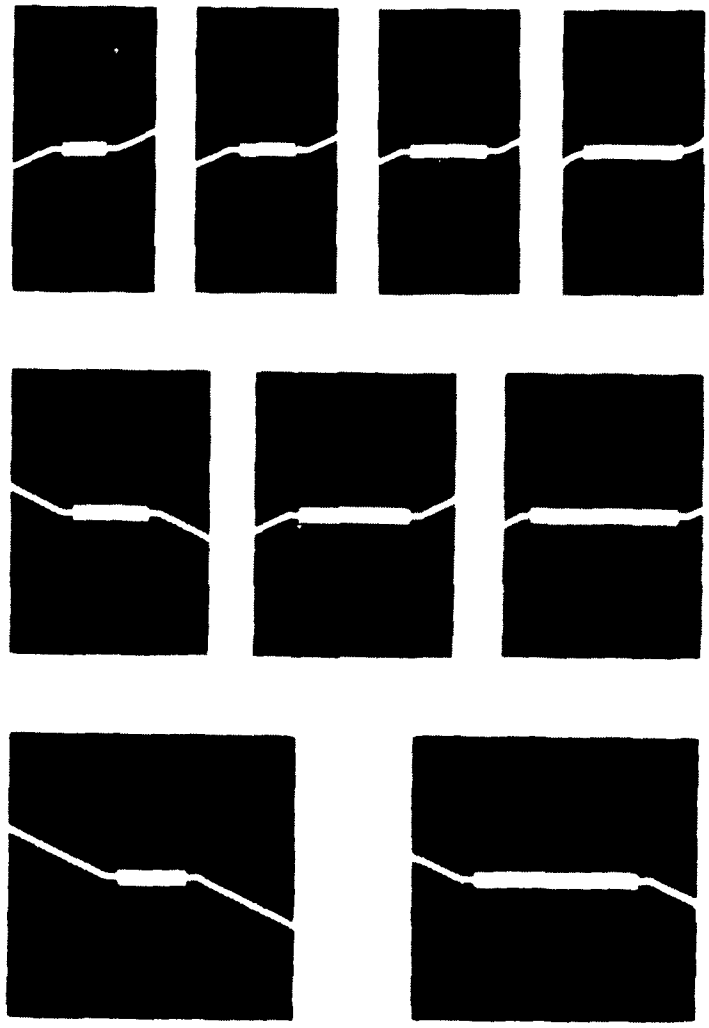

Figure 4. Schematical drawing of results obtained on 2 mm thick aluminum plates. Plate width: upper row: 160 mm; middle row: 240 mm; lower row: 320 mm.

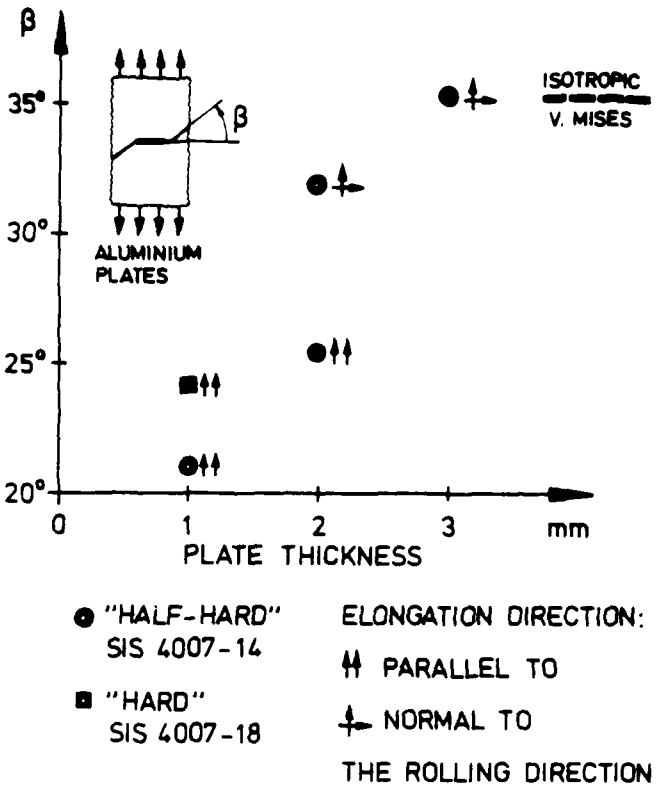

Figure 5. Crack directions in experiments with thin aluminum plates.

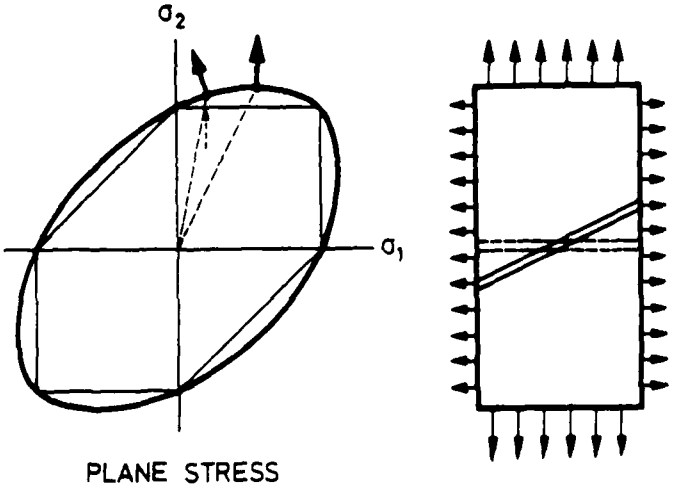

Figure 6. Yield surfaces according to von Mises and Tresca and implications on necking direction.

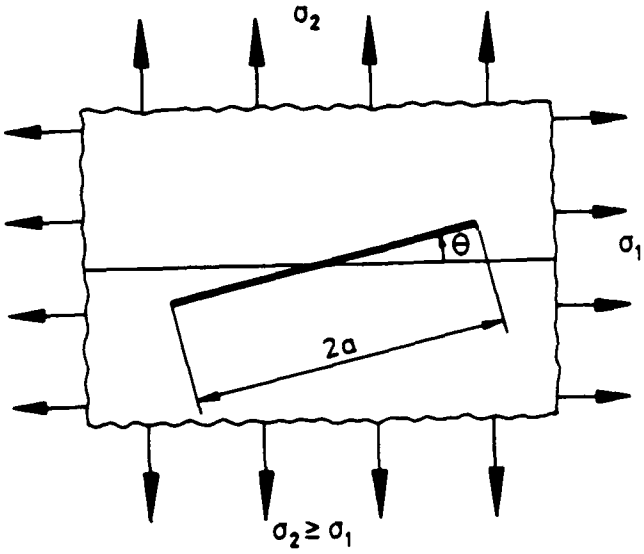

Figure 7. Crack orientation with respect to the principal stresses.

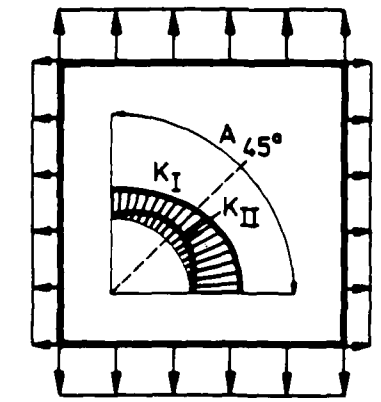

Fig. 8

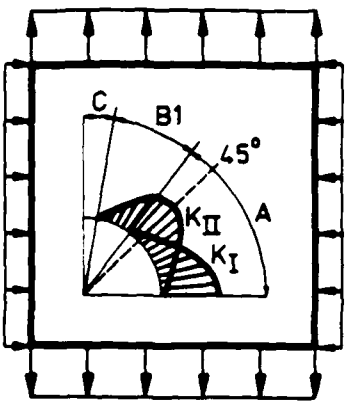

Fig. 9

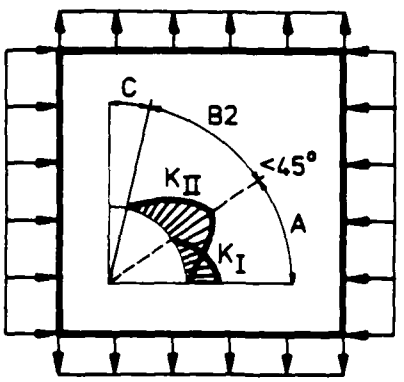

Fig. 10

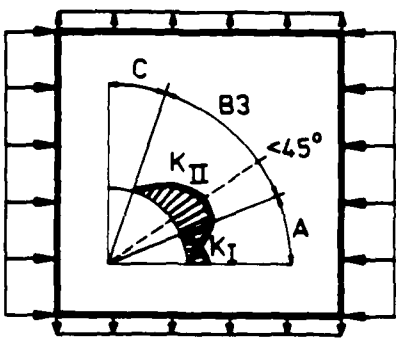

Fig. 11

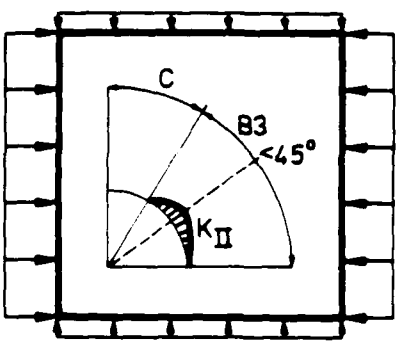

Fig. 12

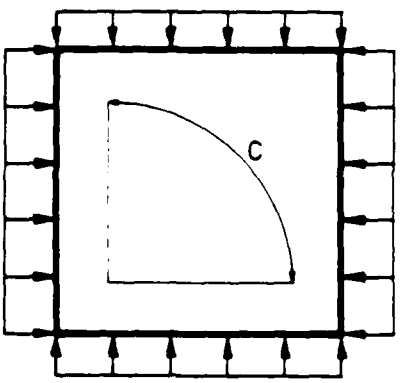

Fig. 13

Figure 8-13. Stress intensity factors K_I and K_{II} for different crack orientations and relations between σ_1, σ_2 and μ (see text).

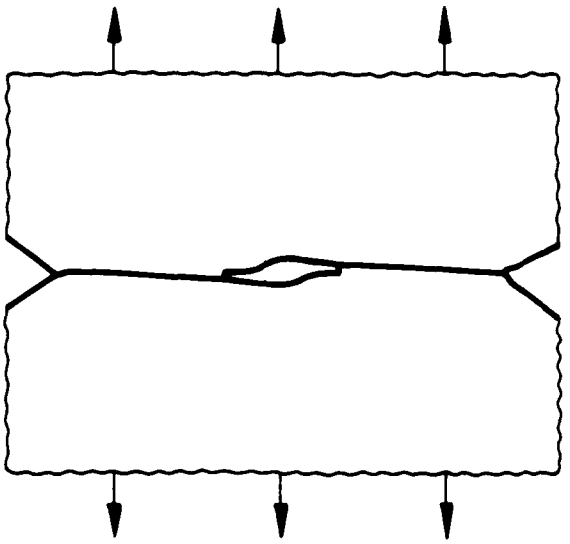

Figure 14. Originally collinear cracks seem to avoid each other.

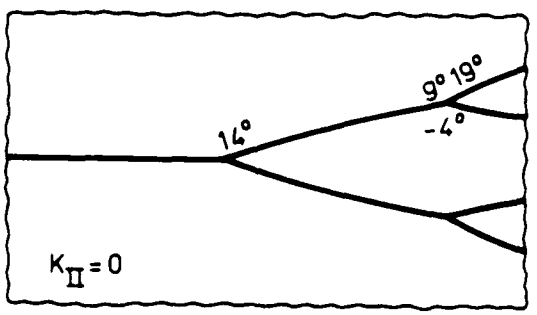

Figure 15. Branching pattern obtained from static FEM-analysis.

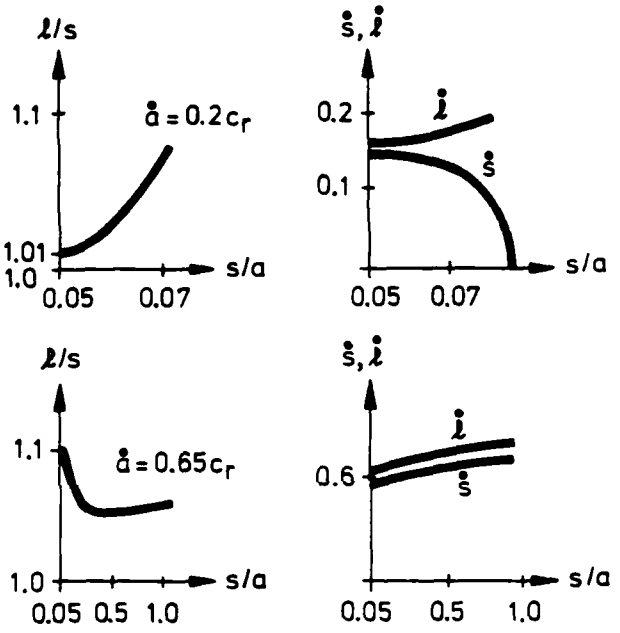

Figure 16. Upper left figure shows the length ratio l/s between two branches, initially of lengths $s = 0.05a$, where a is the half-length of the crack just before branching, and $l = 1.01$ s. Crack velocity just before branching is 20 per cent of the equivoluminal wave velocity c_r. The upper right figure shows the branch velocities $\dot{l}$ and $\dot{s}$. The shorter branch is arrested before it has doubled its assumed initial length.

The lower figures show the same thing except that the crack velocity before branching is 65 per cent of the equivoluminal wave velocity and the relative initial length difference is 10 per cent instead of 1 per cent. One observes that the relative difference in branch length is less than 10 per cent even after the branch has grown to more than the half-length of the original crack before branching.

PATH-INDEPENDENT INTEGRALS IN DYNAMIC FRACTURE MECHANICS

S.N. Atluri and T. Nishioka
Center for the Advancement of Computational Mechanics
School of Civil Engineering
Georgia Institute of Technology

SUMMARY

We first consider linear elastodynamic crack propagation* under mixed mode non-steady conditions with an arbitrary velocity.

Consider, for instance, a two-dimensional problem. Let the velocity of crack-propagation be denoted by the vector $\underline{C}$ (for simplicity, we denote $|\underline{C}| = C$). Consider a small loop Γ_ϵ of radius ϵ, centered around the crack-tip at time t, and assume that the crack-tip moves by an amount $(dt \cdot \underline{C})$ into Γ_ϵ at time t + dt, i.e. $\epsilon > Cdt$ without loss of generality. Let the unit outward normal to Γ_ϵ be $\underline{N}$, and let the kinetic energy density be T [$=(\frac{1}{2})\rho \underline{v} \cdot \underline{v}$, where $\underline{v}$ is the absolute velocity of a material particle and ρ the mass density]. Note that $\underline{v}$ is singular near a propagating crack-tip. Let the strain-energy density be W [which, for a linear elastic material is equal to $(\frac{1}{2})\sigma_{ij}\epsilon_{ij} \equiv (\frac{1}{2})\underline{\sigma} : \underline{\epsilon}$]. From the studies in [1], which were valid for finitely deformed elastic or inelastic solids, it is seen for the present linear elastic case that the rate of release of energy per unit crack growth, G, is given by

$$G = (1/c) \lim_{\epsilon \to 0} \underline{C} \cdot \int_{\Gamma_\epsilon} [(W + T)\underline{N} - \underline{t} \cdot \underline{e}]\, d\Gamma \tag{1a}$$

$$= (1/c)\underline{C} \cdot \underline{G} \tag{1b}$$

where $\underline{e}$ is the displacement gradient; i.e., $\underline{e} = (\nabla \underline{u})^T$, where $\underline{u}$ is the displacement and ∇ the gradient operator in the employed coordinates.

* However, we restrict ourselves to the case of self-similar crack-propagation.

If, for instance, a Cartesian coordinate system is used such that x_1^o is along the crack-axis at time t, and x_2^o is normal to the crack-axis at time t (see Fig. 1), it has been shown in [2] that if the mixed-mode asymptotic solutions are employed in Eq. (1), one obtains:

$$G_1 = \frac{1}{2\mu}\left\{ K_I^2 A_I(c) + K_{II}^2 A_{II}(c) + K_{III}^2 A_{III}(c) \right\} \tag{2}$$

and

$$G_2 = -\frac{K_I K_{II}}{\mu} A_{IV}(c) \tag{3}$$

where μ is the shear modulus, and

$$A_I(c) = \beta_1(1-\beta_2^2)/D(c) \qquad A_{II}(c) = \beta_2(1-\beta_2^2)/D(c) \qquad A_{III}(c) = 1/\beta_2 \tag{4}$$

$$A_{IV}(c) = \frac{(\beta_1-\beta_2)(1-\beta_2^2)}{[D(c)]^2}\left[\frac{\{4\beta_1\beta_2+(1+\beta_2^2)^2\}(2+\beta_1+\beta_2)}{2[(1+\beta_1)(1+\beta_2)]^{\frac{1}{2}}} - 2(1+\beta_2^2) \right] \tag{5}$$

$$\beta_1^2 = 1-(C/C_d)^2 \qquad \beta_2^2 = 1-(C/C_s)^2$$
$$C_d^2 = (\kappa+1)\mu/(\kappa-1)\rho \qquad C_s^2 = \mu/\rho$$

$$\kappa = \begin{cases} (3-\nu)/(1+\nu) : & \textit{plane stress} \\ (3-4\nu) : & \textit{plane strain} \end{cases}$$

$$D(c) = 4\beta_1\beta_2-(1+\beta_2)^2 .$$

In the above, K_I, K_{II}, K_{III} are the time-dependent factors of stress-intensity at the tip of the propagating crack.

Now we consider the problem of analyzing crack-propagation in an arbitrary body, the shape of which and the loading on which, we suppose, preclude any possibility of an analytical solution. Suppose that we have to use a numerical solution Such a numerical solution may be based on a "propagating singular-element" within which the asymptotic mixed mode solution is embedded; and hence the K-factors can be evaluated directly, as demonstrated by the authors [3-6].

However, in order to use a simple numerical procedure, say using distorted (singular) isoparametric finite elements or non-singular isoparametric elements, it is convenient to have available path-independent integrals which have the same meaning as the energy release rate G or $\underline{G}$ of Eq. (1). If so, the integral can be evaluated on a path that is far-removed from the crack tip and hence is insensitive to the details of modeling of crack-tip stress-strain fields.

Such path-independent integrals have been derived based on general conservation laws and given in [1,2]. Here, instead of following [1,2], we present a rather simple, but perhaps didactically unappealing, derivation of a path-invariant vector integral which has the precise meaning of energy release rate in elastodynamic crack-propagation. Let this be identified by $\underline{J}'$. Thus, we are creating a $\underline{J}'$, evaluated on a far-field contour, such that

$$\underline{J}' = \underline{G}(\equiv \int_{\Gamma_\epsilon} [(W + T)\underline{N} - \underline{t} \cdot \underline{e}\,]d\Gamma) \ . \tag{6}$$

Thus, we let

$$\underline{J}' = \int_{\Gamma} [(W + T)\underline{N} - \underline{t} \cdot \underline{e}\,]d\Gamma + \underline{R} \tag{7}$$

where Γ is a far-field contour. In (7), $\underline{R}$ is simply a residue, whose value we check to see if it is no-zero and evaluate it, by comparing Eqs. (6) and (7). Thus,

$$-\underline{R} = \int_{\Gamma}[(W + T)\underline{N} - \underline{t} \cdot \underline{e}\,]d\Gamma - \int_{\Gamma_\epsilon}[(W + T)\underline{N} - \underline{t} \cdot \underline{e}\,]d\Gamma \ . \tag{8}$$

Now, let V_ϵ be the "core" near the crack-tip that is enclosed by Γ_ϵ. Consider the volume $V-V_\epsilon$, which does not include the crack-tip. Hence, the divergence theorem is applicable in $V-V_\epsilon$. (Note that the divergence theorem cannot be applied when the integrand involves non-integrable singularities.) The boundary of $(V-V_\epsilon)$ includes not only Γ and Γ_ϵ but also the crack surfaces Γ_c^+ and Γ_c^- as shown in Fig. 1. Thus, by the application of the divergence theorem in Eq. (8), we see that:

$$-\underline{R} = \int_{V-V_\epsilon} \underline{\nabla} \cdot [(W + T)\underline{I} - \underline{\sigma} \cdot \underline{e}\,] - \int_{\Gamma_c^+ + \Gamma_c^-} [(W + T)\underline{N} - \underline{\bar{t}} \cdot \underline{e}\,]\,d\Gamma \tag{9}$$

In (9), $\underline{\bar{t}}$ are prescribed tractions on the crack face. We assume that W is a single-valued

function of $\underline{\epsilon}$, the strain tensor $[\epsilon = \frac{1}{2}(\underline{e} + \underline{e}^T)]$; and that the solid is in elastodynamic equilibrium; i.e.,

$$\underline{\nabla} \cdot [W\underline{I}] = \underline{\nabla} W = \underline{e}_k [\underline{\sigma} : \underline{\epsilon}_{,k}] \tag{10a}$$

$$\text{and} \quad \underline{\nabla} \cdot \underline{\sigma} + \overline{\underline{F}} = \rho \underline{a} . \tag{10b}$$

Using (10a,b), it is easy to show that

$$\underline{\nabla} \cdot [(W + T)\underline{I} - \underline{\sigma} \cdot \underline{e}] = \underline{\nabla} \cdot (T\underline{I}) - (\rho \underline{a} - \overline{\underline{F}}) \cdot \underline{e} \tag{11}$$

where $\overline{\underline{F}}$ are prescribed body forces (other than inertia). Hence, Eq. (7) can be written as:

$$\underline{J}' = \int_\Gamma [(W + T)\underline{N} - \underline{t} \cdot \underline{e}] + \int_{V-V_\epsilon} (\rho(\underline{a} - \overline{\underline{F}}) \cdot \underline{e} - \underline{\nabla} T) dV$$

$$+ \int_{\Gamma_c} [(W^+ - W^-)\underline{N}^+ + (T^+ - T^-)\underline{N}^+ - \overline{\underline{t}} \cdot \underline{e}] dP \tag{12}$$

where (+) and (-) refer, arbitrarily, to the "upper" and "lower" crack faces, $\underline{N}^+ = -\underline{N}^-$ is the unit normal to Γ_c^+, and $\overline{\underline{t}}$ are prescribed tractions on the crack face. It is evident from the foregoing that $\underline{J}'$, as evaluated through the far-field integral in Eq. (12), is strictly equal to the energy-release rate $\underline{G}$ of Eq. (1). Further, using relations of Eq. (2,13), the K-factors can be evaluated conveniently through Eq. (12).

It should be remarked that the far-field contour Γ in Eq. (12) is fixed in space, and the crack-tip is moving inside Γ. Using a similar space-fixed contour, Aoki *et al.* [7] derived a path-independent integral $\hat{\underline{J}}$, which may be written (although what is given in [7] is somewhat less general) as:

$$\hat{\underline{J}} = \int_\Gamma [W\underline{N} - \underline{t} \cdot \underline{e}] + \int_{V-V_\epsilon} \rho(\underline{a} - \overline{\underline{F}}) \cdot \underline{e}\, dV + \int_{\Gamma_c} [(W^+ - W^-)\underline{N}^+ - \underline{t} \cdot \underline{e}] d\Gamma . \tag{13}$$

It is clear that $\hat{\underline{J}}$ has no meaning as an energy release rate, nor do the relations of (2) and (3) hold between $\underline{J}$ and K_I, K_{II}, contrary to what has been often stated, and used, in recent literature.

It should be remarked that the $\underline{J}'$ integral in Eq. (12) accounts for discontinuities of W and T across the crack faces. Further, in elasto-statics, zero body forces, and traction-free crack faces, $\underline{J}'$

may be written as

$$\underline{J}' = \int_{\Gamma} [W\underline{N} - \underline{t} \cdot \underline{e}]d\Gamma + \int_{\Gamma_c} (W^+ - W^-)\underline{N}^+ \, d\Gamma. \tag{14}$$

Assuming for simplicity that the crack axis is straight, if we use the special coordinate system, x_1^o along the crack axis and x_2^o normal to crack axis, we have,

$$N_1^+ = 0 , \quad N_2^+ = 1 \quad at \quad \Gamma_c \quad (in \; x_1^o \; , \; x_2^o \; system) .$$

Thus, (14) in component form in $(x_1^o \; , \; x_2^o)$ system becomes:

$$(J'_1)_o = \int_{\Gamma} [WN_1 - t_i(\partial u_i/\partial x_1^o)]d\Gamma \tag{15a}$$

$$(J'_2)_o = \int_{\Gamma} [WN_2 - t_i(\partial u_i/\partial x_2^o)]d\Gamma + \int_{\Gamma_c} (W^+ - W^-)d\Gamma. \tag{15b}$$

The expressions in (15a,b) should be contrasted with those given by Budiansky and Rice [8] when a coordinate system similar to above is used:

$$(J_K)_o = \int_{\Gamma} [\, WN_K - t_i u_{i,K}]d\Gamma \qquad K = 1,2 . \tag{16}$$

Thus, it is seen that J_2, as given by Budiansky and Rice, is <u>not</u>, in general, path-independent. This has also been noted by Herrmann and Herrmann [9].

The Use of $\underline{J}'$: Even though the vector-tensor formalism in writing $\underline{J}'$ as in Eq. (12) may appear pretentious at first glance, its' convenience may be appreciated in <u>analyzing</u> problems of the type shown in Fig. 1. In most computations (finite elements?!) one generally uses a global Cartesian system. If the unit base vectors along the <u>crack</u>-<u>tip</u> axes are $\underline{e}_1^o$ and $\underline{e}_2^o$, the computation of $\underline{J}'$ in Eq. (12) can be carried out from the obtained solution in global coordinates, and the components $(J'_1)_o$ and $(J'_2)_o$ along $\underline{e}_1^o$, $\underline{e}_2^o$ are obtained as:

$$(J'_1)_o = \underline{e}_1^o \cdot \underline{J}' ; \quad (J'_2)_o = \underline{e}_2^o \cdot \underline{J}' . \tag{17}$$

If, on the other hand, the more commonplace definitions of the type Eq. (15a,b) are used to compute the $(J'_1)_o$, $(J'_2)_o$ directly, the obtained solution must first be transformed to the local coordinate system x_1^o, x_2^o.

From $(J'_1)_o$ and $(J'_2)_o$ as computed in (17), one may evaluate K_I, K_{II} as follows:

$$K_I = \pm < \frac{\mu}{A_I(c)} \left\{ (J'_1)_o \pm [(J'_1)_o^2 - (A_I A_{II}/A_{IV}^2)(J'_2)_o^2]^{\frac{1}{2}} \right\} >^{\frac{1}{2}} \tag{18}$$

$$K_{II} = \pm < \frac{\mu}{A_{II}(c)} \left\{ (J'_1)_o \mp [(J'_1)_o^2 - (A_I A_{II}/A_{IV}^2)(J'_2)_o^2]^{\frac{1}{2}} \right\} >^{\frac{1}{2}}. \tag{19}$$

The signs of K can be determined as follows: Suppose $(u_i)_o$ are displacements asymptotically close to the crack tip along and normal to the crack-tip axis. Define:

$$\delta_I = (u_2)_o^+ - (u_2)_o^- \; ; \quad \delta_{II} = (u_1)_o^+ - (u_1)_o^- \; . \tag{20}$$

The signs of K_I, K_{II} correspond to the signs of δ_I, δ_{II}. The term in braces { } in Eq. (18) is determined as follows:

$$\text{if} \quad |\delta_I/\beta_1| \geq |\delta_{II}/\beta_2| \; , \quad \textit{take} + \tag{21}$$

$$\text{if} \quad |\delta_I/\beta_1| < |\delta_{II}/\beta_2| , \quad \textit{take} - \tag{22}$$

with similar choices for K_{II}. Further, it is of interest to note from Eqs. (2,3) that

$$(J'_1)_o^2 - (A_I A_{II}/A_{IV}^2)(J'_2)_o^2 = \left\{ \frac{1}{2\mu}(K_I^2 A_I - K_{II}^2 A_{II}) \right\}^2 \geq 0 \; . \tag{23}$$

Hence,

$$|(J'_1)_o| \geq [(A_I A_{II})^{\frac{1}{2}}/A_{IV}] \; |(J'_2)_o| \; . \tag{24}$$

For the static case, $A_I = A_{II} = A_{IV} = (\kappa+1)/4$; hence

$$|(J'_1)_o| \geq |(J'_2)_o| \; . \tag{25}$$

Note that when the global coordinate system is used in computing Eq. (12), the integral on Γ_c is present in both the components J'_1 and J'_2 of $\underline{J}'$ in the global system. Thus, even in the absence of crack-face tractions, the effects of discontinuities of W and T [i.e. $(W^+ - W^-)$ and $(T^+ - T^-)$] are present in both J'_1 and J'_2.

For the problem of Fig. 1, the static solution is first computed. In doing so, both the "quarter-point" isoparametric elements as well as non-singular isoparametric elements are used. Note that the former elements do represent a (1/r) singularity in W near the crack-tip, while the latter do not unless a mesh much finer than in Fig. 1 is employed. In Fig. 2a the computed W for the mixed-mode problem is shown for both the upper and lower faces of the crack. It is clearly seen, since whatever approximations are made in W are present in both W^+ and W^-, that $(W^+ - W^-) \neq o$. This explains the reason as to why Budiansky and Rice's definition of $(J_2)_o$ will not be path-independent, while the present J'_2 will be. Further, since J'_1 and J'_2 as computed in Eq. (12) involve the effect of $(W^+ - W^-)$ and $(T^+ - T^-)$, numerically this will be reflected in $(J'_1)_o$ and $(J'_2)_o$ from which (K_1 and K_{II}) are computed as in Eqs. (18,19). Kitagawa et al. [10] suggested a procedure for computing K_1 , K_{II} which, in retrospect, appears to circumvent the problem with $(W^+ - W^-)$ and $(T^+ - T^-)$ being non-zero. Suppose that the computed global solution for a linear problem for displacement, stress, and strain is transformed into crack-tip local coordinates x_1^q and x_2^q and then decomposed into components that are symmetric and anti-symmetric, respectively $w \cdot r \cdot t$ the x_2^q axis. Thus, the mixed mode problem has been effectively decomposed into a superposition of pure mode I and mode II problems. Thus, for a static problem with traction-free crack faces, $(J'_1)_o$ can be computed from Eq. (15a) for the pure mode I and mode II cases separately. Let these be designated as $(J'_1)_{oI}$ and $(J'_1)_{oII}$, respectively. Thus, K_I and K_{II} can be extracted from the relations (given for the general dynamic propagation case):

$$(J'_1)_{oI} = \frac{1}{2\mu}(K_I^2 A_I(c)) \; ; \quad (J'_1)_{oII} = \frac{1}{2\mu}(K_{II}^2 A_{II}(c)) \; .$$

Of course, for the above decomposed pure mode cases, $(J'_2)_o$ vanishes separately. The strain-energy density functions W^I and W^{II}, for the above decomposed pure mode I and mode II cases, respectively, are shown in Fig. 2b for both the upper and lower crack faces. It is seen from Fig. 2b that both W^I and W^{II} are continuous at the crack face. However, it should be noted that since W^I and W^{II} are quadratically superposed for the mixed mode problem, the total W

is discontinuous as in Fig. 2a.

Thus, in problems wherein separation of modes is easy, the procedure of Kitagawa et al. [10] is more accurate to extract mixed mode K-factors, since it is insensitive to the approximation of W near the crack-tip. However, for nonlinear elastic problems, or general 3-dimensional problems, the present procedure is preferable. A comparison of the results for K_I and K_{II}, in the static case, for the problem of Fig. 1 is shown in Tables I and II.

Table I
(Quarter-point Singular Elements)

	$K_I/\sigma\sqrt{\pi a}$	$K_{II}/\sigma\sqrt{\pi a}$
Present Procedure	1.275	0.569
Kitagawa et al.'s mode decomposition	1.285	0.547
Bowie & Freese [11]	1.27	0.58

Table II
(Non-singular Isoparametric Elements)

	$K_I/\sigma\sqrt{\pi a}$	$K_{II}/\sigma\sqrt{\pi a}$
Present Procedure	1.335	0.365
Kitagawa et al.'s mode decomposition	1.274	0.540
Bowie & Freese [11]	1.27	0.547

The presently computed results for the problem whose configuration is shown in Fig. 1, and wherein the crack propagates in a self-similar fashion are shown in Fig. 3. Here, the variation of K_I, K_{II} with time, or alternatively the crack length (a is the crack length, θ_c the direction of propagation) is shown when the crack velocity C = 0.5 times the shear wave speed C_s.

ELASTO-PLASTIC DYNAMIC CRACK PROPAGATION

Here we confine ourselves to briefly mentioning the yet unpublished work of the authors concerning two integrals which are path-independent in elasto-plastic dynamic crack propagation when a rate theory of plasticity is used. These are:

$$(\Delta \underline{T})_{dp} = \lim_{\epsilon \to 0} \int_{\Gamma_\epsilon} [(\underline{\tau} : \Delta \underline{\epsilon} + \Delta U + \Delta K)\underline{N} - \underline{N} \cdot \underline{\tau} \cdot \Delta \underline{e} - \underline{N} \cdot \Delta \underline{\tau} \cdot \underline{e}]\, ds$$

$$= \int_{\Gamma+\Gamma_c} [(\underline{\tau}:\Delta\underline{\epsilon} + \Delta U + \Delta K)\underline{N} - \underline{N}\cdot\underline{\tau}\cdot\Delta\underline{e} - \underline{N}\cdot\Delta\underline{\tau}\cdot\underline{e}\,]ds$$

$$+ \int_{V-V_\epsilon} [(\nabla\underline{\epsilon} + \tfrac{1}{2}\nabla\Delta\underline{\epsilon}):\Delta\underline{\tau} - (\nabla\tau + \tfrac{1}{2}\nabla\Delta\underline{\tau}):\Delta\underline{\epsilon}$$

$$+ \rho(\underline{a}\cdot\Delta\underline{e} - \dot{\underline{u}}\cdot\nabla\Delta\dot{\underline{u}}) + \rho(\Delta\underline{a}\cdot\underline{e} - \Delta\dot{\underline{u}}\cdot\nabla\dot{\underline{u}})]dV$$

and

$$(\Delta\underline{T})_{dp} = \underset{\epsilon\to 0}{Lt} \int_{\Gamma_\epsilon} [(\underline{\tau}:\Delta\underline{\epsilon} + \Delta U + \Delta K)\underline{N} - \underline{N}\cdot\underline{\tau}\cdot\Delta\underline{e} - \underline{N}\cdot\Delta\underline{\tau}\cdot\underline{e}\,]ds$$

$$+ \int_{V_t-V_\epsilon} [\Delta\underline{\tau} + \tfrac{1}{2}\nabla\Delta\underline{\tau}):\Delta\underline{\epsilon} - (\nabla\underline{\epsilon} + \tfrac{1}{2}\nabla\Delta\underline{\epsilon}):\Delta\underline{\tau}$$

$$+ \rho(\dot{\underline{u}}\cdot\nabla\Delta\dot{\underline{u}} - \underline{a}\cdot\Delta\underline{e}) + \rho(\Delta\dot{\underline{u}}\cdot\nabla\dot{\underline{u}} - \Delta\underline{a}\cdot\underline{e})]dV$$

$$= \textit{path independent when } (\Gamma_\epsilon) \textit{ is replaced by } (\Gamma + \Gamma_c) \text{ and}$$

$$(V_t - V_\epsilon) \textit{ is replaced by } (V_t - v)\ .$$

In the above, $\Delta\underline{\epsilon}$, $\Delta\underline{\tau}$, $\Delta\underline{u}$, $\Delta\dot{\underline{u}}$, $\Delta\underline{a}$ and $\underline{u}$ are incremental, strain, stress, displacement, velocity, acceleration, respectively; and $\underline{\tau}$, $\underline{e}$, $\underline{a}$ are the current stress, displacement gradient, and acceleration, respectively, while V_t is the total volume of the body; ΔU is the incremental stress working density such that $\Delta\underline{\tau} = \partial\Delta U/\partial\Delta\underline{\epsilon}$, and thus can include arbitrary loading/unloading in elasto-plasticity.

ACKNOWLEDGEMENTS

The results presented above were obtained during the course of investigations supported by ONR, whose support is gratefully acknowledged. The authors thank Ms. J. Webb for her careful assistance in the preparation of this manuscript.

REFERENCES

1. Atluri, S.N., Engineering Fracture Mechanics, 16 (1982) 341-364.

2. Nishioka, T., and Atluri, S.N., Engineering Fracture Mechanics, 17 (1983) (in press).

3. Atluri, S.N., Nishioka, T., and Nakagaki, M., in Nonlinear and Dynamic Fracture Mechanics, N. Perrone and S.N. Atluri (eds.), ASME, AMD, 35 (1979) 37-66.

4. Nishioka, T., and Atluri, S.N., Journal of Applied Mechanics, 47 (1980) 570-576 and 570-583.

5. Nishioka, T., and Atluri, S.N., Engineering Fracture Mechanics, 16 (1982) 303-332.

6. Nishioka, T., and Atluri, S.N., Engineering Fracture Mechanics, 16, 2 (1982) 157-175.

7. Kishimoto, K., Aoki, S., and Sakata, M., Engineering Fracture Mechanics, 13 (1980) 841-850.

8. Budiansky, B. and Rice, J.R., Journal of Applied Mechanics, 40 (1973) 201-203.

9. Herrmann, A.G., and Herrmann, G., "On Energy Release Rates for a Plane Crack," Stanford University (1981).

10. Kitagawa, H., Okamura, H., and Ishikawa, H., Proceeding of JSME, No. 760-13 (1976) 46-48.

11. Bowie, O.L., Mechanics of Fracture I, G.C. Sih ed., Noordhoff (1973) 1-55.

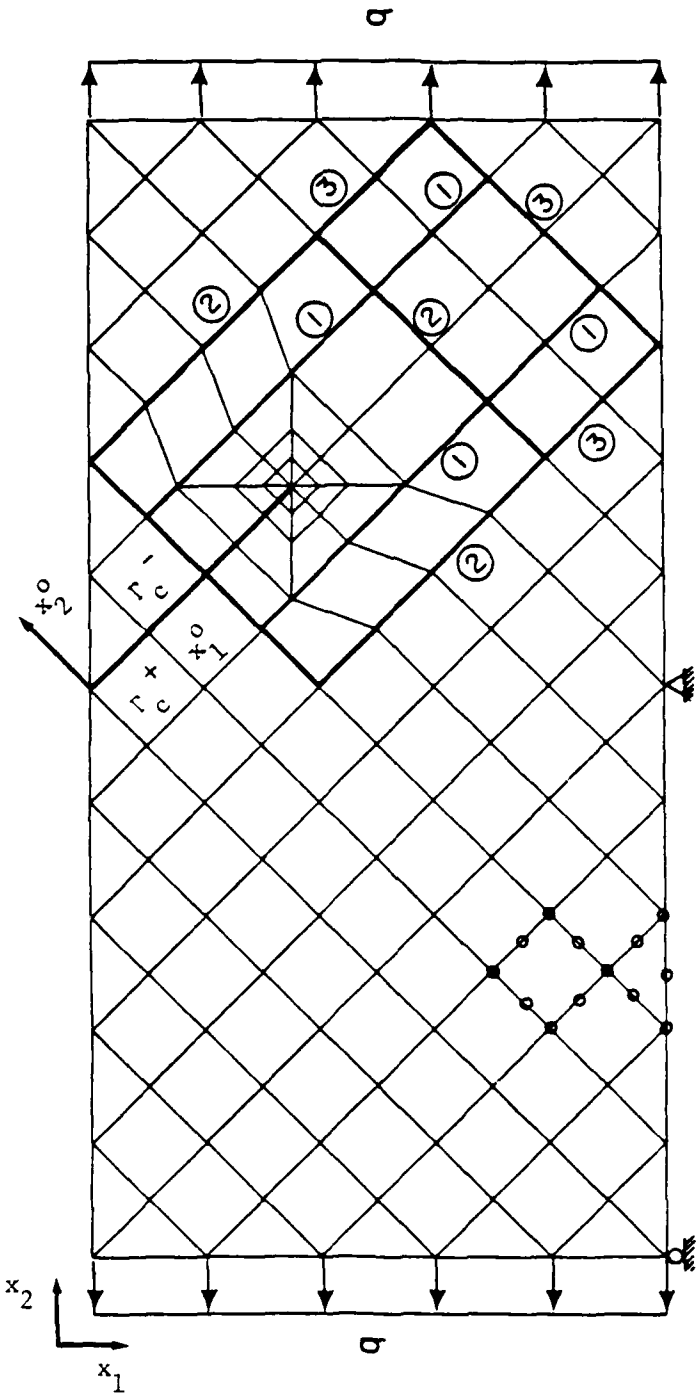

Figure 1.

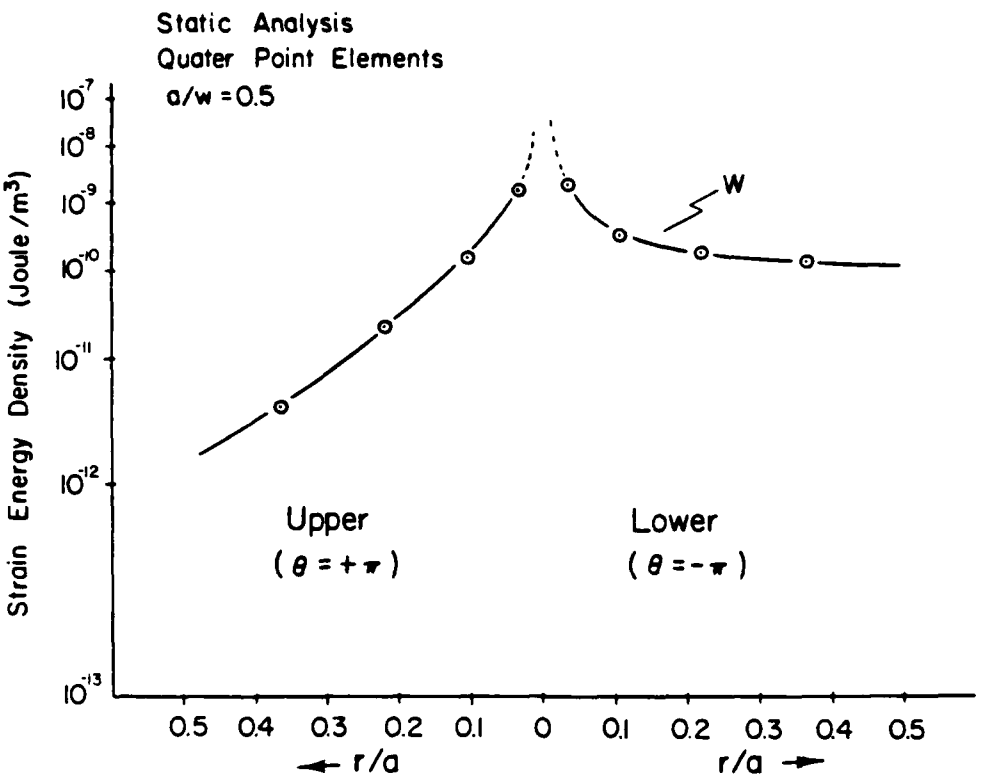

Figure 2a.

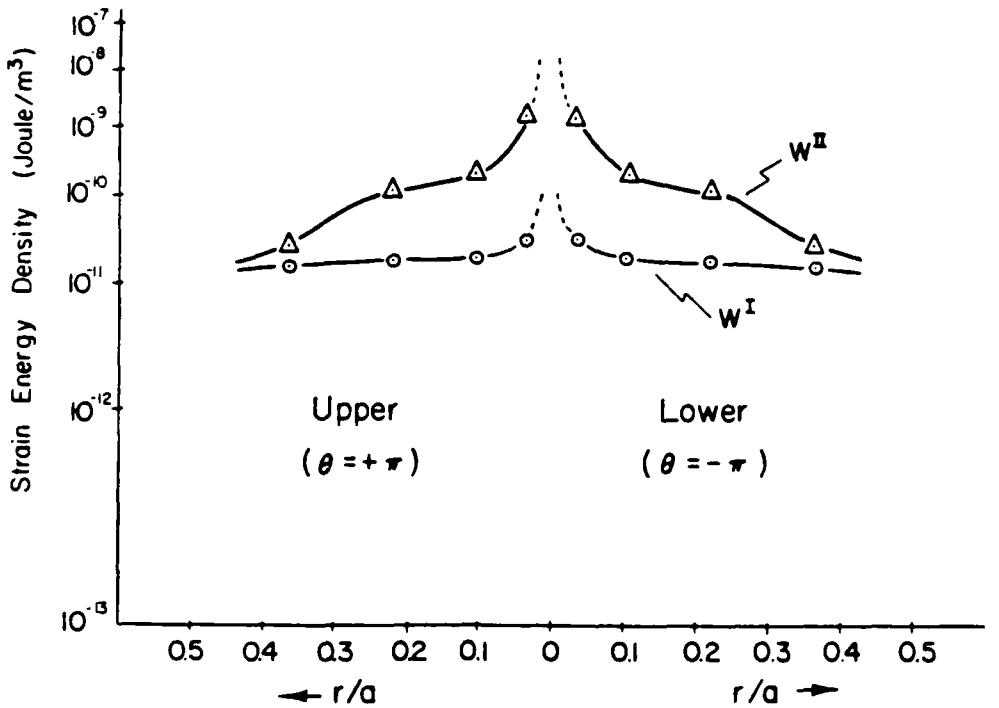

Figure 2b.

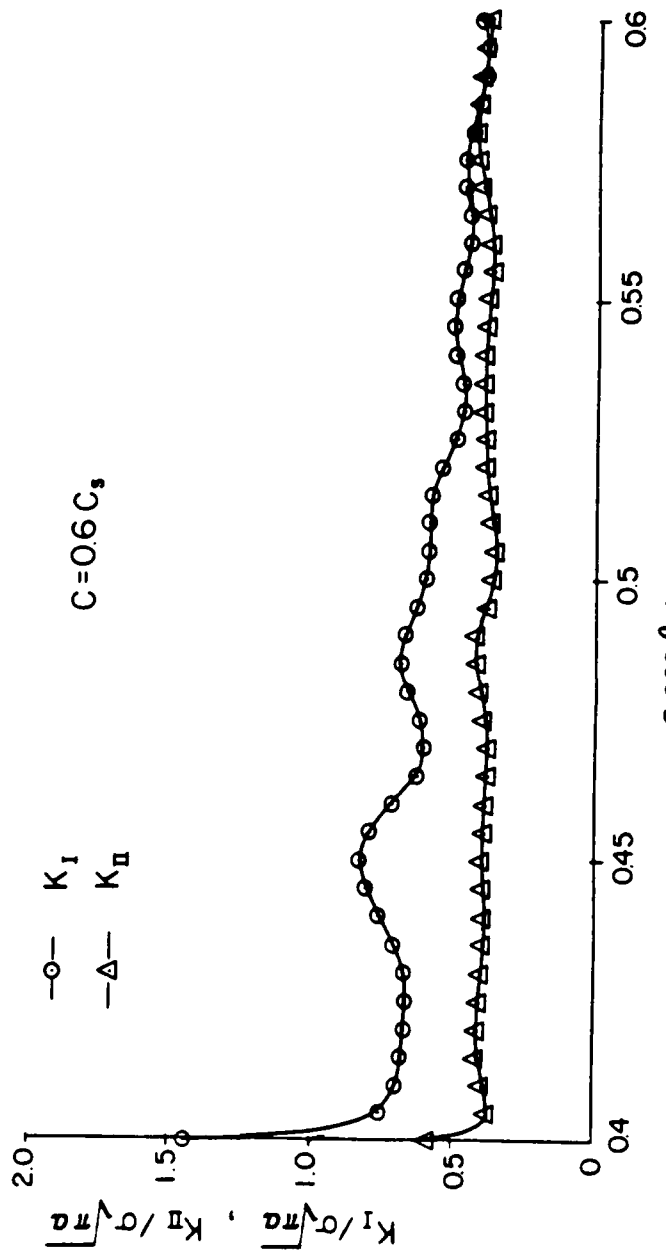
C=0.6 C_s
—o— K_I
—Δ— K_{II}
$K_I/\sigma\sqrt{\pi a}$, $K_{II}/\sigma\sqrt{\pi a}$
2.0
1.5
1.0
0.5
0
0.4
0.45
0.5
0.55
0.6
a cos θ_c/w

Figure 3.

CRACK BRANCHING, CRACK ARREST AND RAPID TEARING

A.S. Kobayashi
Department of Mechanical Engineering
University of Washington

1. INTRODUCTION

For the past several years, the author and his colleagues have been involved in various aspects of dynamic fracture research where dynamic photoelasticity was used to quantify the dynamic fracture parameters associated with a running crack in photoelastic polymers. The experimental data were also used to verify a dynamic finite element code executed in its generation and propagation modes. Experimentally measured crack velocity was then used to drive the verified finite element code in its generation mode to extract dynamic fracture parameters, which could not be measured directly, in metals and ceramics. In the following, some recent results obtained in three research projects on dynamic fracture using the above mentioned techniques are summarized. These results involve dynamic and static crack branching in Homalite-100 plates and metal pipes, dynamic crack arrest in structural ceramics and rapid tearing of thin polycarbonate sheets.

2. CRACK BRANCHING

The crack branching criterion, which was recently proposed in [1,2], requires a critical stress intensity factor to trigger crack branching and a crack curving criterion for predicting the crack branching angle. A review of all past and recent crack branching data on Homalite 100 and polycarbonate photoelastic polymers showed that most cracks would bifurcate upon reaching a branching stress intensity factor. The bifurcated cracks also satisfied the crack curving criterion. This crack curving criterion [3,4], which is a dynamic extension of the static crack curving criterion by Streit and Finnie [5], is the sufficiency condition for the bifurcated cracks to propagate

in a slanted direction in the presence of a positive remote stress component. A negative remote stress component, on the other hand, predicts a self-similar crack extension [6] or no branching which conflicts with the requirement of large energy dissipation. The crack curving criterion is based on the postulate that the micro-cracks ahead of the crack tip dictate the direction of crack propagation. An off-axis micro-void, which is within a critical distance, r_c, to the crack tip, is actuated by a critical crack tip stress field and deflects the crack from its otherwise self-similar propagation path. The distance between the micro-void and the crack tip, r_o, is a characteristic distance which is governed by the singular state of stress as well as the second order term, i.e. the remote stress component. The critical distance, r_c, is assumed to be a material property.

Figure 1 shows the variations in dynamic stress intensity factors, K_I and K_{II}, and the characteristic distance r_o during crack branching in a Homalite-100 single-edged notch specimen. Table 1 shows the crack branching stress intensity factors, K_{Ib}, the critical distance, r_c and measured and predicted crack branching angles. The crack branching angle was estimated by modifying the crack curving criterion for negative remote stress components [7]. Similar results have been obtained from a recently completed dynamic photoelastic analysis of crack branching in polycarbonate single-edged notch specimens [7]. The crack branching criterion was also used to predict the crack branching angle of bifurcated cracks which initiated under static loading at the blunt starter cracks in Homalite-100, wedge-loaded, double-cantilever beam specimens. The crack branching angles in pressurized steel [8,9] and aluminum [10] pipes, as shown in Table 2, were also predicted by this crack branching criterion.

3. CRACK ARREST IN STRUCTURAL CERAMICS

Recent failures of ceramic heat engine components have prompted the use of static fracture mechanics for life-time and failure predictions of the ceramics. Prototype testings show that failures of ceramic components are characterized by complete fracture in contrast to partial crackings observed in alloy steel components. This difference in failure modes has been

attributed by the author and his colleagues to the differences in the dynamic fracture responses of structural ceramics and steel [11].

The dynamic fracture studies involved glass and reaction bonded silicon nitride wedge-loaded double cantilever beam specimens [12,13]. Crack length versus time histories were used to drive a dynamic finite element code from which the dynamic fracture parameters were extracted. Although the cracks started from relatively blunt, machined crack tips, these ceramics exhibited an initial crack acceleration phase which has not been observed in metals and polymers. As a result, the dynamic responses in ceramics were not as pronounced as those of metals and polymers. A distinct crack deceleration phase without crack arrest was also observed. Figure 2 shows the dynamic stress intensity factor, K_I^{dyn}, versus crack velocity, $\dot{a}$, relation of reaction bonded silicon nitride. Also shown for comparison is an idealized dynamic fracture toughness versus crack velocity relation of steel.

In contrast with the well studied steel and photoelastics polymers, Reference [12,13] showed that dynamic fracture analysis of ceramics can be approximated by quasi-static analysis. Also in contrast with metals and polymers, a propagating crack in ceramics will not arrest unless it enters a vanishing stress intensity factor field. This lack of a dynamic crack arrest stress intensity factor results in complete fracture of ceramic components.

4. RAPID TEARING OF POLYCARBONATE SHEETS

Recent dynamic photoelastic analysis of fracturing 1.6 mm thick polycarbonate sheets has shown that the crack velocity is less than 5 percent of the dilatational stress wave velocity and that the propagating crack tip was preceded by a necked region. The former reduced dynamic fracture of thin polycarbonate sheets to quasi-static analysis and the latter justified the use of a Dugdale strip yield zone to model the propagating plastic yield zone. A Dugdale strip yield zone together with two tangential surface tractions, which modeled the residual stresses generated in the wake of rapid tearing, generated isochromatics which resembled the isochromatics surrounding the propagating crack [14].

This modified Dugdale model was further improved by incorporating higher order, non-singular terms in the static crack-tip stress field. This crack-tip stress field contains as disposable parameters the undetermined coefficients associated with the polynomial of $r^{n/2}$ and the undetermined tangential surface tractions. These disposable parameters were determined by least square fitting the isochromatics associated with this modified Dugdale model to the elastic isochromatics in thin fracturing polycarbonate specimens. Figure 3 shows typical experimentally observed isochromatics and those associated with the modified Dugdale model. The fractional fringe orders for the isochromatics in the yield region were estimated through the use of a constant strain-optical coefficient and deformation theory of plasticity. This and twenty other similar results verified the modified Dugdale model for rapid tearing of thin polycarbonate plates [15]. The modified Dugdale model with non-singular mode II crack tip stress field was also used successfully to model the strip yield zone and the stable crack growth from a slanted crack in thin polycarbonate tension specimens [16]. This modified Dugdale model is being used with equal success to model rapid tearing of thin 7075-T6 aluminum plates.

5. CONCLUSIONS

1. A dynamic crack branching criterion, which requires a crack branching stress intensity factor as a necessary condition and a crack curving criterion as a sufficiency condition, has been established.

2. The terminal crack velocity of structural ceramics is less than 5 percent of its dilatational stress wave velocity. A propagating crack in ceramics will arrest only upon entering a vanishing stress intensity factor field.

3. A modified Dugdale model can be used to model the crack-tip stress field associated with rapidly tearing cracks in thin polycarbonate and aluminum specimens.

ACKNOWLEDGEMENTS

The crack branching studies, the crack arrest studies in ceramics and the rapid tearing studies are being funded by ONR Contract N00014-76-0060 NR-064-478, NASA Grant NGL 48-002-004 to the Ceramic Engineering Division and NSF Grant No. CME-792507, respectively.

REFERENCES

1. Ramulu, M., Kobayashi, A.S., and Kang, B. S.-J., "Dynamic Crack Branching - A Photoelastic Evaluation," to be published in Fracture Mechanics, (15th), ASTM STP (1983).

2. Ramulu,M., Kobayashi, A.S., and Kang, B. S.-J., "Dynamic Crack Curving and Branching in Line-Pipe," ASME Journal of Pressure Vessel Technology, 104 (1983) 317-322.

3. Ramulu, M. and Kobayashi, A.S., "Dynamic Crack Curving - A Photoelastic Evaluation," to be published in Experimental Mechanics.

4. Sun, Y.-J., Ramulu, M., Kobayashi, A.S. and Kang, B. S.-J., "Further Studies on Dynamic Crack Curving," Developments in Theoretical and Applied Mechanics, T.J. Chung and G.R. Karr (eds.), The University of Alabama, Huntsville (1982) 203-218.

5. Streit, R. and Finnie, I. "An Experimental Investigation of Crack Path Directional Stability," Experimental Mechanics, 20 (1980) 17-23.

6. Kim, K.S., private communication dated July 15, 1983.

7. Ramulu, M., Kobayashi,A.S., Kang, B. S.-J., and Barker, D., "Further Studies on Dynamic Crack Branching," to be published in Experimental Mechanics.

8. Almond, E.A., Petch, N.J., Wraith, A.E., and Wright, E.S., The Fracture of Pressurized Laminated Cylinders," Journal of Iron and Steel Institute, 207 (1969) 1319-1323.

9. Congleton, J., "Practical Applications of Crack-Branching Measurements," Dynamic Crack Propagation G.C. Sih (ed.), Noordhoff Int. Publ., Leyden, (1973) 427-438.

10. Shannon, R.W.E. and Wells, A.A., "A Study of Ductile Crack Propagation in Gas Pressurized Pipeline," Proceedings of International Symposium on Pipeline, Paper No. 17, Newcastle upon Tyne (1974).

11. Kobayashi, A.S., Emery, A.F., and Liaw, B.M., "Crack Arrest in Structural Ceramics," to be published in Proc. of the 1983 (5th) ASME Failure Prevention and Reliability Conf., Dearborn, Michigan, Sept. 11-14, 1983.

12. Kobayashi, A.S., Emery, A.F. and Liaw, B.M., "Dynamic Fracture Toughness of Glass," to be published in the Proceedings of the 3rd International Symposium on Fracture Mechanics of Ceramics, Plenum Press (1983).

13. Kobayashi, A.S., Emery, A.F., and Liaw, B.M., "Dynamic Fracture Toughness of Reaction Bonded Silicon Nitride," Journal of American Ceramic Society, Vol. 66, No. 2, Feb. (1983).

14. Kobayashi, A.S., and Lee, O.S., "Elastic Field Surrounding a Rapidly Tearing Crack," to be published in Elastic-Plastic Fracture, 2nd Symp., ASTM STP (1983).

15. Lee, O.S., and Kobayashi, A.S., "Crack Tip Plasticity of a Tearing Crack," to be presented at the 16th ASTM National Symposium on Fracture Mechanics, Columbus, Ohio, Aug. 15-18, 1983.

16. Sun, Y.J., Lee, O.S., and Kobayashi, A.S., "Crack Tip Plasticity Under Mixed Mode Loading," to be presented at the ICF Int. Symp. on Fracture Mechanics, Beijing, China, Nov. 22-25, 1983.

Table 1 Crack Branching Data

Homalite-100 Single-Edged Notch Specimens

Specimen No.	Branching		Half Branching Angle	
	K_{IB}	r_c		
	MPa$\sqrt{m}$	mm	Measured	Estimated
B8	2.08	1.2	23	28
B9	2.03	1.3	30	28
W082270	2.03	1.4	26	28
B7	2.03	1.4	30	28
B5	2.08	1.2	30	28
B6	2.09	1.3	28	28
Average	2.04	1.3	27.8	28

Table 2 Crack Branching Data

Pressurized Metal Pipes

Material	Branching		Half Branching Angle	
	K_{Ib}	r_c		
	MPa$\sqrt{m}$	mm	Measured	Predicted
Steel	124	1	66	64
Aluminum	xx	1.3	88	84

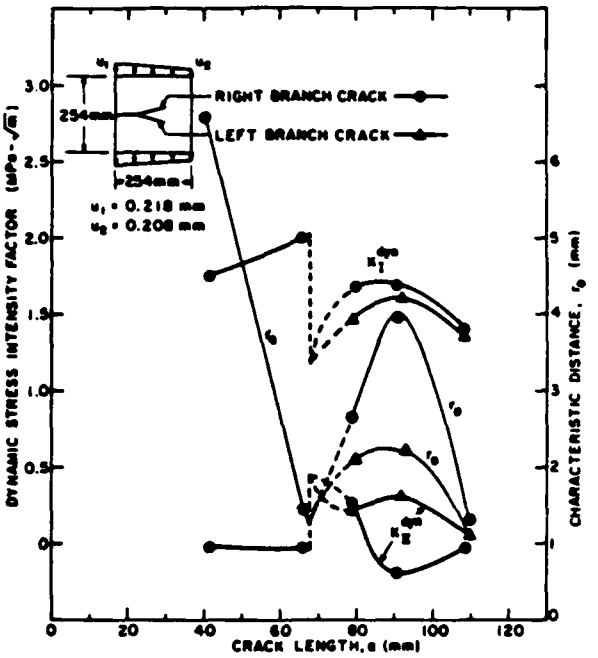

Figure 1. Dynamic stress intensity factors and r_o of branched cracks. Specimen No. B8.

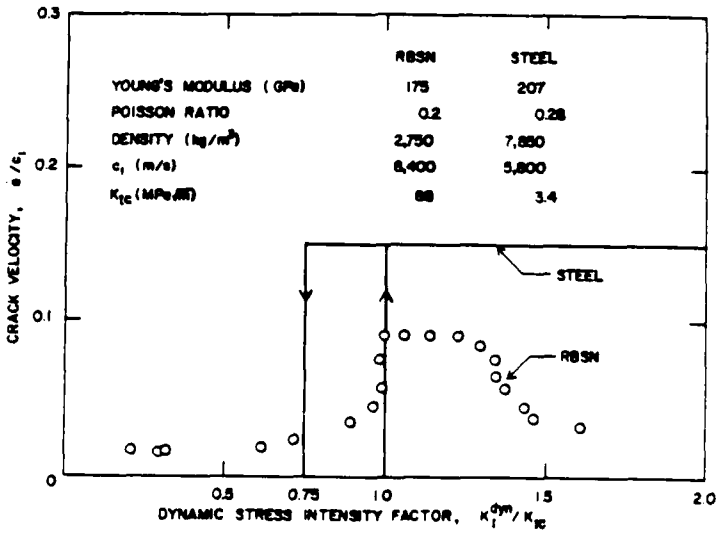

Figure 2. Dynamic stress intensity factor versus crack velocity relation of reaction bonded Silicon Nitride and steel.

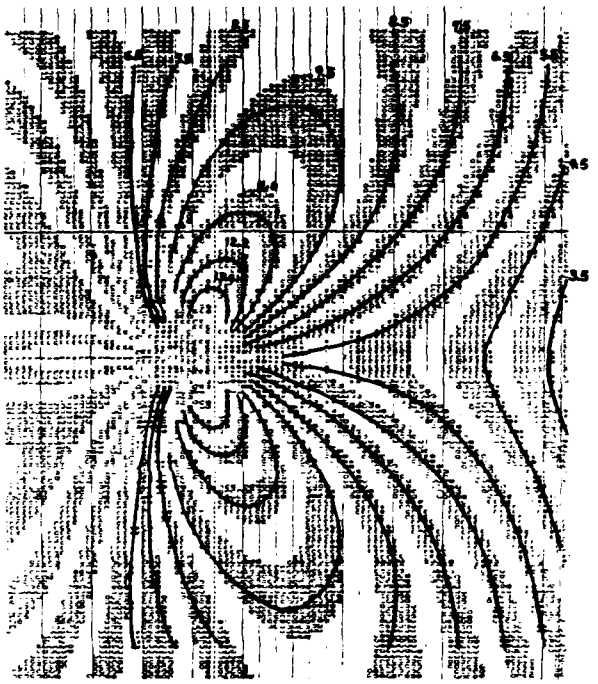

Figure 3. Experimental and theoretical isochromatics surrounding a rapidly tearing crack in a thin polycarbonate sheet.

DYNAMIC KINKING AND BIFURCATION OF CRACKS IN PLANE STRAIN

P. Burgers
Hibbitt, Karlsson and Sorensen, Inc.
Providence, Rhode Island

1. INTRODUCTION

The bifurcation event in dynamic crack propagation is an extremely complicated process. Typically, experiments show that the process is inherently three-dimensional in that the crack front is not straight. Also there is no single instant of bifurcation but in the process zone multiple bifurcation attempts are made by the propagating crack. Only a few of these attempts are successful on a macroscopic scale. For these successful bifurcation attempts, usually there is not a sharp point at which the crack kinks, but a short distance over which the crack direction changes rapidly.

It is only recently that experimental results have been obtained for which the experiments are sufficiently simple that there is any hope of modelling them analytically. The detailed three dimensional situation existing at bifurcation is far too complex to be treated at present. It is true however that providing the microscopic details are not considered, the approximation to planar deformation is not unreasonable. This simplification, in this case to plane strain, is essential. In this spirit, we take a "small scale yielding" approach, and assume that the "process" zone or the region in which significant bifurcation attempts are made is small with respect to any characteristic length in the problem. The process zone (and therefore the length over which the bifurcation cracks are curving rapidly) reduces to a point, giving a well-defined "instant" of bifurcation. This approximation will be valid when the crack branches are "long" with respect to the process zone. The details of deformation in the process zone can then presumably be lumped into a fracture criterion as is typically done in fracture mechanics. The determination of this fracture criterion is the purpose of this work together with much of the other work presented at this workshop.

It should be pointed out that the experimental results obtained for dynamic fracture such as in [1,2] are forced to take the same viewpoint. For example, the dimensions of typical caustic curves are on the order of 1 mm, whereas the process zone is about an order of magnitude smaller.

If the macroscopic viewpoint is taken, experimental results of bifurcation and kinking of cracks can be summarized as follows. The kink angle or half the included angle at bifurcation lies between 10° and 30° to 45° for crack propagating in glass or polymers such as PMMA. The velocity of the bifurcated cracks v_{CT} is of the order of .9 of crack propagation speed before bifurcation, which is usually less than .5 of the Rayleigh wave speed c_R.

2. ANALYSIS AND DESCRIPTION OF THE MODEL

The type of problems that can model dynamic bifurcation or kinking is limited. Currently the most promising technique can handle only self-similar problems; that is, the stresses must be self-similar in the radial coordinate from the bifurcation point r and time from bifurcation t. Also, the initial conditions must be for a stationary semi-infinite crack in a stress free full space, and that bifurcation occurs immediately at load application. This latter restriction will be removed in an approximate manner later.

The loading considered is normal step function in time loading on the crack faces. The wavefront patterns are shown in Fig. 1. As such, the model is fairly close to the experiments done by Ravi-Chandar [1], although the observed that the crack initially propagated straight ahead before bifurcating.

The solutions to the following problem are obtained by constructing Green's functions which consist of shear and edge dislocations which propagate out of the original crack at constant velocity u and whose Burger's vectors grow linearly with time as shown in Fig. 2. To obtain the solutions for these Green's functions the stress field of pairs of edge and shear dislocations in a full space must be first derived.

The stresses are of the form $\underline{\sigma} = \underline{\sigma}(r/t,\Theta,u)$. Along z = 0 we note that any particular stress level propagates out with constant velocity v = r/t. A superposition of normal and shear point loads whose magnitude grows linearly with time and which propagate out at constant velocity along the original crack faces from the origin (see Fig. 3) can be used to cancel the stresses along z = 0, x < 0 due to the dislocations.

The Green's functions are now constructed and the stresses due to either the shear or edge dislocations are self-similar. The velocity of propagation of the dislocations can now be used as a superposition parameter to form an arbitrary distribution of σ_{zz}, σ_{xz} on z = 0, x < 0. This can be expressed as

$$\underline{\sigma}(r/t,\Theta) = \int_0^{v_{CT}} [\, \underline{\sigma}^{EC}(r/t,\Theta,u)\ F^E(u) + \underline{\sigma}^{SC}(r/t,\Theta,u)\ F^S(u)]\ du\ ,$$

where E,S indicate edge and shear dislocations respectively, and $F^E(u)$, $F^S(u)$ are the distribution of edge and shear dislocations. The bifurcated crack tip speeds are v_{CT}.

If the left-hand side is set equal to the stresses required to be removed from (or applied to) the bifurcated (kinked) crack faces, dual Cauchy singular integral equations are obtained, for which there are a number of efficient numerical solution techniques; for example see [3,4].

3. RESULTS AND PREDICTIONS OF POSSIBLE FRACTURE CRITERIA

To understand the sensitivity of the stress intensity factors to the kink angle, we consider normal loading applied to the kinked and bifurcated crack cases. See Fig. 4. We note that for the kinked crack case the kink angle has almost negligible influence. For the bifurcated crack case the more significant dependence of $K_{I,II}$ on δ is due to the cracks interacting with one another. The above results are presented more fully in [4,5].

The results of the more realistic model for bifurcation with step function normal loading on the original crack faces for the kinked and bifurcated crack cases are shown in Fig. 5.

If we use as a criterion for bifurcation the requirement that $K_{II} = 0$, we see that only in the

bifurcated crack case will the crack deviate from straight ahead. In this case, this criterion predicts bifurcation only at $\delta = 0.05\pi$, which is within the observed range for bifurcation.

It must be pointed out here that recently the kinked crack case has been solved asymptotically [6] by expanding the solution in terms of δ about $\delta = 0$. These results compare very well with Fig. 4a due to the result shown in Fig. 3; that is, the kink geometry does not affect the solution very significantly.

4. TIME DELAY IN CRACK INITIATION

To improve the model, a time delay in the start of crack propagation after the application of loading must be included, since it is unrealistic to consider crack initiation under zero stress intensity factor. If the loading is applied at time $t = -\epsilon$ and the crack starts propagating at $t = 0$, an asymptotic solution in ϵ can be obtained by expanding about self-similar problems. The stresses can be expressed as

$$\begin{aligned} \underline{\sigma}(r,\theta,t+\epsilon) &= \underline{\sigma}(r/t,\theta) + \frac{d}{dt}\underline{\sigma}(r,\theta,t+\epsilon)\Big|_{\epsilon=0} + O(\epsilon^2) \\ &= \underline{\sigma}(r/t,\theta) + \epsilon\frac{d}{dt}\underline{\sigma}(r/t,\theta)\Big|_{\epsilon_{fixed}} + O(\epsilon^2) \end{aligned}$$

where $\epsilon = \overline{x} - vt$, $t >> \epsilon$.

This implies

$$\begin{aligned} K^{\bullet}_{I,II}(t+\epsilon) &\simeq K^{\bullet}_{I,II}(t^{\frac{1}{2}} + \epsilon/2t^{\frac{1}{2}}) + O(\epsilon^2) \\ &\simeq K^{\bullet}_{I,II}(t+\epsilon)^{\frac{1}{2}} + O(\epsilon^2), \quad t >> \epsilon \end{aligned}$$

where $K^{\bullet}_{I,II}$ are the abscissal in Fig. 4 and 5. For $t << \epsilon$, we use an analogy with Freund's result [7] at $t = 0^+$ to get

$$K_{I,II}(t+\epsilon) = K^{\bullet}_{I,II}\epsilon^{\frac{1}{2}} .$$

To order ϵ^2 the stress intensity factor for the delay time problem is given by $K_{I,II}(t+\epsilon)^{\frac{1}{2}}$ which is exactly Freund's result for the straight crack case.

We can now consider more realistic criteria for crack initiation. A possible candidate is that the applied energy release rate $G^{applied}$ equal some material property G^{mat} at initiation. Normalized $G^{applied}$ is tabulated for different values of δ and v_{CT}. Case (a) corresponds to normal loading on the new crack faces and case (b) to normal loading on the original crack faces.

Table 1. Normalized Energy Release Rate versus δ.

v_{CT}/c_R	Loading Case	δ/π 0.3125	.125	.25	.375	.485
.1	a	.0485	.0559	.0522	.0376	.0308
	b	.1702	.1590	.1295	.1278	.1723
	c	.3963	.3861	.2964	.2210	.2002
.3	a	.1129	.1374	.1541	.1404	.1221
	b	.0466	.0455	.0565	.0800	.1804
	c	.3028	.3082	.2909	.2313	.1882
.5	a	.1479	.1946	.2482	.3138	.2062
	b	.0112	.0136	.0229	.0442	.0779
	c	.2381	.2667	.2563	.2187	.1150
.7	a	.1478	.2065	.2761	.3788	.3205
	b	.0011	.0025	.0088	.0249	.0529
	c	.1707	.2039	.2106	.1804	.0963
.9	a	.1058	.1419	.1678	.2166	.2081
	b	.0001	.0007	.0038	.0123	.0291
	c	.0934	.1104	.1135	.1004	.0594

If we assume crack bifurcation occurs, we see that for $v_{CT} \geq .3\ c_R$ the crack will tend to propagate straight, indicating bifurcation is unlikely at t = 0. This corresponds to the results obtained by Ravi-Chandar where the crack always propagated straight for a short distance before bifurcating. For $v_{CT} \leq .5\ c_R$ δ would depend on v_{CT} at initiation, which we have no rational way of picking.

For crack growth after initiation, the energy release rate grows linearly with time so neither the model nor fracture criterion can be considered to be correct.

5. CONCLUSIONS

A great deal of progress has been made in analyzing the bifurcation event in dynamic fracture. However, the analysis is still not sufficiently general to model the experimental results accurately. It does seem possible that such generalizations can be made. The case of a crack which is initially propagating under some loading and then bifurcates is the type of problem which must be solved. The difficulty in solving this problem lies in the loss of the self-similarity in the stress fields.

REFERENCES

1. Ravi-Chandar, K., "An Experimental Investigation into the Mechanics of Dynamic Fracture," Ph.D. Thesis, California Institute of Technology (1982).

2. Rosakis, A.J., Duffy, J., and Freund, L.B., "Dynamic Crack Growth Criteria in Structural Metals," Proceedings, Workshop on Dynamic Fracture, Feb. 17-18, 1983, California Institute of Technology, Pasadena, California.

3. Burgers, P., "Dynamic Propagation of a Kinked or Bifurcated Crack in Anti-Plane Strain," J. Appl. Mech. 49 (1982) 371-376.

4. Burgers, P., "Dynamic Kinking of a Crack in Plane Strain," accepted for publication by Int. J. Solids Structures (1983). -

5. Burgers, P. and Dempsey, J.P., "Plane Strain Dynamic Crack Bifurcation," submitted to Int. J. Solids Structures (1982).

6. Achenbach, J.D., Kuo, M.K., and Dempsey, J.P., "Mixed Mode I-II Crack Kinking Under Stress Wave Loading," manuscript form (1982).

7. Freund, L.B., "Crack Propagation in an Elastic Solid Subjected to General Loading - II. Non-Uniform Rate of Extension," J. Mech. Phys. Solids, 20 (1972) 141-152.

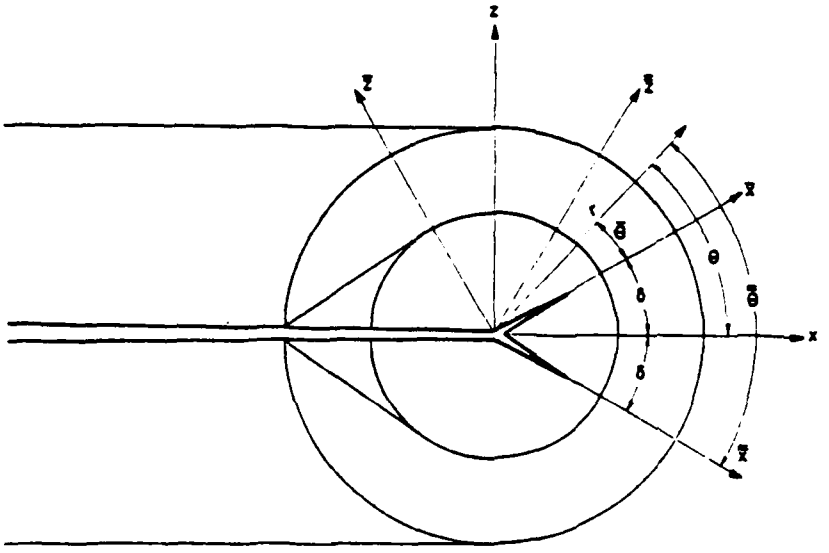

Figure 1. Stress wave pattern for normal step function loading on the original crack faces.

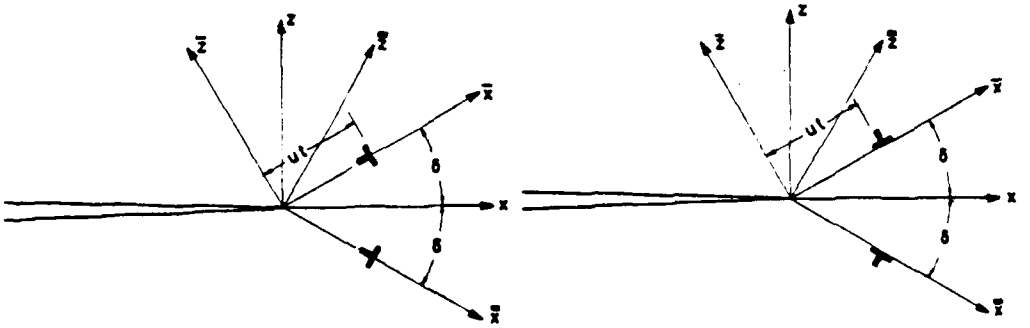

Figure 2. a) Edge and b) shear dislocations propagating out of the tip of a semi-infinite crack in an initially stress free full space.

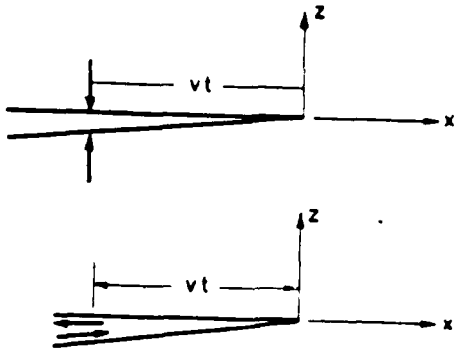

Figure 3. a)Normal and b) shear point loads which grow linearly with time and propagate out at constant velocity along the original crack faces.

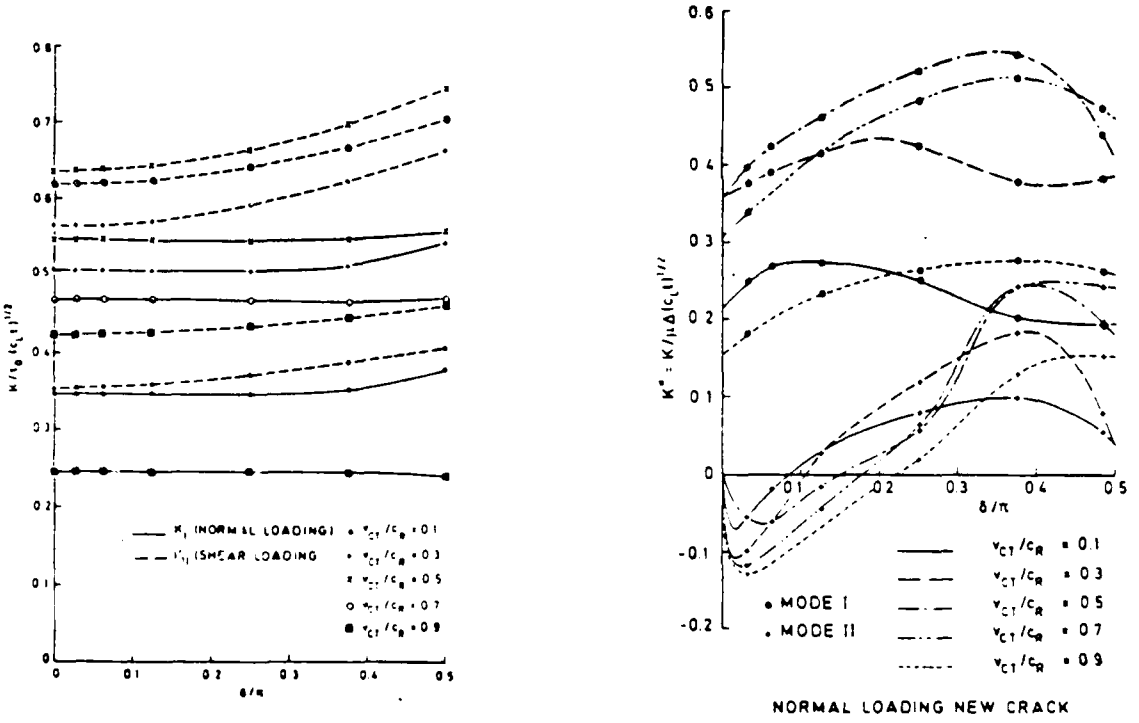

Figure 4. a)Constant normal and shear loading on the new faces of a kinked crack. b) Normal loading on the new faces of a bifurcated crack.

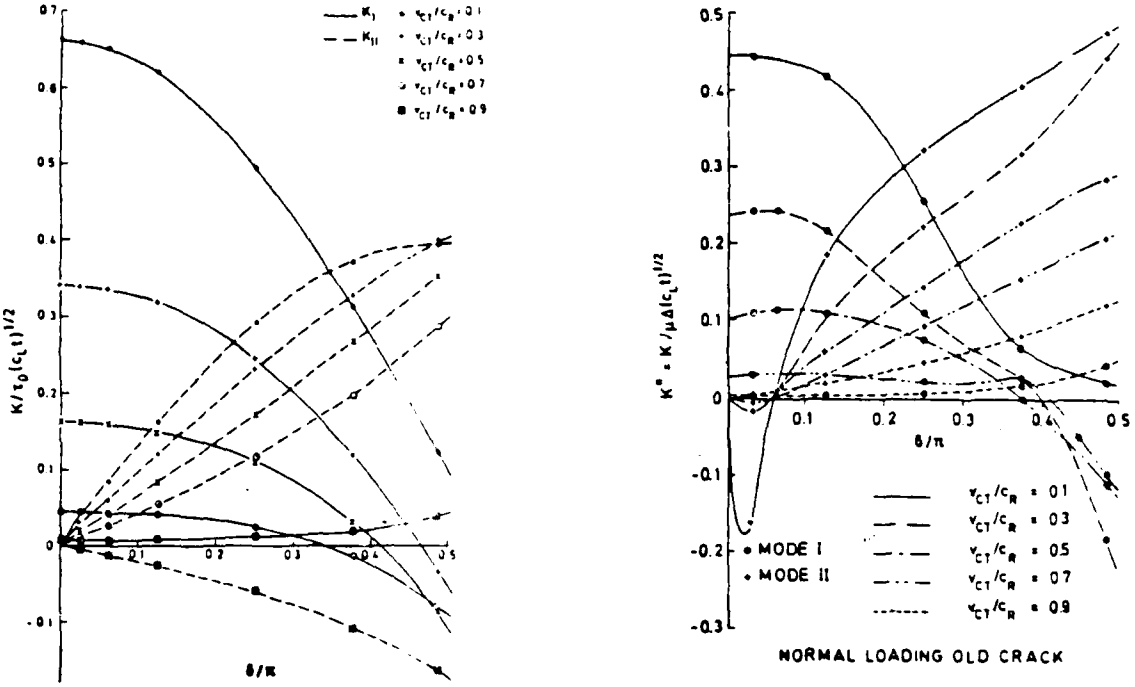

Figure 5. Normal loading on the original crack faces of a) kinked crack, and b) bifurcated crack.

AD-A140 194 WORKSHOP ON DYNAMIC FRACTURE HELD AT PASADENA CALIFORNIA ON 17-18 FEBRUARY 1983(U) CALIFORNIA INST OF TECH PASADENA W G KNAUSS ET AL. OCT 83 3/3

UNCLASSIFIED ARO-19961.1-EG-CF DAAG29-83-M-0101 F/G 11/6 NL

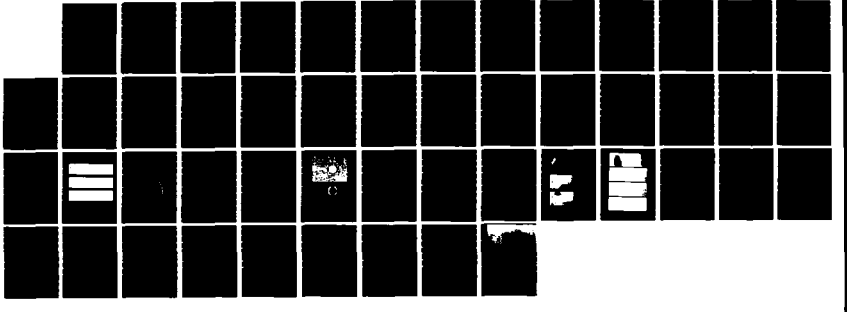

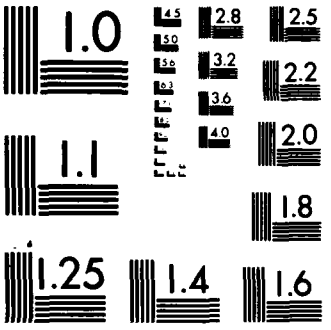

SYNOPSIS OF SESSION IV: INELASTIC CRACK GROWTH

R.J. Clifton
Brown University

J.D. Achenbach reviewed near-tip fields for steady-state dynamic crack propagation in elastic-plastic materials. For linear strain hardening materials he showed that the singularity becomes less severe as the crack-tip speed increases. For perfectly plastic materials he showed that the near-tip dynamic solution does not approach the near-tip quasi-static solution as the crack speed is reduced because the dynamic solution is asymptotically valid only in a zone which shrinks onto the crack-tip as the speed reduces to zero. Solutions for a Mode-III crack in a perfectly plastic material for the case of steady-state crack propagation show that the extent of the region of large plastic strain decreases with increasing crack speed.

Attempts to extend this type of analysis to a Mode-I crack in plane stress have not been fully satisfactory because the resulting system of equations is not closed. Finally, J.D. Achenbach reported that calculations of crack openings based on an elastic-viscoplastic model due to Bodner and Partom show an "overshoot" or "keyhole" phenomenon in which the crack opening is greater near the crack tip than at some locations more distant from the crack-tip.

Walton reviewed solutions for rapid steady-state propagation of semi-infinite Mode-III cracks in a general linearly viscoelastic solid. For the case of an unbounded solid with a smooth, monotonically decreasing relaxation function and for crack-tip velocities less than the "equilibrium" shear wave speed (based on long term properties) the stress in the body is the same as for the elastic case. At velocities greater than the "equilibrium" wave speed, but less than the "glassy" wave speed, the stress intensity factor depends on the relaxation function through a single, easily computed parameter.

J. Walton also considered the case of a layer of finite thickness for which the stress field differs from the elastic field for all crack-tip velocities. The viscoelastic effect in the immediate crack tip vicinity is determined primarily by the slope of the realxation function at t=0.

J. Walton also indicated that the problems on which he currently works include: (i) Mode I analogs of the two problems described for Mode III cracks; (ii) a semi-infinite crack in a layer between two half-planes; (iii) two semi-infinite and parallel cracks; (iv) a single crack in an inhomogeneous material with a power law dependence of the relaxation function on time and on distance from the crack plane. Problem (iv) is undertaken because inhomogeneity could provide a limit to crack speed.

K.S. Kim reported on experiments that approximate conditions of a semi-infinite Mode-I crack in an unbounded viscoelastic material due to ramp loading on the initial crack surfaces. In these experiments the method of caustics is extended to incorporate viscous effects. This was done first analytically and experimentally for the static case. The caustic curve in front of the advancing crack-tip is approximately the same as it is for the elastic case whereas behind the tip it tends to differ due to viscoelastic relaxation.

A major result of these experiments is that, although the inferred stress intensity factor varies with time, the crack tip speed remains constant for heated Homalite 100 (up to $T_g = 100°C$). The crack-tip speed decreases strongly with increasing temperature for a given applied loading due to viscoelastic effects - but results are otherwise in agreement with those reported by K. Ravi-Chandar and W.G. Knauss.

As extensions of the research reported Kim suggested that (i) quasi-static elastic stress fields should be replaced by dynamic viscoelastic stress fields in the caustics relation; (ii) variations in the hydrostatic pressure and in moisture content should be examined along with variations in temperature when studies of the relationship between crack-tip speed and stress intensity factor are conducted in polymers; (iii) fracture surface studies should be extended and a fracture process zone model should be developed; (iv) feedback between developing fractures should be considered.

In the final presentation M.F. Kanninen addressed difficulties in the application of fracture mechanics to important technological problems. Of particular interest was the appropriateness

of quasi-static vs. dynamic analyses. As an example M. Kanninen discussed the thermal shock problem of dynamic crack propagation through the wall of a pressure vessel with a temperature gradient. According to LEFM the crack would be propagating in a region where the stress intensity factor is increasing with distance of propagation and the critical stress intensity factors for fracture initiation and for fracture arrest are also increasing in accordance with the temperature gradient. In this case a quasi-static analysis predicts less crack extension than is predicted by a dynamic analysis. As another example he cited a test of a large edge-cracked plate (0.5 m wide, 3 m long, and 5-10 cm thick) conducted in collaboration with Japanese researchers. From dynamic calculations by Battelle the stress intensity factor during crack advance was approximately 35% less than the values inferred from a quasi-static interpretation of the experiment. He cited the experiments of Kalthoff as indicating that the dynamic approach is very important in modelling fracture arrest. However, even the dynamic approach has its drawbacks: (i) LEFM is not strictly applicable for dynamic crack propagation because the wake region precludes the existence of a small confined process zone; (ii) elastic-plastic fracture mechanics is required, but a generally accepted crack growth criterion is not available; (iii) viscoplastic formulations may be required - lack of well established constitutive equations for the high strain rate regime of dynamic crack propagation impedes progress in viscoplastic modeling of dynamic fracture; (iv) parameters characterizing the crack tip conditions during dynamic crack propagation cannot be measured directly, but must be inferred from analyses based on assumed constitutive models.

As an indication of his current work M.F. Kanninen mentioned fracture in or around welds. Residual stress fields due to welding are simulated by finite element methods. He also mentioned investigations of COA (crack opening angle) as a useful criterion for dynamic elastic-plastic fracture.

PLASTIC DEFORMATION NEAR A RAPIDLY PROPAGATING CRACK TIP

J.D. Achenbach
Department of Civil Engineering
Northwestern University

ABSTRACT

A brief summary is presented of some recent analytical and numerical results for the dynamic fields of stress and deformation near a rapidly propagating crack tip in elastic-plastic materials.

1. INTRODUCTION

The fields of stress and deformation near the tip of a stationary crack in elastic-plastic materials have been studied in some detail for quasi-static conditions, see e.g. [1]. The analysis of fields near a growing crack is more difficult, and only a few continuum plasticity solutions are available [2]. The main difficulty stems from the history-dependent nature of the deformation and the feature that the material experiences a non-proportional straining history when it is loaded and unloaded as the crack tip passes by.

In this report we consider three constitutive models: elastic perfectly-plastic, linear strain hardening and the Bodner-Partom model. These constitutive models have been used in formulations which take into account the mass density of the material. Most of the results are for the steady-state case, i.e., for the case that the fields are time invariant relative to an observer moving with the crack tip.

For the details of the analytical and numerical work we refer to the cited references.

2. LINEAR STRAIN HARDENING

Asymptotic methods have been found very useful for the analysis of the dynamic near-tip fields in the presence of strain hardening. As shown by Achenbach, Burgers and Dunayevsky [3],

for strain hardening the governing equations are elliptic when the crack-tip speed is less than a certain critical value. The usual separation-of-variables asymptotic analysis can then be carried out, which yields singularities of the general type r^s ($-1 < s > 0$) for the near-tip stresses and strains. As the crack-tip speed increases (or alternatively as the strain-hardening curve becomes flatter) the nature of the governing equations becomes, however, hyperbolic, and the near-tip fields change character. Indeed in the limit of elastic perfectly-plastic behavior the stresses become bounded. For linear strain hardening specific results have been obtained by Achenbach and Kanninen [4] and Achenbach, Kanninen and Popelar [5]. These results are very similar to the ones obtained by Amazigo and Hutchinson [6] for the corresponding quasi-static problem.

The parameters in the analysis of [5] are α and M. For the Mode-I case $\alpha = E_t/E$, where E and E_t are the two constants for the bilinear relation between effective stress and effective strain, and $M = v/(E/\rho)^{\frac{1}{2}}$, where v is the speed of the crack tip and ρ is the mass density. Fig. 1 shows the singularity parameter s versus the parameter α for three values of M. For $\alpha = 1$, which implies perfect elasticity, we have the usual singularity defined by $s = -.5$. The curve for $M = 0$ corresponds to the quasi-static case. It is noted that the singularity becomes less severe as the crack-tip speed increases, i.e., as dynamic effects become more important.

3. PERFECT PLASTICITY

Investigations of the dynamic near-tip fields in an elastic perfectly-plastic material have been presented by Slepyan [7] and Achenbach and Dunayevsky [8], for both anti-plane and in-plane deformations.

The solutions that were obtained in [7] and [8] show anomalies in the transition from the dynamic to the quasi-static solution. As the crack-tip speed decreases the expressions for the stresses reduce to the ones for the corresponding quasi-static solution, as might be expected on the basis of intuitive reasoning. This is however not true for the strains, which become unbounded in the limit of vanishing crack-tip speed. In [9] it was shown that the transition from

dynamic to quasi-static conditions with decreasing crack-tip speed is effected because the dynamic solution is asymptotically valid in a small edge zone, which shrinks on the crack tip in the limit of vanishing crack-tip speed. Reference [9] also contains an exact solution for the Mode-III dynamic field in the plane of the crack. The same type of solution has also been obtained by Freund and Douglas [10].

It is of interest to emphasize that for Mode-III a dynamic solution in the plane of the crack, ahead of the propagating crack tip, is relatively easy to obtain. This solution can be based on the following expansions for the stress σ_{xz} and the particle velocity $\dot{w}$:

$$\sigma_{xz}(x,y,t) = -\tau(x,t)y + 0(y^3) \tag{1}$$

$$\dot{w}(x,y,t) = \dot{w}_1(x,t)y + 0(y^3) , \tag{2}$$

where x and y are coordinates moving with the crack tip, and the dot denotes the time-rate at a fixed material point. It is found that τ(x,t) and $\dot{w}_1$(x,t) satisfy the equations

$$\frac{\partial \dot{w}_1}{\partial x} + \frac{\dot{\tau}}{\mu} + \frac{1}{k}\,\dot{w}_1\tau = 0 \tag{3}$$

$$\frac{\partial \tau}{\partial x} + \frac{\tau^2}{K} + \rho\ddot{w}_1 = 0 . \tag{4}$$

Here μ is the stress modulus of initial elasticity, k is the yield stress in shear and ρ is the mass density. Equations (3) and (4) are coupled non-linear partial differential equations whose solution has not yet been obtained.

For the steady-state case (3) and (4) simplify considerably. Now we have $(\dot{}) = -c_F d/dx$ where c_F is the constant crack tip speed. By defining

$$\gamma_x = dw_1/dx, \quad \textit{we find} \quad \dot{w}_1 = -c_F\gamma_x , \tag{5}$$

and (3)-(4) reduce to

$$\frac{d\gamma_x}{dx} + \frac{1}{\mu}\,\frac{d\tau}{dx} + \frac{1}{k}\,\gamma_x\tau = 0 \tag{6}$$

$$\frac{d\tau}{dx} + \frac{\tau^2}{k} + \mu M^2 \frac{d\gamma_x}{dx} = 0 , \qquad M = c_F/(\mu/\rho)^{\frac{1}{2}} . \tag{7}$$

Equations (6) and (7) are coupled non-linear ordinary differential equations. These equations can be solved (see [9]).

For small x a solution of (6)-(7) is

$$\sigma_{xx}(x,0) \sim -k(1 - M)(\frac{y}{x}) , \qquad \frac{\partial w}{\partial x}(x,0) \sim -\frac{k}{\mu}\frac{1-M}{M}(\frac{y}{x}) \tag{8a,b}$$

$$\frac{\partial w}{\partial y}(x,0) \sim \frac{k}{\mu}\frac{1-M}{M} ln(\frac{x}{x_p}) , \tag{9}$$

where x_p defines the position of the elastic-plastic boundary. On the other hand, for the quasi-static problem we have

$$\frac{\partial w}{\partial y}(x,0) = \frac{k}{\mu}\left\{1 - ln(\frac{x}{x_p}) + \frac{1}{2}\left[ln(\frac{x}{x_p}) \right]^2 \right\} . \tag{10}$$

It is of interest to note that (10) does not reduce to (9) in the limit as $M \to 0$.

In [8] it was speculated that the transition from dynamic to quasi-static conditions with decreasing crack-tip speed is effected because the singular part of the dynamic solution is valid in a small edge zone, which shrinks on the crack tip in the limit of vanishing crack-tip speed. In [9] this non-uniform transition was investigated in detail. It was shown that for small crack-tip speed the complete near-tip solution consists of the outer solution, which is a regular perturbation expansion in M, with the quasi-static solution as the first term, and the inner solution which is of completely different nature. The exact solution of Eqs. (6) and (7), which was obtained in [9] displays the connection between the inner and outer solutions.

Fig. 2 shows the shear strain

$$\gamma_y(x,0) = \frac{\partial w}{\partial y}(x,0) \tag{11}$$

versus x/x_p for various values of M, as obtained in [9]. It is noted that the strain magnitude decreases with increasing values of M. The implications of this behavior have been explored by Freund and Douglas [10].

Preliminary results have indicated similar behavior for the plane stress Mode-I case. The quasi-static solution for this case has been given by Achenbach and Dunayevsky [11].

4. BODNER-PARTOM MODEL

A convenient set of constitutive relations for an elastic-viscoplastic model was proposed by Bodner and Partom [12]. Dynamic near-tip fields for this model have been investigated numerically by Aboudi and Achenbach [13]-[16].

ACKNOWLEDGEMENT

This summary was prepared in the course of research sponsored by the Office of Naval Research (Contract No. N00014-76-C-0063) and the Air Force Office of Scientific Research (Grant AFOSR 78-3589-E).

REFERENCES

1. Rice, J.R., "Elastic-Plastic Fracture Mechanics," in The Mechanics of Fracture, F. Erdogan (ed.), AMD. Vol. 19, The American Society of Mechanical Engineers, New York (1975).

2. Rice, J.R., "Elastic-Plastic Crack Growth," in Mechanics of Solids, H.G. Hopkins and M.J. Sewell (eds.), Pergamon Press, Oxford and New York (1982).

3. Achenbach, J.D., Burgers, P., and Dunayevsky, V., "Near-Tip Plastic Deformations in Dynamic Fracture Problems, in Nonlinear and Dynamic Fracture, N. Perrone and S.N. Atluri (eds.), AMD, Vol. 35, ASME, New York (1979).

4. Achenbach, J.D. and Kanninen, M.F., "Crack-Tip Plasticity in Dynamic Fracture Mechanics," in Fracture Mechanics, N. Perrone, H. Liebowitz, D. Mulville, and W. Pilkey (eds.), The Univ. of West Virginia Press, Charlottesville (1978).

5. Achenbach, J.D., Kanninen, M.F., and Popelar, C.H., "Near-Tip Fields for Fast Fracture in an Elastic-Plastic Material," J. Mech. Phys. Solids, 29 (1981) 211.

6. Amazigo, J.C. and Hutchinson, J.W., "Crack Tip Fields in Steady Crack Growth with Linear Strain Hardening," J. Mech. Phys. Solids, 29 (1981) 81.

7. Slepyan, L.I, "Crack Dynamics in an Elastic-Plastic Body," Izv. Akad. Nauk. SSSR, Mekhanika Tverdogo Tela, 11 (1976) 144.

8. Achenbach, J.D., and Dunayevsky, V., "Fields Near a Rapidly Propagating Crack Tip in an Elastic Perfectly-Plastic Material," J. Mech. Phys. Solids, 29 (1981) 283.

9. Dunayevsky, V. and Achenbach, J.D., "Boundary Layer Phenomenon in the Plastic Zone Near a Rapidly Propagating Crack Tip," Int. J. Solids Structures, 18 (1982) 1.

10. Freund, L.B. and Douglas, A.S., "The Influence of Inertia on Elastic-Plastic Antiplane-Shear Crack Growth," J. Mech. Phys. Solids, 30 (1982) 59.

11. Achenbach, J.D., and Dunayevsky, V., "Crack Growth Under Plane Stress Conditions in an Elastic Perfectly-Plastic Material," submitted for publication (1982).

12. Bodner, S.R., and Partom, Y., "Constitutive Equations for Elastic-Viscoplastic Strain-Hardening Material," J. Appl. Mech., 42 (1975) 383.

13. Aboudi, J. and Achenback, J.D., "Rapid Mode-II Crack Propagation in a Strip of Viscoplastic Work-Hardening Material," Int. J. Solids Structures, 17 (1981) 879.

14. Aboudi, J. and Achenbach, J.D., "Numerical Analysis of Fast Mode-I Fracture of a Strip of Viscoplastic Work-Hardening Material," Int. J. Fracture, in press.

15. Aboudi J. and Achenbach, J.D., "Arrest of Mode-III Fast Fracture by a Transition from Elastic to Viscoplastic Material Properties," J. of Appl. Mech., 48 (1981) 509.

16. Aboudi J. and Achenbach, J.D., "Arrest of Fast Mode-I Fracture in an Elastic-Viscoplastic Transition Zone," Engineering Fracture Mechanics, in press.

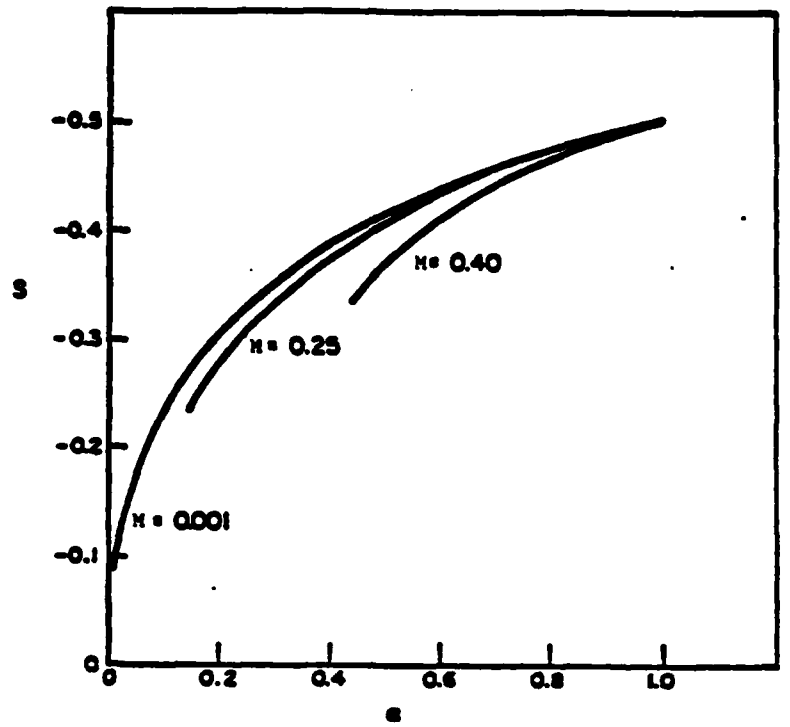

Figure 1. Order of the crack tip singularity of Mode-1 plane stress.

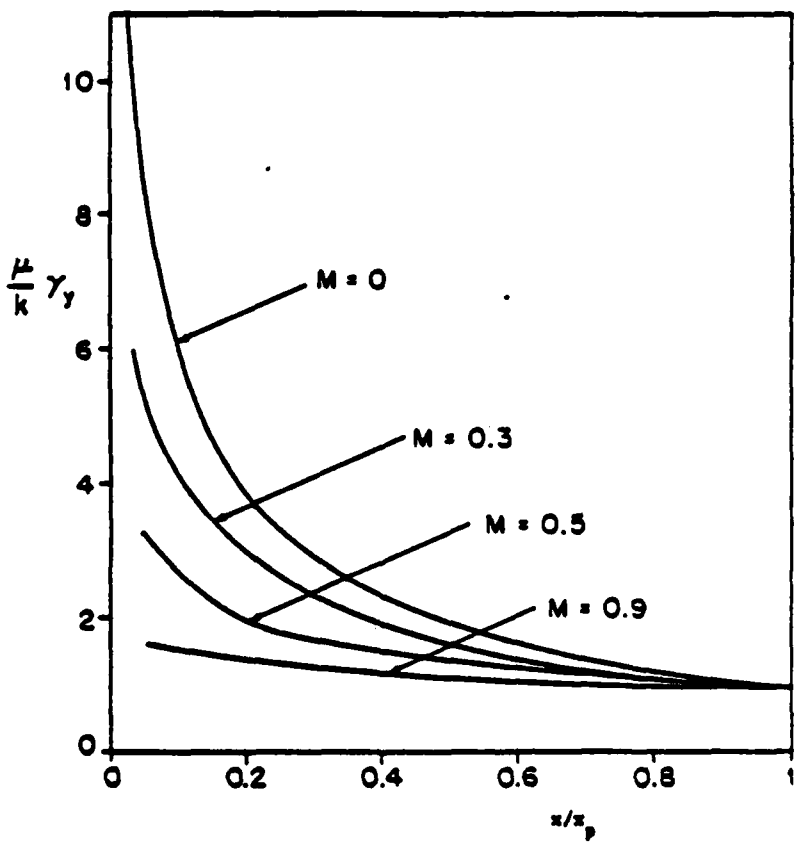

Figure 2. Shear strain γ_y in the plane of the crack ($y = 0$, $x > 0$) versus x/x_p for various crack-tip speeds.

DYNAMIC, STEADY-STATE CRACK PROPAGATION IN LINEAR ISOTROPIC VISCOELASTIC MATERIAL

J.R. Walton
Texas A & M University

ABSTRACT

This paper is a summary of results of some recent analytical studies of dynamic, steady-state crack propagation in linear viscoelastic material. Closed form solutions are presented for the problems of a semi-infinite, anti-plane shear crack propagating with constant speed in an infinite general linear viscoelastic body and in a layer of finite thickness. For both boundary value problems, and for a general class of shear modulus, the solutions obtained exhibit a universal structure that depends in a simple way upon the time dependent shear modulus and crack speed. The forms for the solutions are convenient for the extraction of qualitative and quantitative information about the dependence of the stress field in the body upon the loading, the crack speed and the shear modulus.

1. THE INFINITE BODY PROBLEM

The first problem discussed is the dynamic, steady-state propagation of a semi-infinite, anti-plane strain crack in an infinite, general isotropic and homogeneous linearly viscoelastic body. Subsequently the corresponding problem for a layer of finite thickness is considered. Many of the results presented here for the infinite body analysis appear in the paper [2]. The reader is also referred to that paper for a survey of relevant literature.

The governing field equations for the motion of a linearly viscoelastic material are

$$\sigma_{ij,j} = \rho u_{i,tt} \quad , \quad \epsilon_{ij} = \frac{1}{2}(u_{i,j} + u_{j,i})$$

$$\sigma_{ij} = 2\mu * d\epsilon_{ij} + \delta_{ij}\lambda * \epsilon_{kk}$$

where σ_{ij}, ϵ_{ij} and u_i denote the stress, strain and displacement fields respectively, and $\mu * d\epsilon$ is the Riemann-Stieltjes convolution

$$\mu * d\epsilon = \int_{-\infty}^{t} \mu(t - \tau)\, d\epsilon(\tau) .$$

The deformation of the body is assumed to be anti-plane strain and a semi-infinite crack is assumed to propagate along the x_1-axis with speed v, driven by loads $\sigma_{23}(x_1,0,t) = f(x_1 - vt)$ which follow it. Consequently adoption of the variables $x = x_1 - vt$, $y = x_2$ yields the boundary value problem

$$\begin{aligned}
&\mu * d\Delta u_3 = \rho v^2 u_{3,xx} \quad . \\
&\sigma_{23}(x,0) = \frac{\partial}{\partial y}(\mu * du_3) = f(x) \quad x < 0 \\
&u_3(x,0) = 0 , \qquad\qquad\qquad\quad x > 0 \\
&\sigma_{ij}(x,y) \to 0 , \quad x^2 + y^2 \to \infty
\end{aligned}$$

where $\Delta(\cdot)$ is the two dimensional Laplace operator, $\Delta = \frac{\partial^2}{\partial x^2} + \frac{\partial^2}{\partial y^2}$.

The Fourier transform, defined by

$$\hat{f}(p) = \int_{-\infty}^{\infty} f(x)e^{ixp}\,dx = \int_{0}^{\infty} f(x)e^{ixp}\,dx + \int_{-\infty}^{0} f(x)e^{ixp}\,dx \equiv \hat{f}^{+} + \hat{f}^{-} ,$$

is employed to reduce the above equations to the Riemann-Hilbert problem

$$F^{+}(p) = G(p)F^{-}(p) + g(p) \tag{1}$$

where

$$\begin{aligned}
F^{+}(p) &= \hat{\sigma}^{+}_{23}(p) \\
F^{-}(p) &= \hat{u}^{-}_{3,1}(p) \\
g(p) &= -\hat{\sigma}^{-}_{23}(p) = -\hat{f}(p) \\
G(p) &= -i\, sgn(p)\overline{\mu}\,(-vp)\gamma_1(p) \equiv sgn(p)G_1(p) \\
\gamma_1(p) &= [1 - \rho v^2/\overline{\mu}\,(-vp)]^{\frac{1}{2}} \\
\overline{\mu}\,(-vp) &= \mu(0) + \int_{0}^{\infty} e^{-ivpt}\,d\mu(t) .
\end{aligned}$$

The shear modulus, $\mu(t)$, is assumed only to be positive, continuously differentiable, non-increasing and convex.

A formal solution to (1) is readily constructed in the form (see [2] for details).

$$\begin{aligned} F^{\pm}(z) &= X^{\pm}(z)\ \frac{1}{2\pi i}\ \int_{-\infty}^{\infty} g(\tau)/X^{+}(\tau)\ \frac{d\tau}{\tau - z} \\ X^{\pm}(z) &= \omega^{\pm}(z) X_1^{\pm}(z) \\ X_1^{\pm}(z) &= \exp(\Gamma_1^{\pm}(z)) \\ \Gamma_1^{\pm}(z) &= \frac{1}{2\pi i}\ \int_{-\infty}^{\infty} \log(G_1(\tau))\ \frac{d\tau}{\tau - z}\ . \end{aligned}$$

The functions $\omega^{\pm}(z)$ are branches of $z^{\frac{1}{2}}$ that are analytic in the upper/lower complex plane and such that for real p

$$\omega^{+}(p)/\omega^{-}(p) = sgn(p)\ .$$

A standard asymptotic analysis together with Parseval's equality may now be applied to conclude that as $x \rightarrow 0^{+}$,

$$\sigma_{23}^{+}(x,0) \sim K/\sqrt{x}$$

with

$$\begin{aligned} K &= \frac{|G_1(\infty)|^{\frac{1}{2}}}{\sqrt{\pi}}\ \frac{1}{2\pi}\ \int_{-\infty}^{\infty} g(\tau)/\ X^{+}(\tau) d\tau \\ &= \frac{-\ |G_1(\infty)|^{\frac{1}{2}}}{\sqrt{\pi}}\ \int_{-\infty}^{0} \sigma_{23}^{-}(x,0) h(x) dx \end{aligned} \tag{3}$$

and

$$1/\ X^{+}(p) = \int_{-\infty}^{0} e^{-ipx}\ h(x) dx\ . \tag{4}$$

More generally, for all x > 0,

$$\sigma_{23}^{+}(x,0) = \frac{1}{2\pi}\ \int_{-\infty}^{\infty} e^{-ixp} X^{+}(p) dp\ \frac{1}{2\pi i}\ \int_{-\infty}^{\infty} g(\tau)/X^{+}(\tau)\ \frac{d\tau}{\tau - p}\ . \tag{5}$$

The principal difficulty in deriving useful expressions for the stress intensity factor, K, or for

$\sigma_{23}^{+}(x,0)$ in line (5) is the calculation of $X^{+}(p)$. The assumptions on $\mu(t)$ listed above permit the exploitation of certain analyticity properties of $\overline{\mu}\ (-vp)$ in the evaluation of the integral involved in the construction of $X^{+}(p)$. In that analysis, the consideration of two cases defined by parameters c and c^* arises naturally. Specifically, in [2] it was shown that

$$X^{+}(p) = \begin{cases} (-ip)^{\frac{1}{2}} |G_1(\infty)|^{\frac{1}{2}}, & 0 < v < c^* \\ (q_0 - ip)^{\frac{1}{2}} |G_1(\infty)|^{\frac{1}{2}}, & c^* < v < c \end{cases} \tag{6}$$

where $(c^*)^2 = \mu(\infty)/\rho$, $c^2 = \mu(0)/\rho$ and q_0 is the unique positive number for which

$$vq_0 \int_0^{\infty} \mu^*(t)\, e^{-q_0 vt} dt = (v/c)^2 .$$

The function $\mu^*(t)$ is the normalized modulus, $\mu^*(t) = \mu(t)/\mu(0)$. It should be observed that c^* and c are the equilibrium and glassy shear wave speeds. Combining (3), (4) and (6) we may conclude that the stress intensity factor, K, is given by

$$K = \begin{cases} -\frac{1}{\pi} \int_{-\infty}^{0} \sigma_{23}^{-}(x,0) |x|^{-\frac{1}{2}} dx , & 0 < v < c^* \\ -\frac{1}{\pi} \int_{-\infty}^{0} \sigma_{23}^{-}(x,0) |x|^{-\frac{1}{2}} e^{q_0 x} dx , & c^* < c < c > . \end{cases}$$

Another quantity of interest in fracture mechanics is the energy release rate, E, given by

$$E = \int_{-\infty}^{0} \sigma_{23}^{-}(x,0) u_{3,1}(x,0) dx .$$

Unlike for elastic material, for viscoelastic material it is necessary to know $\sigma_{23}^{+}(x,0)$ for all $x > 0$ in order to calculate E. Combining (5) and (6) it can be shown that

$$\sigma_{23}^{+}(x,0) = \begin{cases} \frac{1}{2\pi x} \int_{-\infty}^{0} \sigma_{23}^{-}(\tau,0) l(\tau/x)(\tau/x) d\tau , & 0 < v < c^* \\ \frac{1}{2\pi x} \int_{-\infty}^{0} \sigma_{23}^{-}(\tau,0) e^{-q_0(x-\tau)} l(\tau/x)(\tau/x) d\tau , & c^* < v < c \end{cases}$$

with $l(x) = \int_0^1 (1-t)^{-\frac{1}{2}} (t-x)^{-\frac{3}{2}} dt.$

Some remarks on the solution given above are in order.

i. If $0 < v < c^*$, the stress in the body is just the elastic stress distribution and, in particular, is independent of v and material properties.

ii. If $c^* < v < c$, the stress field depends on both v and material properties. However, the dependence on $\mu(t)$ is only through the single easily computed parameter q_0. Moreover, there is a simple universal functional form for the stress, $\sigma_{23}^+(x,0)$, ahead of the advancing crack.

iii. It is easily seen that the rate of decay of $\sigma_{23}^+(x,0)$ for $x \to \infty$ is given by

$$\sigma_{23}^+(x,0) = \begin{cases} 0(x^{-\frac{3}{2}}), & 0 < v < c^* \\ 0(x^{-\frac{3}{2}} e^{-q_\sigma x}), & c^* < v < c . \end{cases}$$

iv. The stress intensity factor, K, vanishes in the limit $v \to c$. Indeed, the same is true for $\sigma_{23}^+(x,0)$ for all $x > 0$.

Very recently, the problem of determining the angular dependence of the near crack tip stresses was addressed. We are studying this question for more general viscoelastic crack problems than are discussed here, but we shall present in this summary the results obtained for the problem considered above.

It is easily seen that the stress $\sigma_{23}(x,y)$ in the upper half-plane, $y > 0$, is given by

$$\sigma_{23}(x,y) = \frac{1}{2\pi} \int_{-\infty}^{\infty} \sigma_{23}(s,0)ds \int_{-\infty}^{\infty} e^{-|p|y\gamma_1(p)} e^{ip(s-x)} dp .$$

Adopting local polar coordinates, (r, θ), around the crack tip, we may conclude, after an obvious change of variables,

$$\sigma_{23}(r,\theta) = \frac{1}{2\pi} \int_{-\infty}^{\infty} \sigma_{23}(rt,0)dt \int_{-\infty}^{\infty} e^{-|\tau|\sin(\theta)\gamma_1(\tau/r)} e^{i\tau(t-\cos\theta)} d\tau .$$

After some rather lengthy but routine analytical arguments it can be concluded that the dominant term in the asymptotic expansion of $\sigma_{23}(r,\theta)$ in powers of r as r tends to zero is given by

$$\sigma_{23}(r,\theta) \sim \frac{K}{\sqrt{x}} f(v,\theta)$$

$$f(v,\theta) = \frac{1}{2\pi} \int_0^\infty t^{-\frac{1}{2}} dt \int_{-\infty}^{\infty} e^{-|\tau|\sin(\theta)\gamma_1(\infty)} e^{i\tau(t-\cos\theta)} d\tau \tag{7}$$

where

$$\gamma_1(\infty) = [\ 1 - (v/c)^2\ ]^{\frac{1}{2}} .$$

The integral in (7) is easily evaluated to yield

$$f(v,\theta) = Re\ [\ \cos(\theta) - i\gamma_1(\infty)\sin(\theta)\ ]^{-\frac{1}{2}} .$$

It should be observed that the function f(v,θ) is the same as occurs in an elastic analysis with the glassy shear modulus $\mu = \mu(0)$. So, for example, there is a threshold effect on f(v,θ). That is, for $0 \leq (v/c)^2 \leq \frac{1}{2}$, f(v,$\theta$) is a monotone decreasing function of θ, whereas, for $\frac{1}{2} \leq (v/c)^2 < 1$, f(v,$\theta$) possesses a unique maximum at a point θ_0, with θ_0 tending to $\pi/2$ as v/c tends to one. A thorough discussion of the dynamic elastic analysis is given by Achenbach and Bazant [1].

2. THE FINITE LAYER PROBLEM

Here we assume that the crack is propagating in a layer of thickness 2h, defined by $-\infty < x < \infty$, $-h \leq y \leq h$. As before, the semi-infinite crack lies along $y = 0$, $x \leq 0$. On the layer boundaries, two possible boundary conditions are considered:

I. $u_3(x\ ,\ \pm h) = 0$
II. $\sigma_{23}(x\ ,\ \pm h) = 0$.

As for the infinite body analysis, the boundary value problem is reduced to a Riemann-Hilbert problem

$$F^+(p) = G(p)F^-(p) + g(p) .$$

The function $F^{\pm}(p)$ and g(p) are as before but G(p) is now given by

$$G(p) = sgn(p)\ G_1(p)\ G_2(p)$$

with $G_1(p)$ as before and

$$G_2(p) = \begin{cases} \coth(h\,|p|\,\gamma_1(p)) & I. \\ \tanh(h\,|p|\,\gamma_1(p)) & II. \end{cases} .$$

The solution, $\sigma_{23}^{+}(x,0)$ is still given by lines (3), (4) and (5), but with $X^{\pm}(z)$ such that

$$X^{\pm}(z) = \omega^{\pm}(z)\ X_1^{\pm}(z)\ X_2^{\pm}(z)$$
$$X_2^{+}(p)/\ X_2^{-}(p) = G_2(p)\ .$$

Since $G_2(p)$ for problems I and II are just reciprocals, the same is true for $X_2^{\pm}(z)$. Consequently, we need to consider only one of the cases, say I. The evaluation of $X_2^{+}(p)$ is the central problem. With arguments similar to those presented in [2] we may deduce that

$$X_2^{+}(p) = Y(p) \begin{cases} (ip)^{-\frac{1}{2}} & 0 \leqslant v \leqslant c^* \\ (q_0 - ip)^{-\frac{1}{2}} & c^* \leqslant v < c \end{cases}$$

with

$$Y(p) = \lim_{n\to\infty} \prod_{j=1}^{n} \left(\frac{a_{2j-1} - ip}{a_{2j} - ip} \right) (a_{2n+1} - ip)^{\frac{1}{2}} ,$$

and where the a_k are given by

$$va_{2n} \int_0^{\infty} \mu^*(t) e^{-vta_{2n}}\ dt = (v/c)^2/[1 - (n\pi/ha_{2n})^2]$$

$$va_{2n+1} \int_0^{\infty} \mu^*(t) e^{-vta_{2n+1}}\ dt = (v/c)^2/[1 - (n + \tfrac{1}{2})\pi/ha_{2n+1})^2] .$$

We remark that $a_j < a_{j+1}$, $j = 0,1, \cdots$ and

$$a_0 = \begin{cases} 0 & 0 \leqslant v \leqslant c^* \\ q_0 & c^* \leqslant v < c . \end{cases}$$

For $X^{+}(p)$ we have

$$X^{+}(p) = \lim_{n\to\infty} |G_1(\infty)|^{\frac{1}{2}} \prod_{j=1}^{n} \left[\frac{a_{2j-1}-ip}{a_{2j}-ip} \right] (a_{2n+1} - ip)^{\frac{1}{2}} .$$

The stress intensity factor can be evaluated by computing the Fourier transform of $1/X^{+}(p)$. A convenient scheme for inductively approximating K can be based upon the observation that

$$\prod_{j=1}^{n} \left[\frac{a_{2j}-ip}{a_{2j-1}-ip} \right] = 1 + \frac{b_{n1}}{(a_1-ip)} + \cdots + \frac{b_{nn}}{(a_{2n-1}-ip)} ,$$

with

$$b_{nk} = \frac{\left[\prod_{j=1}^{n} (a_{2j}-a_{2k-1}) \right]}{\left[\prod_{j\neq k}^{n} (a_{2j-1}-a_{2k-1}) \right]} = b_{(n-1)k} \left[\frac{a_{2n}-a_{2k-1}}{a_{2n-1}-a_{2k-1}} \right] .$$

It can be shown that

$$K = \lim_{n\to\infty} K_n \quad , \quad K_n = -\frac{1}{\pi} \int_{-\infty}^{0} \sigma_{23}^{-}(x,0)|x|^{-\frac{1}{2}} h_n(x)dx$$

$$h_n(x) = e^{a_{2n+1}x} - 2x \sum_{j=1}^{n} b_{nj} \int_{0}^{1} \exp[x(a_{2n+1}t^2 + a_{2j-1}(1-t^2))] dt .$$

For the viscoelastic layer problem, the stress field in the body is different from the elastic solution for all values of v, instead of just for $c^* \leq v < c$ as occurs for the infinite body case. However, there is still a universal functional form for the solution that depends upon $\mu(t)$ only through the parameters a_j.

REFERENCES

1. Achenbach, J.D., and Bazant, Z.P., "Elastodynamic Near Tip Stress and Displacement Fields for Rapidly Propagating Cracks in Orthotropic Materials," J. Appl. Mech., 42(1975) 183-189.

2. Walton, J.R., "On the Steady-State Propagation of an Anti-Plane Shear Crack in an Infinite General Linearly Viscoelastic Body," Quart. Appl. Math., (1982) 37-52.

VISCOELASTIC EFFECT ON DYNAMIC CRACK PROPAGATION IN HOMALITE 100

K.S. Kim, K.L. Dickerson
Department of Theoretical and Applied Mechanics
University of Illinois at Urbana-Champaign
W.G. Knauss
Graduate Aeronautical Laboratories
California Institute of Technology

ABSTRACT

The optical method of caustics is used to determine the stress intensity factor for a running crack in a viscoelastic material. A formulation of the quasi-static deformation of materials with rheologically simple shadow-optic creep functions is derived for the caustics, solved numerically and applied to the fracture testing of Homalite-100 at various temperatures (40^oC - 100^oC). Theoretical and experimental caustics show good agreement in shape even for moderately high crack speeds (150 - 300 m/sec). Results also show that the relation between the stress intensity factor and the crack speed for Homalite 100 is highly sensitive to temperature variations.

1. INTRODUCTION

To understand the physics and mechanics of dynamic fracture may be important from the point of view of both prevention as well as intention to cause rapid fracture. The first viewpoint prevails where the need exists to design safe containment vessels (pressure vessels, pipe lines, nuclear reactors) while the second consideration arises in connection with comminution, be this in the pharmaceutical, the mining industry or rapid drilling (armor piercing) operations. Although much has been learned with respect to brittle or metallic structures during past years - and still much more work is uncharted - the effect of viscoelastic material behavior on dynamic fracture problems is virtually unexplored, although the need for a better understanding exists in connection with the performance of many explosives (intentional comminution) and some high

energy solid rocket propellants (often an unintentional comminution process).

Here we present an initial investigation into the fracture of a viscoelastic polymer under dynamic loading. The loading condition is in the form of a time step on the faces of a semi-infinite crack in an unbounded viscoelastic two-dimensional medium. The condition is simulated experimentally by applying on the crack faces electromagnetic forces induced by a nearly-square pulse of high electric current flowing in opposite directions through a doubled-up thin copper strip (0.48 mm thick); this strip, the legs of which are separated by a Mylar insulator 125 μm thick, is inserted into the crack of a large specimen plate (30 x 60 cm and 4.7 mm thick). The schematic of the loading is shown in Fig. 1. In order to control the intrinsic time scale of viscoelasticity, the temperature is changed through the use of the time-temperature shift phenomenon. In these experiments, Homalite-100 is used at different temperatures subjected to different load levels. By adjoining to those temperature-varied tests those conducted on Homalite 100 at "room temperatures" [10] one hopes to gradually clarify the influence of viscoelastic material behavior on dynamic fracture progression.

The result of this study is basically divided into two parts. The first part is the characterization of the stress state near the crack tip, measuring the stress intensity factor K(t) as a function of time in the given load history. This is done experimentally by extending the method of caustics [1-4] to viscoelastic materials. The second part concerns the process of fracture under the characterized stress state at the crack tip. This is investigated by relating the stress intensity factor and the corresponding velocity of the extending crack and by observing the fracture surfaces microscopically.

2. EXPERIMENTAL PROCEDURE

We employ the optical method of caustics to evaluate the stress intensity of the running crack with the aid of a rotating mirror high speed camera [5]. A 5 watt cw laser (Spectra Physics) equipped with a cavity dumper for the emission of high power (50 w) short duration (15 ns) light pulses is used as a light source; a framing rate of 100,000 fps is used consistently [5] throughout

this work. A typical photographic record taken by this camera system on 35 mm film is shown in Fig. 2.

We consider first the method of caustics for the evaluation of the stress intensity factor of a stationary crack, in a viscoelastic plate under disregard of material inertia. We deal here with the case for which the crack tip stresses in a viscoelastic solid are the same as in the elastic counterpart; that situation prevails for traction boundary conditions when no net forces act on the boundaries of holes or cracks. One obtains then the relation between the stress intensity factor K_I and the caustic "diameter" $D_o(t)$[1] as

$$K_I = \frac{\sqrt{2\pi}}{3f^{\frac{5}{2}} z_o d_o} \, |C^{-1}(t)| * D_o^{\frac{5}{2}}(t) \tag{1}$$

where f, z_o, d_o, and $C(t)$, denote, respectively, a multiplication factor [3], the distance from the specimen to the image plane, the thickness of the specimen and the caustic creep function, while $C^{-1}(t)$ indicates the caustic relaxation function. The star notation indicates the convolution $F*G \equiv \int_{-\infty}^{t} F(t-\eta)G'(\eta)d\eta$, with (') denoting the time derivative. This expression reduces to the known results [3] when the material behaves in a linearly elastic manner.

The caustic creep function C(t) is composed of two contributions. One arises from the change of the index of refraction, and the other from the lens-like deformation associated with the plane stress state of the viscoelastic sheet. The former contribution can also be deduced from the mechanical deformation history of the specimen with the aid of the theory of electromagnetic waves in dielectric materials [6]. That theory requires that (for optically isotropic solids) the change of refractive index Δn is related to the mechanical deformation by

$$\Delta n = \frac{-(n^2-1)(n^2+2)}{6n} \, \epsilon_{ii} \tag{2}$$

where n is the index of refraction and ϵ_{ii} is the volume strain of the material.[2] This relation

1. $D_o(t)$ is measured in the direction normal to the crack plane.
2. The material used in this work, Homalite 100, is optically anisotropic (birefringent); however, it turns out that the constant determining the degree of anisotropy is small so that (2) is still valid.

together with the contribution of the lens effect leads to the relation,

$$C(t) = -(n-1)\left\{\frac{[1-2\nu(t)](n+1)(n^2+2)}{6n}+\nu(t)\right\} * E^{-1}(t) \tag{3}$$

where $\nu(t)$ is the relaxation function of Poisson's ratio (for a constant strain jump test) and $E^{-1}(t)$ is the uniaxial creep compliance function. For Homalite 100 the index of refraction is 1.5 so that $C(t) = -[0.59 - 0.68\,\nu(t)] * E^{-1}(t)$. A comparison of this result with experiments is shown in Fig. 3. In this comparison the relaxation modulus from Bebee's work [7] has been used with the approximate relation $E^{-1}(t) \approx [E(t)]^{-1}$. Even with this approximation the comparison shows good agreement.

For our further work, we need to recall that analyses of the dynamic stress intensity factor for moving crack tips are usually formulated so that the state variables such as stress, strain, etc. are expressed in terms of a position vector $\underline{x}$ which has its origin at the running crack tip. In contrast the shadow optic function C(t) is a material property and therefore the appropriate convolution " * " has to be applied with respect to a fixed material point $\underline{X}$ so that the change in path length of the light at a point ΔS is

$$\Delta s = d_o \int_{-\infty}^{t} C(t-\eta)\left(-v\frac{\partial \sigma}{\partial x_1}+\frac{\partial \sigma}{\partial \eta}\Big|_{\underline{x}}\right)d\eta \tag{4}$$

where v is the velocity of the crack tip, assumed to move in the x_1 direction, and σ denotes the sum of the two principal stresses in the $x_1 - x_2$ plane.

Let us now consider an approximation for the caustic in a viscoelastic material arising from a crack tip moving through a two-dimensional geometry; we do this in the context of a state of plane stress. Drawing on the results with the stationary crack in which case this stress at the crack tip could be written as a product function of a time dependent stress intensity factor and a function representing the spatial distribution of the stresses, we write tentatively for the dynamic case

$$\sigma[\underline{x}(\underline{X},t),t] = K(t)f[\underline{x}(\underline{X},t);\mathrm{v}] + a\,. \tag{5}$$

Although there exists an explicit form for the function f ($\underline{x}$;v) for the case of dynamically moving cracks in an elastic material this function has not yet been determined for viscoelastic materials. However, we can arrive at an adequate estimate by noting that the speed of cracks in viscoelastic materials tends to be relatively low. This observation allows us to disregard dynamic effects in this stress distribution so that we may make use of the quasi-static stress distribution as an approximation, so that[3]

$$f(\underline{x}) = \left\{ \frac{x_1 + (x_1^2 + x_2^2)^{1/2}}{\pi(x_1^2 + x_2^2)} \right\}^{1/2} \tag{6}$$

although history effects also may change the spatial function a little. Making use of these assumptions, we obtain for the deflection vector of the light rays in passing through the deformed crack tip area, [5]

$$\underline{w}[\underline{x}(\underline{X},t)] = d_o z_o \nabla \Bigg[\int_{-\infty}^{t} C(t-\eta)\{-K(\eta)\mathrm{v}(\eta)\, \frac{\partial f}{\partial x_1}\, [\underline{x}(\underline{X},\eta)] + \frac{\partial K(\eta)}{\partial \eta}\, f[\underline{x}(\underline{X},\eta)]\}\, d\eta \Bigg]. \tag{7}$$

In order to compute the shape of the caustic we have to make use of the vanishing of the Jacobian J of the transformation, with $\underline{x}' = \underline{x} + \underline{w}$, as

$$J = \frac{\partial(x'_1, x'_2)}{\partial(x_1, x_2)} = 0\,. \tag{8}$$

This relation determines the shape of the caustic. However, we are not really interested in the shape for a given history of the stress intensity factor; rather, we are only interested in the measurement of the stress intensity factor as a function of velocity and time. Indeed, it turns out from experiments described later that the shape of the part of the caustic that precedes the crack tip is

3. Note that the loading history at the crack tip does, in principle, affect the stress distribution there. However, according to latest results (see J. Walton's contribution in this proceedings) these effects seem to be minimal at low velocities.

not much different at all from that for the stationary crack for the velocities encountered in our experiments. In order to determine the geometry of the initial curve, it is therefore not necessary to compute the total shape of the caustic; to determine the stress intensity factor it suffices to cast the caustic in terms of the distance of the initial curve from the crack tip along the x-axis. Denote this distance by r_o[4] and observe that on the x_1-axis one can replace $J=0$ by $(\partial x_1'/\partial x_1)_{x_2=0} = 0$. For a crack in steady motion with velocity v ($\partial K/\partial t \equiv 0$) this condition yields

$$K = \frac{2\sqrt{2\pi}}{3 z_o d_o C_{eff}(\frac{r_o}{v})} r_o^{\frac{5}{2}} \tag{9}$$

where

$$C_{eff}(\frac{r_o}{v}) = \frac{5}{2} \int_o^\infty \frac{C(\frac{r_o}{v}\xi)}{(1+\xi)^{\frac{7}{2}}} d\xi \ . \tag{10}$$

In the limits $v \to 0$ and $v \to \infty$[5] one verifies that C_{eff} tends to appropriate elastic limits. For three different temperatures $C_{eff}(\frac{r_o}{v})$ is shown in Figure 4 for illustrative purposes.

Because the value of r_o cannot be determined from experimental records directly one must generate both the caustic and the initial curve (and thus r_o) mathematically. From the proper caustic one then deduces the appropriate value of r_o. In Figure 5 caustics and associated initial curves are shown at different temperatures and different velocities. These curves are excerpts of complete ray plots, an example of which is shown in the lower portion of Figure 6.

It is of interest to note that for $X_1 > 0$ the caustics and the initial curve have very nearly

4. We remark here that for $x_1 > 0$ the initial curve is very close to a (semi) circle, so that the distance of the initial curve from the origin, but in the x_2-direction is also very nearly equal to r_o.
5. This limit is, of course, not permissible for the physical interpretations later on because of the low-speed approximation made.

behavior of molecular composition in the cohesive zone so that it substantially controls the speed of the crack. In contrast the directional, inhomogeneous roughness derives from a rather macroscopic mechanism, which may control the expenditure of energy on a larger scale.

Another interesting observation is that three dimensional effects near the free surface boundary of the plate specimen develops boundary layers of the fracture roughness. The thickness of this boundary layer increases with temperature. This phenomenon should be studied more with proper fracture process zone models for an improved understanding of this phenomenon which seems to be related to the shear lip formation in the fracture of plastically deforming metals.

4. CONCLUSION

For ready reference, we summarize here the salient points of this investigation:

1. The method of optical caustics is extended for a steadily running crack in a viscoelastic medium and applied to the fracture testing of Homalite 100 at various temperatures. For further study of the crack tip stress field adiabatic conditions should, perhaps, be incorporated in the formulation of the caustics. Also, it should be extended for the unsteady motion of a crack in a viscoelastic material.
2. The relation of the caustic creep function, index of refraction, and the history of mechanical deformation is obtained and compared with experimental results, and shows good aggreement. For further study that relation should be revised for birefringent materials.
3. The dependence of the crack speed on the stress intensity has been clarified for Homalite 100 at various temperatures. For further study a low temperature test should be performed. Also, tests should be conducted above the glass transition temperature.
4. Fracture surfaces have been investigated microscopically and qualitative correlations among the roughness of the surface, stress intensity levels and temperature are observed. For further study a proper microscopic fracture process model should be established for the quantitative understanding of these correlations.

ACKNOWLEDGEMENT

A portion of this work was performed at the California Institute of Technology under ONR sponsorship (Contract No. N00014-78-C-0634). Also support of the University of Illinois is gratefully acknowledged.

REFERENCES

1. Manogg, P., Ph.D. dissertation, University of Freiburg (1964).
2. Theocaris, P.S. and Gdoutos, E.E., Journal of Applied Mechanics, 39 (1972) 91.
3. Beinert, J and Kalthoff, J.F., Chapter in Mechanics of Fracture, VII, G.C. Sih (ed.), (1981).
4. Rosakis, A.J., Engineering Fracture Mechanics, 13 (1980) 331.
5. Kim, K.S., and Knauss, W.G., CIT Technical Report GALCIT SM 81-7 (1981).
6. Lorentz, H.A., Wied. Ann. Phys , 9 (1980) 641.
7. Beebe, W.M., Ph.D. Thesis, California Institute of Tehcnology, (1964).
8. Freund, L.B., J. Mech. Phys. Solids, 20 (1972), 141.
9. Kobayashi, A.S., and Mall, S., Experimental Mechanics, 18 (1978) 11.
10. Ravi-Chandar, K., Ph.D. dissertation, California Institute of Technology (1982).

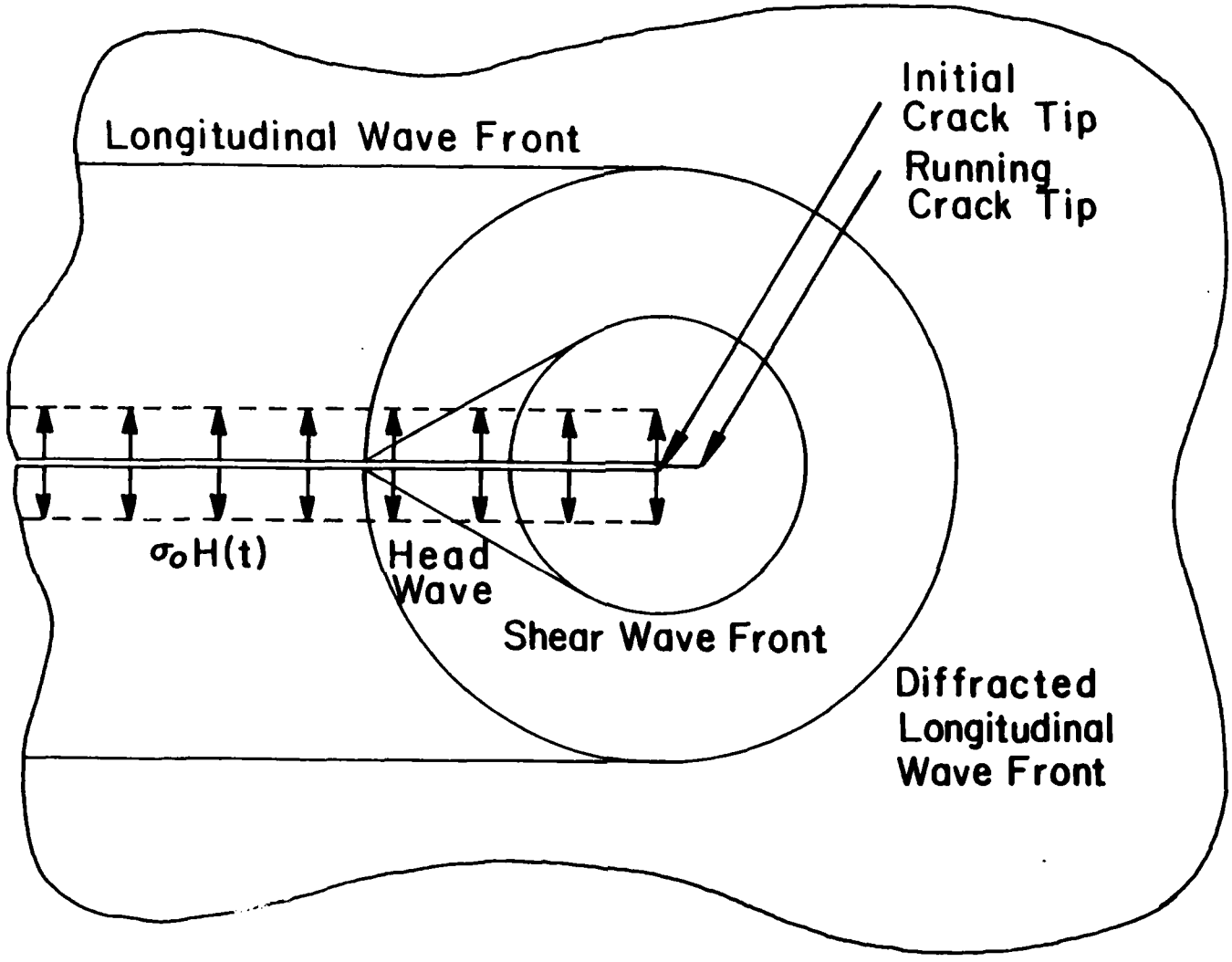

Figure 1. Schematic of Dynamic Loading on Semi-Infinite Crack Faces

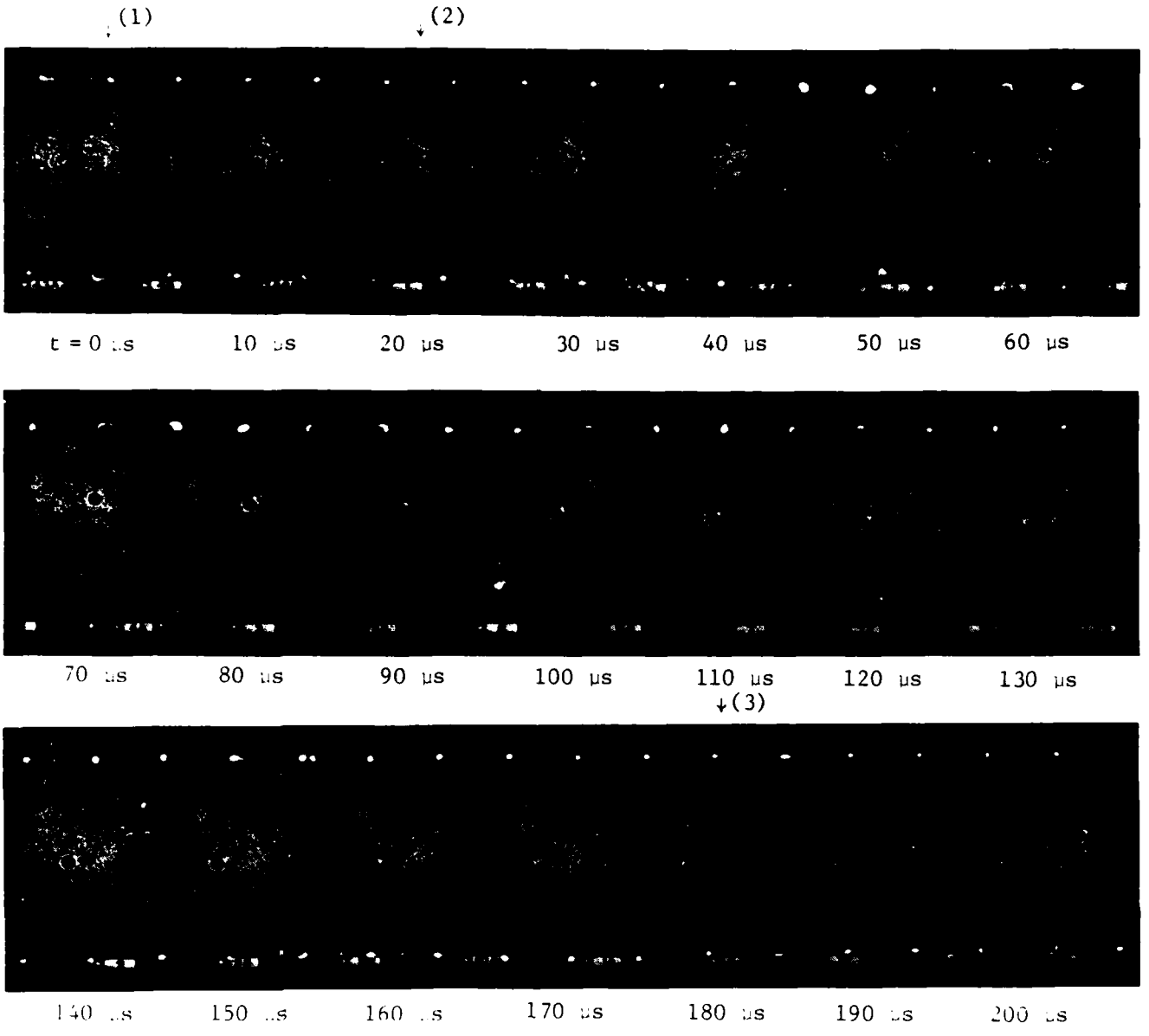

Figure 2. Caustics for a running crack in Homalite-100: (1) Stress-wave arrival; (2) Initiation of running crack; (3) Crack bifurcation. (Pictures taken with high-speed camera at California Institute of Technology.)

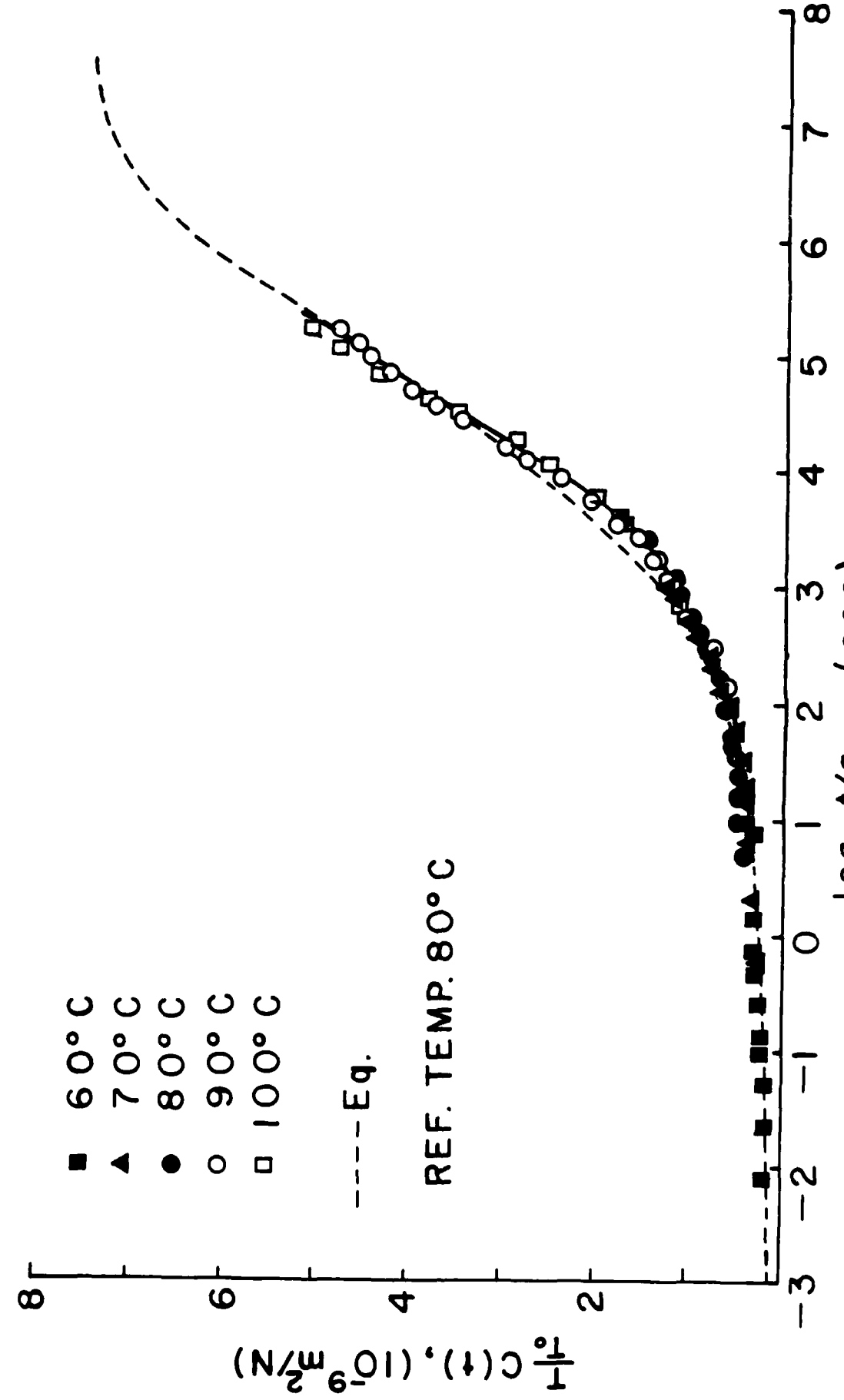

Figure 3. Caustic Creep Function of Homalite-100

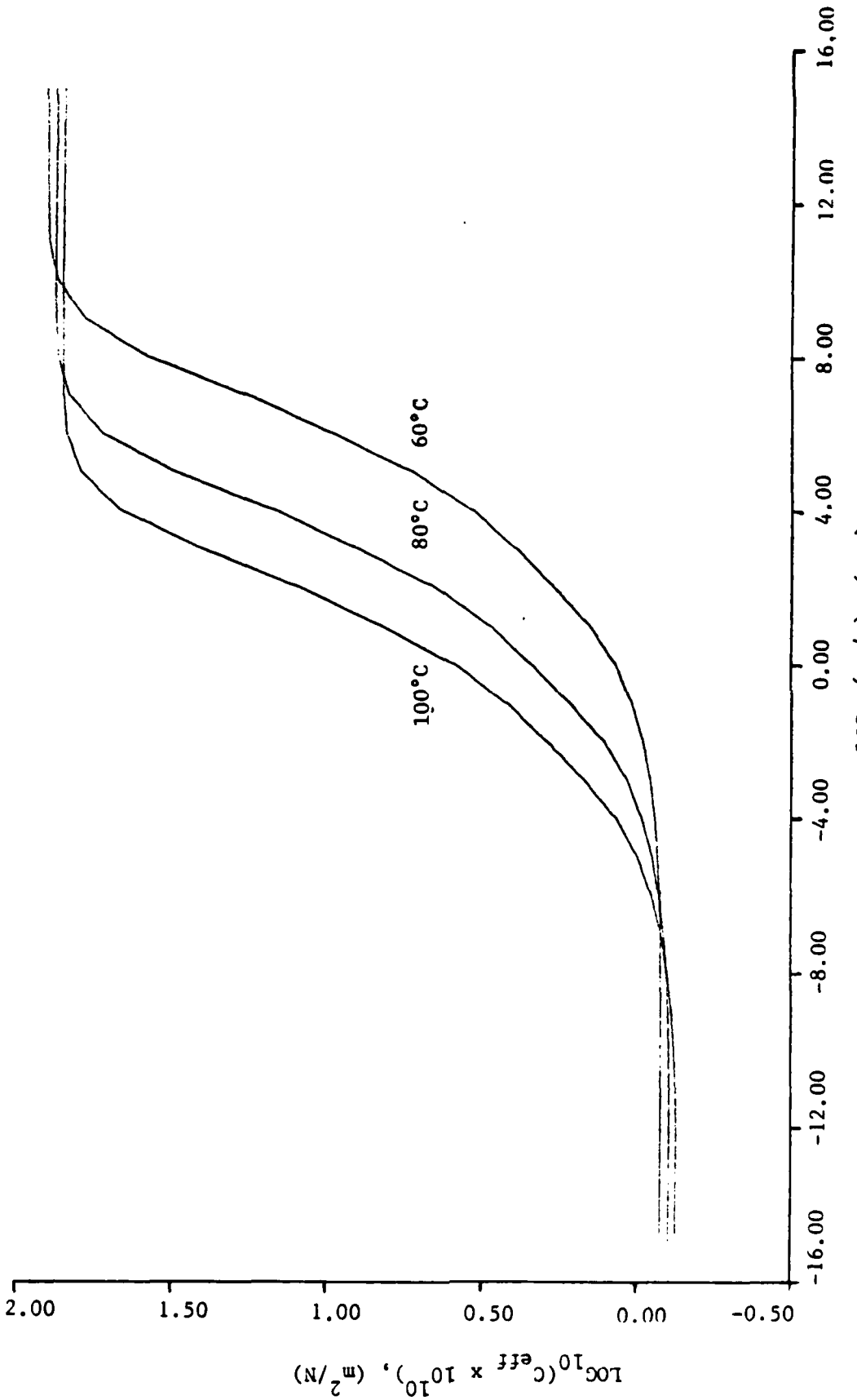

Figure 4. Effective Shadow Optic Constant of Homalite-100

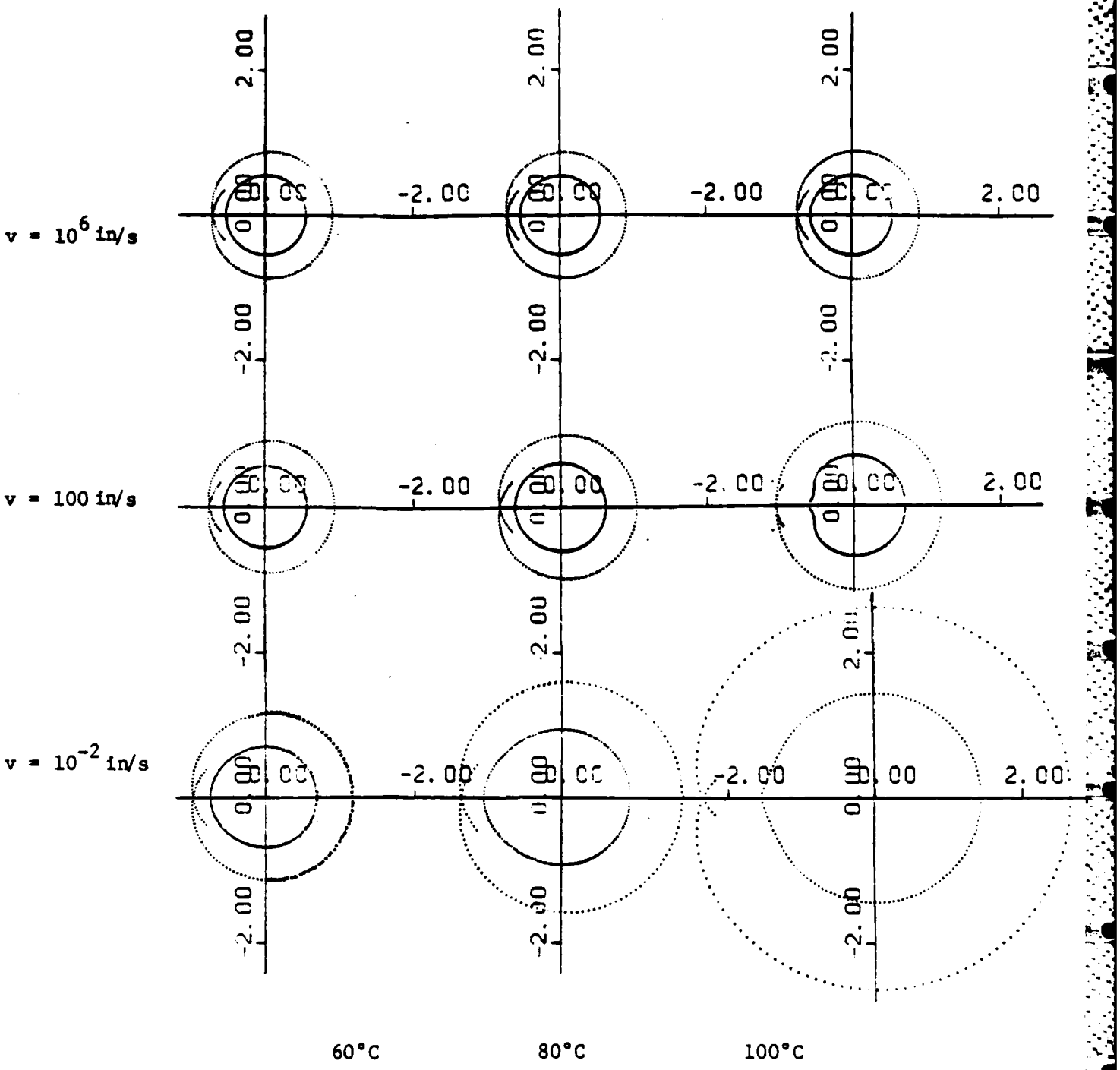

Figure 5. Initial and Caustic Curve for Different Speeds and Temperatures

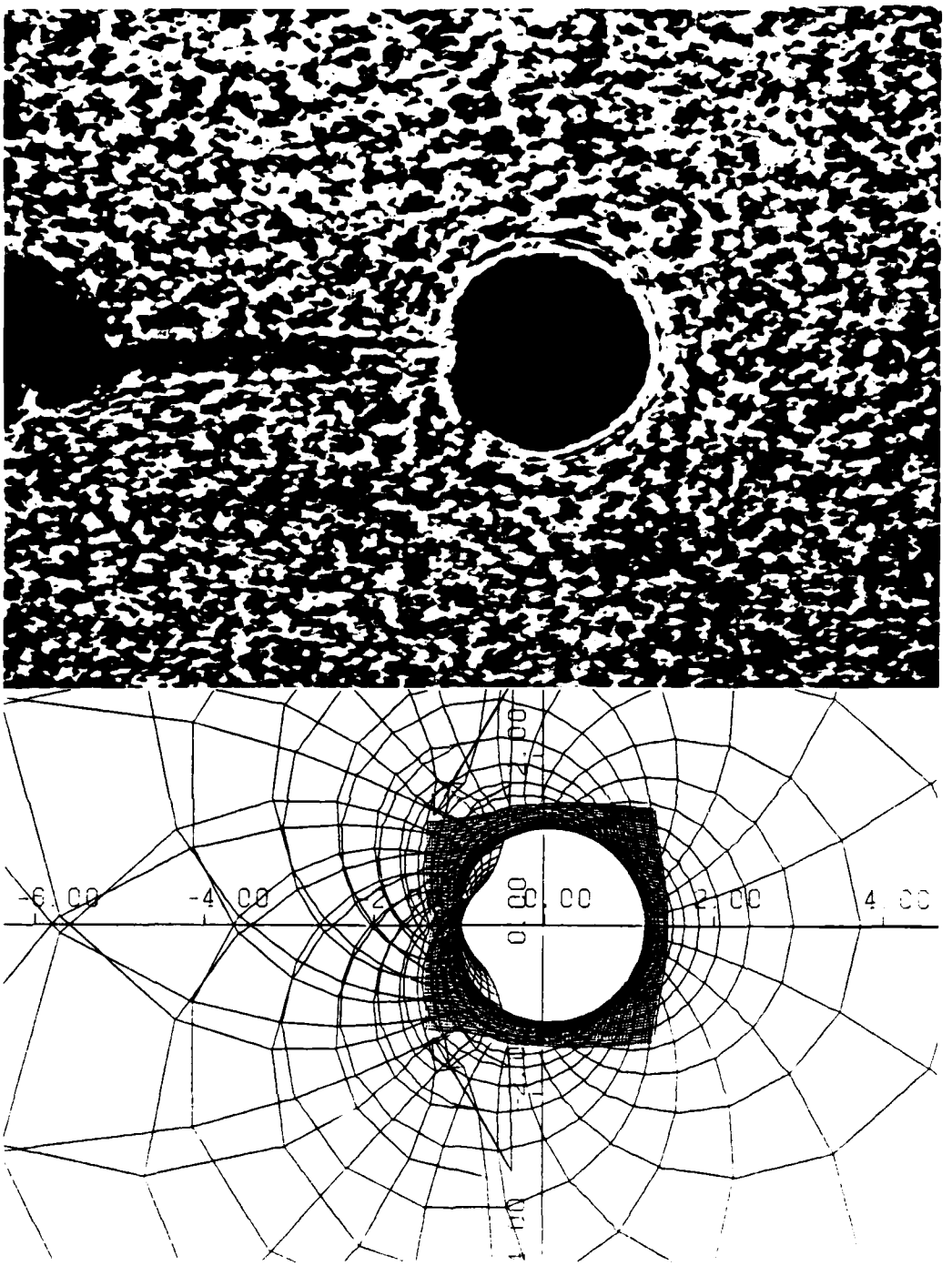

Temp = 100°C, K = 1234 psi(in)$^{\frac{1}{2}}$, v = 9414 in/sec

Figure 6. Comparison of Numerical Caustics to Experimental Caustic for a Running Crack in a Homalite-100

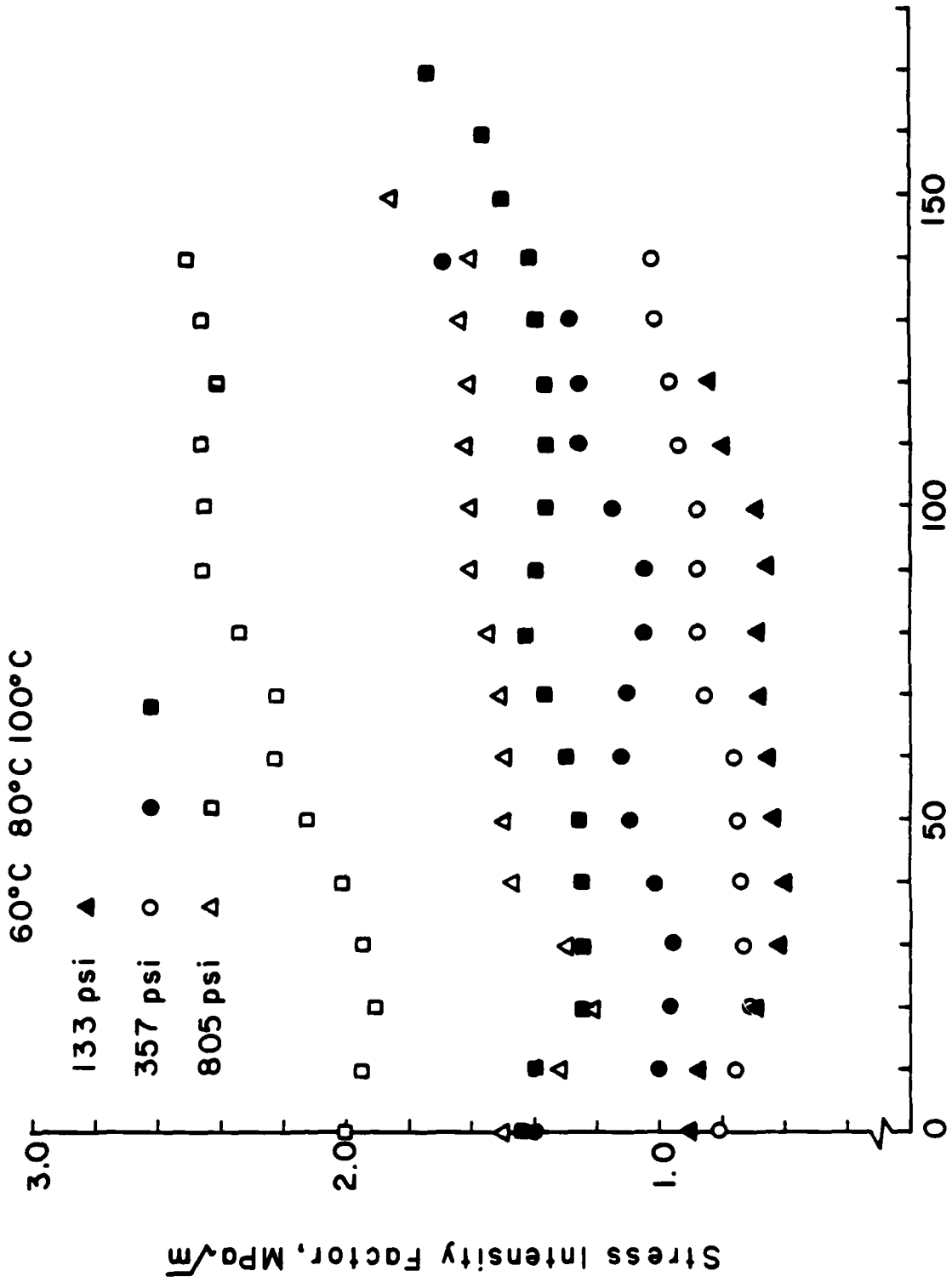

Figure 7. Stress Intensity Variation after Dynamic Crack Initiation

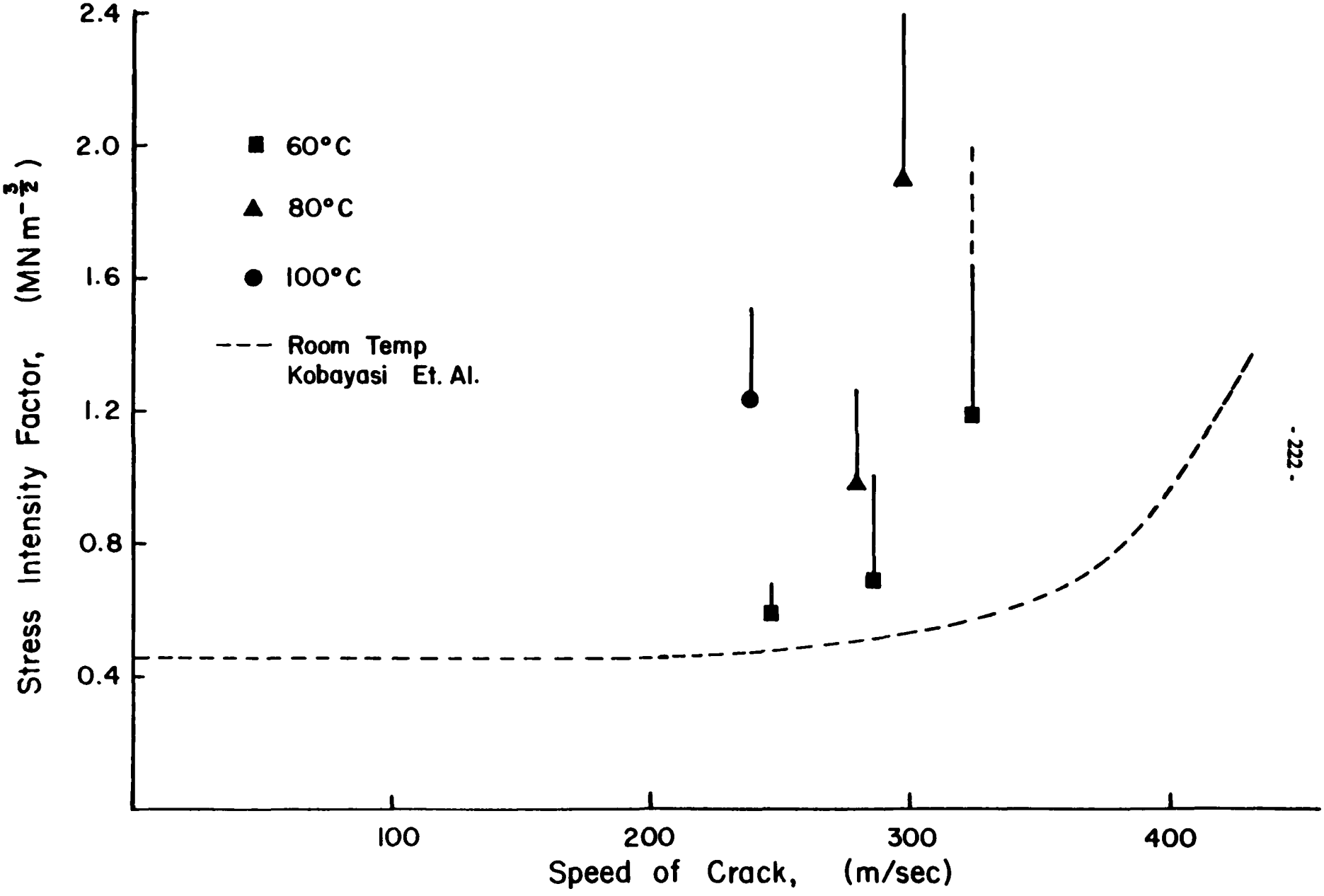

Figure 8(a). K-v Relation of Homalite 100 at Various Temperatures

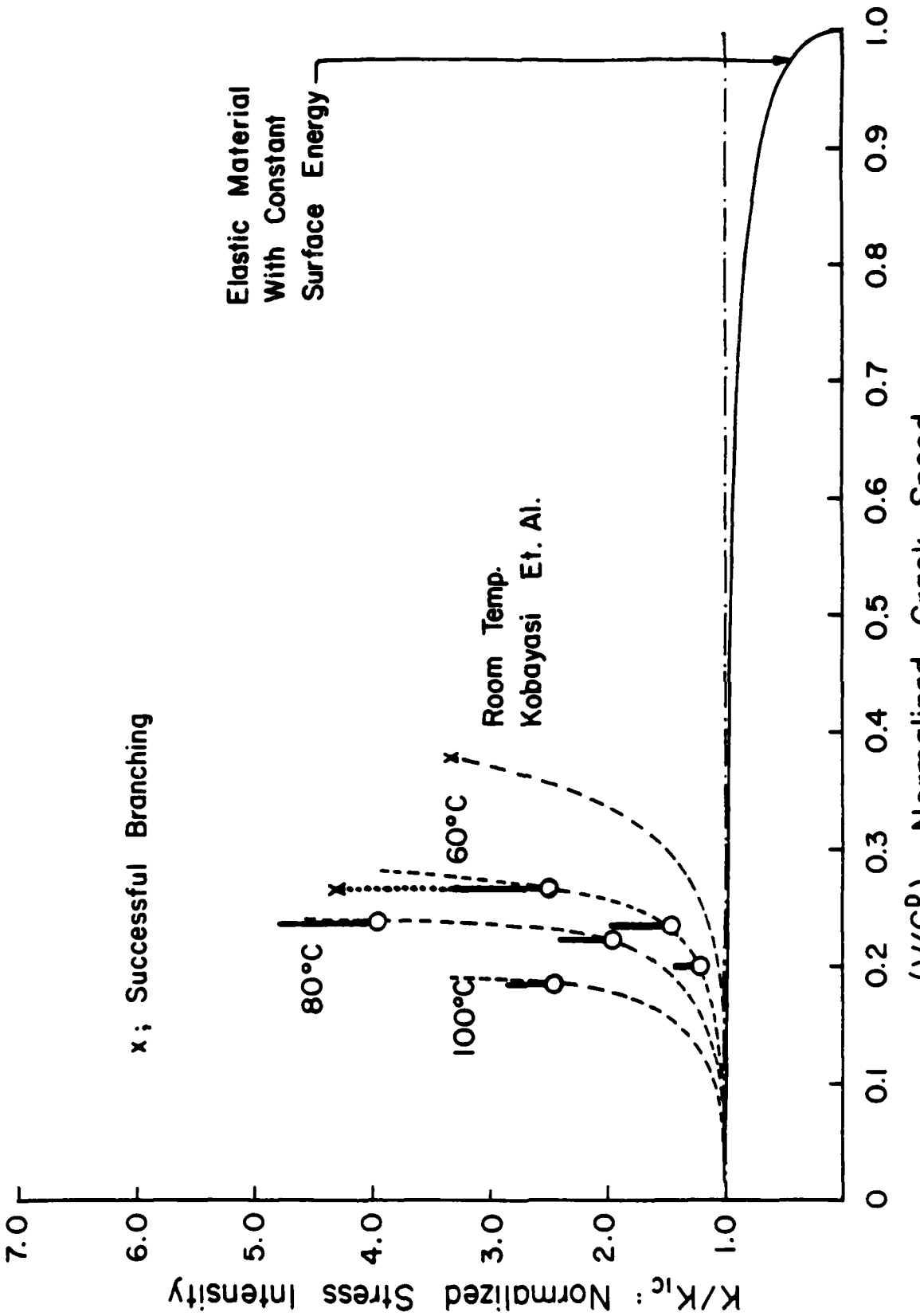

Figure 8(b). Normalized K-v Relation of Homalite 100 at Various Temperatures

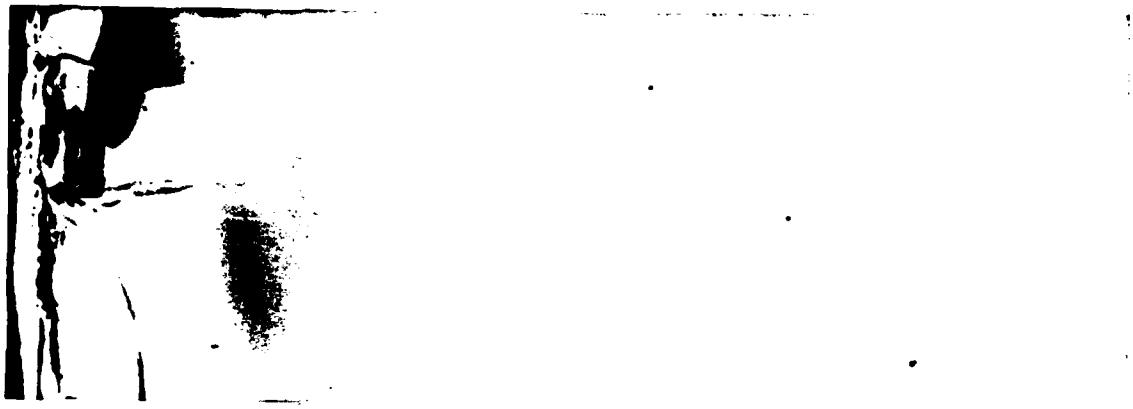

a) 60°C ; 357 psi

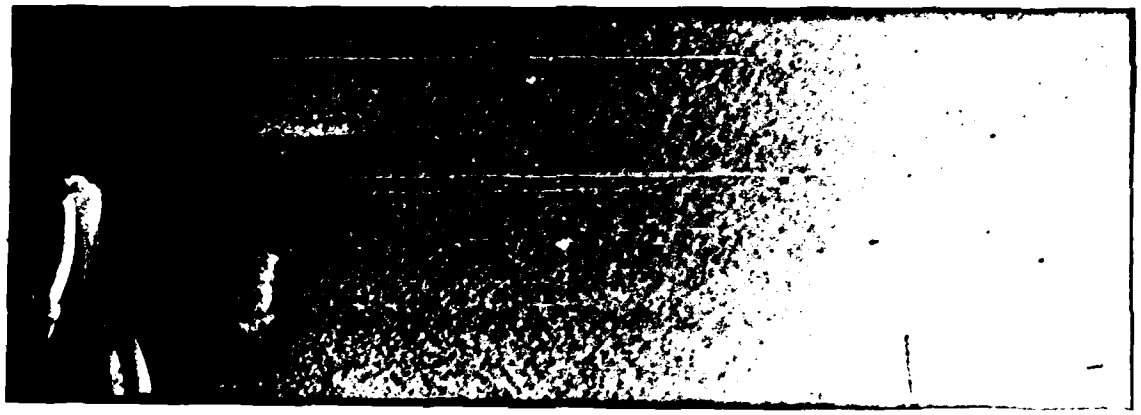

b) 80°C ; 805 psi

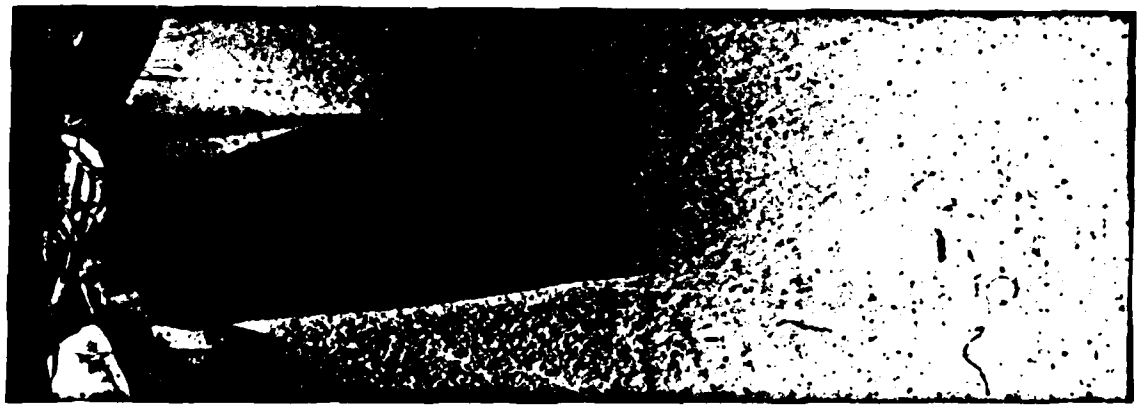

c) 100°C; 805 psi

Figure 9. Surface roughness at various temperatures.

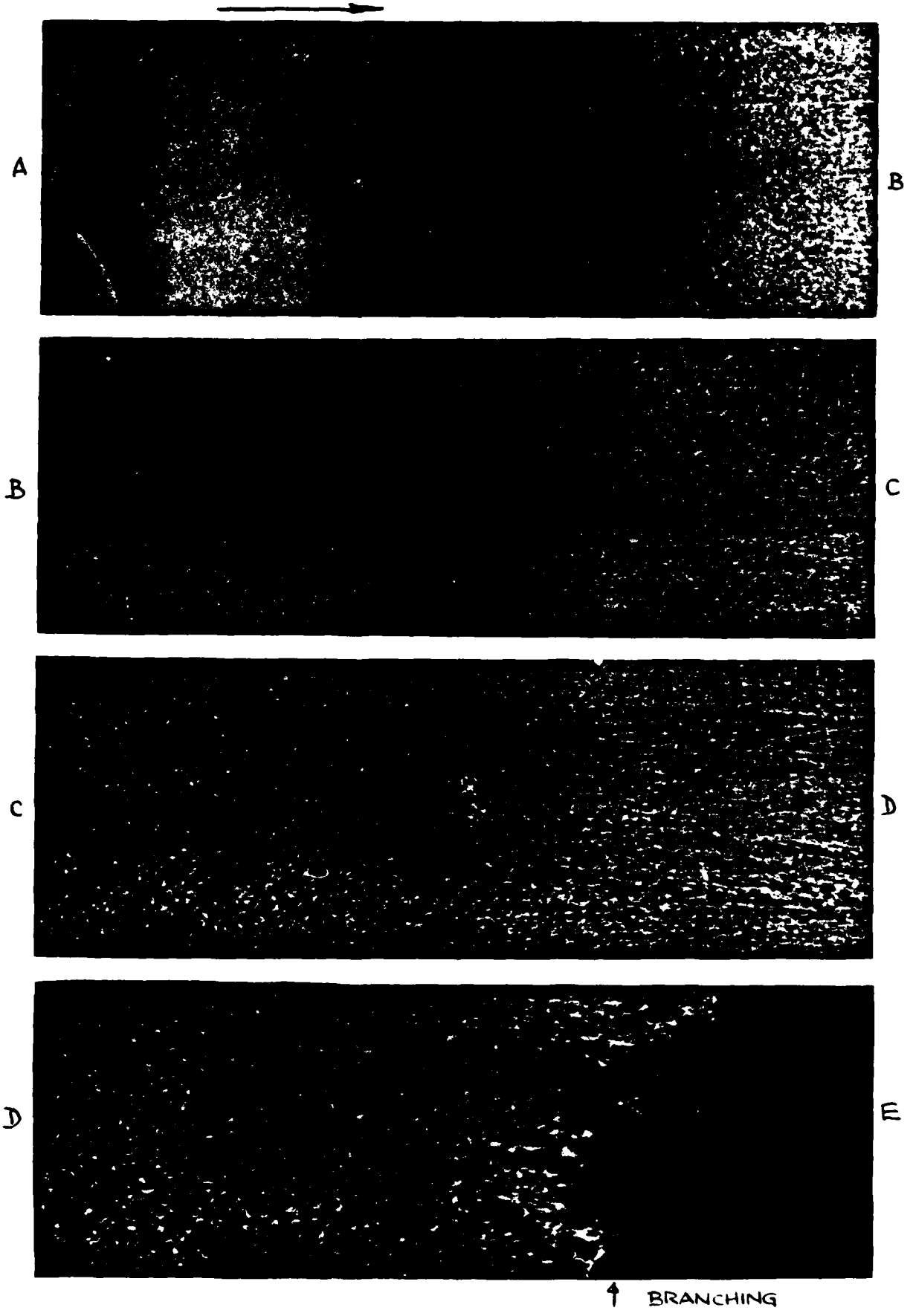

Figure 10. Change of surface roughness along with the stress intensity in a single specimen (805 psi, 60°C).

SOME THOUGHTS ON THE SUBJECT OF DYNAMIC ELASTIC-PLASTIC ANALYSES OF RAPID CRACK PROPAGATION AND CRACK ARREST

M.F. Kanninen
Battelle, Columbus Laboratories

1. INTRODUCTION

Despite the fact that the basic assumption of linear elastic fracture mechanics - contained-yielding - is violated for a crack that grows, most attempts to characterize rapid crack propagation and arrest are nevertheless rooted in LEFM. Together with the growing necessity to analyze crack arrest under conditions where large scale plasticity is expected, this fact is prompting researchers to develop dynamic elastic-plastic analyses. Starting from LEFM-based analysis procedures that form the current state-of-the-art, this paper attempts to provide some perspective for this evolutionary trend in dynamic fracture mechanics. Emphasized are some of the potential dilemmas that face the researchers pursuing this subject.

2. BACKGROUND

The current state-of-the-art in the application of dynamic fracture mechanics to rapid crack propagation and arrest is based upon the use of quasi-static linear elastic fracture mechanics (LEFM). Specifically, $K = K_{IC}$ is used for the initiation of unstable crack propagation and $K = K_{Ia}$ for its termination, where K in both instances is calculated as if the crack were stationary. For example, the thermal shock problem for nuclear pressure vessels, an application that is receiving a great deal of attention at present, is being handled in just this way [1]. It can be noted that this point of view does not include (nor could it) any consideration of the rapid crack propagation event that links the initiation and arrest points.

The quasi-static view requires crack arrest to occur smoothly with an intimate connection between the slowing down process and the static deformation state long after arrest. However,

there is ample evidence to suggest that crack arrest instead occurs quite abruptly. A point of view that gives direct consideration to crack propagation, with crack arrest occurring only when continued propagation becomes impossible, is free from the erroneous assumption inherent in the quasi-static approach. Within the confines of elastodynamic behavior, unstable crack propagation occurs under the condition that $K = K_{ID}(\dot{a})$ with arrest occurring (generally abruptly) at a position and time for which $K < \min(K_{ID})$ for all greater times [2]. The experiments of Kalthoff and others have shown clearly that the dynamic approach that considers arrest as the termination of unstable propagation is the more correct and that the use of K_{Ia} as a material property is therefore not well founded [3].

Specifically, Kalthoff, et al. showed by direct measurements (using the method of caustics and the DCB test specimen) that cracks propagating deeper into the specimen arrested at the same value of the dynamic stress intensity factor, with the K_{Ia} values being markedly different in each instance [3]. This finding corroborated the theoretical analysis prediction made earlier by Kanninen who showed that a systematic decrease in K_{Ia} with crack jump length is a direct consequence of a dynamic approach [4]. Nevertheless, this view still is not universally accepted. There are strong advocates, e.g., Crosley and Ripling [5], for the K_{Ia} as a material property approach.

Confusing the situation are the many practical problems where the differences between the predictions of the two approaches are not great. These applications are typified by (1) the use of K_{Ia} values measured from short crack jumps (whereupon K_{Ia} approximates the mimimum value of K_{ID}), and (2) component boundaries that do not reflect stress waves back to the running crack tip. The through-the-wall propagation of a long axial crack in a circular cylinder (e.g., the thermal shock problem) is an example where (2) is fairly well (but not exactly!) satisfied; the double cantilever beam (DCB) test specimen is one where it decidedly is not. The decisive observations of run/arrest events in the DCB specimen are sometimes brushed aside on the grounds that it is "too dynamic" to represent actual applications. Whether or not this is so, such observations

clearly demonstrate the anti-conservative nature of a quasi-static treatment - a crack is always predicted to propagate further in a dynamic analysis than in a quasi-static analysis.

3. BASIS FOR ELASTOPLASTIC DYNAMIC ANALYSES

Until fairly recently, the view that elastodynamic analyses coupled with K_{ID} values that are properties of the material is the appropriate way to predict crack arrest generally prevailed, at least within the research community. Then, further work began to reveal discrepancies [2]. It was first found that K_{ID} exhibited significant geometry-dependence. Next, the conditions under which the crack was initiated were also found to influence the subsequent propagation. These, of course, cannot be reconciled with the concept of K_{ID} being a material property dependent, at most, upon crack speed, temperature and degree of constraint (i.e., specimen thickness). To begin to understand the reasons for such aberrant behavior, the author and his associates at Battelle began to question the basic concepts of elastodynamic crack propagation [6]. Not coincidentally, work in the area of elastic-plastic fracture mechanics (in regard to the validity of J in characterizing stable crack growth) was pursuing a similar course at the same time [7]. Of some importance, this work has identified the crack tip opening angle (CTOA) parameter as an appropriate crack tip characterizing parameter for extended crack growth under elastic-plastic conditions.

It is generally known that LEFM is valid under the condition that the inelastic deformation surrounding the crack tip is "dominated" by the elastic K field. But, because a moving crack inevitably leaves a wake of relaxed plasticity behind, except for very short crack jumps, LEFM cannot in principle be valid at the point of crack arrest. The limit of validity could probably be shown in an analogous manner to that used by Hutchinson and Paris [8] if there was any need to do so.

The same conceptual difficulty arises in fatigue (at generally much lower stress levels) where it is dealt with by appealing to the idea of "similitude". That is the parameters governing the crack growth rate must be measured for the same type of load history as in the application of

interest. When similitude is violated, the fatigue relations do not work, e.g., as in crack growth retardation following an overload, owing to the lack of similitude in the plastic zones. One should expect the same kind of effects in dynamic fracture. This provides some of the incentive for the current efforts of several researchers to develop elastic-plastic dynamic crack propagation analyses. Recent work by J.D. Achenback, S.N. Atluri, L.B. Freund, G.T. Hahn, M.F. Kanninen and A.S. Kobayashi has been performed in this area and can be found in reference 9.

A difficulty that immediately arises in elastic-plastic analyses lies in identifying the proper crack growth criterion. A critical strain at a critical distance ahead of the crack tip is being used. But such a parameter is somewhat unappealing - it cannot be measured and is not in any event palatable unless it can somehow be connected to a micromechanical picture. Alternatives such as the CTOA are attractive both from a computational point of view, and for the evidence which exists indicating its constancy in stable crack growth. But it will similarly require a proper theoretical basis. Accordingly, one of the most important concerns is the need for an appropriate inelastic criterion. Nevertheless , this is still not the only issue. The possibility exists that elastic-plastic treatments are really not appropriate at all! The suggested reasons are as follows.

4. DYNAMIC VISCOPLASTIC FORMULATIONS

Because plasticity is inherently a time-dependent process (cf. the effect of loading rate on the yield stress in tension), the plastic zone accompanying a rapidly propagating crack requires time to form. Hence, it could be much smaller than for the same crack length and applied load under static conditions. On this basis it has been suggested by Vagins [10] that very high crack arrest values (e.g., $K_{Ia} = 400 ksi\ in^{\frac{1}{2}}$) are tolerable within the static LEFM approach. This is an intriguing idea. But in order to investigate it, one could not use either LEFM (for obvious reasons) or elastic-plastic analyses that do not contain the rate-dependence of yielding. A viscoplastic formulation therefore is needed.

Some work is progressing in this direction. Achenbach (unpublished work), for example, has

suggested making use of the Bodner-Partom model [11] for an asymptotic analysis in the sense of the treatment of Achenbach, Kanninen and Popelar [12]. Use of such models appears to be limited, however, by the lack of data that can be used to evaluate the constants that they contain at the strain rates encountered in a propagating crack problem. Clearly, these can be very much higher than in more conventional problems. So, progress towards quantitative dynamic viscoplastic assessments of rapid crack propagation and crack arrest can be expected to be slow. In the meanwhile, it is natural to turn to the existing experimental results to see what insights might be gained from them.

Rapid crack propagation/arrest experiments can be classified as either direct or indirect, depending upon whether crack tip characterizating parameters are measured during the event or are inferred from a supplementary analysis. In the first category are the experiments on photoelastic and reflective materials where a shadow spot (caustic) or a fringe pattern is photographed by high speed cameras. The second category contains experiments where timing wires are broken by the advancing crack. The resulting crack length versus time data can then be used as input to, say, a finite element computation in which details (e.g., the dynamic stress intensity factor) that cannot be measured could then be calculated.

In both types of experiments some assumption about the constitutive behavior of the material during rapid crack propagation is required. While this is obvious in the indirect approach, it is equally true in the direct approach. The size of a reflected shadow spot may indeed correspond to the dimensions of the crack tip plastic zone, but its relation to other features of the deformation will depend upon the material behavior at the strain rates experienced by the crack tip. It follows that the experiments that have been performed cannot really discriminate among the various types of constitutive behavior that are possible. It can nevertheless be concluded that the viscoplastic nature of rapid crack propagation does not justify the use of the quasi-static LEFM parameter for crack arrest. The reason is that it relies upon two conflicting assumptions.

On the one hand, for K_{Ia} to be meaningful, there must be a direct connection between the dynamic deformation state of the crack at the instant of crack arrest and the static state that

exists at some (relatively long) time later. At the same time, if viscoplastic effects are significant, the plastic zone of the propagating crack as it approaches the arrest point will necessarily be considerably smaller than that corresponding to the arrested crack long after arrest. A smooth slowing down to arrest, which is contrary to the experimental evidence in any event, would not reconcile this dichotomy. If the crack arrests with a large enough plastic zone - a necessary condition for the warm prestress effect on subsequent reinitiation [13] - then LEFM is invalid regardless of the plastic zone sizes that precede arrest.

5. SUMMARY AND CONCLUSIONS

To summarize, the long-standing disagreement between the two opposing views of crack arrest still exists. These are that (1) crack arrest is the reverse in time of crack initiation, whereupon it is characterizable by a single material property, e.g., K_{Ia}; or (2) crack arrest is the termination of unstable propagation whereupon it is characterized by the same speed-dependent properties that govern its motion; e.g., K_{ID}. While the weight of the evidence definitely favors the second of these two views, there are many practical applications where the much simpler analysis procedures offered by the first will suffice. Further confusing the situation are doubts that now exist concerning the underlying assumptions in the second view; at least insofar as its implementation via elastodynamic procedures is concerned.

Efforts to clarify the situation, as well as to extend the applicability of dynamic fracture mechanics to more ductile materials [14], have generally proceeded through the use of elastic-plastic analyses. However, these are now being called into question on the basis that the viscoplastic nature of rapid crack propagation is thereby neglected. General agreement on the proper crack growth criterion does not exist for elastic-plastic conditions, much less for viscoplastic conditions. Moreover, the use of viscoplastic models suffers from a lack of the proper material constants. The resolution of these questions would therefore appear to be well in the future when analyses based upon well-documented constitutive behavior can be coupled with precisely conducted experiments to elucidate the load/structure/crack size-independent crack tip

characterizing parameter that governs crack propagation/arrest. Nevertheless, it is in this direction that research is focussed and, in the author's view, properly so.

ACKNOWLEDGEMENT

This paper was prepared as part of a research program supported by the Office of Naval Research under Contract No. N00014-77-C-0576. The author would like to express his appreciation to Dr. Yapa Rajapakse of ONR for his continued encouragement of this work.

REFERENCES

1. Cheverton, R.D., Bolt, S.E., Holz, P.P., and Iskander, S.K., "Behavior of Surface Flaws in Reactor Pressure Vessels under Thermal-Shock Loading Conditions," Experimental Mechanics, 22, (1982) 155-162.

2. Kanninen, M.F., "Whither Dynamic Fracture Mechanics?", in Numerical Methods in Fracture Mechanics, D.R.J. Owen and A.R. Luxmore, (eds.), Pineridge Press, Swansea, U.K., (1980) 433-456.

3. Kalthoff, J.F., Beinert, J., and Winkler, S., "Measurements of Dynamic Stress Intensity Factors for Fast Running and Arresting Cracks in Double-Cantilever-Beam Specimens," in Fast Fracture and Crack Arrest, G.T. Hahn and M.F. Kanninen (eds.), ASTM STP 627 (1977) 161-176.

4. Kanninen, M.F., "An Analysis of Dynamic Crack Propagation and Arrest for a Material Having a Crack Speed Dependent Fracture Toughness," in Prospects of Fracture Mechanics, G.C. Sih, et al. (eds.), Noordhoff, Leyden (1974) 251-266.

5. Crosley, P.B., and Ripling, E.J., "Comparison of Crack Arrest Methodologies," in Crack Arrest Methodology and Applications, G.T. Hahn and M.F. Kanninen, (eds.), ASTM STP 711 (1980) 211-227.

6. Kanninen, M.F., Gehlen, P.C., Barnes, C.R., Hoagland, R.G., Hahn, G.T., and Popelar, C.H., "Dynamic Crack Propagation Under Impact Loading," in Nonlinear and Dynamic Fracture Mechanics, N. Perrone and S.N. Atluri (eds.), ASME AMD 35 (1979) 185-200.

7. Kanninen, M.F., Popelar, C.H., and Broek, D., "A Critical Survey on the Application of Plastic Fracture Mechanics to Nuclear Pressure Vessels and Piping," Nuclear Engineering and Design, 67 (1981) 27-55.

8. Hutchinson, J.W., and Paris, P.C., "Stability Analysis of J-Controlled Crack Growth," in Elastic-Plastic Fracture, J.D. Landes, et al. (eds.), ASMT STP 668 (1979) 37-64.

9. Proceedings of the 29th Sagamore Army Materials Research Conference, Plenum, New York, in press, 1983.

10. Vagins, M., Private Communication, (1982).

11. Bodner, S.D., and Partom, Y., "Constitutive Equations for Elastic-Viscoplastic Strain-Hardening Materials," Journal of Applied Mechanics, 42 (1975) 385-390.

12. Achenbach, J.D., Kanninen, M.F., and Popelar, C.H., "Crack-Tip Fields for Fast Fracture of an Elastic-Plastic Material," Journal of the Mechanics and Physics of Solids, 29 (1981) 211-225.

13. Loss, F.J., Gray, R.A. Jr., and Hawthorne, J.R., "Investigation of Warm Prestress for the Case of Small ΔT During a Reactor Loss-of-Coolant Accident," Journal of Pressure Vessel Technology, 101 (1979) 298-304.

14. Kanninen, M.F., Brust, F.W., Ahmad, J., and Abou-Sayed, I.S., "The Numerical Simulation of Crack Growth in Weld-Induced Residual Stress Fields," Residual Stress and Stress Relaxation, Plenum, New York (1982) 227-248.

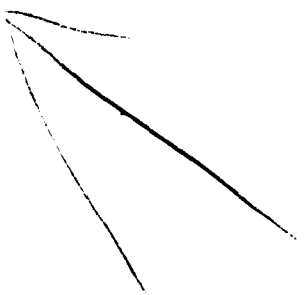

LIST OF PARTICIPANTS

J.D. Achenbach	Northwestern University The Technological Inst. Evanston, IL 60201
S.N. Atluri	School of Civil Engineering Georgia Institute of Tech. Atlanta, GA 30332
C.D. Babcock	Graduate Aeronautical Laboratories California Institute of Technology Pasadena, CA 91125
K.B. Broberg	Div. of Solid Mechanics Lund Institute of Technology Box 725, S-22007 Lund, Sweden
L.M. Brock	Dept. of Engineering University of Kentucky Lexington, KY 40506
P. Burgers	Hibbit, Karlsson & Sorensen, Inc. 35 S. Angell St. Providence, RI 02901
R.J. Clifton	Div. of Mechanical Engineering Brown University Providence, RI 02901
J.P. Dempsey	Dept. of Civil and Environmental Engineering Clarkson College of Technology Potsdam, NY
J. Duffy	Div. of Mechanical Engineering Brown University Providence, RI 02901
F. Erdogan	Dept. of Mechanical Engineering and Mechanics Lehigh University Bethlehem, PA 18015
W.L. Fourney	Dept. of Mechanical Engineering University of Maryland College Park, MD 20742
L.B. Freund	Div. of Engineering Brown University Providence, RI 02912

G.T. Hahn — Materials Sciences Dept.
Vanderbilt University
Box 23, Station B
Nashville, Tenn. 37235

G. Herrmann — Dept. of Applied Mechanics
Stanford University
Stanford, CA 94305

W.G. Hoover — Lawrence Livermore Lab.
L-798, P.O.Box 808
Livermore, CA 94550

J.F. Kalthoff — Fraunhofer-Insitut für Werkstoffmechanik
Rosastrasse 9, Freiburg i.B., West Germany

M.F. Kanninen — Southwest Research Institute
Post Office Drawer 28510
6220 Culebra Road
San Antonio, TX 78284

K.S. Kim — Dept. of Theoretical &
Applied Mechanics
University of Illinois
Urbana, IL 61803

V.K. Kinra — Aerospace Engineering Dept.
Texas A & M University
College Station, TX 77843

W.G. Knauss — Graduate Aeronautical Laboratory
California Institute of Technology
Pasadena, CA 91125

A.S. Kobayashi — Dept of Mechanical Eng.
Univ. of Washington
Seattle, Wash. 98105

T. Kobayashi — SRI International
Poulter Lab. 333R
333 Ravenswood Ave.
Menlo Park, CA 94025

C.H. Popelar — Ohio State Univ.
Columbus, OH 43210

K. Ravi-Chandar — Graduate Aeronautical Laboratory
California Institute of Technology
Pasadena, CA 91125

A.J. Rosakis	Graduate Aeronautical Laboratory California Institute of Technology Pasadena, CA 91125
D.A. Shockey	SRI International Poulter Lab 333 Ravenswood Ave. Menlo Park, CA 94025
A. Shukla	Dept. of Mechanical Engineering and Applied Mechanics Univ. of Rhode Island Kingston, RI 02881
J.R. Walton	Texas A & M University College Station, TX 77843
M. L. Williams	Univ. of Pittsburgh 240 Benedum Engineering Hall 3900 O'Hara Street Pittsburgh, PA 15261
C.J. Astill	National Science Foundation Washington, D.C. 20550
J. Baley	U.S. Army Research Office Research Triangle Park, NC 27709
G. Moss	Ballistic Research Laboratory Aberdeen, MD 21005
E.A. Saibel	U.S. Army Research Office Research Triangle Park, NC 27709
M. Vagins	U.S. Nuclear Regulatory Commission Rockville, MD 20852

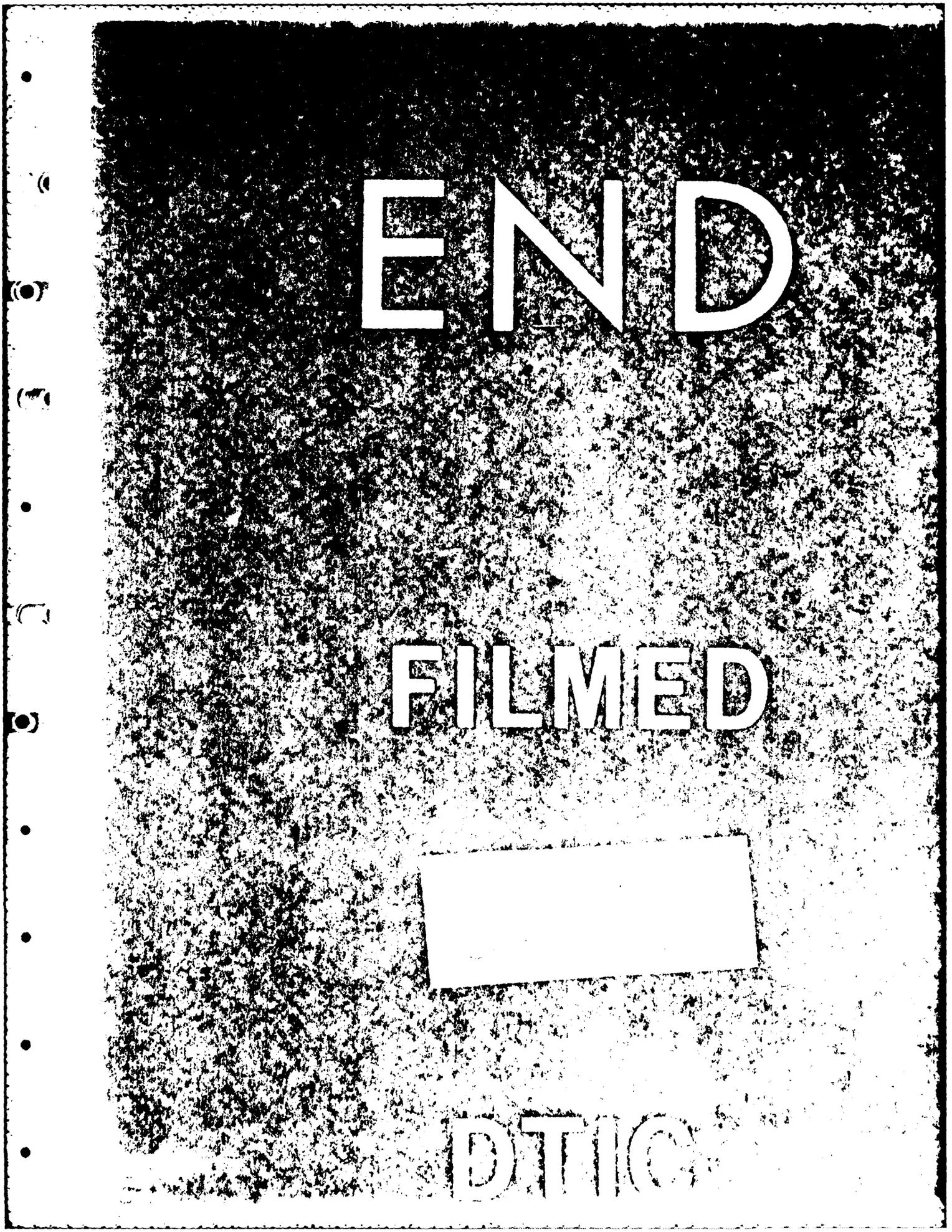
END
FILMED
DTIC